UNIVERSITY OF SOUTHAMPTON

IMPROVED MODELS FOR THE PREDICTION OF SOUND TRANSMISSION THROUGH PARTITIONS AT LOW FREQUENCIES

by

Max De Castro Magalhaes

Institute of Sound and Vibration Research

Faculty of Engineering, Science and Mathematics

Thesis submitted for the degree of

Doctor of Philosophy

April 2004

This thesis is dedicated to my parents, who have made many sacrifices in order that I could pursue my academic career. It was from them that I derived the strength to complete this project.

UNIVERSITY OF SOUTHAMPTON

ABSTRACT

FACULTY OF ENGINEERING AND APPLIED SCIENCE
INSTITUTE OF SOUND AND VIBRATION RESEARCH

Doctor of Philosophy

IMPROVED MODELS FOR THE PREDICTION OF SOUND TRANSMISSION THROUGH PARTITIONS AT LOW FREQUENCIES

by Max De Castro Magalhaes

Although the phenomenon of sound transmission through partitions has been investigated over many years, the problem of low frequency sound insulation in buildings is still an active research area. Modal methods are widely used for the low-frequency analysis of vibro-acoustic problems, including the problem of sound transmission between coupled rooms. A generic modal model is developed and implemented for better representation of the airborne sound transmission in buildings. Subsequently, the model is validated experimentally and showed good agreement when compared to previously published results.

This model also provided some information in terms of the variability and sensitivity of sound insulation parameters (e.g. the Noise Reduction) to the geometry and material properties of the system.

The effects of the imposition of common velocity on the acoustic-structural interface have been incorporated using a novel development of the Component Model Synthesis Method (CMS). The formulation of the structural-acoustic problem in terms of 'components' is described. The results obtained via the CMS method are then compared

to those obtained using both a one-dimensional wave approach and the standard modal analysis for a one dimensional acoustic system. Very good agreement was found between the one-dimensional wave model and the CMS model. Finally, the CMS approach is developed and extended to three-dimensional acoustic systems. Results are provided for the case of an elastic partition coverage of a common interface.

In summary, improved models have been developed and implemented in order to make a better assessment of the sound transmission between two rooms coupled by a common structural partition.

Table of Contents

Acknowledgments

I would like to acknowledge with deep appreciation the academic guidance, understanding and continuous encouragement provided by my supervisor, Dr. Neil Ferguson, throughout this work. His patience and friendship were extremely valuable on the successful completion of this project.

I greatly appreciate the feedback and useful advice from Professor Mike Brennan and Dr. David Thompson who internally reviewed my progress. I also wish to acknowledge my indebtedness to all ISVR staffs who contributed to the realization of this work.

In particular, I gratefully acknowledge the financial support provided by the University of Southampton and Institute of Sound and Vibration Research (ISVR).

I am indebted to all my colleagues from the Department of Engineering Materials and Construction, (State University of Minas Gerais - UFMG, Brazil), who have been immensely supportive during my PhD studies.

I am also profoundly indebted to Professor Samir N. Y. Gerges (LVA, State University of Santa Catarina, Brazil) for his support and help.

I am grateful to all members of the Verbum Dei Community (Southampton) and Catholic Society of Southampton University, who took care of me with their spiritual advice and friendship.

List of Symbols

A a particular internal room surface

A_s complex forward travelling wave amplitude (equation (5.1))

B_n complex pressure amplitude (equation (2.18))

B_s complex backwards travelling wave amplitude (equation (5.1))

C_{ct} matrix of constraint equation (equation (5.15))

C_d matrix of modal damping

C_{n_1p}, C_{n_2p} spatial structural-acoustic coupling coefficient for the source and receiving rooms respectively

C_r complex forward travelling wave amplitude (equation (5.2))

$C(t)$ Amplitude decay curves

C_1^{3D} modal damping matrix for the fluid column

C_1, C_2 constraint equations (equations (6.20) and (6.21))

D damping dissipation function (equation (6.38))

D bending stiffness of a thin plate (= $Eh^3/12(1-\upsilon^2)$)

D_r complex backwards travelling wave amplitude (equation (5.2))

E Young's modulus of elasticity

E_i spatial averaged, time averaged energy in subsystem i

$E(t)$ complex voltage amplitude

F_o An arbitrary complex force

F_1 force exerted on component 1

$\overline{G}$ matrix containing the generalized coordinates of the uncoupled components

$\overline{G}^s$ rearranged global matrix $\overline{G}$

G subscript of global matrix of coupled system

$G(r \mid r_o)$ Green's Function (solution of equation (2.11))

H Hilbert Transform

$H(f)$ frequency response function

I Identity matrix

Im imaginary part

K_1, K_2 matrices of the modal stiffness of components *1* and *2* respectively

K_1^{3D} modal stiffness matrix for the fluid column

L Lagrangian for the system of coupled components (equation (6.39))

L_{py}, L_{pz} width and length of the partition respectively

L_{x1}, L_{y1}, L_{z1} length, height and width of room 1

L_{x2}, L_{y2}, L_{z2} length, height and width of room 2

L' is the total perimeter of the room

M_1, M_2, M_p modal mass matrix of components *1*, *2* and *limp* partition *p* respectively

ML subscript for results obtained using the Mass Law theory

$\mathbf{M_1}$, $\mathbf{M_2}$ Modal Overlap factor for subsystem 1 and 2 respectively

M_{comb}, N_{comb} combined modal overlap factor and number of modes respectively

M_1^{3D} modal mass matrix for the fluid column

N total number of acoustic modes

P total number of structural modes

P_k pressure measured at the k^{th} response point

P_o reference pressure measured at the excitation point (loudspeaker near-field pressure) of the acoustic system

P_{diss}, P_{in} time averaged dissipated power and input power respectively

P_{ij} net power transmitted from subsystem *i* to subsystem *j*

Q_0 Acoustic volume velocity

Q_i, Q_n the time-dependent generalized volume velocity source strength

Q_1^{3D} column matrix of generalized volume velocity source strength

R_1, R_2 sub-matrices defined in equation (5.18)

R_c coefficients of the matrix constraint equation (equation (5.18))

R_c^s rearranged coefficients of the matrix constraint equation (equation (5.27))

Re real part

S area of the partition

SRI Sound reduction Index

S' total surface area of a room

$S_{xy}(f)$ cross-spectral density of an input and output signal

$S_{xx}(f)$ auto-spectral density of an input signal

T_A kinetic energy (equation (6.31))

T_r transformation matrix.

T superscript to indicate the transpose of the matrix

T_{60}, $T_{60,i}$ Reverberation Time and Reverberation Time for subsystem i respectively

U loudspeaker velocity

V_A potential energy (equation (6.37))

V volume of the acoustic room

1, 2 subscripts for component 1 and 2 respectively.

a plate height in equations (2.8)-(2.9).

b half-power point bandwidth; plate width in equations (2.8)-(2.9)

c subscript for constraint modes

c_o sound speed in air

d subscript for diffuse field

f subscript for field incidence

f_B measured first resonance frequency of the plasterboard beam

$f(t)$ input excitation force (equation (3.1))

f_n measured resonance frequency of a plasterboard partition mounted *in situ*

f_s 'Schroeder' frequency or 'large room' frequency (equation (4.1))

h thickness of the partition

$h(t)$ impulse response of the system

i,j subscript for subsystems i and j.

j $\sqrt{-1}$

$\vec{i}, \vec{j}, \vec{k}$ unit vectors in the positive directions of the axes of a Cartesian coordinate system

k acoustic wavenumber $= \dfrac{\omega}{c_o}$

k_n acoustic wavenumber corresponding to mode n

k_b wavenumber of free-bending waves in an elastic plate

k_{pz} structural wavenumber component in the z direction for an elastic plate

k_{py} structural wavenumber component in the y direction for an elastic plate

k_x, k_y, k_z acoustic wavenumber in the x, y and z direction

l subscript which denotes the normal mode number of a mode in the y direction (equation (6.3))

m modal mass defined in equation (5.12)

m panel mass per unit area

m' mass per unit length of the test beam (equation (3.6))

n subscript for acoustic normal mode number; normal incidence and normal mode number of a particular mode in the x direction (see equation (6.2))

n_1, n_2 modal densities for subsystems 1 and 2 (equation (4.1))

n_y, n_z acoustic mode number in the y and z directions.

p subscript indicating the partition; panel mode number

p_{bL} modal generalized force (blocked pressure on the partition)

$p_i(y, z, \omega)$ incident field amplitude of pressure on the partition

$\left\langle \overline{p}_i^2 \right\rangle$ spatially averaged mean square sound pressure in subsystem i

p_n acoustic modal pressure amplitude

$\overline{p}$ steady-state sound pressure amplitude (equation (2.17))

$\overline{p}_{n_2}$ receiving room generalized modal pressure

$\overline{p}_R$ generalized pressure over the partition in the receiving-room (equation (2.38))

q subscript indicating a panel mode number (equation (2.12)) and subscript which denotes the normal mode number of a mode in the z direction (equation (6.4))

q_b vibration of the panel surface (equation (2.27))

q_i generalized coordinate

$\overline{q}_i$ linearly independent coordinates of the coupled system

q_s distribution of external source inside the room

r, s represent the panel mode numbers.

$s(t)$ signal received at a receiving transducer (equation (3.1))

t time

u_x, u_y, u_z fluid particle velocity components in the x, y and z directions

$w(z, y, \omega)$ normal displacement of the plate surface into the fluid

w_p generalized normal panel velocity

w_{inc} incident sound power

w_{trans} transmitted sound power

x, y, z Global Cartesian coordinates

z_a real specific acoustic impedance

$\Lambda_{n1,p,n2}$ modal generalized mass for the source room, elastic panel and receiving room respectively

Φ scalar function termed velocity potential

$\overline{\Phi}$ generalized displacement potential (scalar quantity)

$\dot{\overline{\Phi}}$ generalized velocity potential (scalar quantity)

$\prod(\omega)$ time and space averaged power radiated into the half-space from a vibrating partition

∇^2 Laplace operator [79] which is given by $\nabla^2 = (\partial^2/\partial x^2)+(\partial^2/\partial y^2)+(\partial^2/\partial z^2)$

∇^4 operator governing the elastic forces in the plate; It is given by $\nabla^4 = (\partial^4/\partial y^2)+(\partial^4/\partial y^2\partial z^2)+(\partial^4/\partial z^4)$.

Ψ normalized modal matrix of assumed-modes

Ψ_x, Ψ_y, Ψ_z matrices which consist of pre-selected orthogonal normal modes plus constraint modes in the x, y and z directions respectively (equations (6.2), (6.3) and (6.4)

Ω_n acoustic pressure mode shape n for the room volume (equation (2.12))

α diffuse absorption coefficient for an internal room surface A

β generalized modal damping coefficient (equations (2.31), (2.32) and (2.33))

$\delta(x-x_o)$ one-dimensional Dirac Delta function

$\delta(\mathrm{r}-\mathrm{r}_o)$ three-dimensional Dirac Delta function

$\varepsilon(x,t)$ fluid displacement function at position x and time t.

$\dot{\varepsilon}$ fluid velocity function

$\overline{\varepsilon}$ generalized coordinates of the component displacements.

ε_1 fluid loading parameter (see equation (2.9))

ς global matrix of modal damping of the system (acoustic components 1, 2).

ζ_N modal damping ratio matrix of the component

η total loss factor o mechanical damping factor in equations (2.8)-(2.9)

η_i internal loss factor for subsystem *i*

η_{ij} Coupling Loss Factor from subsystem *i* to subsystem *j*

η_{ML} Coupling Loss Factor defined in equation (4.10)

κ compressibility of the fluid (equation (6.33))

λ Lagrange multiplier vector

μ global matrix of the modal mass of the system

v particle velocity on the panel surface

ρ_o density of air.

σ^2 variability defined in equation (4.11)

ρ density of the partition

τ transmission efficiency parameter (equation (2.1))

τ_{12} transmission efficiency calculated for volume velocity source located in room 1

τ_{21} transmission efficiency calculated for volume velocity source located in room 2

τ_∞ diffuse field transmission efficiency

$\tau(\theta)$ transmission efficiency for a given angle of incidence θ

τ_{Lep} transmission efficiency according to Leppington's [16].

τ_{nr} transmission efficiency of the non-resonant contribution

τ_{res} transmission efficiency of the resonant contribution.

υ Poisson's ratio

ϕ_n, ϕ_c set of matrices of normal displacement and constraint modes respectively.

ϕ_p normal displacement mode shape *p* for a simply-supported rectangular panel (see equation (2.11))

χ global stiffness matrix of the system (acoustic components *1*, *2*).

ψ matrix of shape functions defining the normalized modes (equations (10-11)).

ω angular frequency (rad/s)

ω_c critical frequency of a simply-supported rectangular panel.

ω_N modal matrix of natural frequencies

ω_p *in vacuo* natural frequencies of the partition

ω_n natural frequencies of a rigid-walled rectangular space

List of Figures

List of Tables

Chapter 1

INTRODUCTION

1.1 – General background

Sound insulation requirements for buildings depend on many factors. These include activities of people involved, e.g. listening to music, shopping, etc., and also on the background noise, which may be considered as part of the work or home environment. Although the frequency range of human hearing is considered to be between 20 Hz and 20,000 Hz, a source of noise operating at frequencies below 20 Hz can be perceived (if one considers a signal that has a high sound pressure level) and also detected through the human body [1]. Hence, there is a need to predict, quantify and understand the behaviour of sound transmission over a wide range of frequencies.

The phenomenon of sound transmission is an important subject in noise control for buildings. Usually, noise is communicated between rooms via many different paths. The two methods of sound transmission in buildings are characterized as airborne and structure-borne sound transmission. In airborne sound transmission the noise originates and travels in the air. The noise sources may be elsewhere in the building and/or outside the building. In structure-borne sound transmission, the sound is either generated or transmitted by vibrating solid bodies. Subsequently, the vibration may produce radiated noise into a receiving space. In this thesis, the phenomenon of structure-borne sound transmission is not directly addressed. Therefore, indirect paths of transmission or as they are often called 'the flanking transmissions' are not included in this work. Thus the sound transmission will only be considered through a common partition separating two acoustic volumes. This is the simplest of cases and is often sufficient in quantifying the noise levels.

1.1.1 – The definition of Noise Reduction (NR) and Sound Reduction Index (SRI)

For practitioners in the field of building acoustics the quantification of the 'sound insulation' is typically described in terms of some simple quantities which are relatively easier to comprehend and use than the physical response in terms of pressure and velocity.

Generally, the term 'sound insulation' refers to the predicted or measured sound level difference, or Noise Reduction (NR), and also the Sound Reduction Index (SRI). The latter is the logarithmic index of the inverse of the sound transmission efficiency [2]. The sound transmission efficiency is defined as the ratio of the transmitted sound intensity through a partition or wall to the incident intensity on a partition or wall. For a diffuse field, the formula or expression for the NR is given by [2]

$$\mathrm{NR} = L_S - L_R = SRI + 10\log_{10}\left(10^{-\frac{SRI}{10}} + \frac{A}{S}\right) \tag{1.1}$$

where L_S and L_R are the spatially averaged sound pressure levels in the source and receiving rooms respectively, S is the area of the partition and A is the Sabine absorption of the receiving room. Equation (1.1) is a consequence of the need for the overall system to obey the conservation of energy principle.

By assuming that in the receiving room the power loss from its reverberant field is much greater than the power being transmitted to the source room, the first term in the bracket is therefore negligible in comparison with the other one. Thus, equation (1.1) can be simplified and rewritten as

$$\mathrm{NR} = L_S - L_R = SRI + 10\log_{10}\left(\frac{A}{S}\right) \tag{1.2}$$

Typically experiments are conducted to measure the Noise Reduction and equation (1.2) can then be used to evaluate the Sound Reduction Index. The latter is primarily a measure of the transmission properties of a partition and it is not easy to measure acoustic intensities in many cases. For instance, at low frequencies, the limitation of a sound intensity measuring system, i.e. the phase mismatch between the pressure transducers and the associated signal conditioning channels, can significantly affect the accuracy of any particular measurement.

Furthermore, well separated microphones are required to measure intensity at low frequencies, as one needs some phase measurement which is very small and subject to significant errors unless the instrumentation is well matched. On the other hand, at high frequencies closely spaced microphones are required. In addition, there is a physical limitation on their closeness and also how close one can get to partition surfaces [3].

These two quantities are used as design parameters or guidelines, which provide sufficient information for detailed calculations or comparison against standards or other configurations. Essentially better sound insulation corresponds to higher values of Noise Reduction and Sound Reduction Indexes. Also, many practitioners use such descriptors in cases where strictly either the room volumes are small, the frequencies are low or the absorption high and then the diffuse field assumption is strictly invalid.

1.1.2 – The main methods used to predict sound transmission

The problem of calculating analytically or numerically the sound transmission between rooms has been the subject of investigation over many years [1-3]. The five main approaches have been the Conventional Wave Approach [4], Modal Analysis [5], numerical techniques such as the Finite Element Method (FEM) and the Boundary Element Method (BEM) [6], the Wave Based Method (WBM) [7] and Statistical Energy Analysis [8].

A brief overview of each method is presented as follows.

In the Conventional Wave Approach, infinitely extended panels are used in sound transmission models and for simplicity a diffuse field is often assumed. The models initially consider the transmission of sound when plane waves are incident upon a panel. The diffuse field transmission results from the integration from all of the transmitted power due to all of the equal amplitude acoustic plane waves in the incident acoustic diffuse field.

For the infinite panel, boundary effects are neglected and the walls are assumed to be homogeneous and to have no leaks. The resulting Mass Law (ML) formula, which assumes transmission through a limp panel, has been successfully applied to many situations where the frequencies are well below the critical frequency* of the panel. In this scenario the transmission is controlled by non-resonant lower order modes of a finite panel which couple spatially with the acoustic field at frequencies above their natural frequencies and their response is mass-controlled.

However, the assumptions provided are unsatisfactory in a large number of real panels whose dimensions are less than or equal to the wavelength of the incident sound wave, especially the case at lower frequencies. In addition, the geometry of the system is not

* It is the frequency at which the speed of free bending waves in the panel equals the sound speed in air.

taken into account and, at low frequencies or for real rooms, the assumption of an incident diffuse field is incorrect.

Alternatively, Modal Analysis [5] allows the geometric parameters of the system to be incorporated into the models and subsequent predictions. The frequency response of a finite system normally has peaks and dips, due to the resonance phenomenon that involves modal behaviour and fluid-structure spatial coupling of wall (plate) and room modes. This approach will be developed later and the limitations/assumptions will be identified and discussed. Typically Modal Analysis using analytical modes is restricted to simple regular geometrical shapes otherwise it requires numerical modal techniques discussed below.

Deterministic numerical techniques, involving for example a Finite Element (FE) model of the room volumes and partitions [6] or a Boundary Element (BE) model for the acoustic volumes and a FE model for the partitions, do not have the limitation on geometry, but for computational and accuracy reasons are applicable primarily for low frequency predictions. These approaches discretise the physical system and equations of motion in the modal degrees of freedom are obtained.

Similarly such an approach is inefficient for simulations involving a large number of geometric variations. The acoustic sources can be explicitly defined and the effect of room geometry, surface absorption and partition properties incorporated. The modes of either the uncoupled or coupled acoustic-structural system can be obtained and a modal basis for the forced response obtained, if required.

Recently, an alternative technique, namely the Wave Based Method [7], has been developed for the analysis of coupled vibro-acoustic problems in the mid-frequency range. It is based on the expansion of dynamic response variables in terms of wave functions, which are the exact solutions of the governing differential equations. These individual solutions are combined and constrained to solve the system with more general geometry or boundary conditions. It has been shown that the WBM model exhibits better convergence properties than the FEM model, especially at higher frequencies, and is more computationally efficient.

Finally, Statistical Energy Analysis (SEA) considers the power flow balance between linear coupled systems and has been applied successfully to noise transmission in buildings for mid to high frequencies, where there are a reasonable number of modes in a

band and a frequency averaged band result is sufficient. The estimates of subsystem energies are obtained on the basis of known values for the loss factors and power inputs, with coupling loss factors either measured or calculated from known formulae. Thus, the response of each subsystem is only described by the time, frequency and spatial averaged energy response.

For noise transmission, the SEA limitations include assuming diffuse and reverberant acoustic volumes, high modal overlap for reduced variability and approximations for the geometry. Consequently, no information about the spatial distribution of the response variables (e.g. pressure, particle velocity, etc) is available. Moreover, whilst there are no rigid rules which restrict the choice for the subsystems, a judicious choice is vital for successful application of the method.

1.1.3 – A review of predictive methods for the sound transmission through partitions

In most cases, it has been possible to consider a simpler configuration, namely sound transmission between acoustic volumes separated by a partition. This has provided insight into the physical phenomenon and a brief overview of most relevant research, both theoretical and experimental, now follows. The majority concentrates on finite panels to overcome the approximation and assumptions used in the Mass Law formulation.

Dowell *et al* [9] analyzed the transmission of a reverberant sound field through a rectangular baffled partition by means of a mode expansion method. According to the formulae derived, valid for non-resonant partition transmission, the problem was well predicted provided that the mass of the partition was significant. In general, the non-resonant transmission was found to be the most important contribution for frequencies below the critical frequency of a particular partition.

Below the critical frequency the spatial matching is best achieved by lower order structural modes. The corresponding acoustic frequency that matches the structural wavelength is higher than the structural natural frequencies. Hence the response of these modes is controlled by mass and not stiffness or damping. Although resonant panel modes might have greater amplitude than the forced modes, they are poorer radiators.

The effect of panel mass on forced-wave transmission is quantified by Fahy [5]. It is seen that the greatest contribution of a particular mode to sound transmission occurs in a

frequency range greater than its natural frequency where the frequency response is mass-controlled. In addition, the radiation efficiency of the forced or non-resonant modes is not only greater than that of the resonant modes but also dependent on the panel boundary conditions.

In these conditions, Dowell *et al* [9] observed that the imaginary part of the fluid wave impedance in the receiver volume was significantly greater than its real part. Therefore it ensured that the forced vibration, or *mass law* contribution, dominated the transmission factor. A detailed review of acoustic-structural coupled systems was also presented. The theoretical model developed for arbitrary wall motions was formulated using Green's Theorem. From the point of view of applications, a simplified formulation was also presented for sound pressure level predictions in terms of the acoustic and structural parameters.

The effects of panel boundaries on sound transmission, including a comparison with an infinite panel, were discussed in refs [10-11]. A simple two-dimensional model was used for evaluating the sound transmission characteristics of finite panels. The analysis of the transmission, through a baffled plate of finite width and infinite length, was conducted rigorously. The effects of panel size were verified in regions below, above and at the critical frequency. Estimates of averaged response over a particular frequency range were also presented. Sound transmission for the diffuse field was hence obtained via direct numerical integration over all angles of incidence.

More recently Osipov *et al.* [12] produced an analysis of sound transmission in buildings based on a room-plate-room model that takes into account the coupling between the flexural modes of a simply supported plate and the acoustic modes of the source and receiving rooms. The thin plate bending wave equation of motion, which is based on the Kirchhoff's theory [3,13], was considered in the analysis. The equations of motion, in terms of the modes, are essentially formulated in the same manner as Dowell [9].

Similarly, Gagliardini *et al* [14] used a modal basis model, which considers the fluid-structure interaction, to predict the influence of some parameters on the Sound Reduction Index. Nevertheless, the results are shown for a limited number of cases due to significantly increased computational time when the dimensions of the rooms and partition, in addition to frequency range, are varied.

Leppington *et al* [15,16] presented an alternative analytical formulation for the calculation of sound transmission through a baffled panel. The model assumed the panel in the problem to be simply supported. These predictions, which were based on modal analysis, have been considered an improvement on previous theories, such as the Mass Law theory. A random field was considered as an infinite sum of uncorrelated plane-waves impinging on the finite-panel surface. Moreover, the transmission problem was described in terms of two distinct mechanisms. The first one is dominant at the region of the spectrum above the critical frequency, where free bending waves interact to cause resonance. In this frequency range the partition is a good radiator and also couples well with the incident sound field. In fact, its radiation efficiency is always greater than or equal to unity. For the region below the critical frequency, both free and forced bending waves are generated. In this frequency range (below the critical frequency), the dominant partition behaviour is that which is forced and responds at the acoustic wavenumbers. At these frequencies the panel is less efficient in coupling to the acoustic excitation and the transmission is governed by the mass law response of modes at frequencies above their resonances, whose modal wavenumber description better match those in the incident acoustic field [15].

Subsequently, Leppington [17] developed a simpler and more direct method to estimate the transmission efficiency which accounts for the non-resonant contribution of sound power transmission. The main assumption was to consider the random field as a diffuse field, neglecting the presence of the boundaries. The transmission phenomenon can then be considered as a summation of the non-resonant or forced transmission, and the resonant transmission.

According to Fahy [18], the two main differences between the unbounded panel and a finite baffled panel in terms of sound transmission performance are the existence of standing waves and diffraction by the aperture in the baffle containing the panel. Although simply supported edges will be considered in this work as has been used by others for reason of simplicity, complex boundary conditions have also been discussed in the literature [19-22].

1.1.4 –Overview of experimental sound transmission investigations

The experimental investigation and quantification of sound transmission has likewise seen developments and improvements. The main concern whilst performing any noise or vibration experimental test is to make valid and accurate measurements which represent the real problem. For instance, the accurate determination of room responses at low frequencies is a difficult task to be tackled. In general, laboratory measurements at these frequencies do not produce acceptable reproducibility due to the poor diffuseness of the acoustic field [23, 24].

Although much research have been devoted to the experimental investigation of sound transmission through partitions at low frequencies, poor sound insulation between dwellings has been a matter of concern for many people. As a result, experimental studies on sound insulation in buildings at low frequencies are still being carried out nowadays. More recent techniques have included nearfield acoustic holography [25], which can allow mapping of the individual intensities of the sound transmitted through partitions, windows, doors, gaps, etc. but are restricted to particular configurations.

Some of the earliest work was also conducted to validate predictions. Petyt *et al* [26] employed a pure sinusoidal excitation technique for the identification of the natural frequencies of rooms. In this procedure, the room was excited at a single frequency of interest and the pressure response (amplitude and phase) measured using an oscilloscope. Nevertheless, this technique is extremely time consuming and not very efficient. Since the advent of two channel FFT analyzers, the identification of modal parameters from measured frequency response functions has been widely used.

Various investigators, over a number of years, have conducted measurements on the sound transmission between two rooms separated by a common wall [27, 28]. Results presented include discussion on the influence of the measurement facilities on the results in terms of sound insulation. In 1972, Lang [29] showed and identified that the differences between field values of airborne sound insulation and the results of measurements made in laboratory were due to the energy transmission via flanking walls.

Guy *et al* [30], studied the effect of panel size upon the laboratory measurements; and a correction factor was presented in order to produce closer agreement between experiments and the classical mass law theory [14]. Craik, [31] similarly assessed the

influence of the rooms conditions and the test partition on the performance of the whole system.

The interesting studies in ref. [32, 33] concluded that laboratory measurements of sound insulation at low frequencies produce not only poor reproducibility but also poor repeatability. The concepts of reproducibility and repeatability are significant in assessing the closeness of agreement between individual and successive results respectively [34]. The former is defined for results obtained under different conditions, such as operators, apparatus, laboratories and intervals between measurements. On the other hand, repeatability is defined for results obtained for the same conditions. Some further work [35, 36] provided alternative solutions in order to improve laboratory conditions. The use of absorbers positioned in the corners of rooms was suggested, in order to improve the repeatability of measurements at low frequencies.

Recently, Maluski [37, 38] has shown that all the present methods of measurements are not appropriate in the low frequency ranges where the sound field is strongly dependent on its modal behaviour. For instance the standard method defined in the International Standard ISO 140 – part 3 [41], which is probably the most widely used nowadays, was initially defined for reverberant diffuse fields. As specified in ISO 140-3, a partition to be tested is positioned between two reverberant rooms. Subsequently, a broadband noise source generates an approximation to a diffuse field in the source room and the spatial-average mean square sound pressure is measured in different positions inside both rooms. It was observed that at low frequencies certain modal patterns inside the rooms dominate over others. Nevertheless, in ref. [38], measurements of sound pressure levels inside rooms at low frequencies were still performed on the basis of the method described in ISO 140-3.

Alternative techniques have been proposed for determination of the Sound Reduction Index [39, 40]. They are based on sound intensity measurements that require signals proportional to the instantaneous sound pressure and the corresponding instantaneous particle velocity vector. The measurements can be made by using an intensity probe which is a transducer system that comprises a pair of phase-matched pressure microphones separated by a small distance.

Basically, experimental validation of theoretical models for predicting sound transmission through partitions involves preliminary tests in order to obtain the

acoustical and structural properties of rooms and partitions respectively. In general, the measurement and quantification of the source volume velocity used on the tests is essential for the validation process. Likewise, the analysis and measurement of damping of structural elements and rooms are also fundamental.

In this thesis, sound pressure measurements based on the conventional method [41] were made in order to compare and validate an acoustic modal model, which is comprehensively described and presented in chapter 2 of this thesis. (Magalhaes and Ferguson [42] having published some initial work on the modal model prior to this date). In addition, the measure of the reverberation time (RT) was based on ISO 354 [43] and Schroeder's method [44]. Thus, the measured RT values were used to calculate the modal damping of the theoretical model [45], which might introduce errors because of the assumptions not being truly applicable. Furthermore, confidence intervals and sample mean values [46] were calculated for the sound pressure measurements.

Alternatively, Tohyama *et al* [47] used the envelope of the signal for the determination of its decay rate. In general, the damping of enclosed fluid volumes can usually be represented either by the loss factor or the absorption coefficient [48]. The half-value bandwidth technique [48] is one of the most popular methods of obtaining the damping of a particular system. For instance, the damping of a plate can directly be obtained from the measurement of its frequency response (e.g. using a laser vibrometer [49]). Alternatively, the damping can also be obtained from the conventional estimate of the Reverberation Time [50].

Moreover, the test facility characteristics and environment conditions can significantly affect the measured variables. General guidelines for analysis of experimental data and measurement procedures can be found in ref. [51]. For instance, by measuring the Sound Reduction Index (SRI) of a plasterboard partition, Mulholland and Lyon [52] found that the SRI obtained could be very low at low frequencies. This phenomenon was justified by the strong fluid-structure coupling which was related to the dimensions of the rooms and partition.

Warnock [53] investigated the influence of the position of a specimen in different positions in the recessed aperture between two reverberant rooms. The test, made for a plasterboard partition, indicated that the SRI was increased when the partition was positioned on the receiver side of the aperture. This investigation concerning the effect of

some laboratory design and mounting conditions on SRI was also related to a previous work presented in ref. [54]. Nevertheless, at very low frequencies, the partition depth does not have any significant effect on sound transmission, as one might expect, as the acoustic wavelength is large compared to the recessed depth.

1.1.5 - Parametric studies of the variation in sound transmission and insulation

Although many researchers have considered the influence of the geometrical and other parameters on the sound transmission phenomenon between two coupled rooms at low frequencies, there is a limited number of published papers showing a parametric study of the variation of the sound insulation with subsystem properties [12, 22]. In a parametric study, numerical techniques for solving coupled equations of motion can be performed to a high degree of precision, which is subject to the limitations of the computer [55].

Osipov *et al* [12] evaluated some numerical examples in order to verify the influence of the dimensions of rooms and partitions on noise transmission. In their work, three distinct theoretical models (infinite plate theory and modal analysis for a baffled partition and for a room-plate-room system) were compared and validated with experimental results. The first set of results was obtained by varying the depth of the receiving room. The number of modes in the receiving room was then increased considerably. The second set was then obtained by varying the width of both rooms. Thus, the number of modes in the source and receiving rooms and partition were all altered significantly.

According to the results presented for SRI, variations of up to 15 dB occurred in one third octave bands. Alternatively, Noise Reduction was also predicted for different panel positions in the wall separating two adjacent rooms. In the next chapter, some numerical results for variability are presented and compared to those obtained in ref. [12].

In general, the sound transmission between two coupled rooms at low frequencies is primarily governed by the individual modes of the rooms [52]. Kihlman *et al* [56] studied the possibility of improving sound insulation at low frequencies (50-150 Hz) by optimizing the design of rooms and their common partition (geometrical properties and damping). The results, which were obtained by using Modal Analysis and the Finite Element Method, indicated that the matching of room modes on both sides of the partition had the most significant effect on the Sound Reduction Index. In this situation, the SRI levels are sharply decreased due to the good coupling and matching resonance frequencies of both source and receiving rooms as would be expected.

Kropp and Pietrzyk [57] developed statistical predictors for analyzing the influence of room dimensions on the airborne sound insulation between rooms. Considering two coupled rooms with different lengths, the first predictor was based on the ratio of the smaller length to the greater one. The second one, which was based on the modal approach, was developed under the assumption that each mode of the source room can only couple with its corresponding one in the receiving room. In other words, this model was strictly limited and is only valid for similar cross section source and receiving rooms and the results cannot be generalized.

Recently, Magalhaes and Ferguson [42] undertook an initial study on the effects of spatial fluid-structural coupling and non-resonant contributions on sound insulation between two rooms. Some of the preliminary analyses showed the influence of the room dimensions, weight of a flexible partition and its position in the common rigid wall, etc. The results of analyses were converted to one third octave band levels to make comparisons with other data possible.

Whilst variability investigations for acoustic-structural transmission were limited, there are some recent variability studies on structural coupling and the importance of both source and receiver subsystems. For example, Park *et al* [58] developed an empirical model for predicting the variability in the effective Coupling Loss Factors (CLF) for rectangular plates [8]. This empirical model has been considered and shown for comparison with the confidence interval levels found for a fluid-structure coupled system comprising two rooms connected by a single partition.

Finally, the problem of fluid-structure interaction for a particular system can be formulated in terms of energy and power balance and this is made in SEA [59, 60], e.g. considering normal surface displacement for the structural partition and velocity potential for the enclosed volumes of fluid, which represent the response of each sub-system involved. For instance, Craik and Smith [21] used spatial functions on this type of problem, although some limitations were identified at low frequencies where the model became less accurate. Hence typically SEA is used at higher frequencies where the confidence limits are reasonable.

The use of SEA for the analysis of airborne sound transmission at low frequencies is usually subject to some limitations, such as the small number of modes within a particular frequency band [61]. Although the choice of the transmission path to be

considered in the analysis is crucial [62], in practice it is not always possible to identify which transmission mechanisms are dominant and which can be ignored. For instance, several different models may be required depending on the details of construction and frequency range of interest [63]. It is known that the coupling between subsystems and losses of energy are described by the dissipation and coupling loss factors respectively. Nevertheless, in practice they are not known or only partly known. Thus, different experimental techniques for the determination of loss and coupling loss factors were proposed in refs [64, 65].

To summarize, although a vast amount of research concerning acoustic-structural coupling has already been published, little information is available on the sensitivity and variability of the response at low frequencies. For instance, the sensitivity of the transmission efficiency parameter (and consequently the SEA Coupling Loss Factor at higher frequencies) to the room dimensions, panel position, material properties, etc. has not been fully explored in an in-depth study. Similarly, there are assumptions within the modal formulations that should be investigated. For instance, a large amount of work has been performed in the analysis of sound transmission phenomena considering only the solution in terms of 'rigid-walled' acoustic modes for the acoustic volumes. Such an assumption is an approximation when a flexible partition is introduced.

In summary, this thesis is aimed at the implementation of mathematical models that incorporate additional features, which can also provide a more realistic representation of the physical problem concerning sound transmission through lightweight partitions at low frequencies.

1.2 – Problems highlighted and the CMS method

The review of noise control in buildings has highlighted that it is still a matter of concern since adverse conditions have contributed to less than satisfactory sound insulation between dwellings, e.g. the use of very low-frequency sources, such as those generated by hi-fi sets, has become a common practice. Consequently, building designs involving wall and ceiling constructions used in dwellings no longer provide sufficient attenuation at very low frequencies compared to the satisfactory noise reduction produced at higher frequencies. Likewise, there is a trend for designing smaller and more practical spaces that might not be reverberant, as typically assumed in noise prediction models available

to consulting/design engineers. Furthermore, lightweight structural elements are increasingly used because of their reduced cost and ease of use compared to some traditional materials such as masonry and concrete.

Hence there is a requirement to have models that incorporate smaller rooms or very dissimilar rooms in addition to lighter partitions in a more accurate way, especially at low frequencies and in cases where the assumptions normally made are no longer valid. Also to assist designers, it is useful to attempt to quantify what variability one might expect when comparing real rooms with existing formulations, such as the Mass Law.

The literature survey in the previous section has also revealed that the boundary condition at the interface between two coupled rooms, which is due to the velocity of the partition, has not yet been replicated in any of the existing formulations. Therefore, the use of a numerical method [13], namely Component Mode Synthesis Method (CMS), for fluid-structure interaction problems involving sound transmission between coupled rooms has been developed in this thesis in order to quantify the significance of the kinematic compatibility and show that this model is applicable to such problems and is not limited to structural configurations. This new approach of the method in this thesis has required an analytical formulation for the coupled fluid and structural components.

The CMS Method has previously been developed to solve large structural dynamics problems, which consist of several components or substructures [13]. It involves the selection of component modes and the solution for the overall system response in terms of a synthesis involving the modes. Typical component modes consist of normal modes with either free or fixed boundaries plus the constraint modes. The constraint modes are additional functions which provide 'extra' degrees of freedom (displacement, velocity, etc.) for the subsystem. The combination of the component modes is used to satisfy the differential equations of motions for the individual subsystems, and the interface conditions between the components.

For instance, Hou [66] presented a new approach for the method by concentrating on undamped free vibration systems, simplifying the formulation and the computation scheme. A simple error analysis technique was adopted to ensure the success of the method. At the component interfaces kinematic compatibility and force equilibrium conditions were also considered. Subsequently Benfield *et al* [67] showed that better accuracy is obtained using a fixed-interface coordinates method. The generalized

coordinates of the static constraint modes are substituted by the use of components whose displacements are defined relative to the interface.

Recently, Craig [68] published a tutorial paper in which a review of the basic procedures used on substructure analyses, or CMS method, was presented. In addition, the performance of some of the methods available in the literature was verified by comparing the CMS convergence properties.

Basically, the different approaches of the method presented differ in terms of the type of component modes selected. Considering an acoustic-structural coupling model, an additional acoustic 'static' mode, or constraint mode, is added to the set of normal modes to improve the accuracy of approximations and ensure correct convergence. It will be shown in this thesis that this constraint mode affects the sound pressure as a result of enforcing particle velocity compatibility between the two acoustic spaces for transmission between two rooms, for example. Furthermore, the components of complex systems can be analyzed separately using the CMS method [69-77].

The main limitation of the method, in the same way that existing Modal Methods are restricted, is due to the increasing number of assumed modes for complex problems or higher frequencies which have to be analyzed. A possible advantage may be the introduction of variability with the choice of the subsystem geometry, etc., and a relatively quick calculation of the response of the perturbed system.

1.3 – Main objectives

This thesis is focused on the development and validation of mathematical models that better represent the airborne sound transmission mechanism in view of the new requirements for design and modelling approaches. The work undertaken in this research was twofold in that variability investigations were required and there is a need to develop improved models that can better predict airborne sound transmission through lightweight partitions at low frequencies. Therefore, the aims of this thesis are to present variability investigations and the development and use of improved analytical tools, via a modal approach and the Component Mode Synthesis (CMS) method that can better predict the required sound transmission parameters.

The main objectives covered by the project can then be summarized as follow.

- Firstly, a modal model has been developed and implemented. It provides the numerical tool for an investigation into the sensitivity of some geometric factors, panel position, material properties, etc., on the noise transmission between two coupled volumes. The modal model is then validated using experimental tests. Comparison with other methods, published results and simulations is also made.

- Subsequently, a parametric study has been conducted into the sensitivity and variability of the coupled response using the modal model. For instance, this has been tackled by considering the influence of physical geometry and partition location, room absorption, internal loss factor, etc., on both NR and SRI.

- The next objective was to investigate the importance of kinematic compatibility (at the common interface between two-coupled rooms) for prediction of airborne sound transmission. The one-dimensional implementation of the CMS method provided the basic framework for a relatively simple system that has an exact analytical solution for validation. In particular, the CMS approach allows one to analyze and quantify the effects of imposing the condition of velocity continuity at an interface of an acoustic volume with a structure. Numerical results presented include spatial pressure and velocity distributions at different frequencies, spatial-averaged mean square pressures and velocities. In addition, the Sound Reduction Index (SRI) and Noise Reduction (NR) parameters have been calculated.

- The CMS method was also extended for the three-dimensional problem and implemented numerically. A comparison between the CMS and the Modal model was made for the three-dimensional case. Some numerical examples were used to compare both models and identify their benefits and shortcomings. As far as the author is aware, based on a literature review of published papers, this is an original approach and use of the CMS method for fluid-structure interaction.

- Finally, using the transmission coefficients obtained from the predictions, an important SEA (Statistical Energy Analysis) parameter, namely Coupling Loss Factor (CLF) was evaluated. This could better incorporate the geometric features and both resonant and non-resonant contributions in airborne transmission. Further limited investigation has been included which has considered predicted variability versus parameters such as the modal density and modal overlap. The

consequences of the findings for SEA, using the two approaches, have been noted for future work.

1.4 – The contribution of thesis to knowledge

The main contributions of this thesis are therefore

- Implementation of a modal model. Subsequently, results for geometric and partition design changes are presented. Comments are provided on the variability.
- Better models for the representation of the airborne sound transmission mechanism through partitions at low frequencies have been developed. This will consequently provide additional information in terms of sound insulation for designing lightweight common walls. The main originality in the modelling is the use of CMS for the fluid-structure interaction.
- Low frequency experimental investigation of sound transmission through a lightweight partition is presented in order to validate the modal and CMS models implemented.

1.5 – Thesis layout

The remaining chapters of this thesis are arranged as follows.

Chapter 2 emphasizes the derivation and implementation of a mathematical modal model to predict the sound transmission efficiency and noise reduction of a system comprising two arbitrary rooms coupled by a single-leaf partition. The fluid-structure interaction analysis is shown to be dependent on the spatial coupling between the acoustic and structural modes. The main assumptions and limitations of the model are also discussed. Simulations show the effect of geometrical coupling coefficients on the Noise Reduction (NR). Finally, a comparison between the Modal model and other published approaches and results, such as the Mass Law Theory and Leppington's prediction [16], is made for Noise Reduction and Sound Reduction Index values.

Chapter 3 presents the experimental validation for the modal model derived in chapter 2. First, the measurement of damping for the structural partition and absorption for the rooms is made. Second, some preliminary experimental tests are made in a single room to verify the accuracy and applicability of measuring and predicting sound pressure

levels in a small volume. Next, the coupled two-room modal model is experimentally validated using the ISVR teaching laboratory. Finally, the partition normal velocity is experimentally determined (by using a Scanning Laser Doppler Vibrometer) and the results are compared to theoretical predictions.

In Chapter 4 a variability investigation and the corresponding results are presented. The results obtained take into account the influence of panel positions on NR; the simulations are then compared to classical formulations. Next, a parametric study assessing the influence of room dimensions on NR is performed. Furthermore, the influence of the room absorption on NR is quantified by assuming uniform absorption distribution inside the rooms. Finally, the Coupling Loss Factor (CLF) is evaluated using power balance and assuming that a two subsystem SEA model represents the problem. Its variability versus the room modal density and modal overlap is presented, in order to consider and comment upon the consequences for subsequent SEA models.

In Chapter 5 the effects of the imposition of velocity continuity on the acoustic-structural interface are considered using an original development of the Component Mode Synthesis Method (CMS) for this problem. The formulation and equations of the structural-acoustic problem in terms of 'components' is described. The model is then validated by comparison of numerical results including the CMS model and a one dimensional wave approach. Moreover, the CMS model is also compared with the modal model. Finally, conclusions are drawn based on the analysis of the results and the extension to three-dimensional acoustic systems discussed.

In Chapter 6 the CMS method is further extended and developed for predicting sound transmission through a partition in the three-dimensional case. The effect of velocity continuity on the spatial pressure and velocity distributions is discussed and presented for three-dimensional models with an elastic partition. Some results show a comparison between the 3D CMS and the modal model. Comparison with experimental results from chapter 3 is given and discussed.

Finally, a concise account of the main findings, and the inferences drawn from the results of each individual chapter are reported in Chapter 7. Next the main conclusions for the complete project are summarized. For completeness, discussion and recommendations for future work are presented.

Chapter 2

STRUCTURAL-ACOUSTIC COUPLING ANALYSIS - A MODAL MODEL

2.1 – Introduction

The aims of this chapter are to provide further background description and present and implement a modal approach, the latter assisting in providing improved understanding of the noise transmission phenomenon in buildings. For instance, better visualization of the spatial distribution of acoustic pressure and particle velocity for a two coupled room model is presented using the concept of modal expansion. The theoretical background for understanding the sound transmission mechanism is presented in section 2.2. A preliminary formulation is presented in terms of a set of coupled modal equations for predicting sound transmission through a cavity-backed finite plate. Finally, a complete acoustic-structural coupled modal model (room-plate-room) is developed and implemented in section 2.3. This model, also represented by a set of integro-differential modal equations, is therefore a straightforward extension of the previous formulation.

A complete modal model for predicting sound transmission between two coupled rooms is presented here whilst retaining the conventional assumption of rigid-walled acoustic modes. With a point noise source placed in either of the rooms, the aim is to predict the Noise Reduction (NR) and the Sound Reduction Index (SRI) of the system due to resonant coupling involving modal behaviour, spatial fluid-structural coupling and non-resonant contributions.

The derivation and numerical examples presented in this chapter show how transmission efficiency is affected by room geometry. The transmission of sound between similar or dissimilar rooms, e.g. for the latter consider rooms attached to corridors, can equally be predicted using the Modal approach. In addition, the simulation is evaluated for two different panel sizes. Firstly, a whole flexible panel is considered over the common wall. Secondly, a small flexible panel is considered, so that all other parts of the common wall are rigid. The narrowband results of analyses were converted to one-third octave band spectra, to make comparisons with other data possible. Finally, a general discussion,

based on the findings of the results obtained, is presented with some observations concerning potential improvements that can be considered.

Two different analytical models are used throughout this chapter for comparison with the developed and implemented modal model. The first one is the Mass Law theory [4] and the second model is Leppington's prediction [16]. These are described in some detail in the next section.

In summary, the main goal of this chapter is to offer insight into the physics and the important parameters in sound transmission between acoustic spaces separated by a flexible partition. This has applications in the field of architectural acoustics.

2.2 – Theoretical background of the sound transmission mechanism

The mechanism of sound transmission may be considered in terms of the radiated sound field from an elastic partition, itself excited by a sound field in a source room. The partition, modelled by a thin plate, has a response to acoustic excitation, which consists of both free and forced bending waves. Freely travelling bending waves are generated when the plate is excited at its natural frequencies. As a result of the plate edges, these waves interact with each other producing the plate mode of vibration. On the other hand, forced waves occur due to pressure fluctuations which force the plate to move in such a way that free-bending waves are not significantly generated. The spatial distribution of the forcing produces a response that is similar in its spatial response.

In terms of radiation efficiency, which is a non-dimensional measure of the sound power radiated by a vibrating surface into an adjacent fluid [78], the generation of free bending waves is more important at frequencies above the critical frequency of the panel, where the natural modes of the partition consist of wave motion with phase velocity greater than the speed of sound travelling in air. In this condition, sound power is radiated efficiently [5]. Below the critical frequency, the free waves are produced but are not significant for sound transmission.

Forced waves at the acoustic wave number are predominant when a panel vibrates at frequencies lower than its critical frequency. They are common when a panel is excited acoustically [15]. In addition, when a sound wave is incident upon a partition, the response, which is frequency dependent, is also dependent on the radiation impedance of

the modes of the partition. Thus, the air or fluid on the receiver side of the plate is excited, and sound waves propagate away from the plate into the receiving volume.

Below the first panel resonance, there is an increase in SRI with decreasing frequency. In this frequency range, the panel moves with the pressure fluctuation to transmit sound and has a very small frequency response. The vibration can be reduced by stiffening the panel hence causing an increase in the SRI.

2.2.1 – Sound transmission through an infinite partition

In general, the sound transmission theory for uniform and unbounded panels has widely been used to approximate the sound transmission loss of a bounded panel in a baffle. Of course, some assumptions, such as the random-incidence field over the partition, as well as a limited frequency range (in which the acoustical wavelength is smaller than the plate size), have been considered. For instance, the normal incidence Mass Law theory is basically derived from an idealized model of normal incidence transmission through an unbounded partition [2]. On the other hand, the diffuse field transmission coefficient can be obtained by considering the whole range of incident angles with equal likelihood. In room acoustics there is an important parameter, namely the 'Schroeder' frequency [59], at which the frequency or modal overlap of the room modes is large enough for the sound field to be considered diffuse. The 'Schroeder' frequency or 'large room' frequency f_s is given by [59]

$$f_s = 2000\left(\frac{T_{60}}{V}\right)^{1/2} \tag{2.1}$$

where T_{60} is the reverberation time and V is the room volume.

Two measures of the effectiveness of a partition in reducing sound transmission are the transmission efficiency and the Sound Reduction Index. A transmission efficiency parameter τ is defined as the ratio of transmitted to incident acoustic power and is given by [18]

$$\tau = \frac{w_{trans}}{w_{inc}} \tag{2.2}$$

where w_{trans} is the transmitted sound power and w_{inc} is the sound power incident on the source side of the partition.

A classical index, known as Transmission Loss (TL), in some countries, or Sound Reduction Index (SRI) is defined as [5,78]

$$\mathrm{SRI}(\theta) = 10\log_{10}(1/\tau(\theta)) \ \text{(dB)} \qquad (2.3(a))$$

where $\tau(\theta)$ is the transmission efficiency for a given angle of incidence θ measured from the normal to the plate. This is so defined such that a positive value of the Sound Reduction Index corresponds to a reduction of the transmitted power compared to the incident.

For a plane wave incident on an infinite panel for frequencies below the critical frequency this can be derived as [5]

$$\tau(\theta) = \frac{1}{\left(1+\left(\frac{\omega m\cos\theta}{2\rho_0 c_0}\right)^2\right)} \qquad (2.3(b))$$

where ω is the angular frequency (in radians/s), m is the panel mass per unit area(kg/m^2), ρ_o is the air density and c_o is the sound speed in air. The derivation of equation (2.3 (b)) was based on the assumption that the influence of the partition stiffness on sound transmission is negligible compared with its mass.

The mass law SRI expressions for normal ($\mathrm{SRI_n}$), field ($\mathrm{SRI_f}$) and diffuse ($\mathrm{SRI_d}$) incidence are given by [18]

$\mathrm{SRI_n} \approx 20\log_{10}(mf) - 42$ (dB) for the 'normal incidence Mass Law' (2.4)

$\mathrm{SRI_f} \approx 20\log_{10}(mf) - 47$ (dB) for the 'field incidence Mass Law' (2.5)

$\mathrm{SRI_d} = \mathrm{SRI_n} - 10\log_{10}(0.23\ \mathrm{SRI_n})$ (dB) for the diffuse incidence 'Mass Law' (2.6)

where f is frequency (Hz). They are valid if $\omega m\cos\theta >> 2\rho_o c_o$.

Equation (2.4) is the result of considering an angle of incidence θ (measured from the normal to the plate) equal to zero. Similarly, Equations (2.5) and (2.6) can be obtained by considering θ varying from 0° to 78° and from 0° to 90° respectively. In equation (2.4), the characteristic impedance of the air is assumed the same on both sides of the plate. Moreover, it is assumed that the partition loss factor is null. The $\mathrm{SRI_n}$ increases by

approximately 6 dB for each doubling of the frequency or the plate mass per unit area. Furthermore, equation (2.6) is only accurate if SRI_n is greater than 15 dB and the incident field is highly diffuse [82].

2.2.2 – Sound transmission through a finite partition in a baffle

A finite-size and baffled rectangular plate is a more realistic model than the infinite one described previously. The transmission is characterized by boundary effects, which lead to the formation of standing-wave modes and resonance. Leppington [16] proposed a different formula for the transmission efficiency τ_{Lep} averaged over all incidence angles and over a frequency band. For frequencies below the critical frequency ω_c of a simply-supported rectangular panel, it is given by

$$\tau_{Lep} = \tau_{res} + \tau_{nr} \text{ ; considering } \omega << \omega_c \tag{2.7}$$

where $\omega_c = c_o^2 (m/D)^{1/2}$, m is the partition mass per unit area and D its bending stiffness per unit width.

The resonant τ_{res} and non-resonant contributions τ_{nr} are expressed by [16] as

$$\tau_{res} = (2/k^2\eta)\varepsilon_1^2(\mu_o^2-1)^{-3}\left\{1/a^2+1/b^2\right\}\left\{\mu_o^2(5\mu_o^2-4)\sin^{-1}(1/\mu_o)+(\mu_o^2-1)^{1/2}(3\mu_o^2-2)\right\} \tag{2.8}$$

$$\tau_{nr} = 4\varepsilon_1^2(1-\mu_o^{-4})^{-2}\left\{\ln(ka^{1/2}b^{1/2})+0.160-U(b/a)+\frac{1}{4}\mu_o^{-6}\left[(2\mu_o^2-1)\right.\right.$$

$$\left.\left.(\mu_o^2+1)^2\ln(\mu_o^2-1)+(2\mu_o^2+1)(\mu_o^2-1)^2\ln(\mu_o^2+1)-4\mu_o^2-8\mu_o^6\ln(\mu_o)\right]\right\} \tag{2.9}$$

where

$$U(x)=\frac{1}{2\pi}\left(x+\frac{1}{x}\right)\ln(1+x^2)-\left(\frac{1}{2}+\frac{x}{\pi}\right)\ln(x)-\frac{\ln(2)}{\pi}-\frac{2}{\pi}\int_x^1\frac{\arctan(t)}{t}dt,$$

ε_1 is the fluid loading parameter which is defined as $\varepsilon_1 = \rho_o/(mk)$, μ_o is given by $\mu_o = k_b/k$ and η is the mechanical damping factor (or internal loss factor) for the panel; ρ_o is the density of air, k is the acoustic wavenumber, k_b is the wavenumber of free bending waves in the partition; a, b are the plate dimensions.

The resonant contribution τ_{res} is due to the modes excited at or near resonance, which produce a large partition deflection but are inefficient in terms of sound power radiation. The non-resonant contribution τ_{nr} corresponds to that from the small amplitude off-resonant modes. However, for these non-resonant modes sound energy is radiated efficiently and their wavenumbers are smaller than the acoustic wavenumber. According to Leppington [16], there is good agreement between the transmission values obtained via solely the non-resonant contribution τ_{nr} and experimental tests with no need for an *ad hoc* correction. As mentioned previously, it is assumed that the plate is simply-supported. It is also assumed that the transmission efficiencies, which are defined in equations (2.8) and (2.9), represent an average over a large number of modes and over all incidence angles.

For instance, Figure 2.1 shows the SRI values for a finite panel (2m x 2m) with average surface mass per unit area equal to 78.5 kg/m^2 calculated using the above formulae. It is seen that the SRI for Leppington's resonant contribution is higher than the other values, as expected. The frequency range shown is below the critical frequency, which for this model equals 1.2 kHz and hence the non-resonant contribution is the appropriate term.

2.3 – Coupling between a room and a finite plate

Consider the case of a rectangular partition (panel) modelled as a flexible plate on one face ($x = x_0$) of a rectangular acoustic volume, which has rigid walls on all of its other surfaces. The equation of motion for a flexible thin plate vibrating at frequency ω can be given in rectangular Cartesian coordinates (z,y) by

$$D\nabla^4[w(z,y,\omega)]-\omega^2 m(r_s)\,w(z,y,\omega)=0 \qquad (2.10)$$

where D is the bending stiffness, ∇^4 is the square of the Laplace operator, and $m(r_s)$ is the mass per unit area of the partition and $w(z,y,\omega)$ is the normal displacement of the plate surface into the fluid. In equation (2.10) and the following equations the term in time $e^{j\omega t}$ has been suppressed.

The plate is assumed to be simply-supported mounted in the (y,z) plane of the Cartesian coordinate system. The basis function, used in the expansion for the panel deflection,

must ensure a vanishing normal displacement on the contour of the panel. It satisfies the simply supported boundary conditions and is given by

$$\phi_p(z,y) = \sin(k_{pz} z)\sin(k_{py} y) \tag{2.11}$$

where $k_{pz} = \left(\frac{r\pi}{L_{pz}}\right)$ and $k_{py} = \left(\frac{s\pi}{L_{py}}\right)$.

L_{pz} is the length of the panel, L_{py} is the width of the panel, and *r, s* represent the panel mode numbers and $k_{pz}^2 + k_{py}^2 = k_b^2$ corresponds to the *in vacuo* plate eigenvalues or corresponding natural frequencies given by $\omega = \sqrt{\frac{D}{m}}\, k_b^2$.

Furthermore, the infinite set of *in vacuo* modes, defined by equation (2.11), represents a set of orthogonal functions, which satisfy the following orthogonality relationships

$$\int_S \phi^T{}_q\, m(r_s)\, \phi_p\, dS = \begin{cases} 0 \; if \; p \neq q; \\ \Lambda_p \; if \; p = q. \end{cases}$$
$$\int_S D\nabla^2 \phi_q \nabla^2 \phi_p\, dS = \begin{cases} 0 \; if \; p \neq q; \\ \omega_p^2 \Lambda_p \; if \; p = q. \end{cases} \tag{2.12}$$

where $\Lambda_p = \int_S m(r_s)\, \phi_p^2\, dS$ is the modal generalized mass, ω_p is the *in vacuo* natural frequencies of the partition, D is the bending stiffness of the partition, r_s is the position vector of a point in the y-z plane, ∇^2 is the two-dimensional Laplace operator and *p, q* are the mode identifiers [5].

To determine the far-field radiated sound intensity, the sound field generated by a harmonic vibrating surface has to be evaluated. The sound field generated by a baffled harmonic vibrating surface **S** at position **r** in the fluid is given by a particular form of Kirchhoff-Helmholtz integral equation, which is termed the Rayleigh Integral [2]. The key function of this problem is to obtain the pressure difference across the panel or plate involved in the sound transmission.

The total surface pressure internal to the enclosed volume is hence the summation of the *blocked pressure* and the radiated pressure. This *blocked pressure* is defined as the summation of the incident field and the reflected field produced as if the plate were rigid

(infinite mechanical impedance). The radiated pressure is the field produced as a result of the elasticity of the plate, and subsequent motion producing sound radiation [2]. The equation of motion of an elastic partition in the absence of sound radiation, from equation (2.10), can be written

$$D\nabla^4[w(z,y,\omega)]-\omega^2 m(r_s)\,w(z,y,\omega)= p_{bL}(z,y,\omega) \tag{2.13}$$

where p_{bL} is the blocked pressure due to the incident and reflected sound fields.

The partition response w can be expressed by series expansion in the free vibration mode shapes as

$$w(z,y,\omega)=\sum_{p=1}^{P} w_p \phi_p \tag{2.14}$$

where P is the total number of structural modes considered. Equation (2.14) is an expression for the partition displacement in terms of a summation of its assumed-modes.

In addition, the total blocked pressure on the partition is given by

$$p_{bL}=2p_i(y,z,\omega) \tag{2.15}$$

where p_i $(y,\ z,\ \omega)$ is the incident field amplitude of pressure.

In equation (2.13) the time term $e^{j\omega t}$ has been suppressed.

Let $p(x,y,z,t)$ be regarded as small amplitude perturbation (acoustic pressure variation) from its equilibrium value. The wave equation, which results from the linear acoustic equations, is given by [2]

$$\begin{aligned}
&\nabla^2 p-\frac{1}{c_o^2}\frac{\partial^2 p}{\partial t^2}=0\\
&\frac{\partial p}{\partial n}=0 \text{ on the rigid walls of the room}\\
&\frac{\partial p}{\partial n}=-\rho_o\frac{\partial^2 w}{\partial t^2} \text{ on the flexible partition}
\end{aligned} \tag{2.16}$$

where w = the displacement of the flexible partition in the normal direction directed outwards from the fluid volume, c_o is the sound speed in the air and ρ_o is the air density.

The steady state solution is obtained through the Fourier Transform of the time domain wave equation, yielding the Helmholtz Equation [5]

$$\nabla^2 \bar{p} + k^2 \bar{p} = 0 \tag{2.17}$$

where $\bar{p}$ is the steady-state sound pressure amplitude and k is the acoustic wavenumber.

If $\bar{p}$ is expressed as an expansion of eigenmodes for the room, corresponding to the natural frequencies of a rigid boundary space, a solution to the Helmholtz Equation may be written as

$$\bar{p} = \sum_n B_n \Omega_n \tag{2.18}$$

where Ω_n is the acoustic mode shape n of a rigid-walled room and B_n the corresponding complex pressure amplitude.

The substitution of equation (2.18) into equation (2.17) yields

$$\nabla^2 \Omega_n + k_n^2 \Omega_n = 0 \tag{2.19}$$

Likewise, a Green's function G can be obtained satisfying the same conditions for a point source located in the fluid

$$\begin{aligned} &\frac{\partial G(r \mid r_o)}{\partial n} = 0 \qquad r \in S_r \\ &\nabla^2 G(r \mid r_o) + k^2 G(r \mid r_o) = -\delta(r - r_o) \\ &G(r \mid r_o) = \sum_n A_n \Omega_n(r) \end{aligned} \tag{2.20}$$

where S_r is the surface area of the rigid walls, $\delta(r - r_o)$ is the three-dimensional Dirac delta function representation of a unit volume velocity source, $G(r \mid r_o)$ is the solution (Green's function) of equation (2.20) and Ω_n = acoustic pressure mode shape of the room. A_n is simply an amplitude term in the series expansion of $G(r \mid r_o)$.

The spatial form for the three-dimensional eigenfunctions Ω_n, corresponding to the natural frequency ω_n of the rigid-walled rectangular space of dimensions L_x, L_y and L_z may be written as

$$\Omega_n = \cos\left(\frac{n_x \pi . x}{L_x}\right)\cos\left(\frac{n_y \pi . y}{L_y}\right)\cos\left(\frac{n_z \pi . z}{L_z}\right) \tag{2.21}$$

This set of orthogonal modes satisfies the following relationship

$$\begin{aligned} &\int_V \Omega_m \Omega_n \, dV = \begin{cases} 0 \; if \; m \neq n; \\ \Lambda_n \; if \; m = n. \end{cases} \\ &\Lambda_n = \int_V \Omega_n^2(x,y,z) \, dV \end{aligned} \tag{2.22}$$

Since Ω_n is an eigenfunction of the room, it has a corresponding eigenvalue k_n which must satisfy

$$\begin{cases} k_n^2 = \left(\frac{n_x \pi}{L_x}\right)^2 + \left(\frac{n_y \pi}{L_y}\right)^2 + \left(\frac{n_z \pi}{L_z}\right)^2 \\ \nabla^2 \Omega_n + k_n^2 \Omega_n = 0 \end{cases} \text{ and hence } \omega_n = k_n c_o \tag{2.23}$$

Therefore, using the previous relationships, equation (2.20) can be written as

$$\sum_n A_n(-k_n^2 + k)\Omega_n = -\delta(r - r_o) \tag{2.24}$$

Multiplying each side of equation (2.24) by $\Omega_m(x,y,z)$ and integrating over the volume of the room one has, by orthogonality, the expression

$$A_n = \frac{\Omega_n(x_0, y_0, z_0)}{\Lambda_n(k_n^2 - k^2)} \tag{2.25}$$

Often the sound pressure response in a room for known sound sources is of interest. Thus, adding a right-hand side term, which corresponds to the rate of change of mass flux per unit volume, to equation (2.16), the wave equation in terms of sound pressure then becomes [5]

$$\nabla^2 p + \frac{\omega^2}{c_o^2} p = -\rho_o j\omega(q_b + q_s) \tag{2.26}$$

and

$$q_b = -2(j\omega w)\delta(x - x_o) \tag{2.27}$$

where $\delta(x-x_o)$ represents a one-dimensional Dirac delta function, q_b is the vibration of the panel surface in terms of a distribution of source volume velocity per unit volume and q_s represents the distribution of 'external' sources, e.g. one or more monopole sources inside the room.

The sound pressure $p(x,y,z)$, which can be expressed as a summation of the orthogonal modes Ω_n, is given by

$$p(x,y,z)=\sum_{n=1}^{N} p_n\,\Omega_n(x,y,z) \tag{2.28}$$

where p_n is the complex pressure amplitude of mode n at frequency ω.

Alternatively, the incident field amplitude of pressure $p_i(y,z,\omega)$, (cited in equation (2.15)), can then be defined in terms of the acoustic pressure modes as

$$p_i(y,z,\omega)=\frac{1}{2}\left(\sum_{n=1}^{N} p_n\,\Omega_n(y,z)\right)e^{-jk_{x,n}x_o} \tag{2.29}$$

where x_o is the coordinate of the partition position in the 'x' direction of the acoustic field and $k_{x,n}=\sqrt{k_n^2-(n_y\pi/L_y)^2-(n_z\pi/L_z)^2}$. As in equation (2.15), the time dependency $e^{j\omega t}$ has been omitted in equation (2.29) for clarity assuming everything is at the same harmonic frequency.

By substituting equation (2.19) and (2.28) into equation (2.26), one obtains

$$\sum_{n=1}^{N}-k_n^2\,p_n\,\Omega_n(x,y,z)-\frac{1}{c_o^2}\sum_{n=1}^{N}\left(-\omega^2 p_n\,\Omega_n(x,y,z)\right)=2\rho_o\left(-\omega^2 w\right)\delta(x-x_o)-\rho_o\left(j\omega\,q_s\right) \tag{2.30}$$

Multiplying by Ω_m and integrating over the fluid volume, applying the orthogonality condition (see equation (2.22)), a set of coupled differential equations for the modal pressure is then obtained and given by

$$-\omega^2 p_n+\omega_n^2 p_n=\left(\frac{-\rho_o c_o^2}{\Lambda_n}\right)\int_S\left(-\omega^2 w\Omega_m(x,y,z)\right)dS+\left(\frac{j\omega\rho_o c_o^2}{\Lambda_n}\right)Q_n \tag{2.31}$$

where n = 1,2, .N. The 'loading' applied to the acoustic volume is represented by the generalized volume velocity source strength in the fluid as

$$Q_n = \int_V q_s(x_o, y_o, z_o)\Omega_n(x, y, z)\delta_1(x-x_o)\delta_1(y-y_o)\delta_1(z-z_o)\,dV \tag{2.32}$$

and $Q_n = q_s\Omega_n(x_o, y_o, z_o)$ for a point source.

where δ_1 is the one-dimensional Dirac delta function (with dimension m^{-1}), the coordinate (x_o, y_o, z_o) is the source position for a point source in the volume, the subscript n refer to the acoustic volume mode number, p_n is the complex modal pressure amplitude, c_o is sound speed in air and S is the surface area of the partition and Λ_n is defined in equations (2.22). Equation (2.32) can be easily extended in the case of a distributed source in the volume.

Substituting equation (2.14) into equation (2.31), one obtains

$$-\omega^2 p_n + \omega_n^2 p_n = \left(\frac{-\rho_o c_o^2 S}{\Lambda_n}\right)\sum_{p=1}^{P}\left(-\omega^2 w_p C_{np}\right) + j\omega\left(\frac{\rho_o c_o^2}{\Lambda_n}\right)Q_n \tag{2.33}$$

where the spatial structural-acoustic coupling coefficient C_{np} is defined by

$$C_{np} = \frac{1}{S}\int_S \Omega_n\,\phi_p\,dS \tag{2.34}$$

In summary, on the right-hand side of equation (2.33) the first and second terms correspond to the sources due to the motion of the flexible panel and to discrete monopole sources in the fluid respectively.

Substituting equations (2.14) and (2.15) into equation (2.13), multiplying by ϕ_p and integrating over the partition surface at $x = x_p$ yields

$$D\nabla^4\int_S\left(\sum_{q=1}^{P} w_q\phi_q\phi_p\right)dS - \omega^2 m\int_S\left(\sum_{q=1}^{P} w_q\phi_q\phi_p\right)dS = \int_S p(x_p, z, y, \omega)\phi_p\,dS \tag{2.35}$$

Substituting equation (2.29) into equation (2.35) and using the orthogonality relationships (2.12), one obtains

$$-\omega^2 w_p + \omega_p^2 w_p = \frac{S}{\Lambda_p}\sum_{n=1}^{N} p_n C_{np} \tag{2.36}$$

where the subscripts n and p refer to the acoustic volume and panel mode numbers respectively, N indicate the total number of acoustic modes adopted in the analysis, p_n is the modal pressure amplitude, Λ_p is the modal generalized mass defined in equation (2.12) and C_{np} is geometric coupling coefficient defined in equation (2.34). Equations (2.33) and (2.36) are coupled modal equations.

A review of velocity potential concepts may also be important if one uses an alternative formulation in terms of velocity potential. The main advantage of using this formulation in terms of velocity potential is that the equations become symmetric. For an inviscid-flow (viscous effects are neglected), low-speed flows are irrotational [20,79]. This means that if $\nabla V \equiv 0$ then $V = \nabla\Phi$, i.e. the velocity components can all be expressed in terms of a scalar function Φ. Therefore,

$$u_x = \frac{\partial\Phi}{\partial x},\ u_y = \frac{\partial\Phi}{\partial y},\ \text{and}\ u_z = \frac{\partial\Phi}{\partial z}, \tag{2.37}$$

where V is fluid velocity, u_x, u_y, u_z are the fluid velocity components and Φ is the scalar function termed velocity potential.

Therefore, the velocity potential function allows one to obtain all other acoustic parameters through the relationship for the pressure

$$p = -\rho_o j\omega\,\Phi \tag{2.38}$$

Equations (2.33) and (2.36) can therefore be rewritten in terms of the modal acoustic velocity potential amplitude Φ_n and with additional viscous damping terms as [5]

$$-\omega^2\Phi_n + j\omega\beta_{n_1}\Phi_{n_1} + \omega_n^2\Phi_n = \left(\frac{c_o^2 S}{\Lambda_n}\right)\sum_{p=1}^{P}\left(j\omega w_p C_{np}\right) - \left(\frac{c_o^2}{\Lambda_n}\right)Q_n \tag{2.39}$$

$$-\omega^2 w_p + j\omega\beta_p w_p + \omega_p^2 w_p = \frac{-\rho_o S}{\Lambda_p}\sum_{n=1}^{N}\left(j\omega\Phi_n C_{np}\right) \tag{2.40}$$

where β_{n_1} and β_p are the generalized modal damping coefficients for the room (subsystem 1) and partition (subsystem 2) respectively; ω is the excitation frequency in radian/s.

Thus, on the left-hand side of equation (2.39) an additional term $j\omega\beta_{n_1}\Phi_{n_1}$, in terms of the velocity potential, is inserted in order to include viscous damping in subsystem 1. Likewise, the term $j\omega\beta_p w_p$ is added on the left-hand side of equation (2.40) in order to represent the damping of the structural partition. Thus, the problem considering fluid loading can be solved. Alternatively, the response of fluid in a single room with rigid-walls to harmonic excitation by a point monopole source can be obtained using equation (2.39) with the first term on the right-hand side, which contains the variable w_p, set to zero. Other types of damping models and terms can be used instead of viscous damping, which is given in the preceding equations.

2.4 – Derivation of a modal-interaction model for a system comprising two rooms coupled by a common partition

In the present analysis, the room-panel-room system is selected as the fundamental model, which may represent a typical real situation in a building. The physical mechanisms involved in the control of sound transmission in buildings can hence be evaluated.

The analytical modal model developed and implemented here is an extension of the set of integro-differential equations presented in section 2.3 to a system comprising two coupled rooms and a simply supported partition. Thus, the problem involving sound transmission between two connected rooms can be tackled.

As mentioned before, the acoustic and the structural response fields are expressed in terms of their uncoupled normal modes by means of differential equations for each mode. Therefore, the structural motion has been expressed as a summation over the response of the *in vacuo* natural modes driven by fluid loading. The acoustic field of the rigid-walled rectangular rooms has been determined by the summation of the acoustic modes over the fluid volume. In fact, these acoustic modes in the source room were excited by a generalized volume velocity source. According to Fahy [5], the correct convergence of the modal pressure on the partition surface is obtained due to the Gibb's phenomenon, which is an overshoot that occurs whenever basis functions (for instance acoustic mode shapes) are used to represent spatial distributions [78] containing discontinuity of slope.

Interaction analysis is considered and described when a system comprising two fluid volumes connected by a thin plate is excited by a point monopole source placed in one of the volumes. Therefore, the results presented were not averaged for different source positions. Solid surfaces, which bound volumes of air V_1 and V_2 are considered.

Equations (2.39) and (2.40) were extended in order to represent the two volume case. Therefore, on the right-hand side of equation (2.40) another coupling term is added in order to represent the influence of room 2. Moreover, an *extra* set of equations of motion representing room 2 is added to the system of equations (2.39) and (2.40).

Therefore, the response of a coupled system (comprising two rooms connected by a common partition) to a forcing harmonic function may be represented in terms of the uncoupled modes of both rooms and the uncoupled panel modes as

$$-\omega^2\Phi_{n_1} + j\omega\beta_{n_1}\Phi_{n_1} + \omega_{n_1}^2\Phi_{n_1} = \left(\frac{c_o^2 S}{\Lambda_{n_1}}\right)\sum_{p=1}^{P}\left(j\omega w_p C_{n_1 p}\right) - \left(\frac{c_o^2}{\Lambda_{n_1}}\right)Q_{n_1} \tag{2.41}$$

$$-\omega^2 w_p + j\omega\beta_p w_p + \omega_p^2 w_p = -\left(\frac{\rho_o S}{\Lambda_p}\right)\sum_{n_1=1}^{N_1}\left(j\omega\Phi_{n_1} C_{n_1 p}\right) + \left(\frac{\rho_o S}{\Lambda_p}\right)\sum_{n_2=1}^{N_2}\left(j\omega\Phi_{n_2} C_{n_2 p}\right) \tag{2.42}$$

$$-\omega^2\Phi_{n_2} + j\omega\beta_{n_2}\Phi_{n_2} + \omega_{n_2}^2\Phi_{n_2} = -\left(\frac{c_o^2 S}{\Lambda_{n_2}}\right)\sum_{p=1}^{P}\left(j\omega w_p C_{n_2 p}\right) \tag{2.43}$$

where the indices n_1, n_2, and p refer to source room, receiver room and panel mode numbers respectively and β is the generalized modal damping coefficient introduced for the acoustic volumes and structural modes. The other variables were already defined in the previous section and/or list of symbols.

In general, it is necessary to consider dissipation in the system. For the structural system, it is common to introduce a complex Young's modulus of elasticity, using a loss factor from measured or assumed values. For fluid volumes, an average absorption coefficient is usually considered in terms of the corresponding modal loss factor. Thus, in equations (2.41), (2.42) and (2.43), the effect of the absorbing material is approximated by the equivalent damping factors β_n.

Neglecting the cross-modal coupling terms introduced by the absorption on the boundary of the volume, and assuming that a single room mode is dominant, the approximation for

the generalized modal damping for the source room β_{n_1}, receiving room β_{n_2} and partition β_p may then be given by [5]

$$\beta_{n_1} = \omega_{n_1}\eta_{n_1} \tag{2.44}$$

$$\beta_{n_2} = \omega_{n_2}\eta_{n_2} \tag{2.45}$$

$$\beta_p = \omega_p\eta_p \tag{2.46}$$

where η_{n_1} and η_{n_2} are the corresponding modal loss factors for the source and receiving rooms. η_p is the modal loss factor for the panel.

The total loss factor η can be expressed in terms of the reverberation time T_{60} by [8]

$$\eta = \frac{\ln(10^6)}{2\pi f T_{60}} \tag{2.47}$$

where f is frequency in Hz and T_{60} is the reverberation time, which is the time taken for the system energy to decay by 60 dB.

The numerical evaluation of the eigenvalues and eigenfunctions for the coupled system was obtained using a dynamic matrix formulation for the problem (see Appendix A). Numerical analysis was applied to the free vibration problem of the coupled room-panel-room system in order to determine the eigenvalues and eigenvectors for the coupled system. Subsequently, for the forced vibration problem a solution in terms of the uncoupled modal contributions was then performed. The results, namely the acoustic pressure and panel displacement, can be used to evaluate two measures of the noise insulation that could be provided. Those quantities are the Sound Reduction Index and Noise Reduction respectively.

The Sound Reduction Index (SRI) can be expressed in terms of the ratio of the incident to the transmitted intensity [78], i.e.

$$SRI = 10\log_{10}\left(\frac{\langle I_i \rangle}{\langle I_t \rangle}\right) \tag{2.48}$$

where $\langle I_i \rangle$ and $\langle I_t \rangle$ are the time-averaged incident and transmitted sound intensity respectively.

Considering the assumption of diffuse field condition, the SRI can be expressed in terms of the Noise Reduction (NR) by [86]

$$SRI = NR + 10\log_{10}\left(\frac{c_o S_p}{8\pi f \eta V_2}\right) \tag{2.49}$$

where S_p is the partition surface area in m^2, V_2 (m^3) and η are the receiving room volume and total loss factor respectively and f is frequency in Hz.

The spatially averaged sound pressure level difference, namely Noise Reduction (NR), is given by [18]

$$NR = 10\log_{10}\left(\frac{\sum_{n_1=1}^{N_1}\left|p_{n_1}\right|^2 \Lambda_{n_1}/V_1}{\sum_{n_2=1}^{N_2}\left|p_{n_2}\right|^2 \Lambda_{n_2}/V_2}\right) \tag{2.50}$$

where Λ_{n_1}/V_1 and Λ_{n_2}/V_2 are included due to the definition of the modal pressure amplitudes p_{n_1} and p_{n_2}.

NR is dependent upon the absorption in the room, whilst it is assumed that SRI is independent of the room absorption and is a property of the sound transmission through the panel.

The theoretical routines were developed according to the flowchart below:

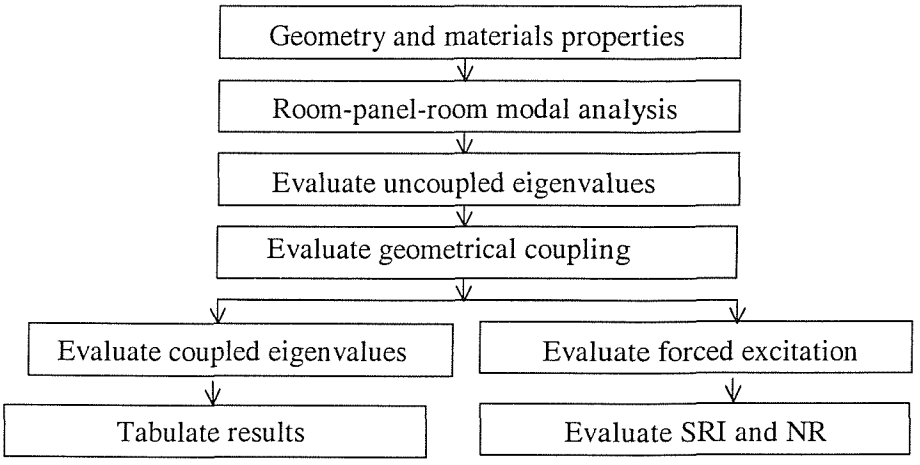

The transmission parameters obtained from the modal room-panel-room model, finite-panel predictions [15,16] and a classical approach can then be compared graphically as a

function of frequency. The values for the coupled natural frequencies can also be considered when examining the response of the forced system, in order to identify which subsystems either structural of acoustic are the most important contributor.

2.5 – Results

2.5.1 – General description of models

The models adopted comprised three subsystems: a source room, a common wall and a receiving room (Figures 2.2 and 2.3). In 'model 1' both rooms have the same width and height whereas in 'model 2' the receiving room is wider than the source room. For the model 3 the partition height and width are 2m and 1.8m respectively. Thus, the rooms of model 3 are slightly different from those of model 1. The source room was defined as an acoustic volume excited by a broadband acoustic point source placed at a corner position. Although the source position does not alter the spatial coupling coefficients between structural and acoustic modes, it has significant influence on exciting the source room modes. Thus, with the source located at one of the source room corners, all modes within a specific frequency range were excited.

The results obtained from the numerical examples provide information about the sensitivity of the modal model to parameters, such as geometrical coupling coefficients and number of modes considered within a particular frequency band. In addition, they also show the spatial distribution of pressure and particle velocity in the acoustic volumes. Finally, some results for the modal model are compared to those obtained by different formulations. The geometric dimensions used for the models are shown in Figures 2.2a, 2.2b and 2.3.

The system properties are described as follows. For a partition made of plasterboard material, a value of $\upsilon = 0.24$ and $E = 2.12 \times 10^9$ N/m^2 were assumed for the Poisson's ratio and Young's modulus respectively. Also a density value of $\rho_s = 806$ kg/m^3 and a thickness of 0.01 m [21] were assumed for the material. On the other hand, for a partition made of steel, a value of $\upsilon = 0.24$ and $E = 210 \times 10^9$ N/m^2 were assumed for the Poisson's ratio and Young's modulus respectively. Also a density value of $\rho_s = 7850$ kg/m^3 and a thickness of 0.01 m [21] were assumed.

The assumption of only pure bending waves propagating in the panel remains valid as the panel thickness is much smaller than the wavelength at the highest frequency

considered herein. When varying the other parameters, the receiving and source room surfaces were considered as being covered by a soft material with a constant modal frequency-average absorption coefficient.

The loss factor for the rooms was chosen as a constant value $\eta = 0.01$ over the whole frequency range. The corresponding T_{60} that results using this constant loss factor is plotted in Figure 2.4.

In ref. [86] typical values for the absorption properties of a room are presented. If one used these absorption values the corresponding loss factor values η would vary from 0.001 to about 0.1 for some commonly used materials in buildings. An important approximation to note here is that the mode functions used have been chosen as the mode shapes of a volume bounded by rigid walls and that absorption has been introduced via a modal description, rather that involving a complex wall impedance in the model. The latter is much more complex and is unnecessary in the present case of rooms with low absorption; both models would produce similar results.

Moreover, the acoustic source strength applied to the source room was a volume velocity equal to $3x10^{-5}$ m^3/s. The source was placed at the corner of the room for all of the simulations presented. The Noise Reduction (NR) parameters obtained from the modal and classical approaches [14,16] were compared graphically as a function of frequency. It was verified in ref. [16] that Leppington's prediction approaches the values obtained from the infinite plate theory when the non-resonant transmission is modelled.

The results are organized as follows. In section 2.5.2, normalized spatial coupling coefficients illustrate the contributions of modes for a frequency range 0-300 Hz. In addition, the spatial averaged mean square pressure and particle velocity distribution are shown for the source and receiving room.

In section 2.5.3, the calculated values of the acoustic and structural natural frequencies are presented. They are also compared with the coupled natural frequencies of the system. Some results show the influence of the number of selected modes on the frequency response of the model within the frequency range considered.

Finally, in section 2.5.4, the modal model results for NR are compared with results using Leppington's expressions [16,17] and also with the diffuse and field incidence mass law theories [14]. The modal model is also compared with Osipov's predictions [12] in terms of NR.

2.5.2 –The coupling coefficients of the system

Tables 2.1-2.5 list the natural frequencies of the rooms and panels considered. These show the occurrence of degenerate modes [78], which are modes that have identical eigenvalues but different eigenfunctions. The effects of the degenerate modes are discussed in the next subsection.

The geometrical coupling values were obtained according to equation (2.34). For a flexible panel in the common wall, equation (2.34) shows that C_{np} is dependent upon panel position and size. The coefficients were normalized by their maximum absolute value in order to compare both models 1 and 2 (Figures 2.1 and 2.2). For a 'whole wall' partition, the peak value for the coupling between uniform pressure acoustic mode (namely the bulk mode) and the fundamental mode of the panel is $4/\pi^2$.

Figures 2.5-2.8 show the contribution of particular modes to the normalized coupling coefficients for the source and receiving rooms. For instance, Figures 2.5 and 2.6 show the contribution of the bulk, axial, tangential and oblique modes to the coupling coefficients $C_{n_1 p}$, which were normalized by the same factor. It is seen that the tangential modes (44 modes) followed by the oblique modes (31 modes) contribute most to the panel-source room coupling. Likewise, Figures 2.7 and 2.8 show the individual contribution of different types of modes to the coupling coefficients $C_{n_2 p}$.It is also evident that the most important contributors were the tangential (28 modes) and the oblique modes (19 modes).

According to the results shown in Figures 2.9-2.12, the coupling relationship between the uncoupled structural and acoustic mode shape functions exhibited the largest contributions for the lower order modes. Figures 2.9 and 2.11 show the coupling coefficients, considering the whole wall flexible, for models 1 and 2 respectively. The coupling coefficients for the source room are similar in both models. On the other hand, they differed significantly for the receiving room. This is mainly due to the larger dimensions of the receiving room for model 2, which led to the increase in the number of coupling acoustic modes.

Figures 2.10 and 2.12 show weak coupling conditions for the configuration when the flexible partition is located in the middle of the common rigid wall. Likewise, the coupling coefficients for the source room are identical in both models (Figures 2.9-a and

2.12-a). However, Figures 2.10-b and 2.12-b show that they provide different values for the panel-receiver room coupling for both models.

Some simplifications, considering 'poor' spatial coupling of higher order modes, have been suggested by some authors [22]. Despite the fact that there were many 'weak coupling coefficients', their summation may be significant to the total coupling and response. Therefore, all modes below 300 Hz including non-resonant contributors were considered in the simulations.

Tables 2.6, 2.7 and 2.8 show the coupled resonance frequencies for the models. By comparing the Tables, it is seen that the modes with frequency at 9 Hz correspond to the uncoupled structural modes (2,1) and (1,2) and these did not couple well to the bulk mode (no net volume associated with these modes) and remained unaltered. On the other hand, the (1,1) structural mode coupled well with the bulk mode and had a coupled frequency that was increased and this then is at 11 Hz due to the stiffening effect. Tables 2.9, 2.10 and 2.11 show the calculated natural frequencies of the uncoupled subsystems and their geometric mode-shape coupling coefficients normalized to their maximum value.

Figures 2.13-2.18 show the dynamic behaviour of the structural-acoustic coupled systems shown in Figures 2.2a, 2.2b and 2.3 in order to illustrate the influence of the geometric mode shape coupling coefficients and structure mass upon the degree of coupling between the elements. Firstly, Figures 2.13 and 2.14 show the predicted responses of the structural-acoustic coupled system presented in Figure 2.2a for partitions with mass per unit area equal to 8.1 kg/m^2 and 78.5 kg/m^2 respectively. Secondly, Figures 2.15 and 2.16 present the frequency response results for model 2 (Figure 2.2b). Finally, Figures 2.17 and 2.18 show the results for model 3 (see Figure 2.3).

Figures 2.13-a and 2.13-b show the frequency responses in terms of sound pressure level for the source and receiving rooms respectively. Figure 2.13-c shows the predicted response of the structural partition in terms of its mean square normal velocity. The results are presented for model 1 which considers the partition dimensions equal to (2m x 2m). The source and receiving room dimensions are equal to (5m x 2m x 2m) and (3m x 2m x 2m) respectively.

For this first model (see Figure 2.2a) the first two peaks (between 10 Hz and 20 Hz) shown in Figures 2.13a and 2.13b are due to the strong coupling with the structural

modes (1,1), (1,3) and (3,1). For instance, the coupled frequencies shown in Table 2.6 at 10.98 Hz, the coupled version of the (1,1) mode, and 19.04 Hz, the coupled version of the (1,3) and (3,1) mode for the square plate, corresponding to peaks in the response in Figures 2.13a-c.

In Figure 2.14-a, a partition with mass per unit area equal to 78.5 kg/m^2 was used in the predictions. The sharp peak at about 12.5 Hz shows the strong structural coupling effect near the structural natural frequency equal to 12 Hz (see Figure 2.14-c). In fact, it corresponds to the coupled frequency 12.53 Hz shown in Table 2.5. The second peak at about 34 Hz corresponds to the uncoupled acoustic mode (1,0,0) shown in Table 2.1. Figure 2.14-b clearly shows a pronounced peak in the receiver room at about 12 Hz, which is also related to the coupling effect with the first structural natural frequency (see Table 2.3).

Figure 2.15 presents the predicted responses for model 2 considering a partition with mass per unit area equal to 8.1 kg/m^2. The first peak at about 9 Hz is due to the strong coupling with the structural mode (1,1) which corresponds to the uncoupled resonance frequency equal to 3.79 Hz. In other words, the coupled version of the (1,1) type structural mode corresponds to the peak at about 9 Hz shown in Figures 2.15a-c. By comparing Figures 2.15-c and 2.13-c, it is shown that the degree of coupling between the structural and acoustic modes for model 1 (see Figure 2.13-c) is greater than that for model 2 (Figure 2.15-c) as expected compared to a model composed of two similar rooms. It can be seen that the coupled frequency at 10.98 Hz shown in Figure 2.13 is more shifted from the *in vacuo* natural frequency, which corresponds to the structural mode (1,1), than the one shown in Figure 2.15, which corresponds to the first peak in the response.

In Figure 2.13-c, the acoustic coupling effect on the structural modes is evident. For instance, the coupled mode at about 18 Hz in Figure 2.13-c is made up of significant contribution of the (1,3) and (3,1) uncoupled structural modes. Similarly, the second and third peaks shown in Figure 2.15a (at about 18.5 Hz and 24 Hz) correspond to the coupled frequencies 18.51 Hz and 24.08 Hz shown in Table 2.4.

Likewise, Figure 2.16 shows the predicted responses for model 2 considering a heavyweight partition with mass per unit area equal to 78.5 kg/m^2. In Figure 2.16a it is seen that the first peak at about 12.3 Hz corresponds to the coupled frequency 12.28 Hz

shown in Table 2.5. Comparing Figures 2.15 and 2.16, it is seen the degree to which the coupling effect reduces as the partition mass increases (i.e. similar to the Mass Law).

Figures 2.17 and 2.18 present the predicted responses of model 3 for both light and heavyweight partitions respectively. This model considers a non-square partition with dimensions equal to (2m x 1.8m). By comparing Figures 2.13 and 2.17 it is seen that 'additional' peaks occur in the response of model 3. For instance, a peak at about 24Hz corresponds to the coupled frequency of 24.2 Hz shown in Table 2.6, as the (3,1) and (1,3) modes have different resonance frequencies in the non-square case. However, apart from this, the sound transmission is not significantly different from that for model 1. Figure 2.18 shows the predicted responses considering a heavyweight partition. It is seen that the first peak corresponds to the coupled frequency 13.9 Hz (Table 2.7), which corresponds to the coupled version of the structural mode (1,1) (see Table 2.5).

2.5.3 –The structural and acoustic modes of the system

It is observed that the location of the resonance peaks for the harmonic forced response coincide with the eigenvalues obtained from the coupled analysis. For room dimensions of 5x2x2 m^3, 3x2x2 m^3 and 3x2x5 m^3, 90, 59 and 130 uncoupled room modes were respectively obtained for a frequency range up to 300 Hz. For panel dimensions of 2x2 m^2 and 1x1 m^2, a total of 112 and 24 modes were considered respectively for the same frequency range.

It is known that the total damping of a lightly damped system (e.g. highly reverberant rooms and partitions with low internal loss factor) has little effect on shifting the eigenfrequencies of an undamped one. However, the results show that spatial coupling between the panel and the volumes played a significant role. This can be confirmed in Table 2.6, which shows the natural frequency values obtained for the first modes of the coupled system. Thus, a coupled mode of the entire room-panel-room system consists of relative amounts of energy corresponding to the rooms' acoustic fields and some energy associated with the panel vibration. Hence, two types of coupled modes, namely mainly panel-controlled and/or room-controlled modes, can exist. For instance, by comparing Tables 2.1, 2.2 and 2.6, it is seen that most of the modes shown in Table 2.6 should be panel-controlled modes as the first acoustic mode is at 34 Hz. Therefore, they have most of their energy stored as vibrational energy in the panel.

The sound power transmission from a source room into a receiving room is mainly affected by the closeness of the separate uncoupled natural frequencies of the rooms and

panel and the degree of spatial matching between the acoustic pressure modes and structural displacement modes. For instance, the fundamental natural frequency of a panel with dimensions equal to 1m x 1m was lower than the lowest natural frequency of the source room (34 Hz). Hence, the corresponding acoustic mode contributes an equivalent mass effect on the panel mode (1,1). Nevertheless, the acoustic bulk mode (0,0,0) always contributes equivalent stiffness. For example, Table 2.8 shows the coupled frequency 15.52 Hz for model 1 with a 1m x 1m partition. It is seen that it is higher than the *in vacuo* natural frequency. This is due to the stiffness contribution from the room bulk mode.

The fundamental coupled natural frequency of models 1 and 2 was about 15 Hz. It is evident from Table 2.6 that it corresponds to a panel-controlled mode as the fundamental uncoupled panel natural frequency was 15.15 Hz.

Figures 2.19 and 2.20 show the mean square sound pressure and particle velocity distribution (in the x direction normal to the panel) with respect to the horizontal plane y = 1m at 120 Hz. Figure 2.19-a and 2.20-a show the surface plot for the pressure and particle velocity respectively. It is observed that there is pressure discontinuity at the interface coordinate $x = 0$ (where there is a flexible partition in the whole common wall) as expected. On the other hand, the particle velocity just goes to zero at the interface. The results are also not constant across the cross-section or symmetric, due to the source location being positioned in one corner of the room (-5,0,0) and the frequency being above the first acoustic mode with a half-wavelength across the section (85 Hz). Figures 2.19-b and 2.20-b show the corresponding contour levels.

The numerical accuracy of the modal model in terms of the number of selected modes used in the calculation was verified in Figures 2.21, 2.22 and 2.23. Spatially averaged mean square pressures were obtained directly from the integration of the square of the pressure given in terms of the orthogonal room modes (see equations 2.12 and 2.28). Figure 2.21 shows the spatial averaged mean square pressure levels predicted from the modal model considering 265 and 90 modes for the source room respectively, which correspond to results obtained when all modes are considered within the frequency range 0-400 Hz and 0-300 Hz respectively. It is seen that the results are almost identical.

Likewise, Figure 2.22 shows the spatial averaged sound pressure levels for the receiving room. Although Figure 2.22-a shows slight differences of about 1-2 dB within the

frequency range 250-300 Hz, (considering 59 and 166 modes for the receiving room) those differences are much less significant in one-third octave bands (Figure 2.22-b).

The Noise Reduction shown in Figure 2.23 presents similar values when a total of 261 modes are considered against 606 modes. The results being presented in both narrow and one-third octave bands. It is seen in Figure 2.23-b that an insignificant difference between the models occurs within the frequency range considered. It can be seen that negative values for NR occurred below the first room mode, which is 34 Hz.

2.5.4 – Comparison of NR obtained via the modal model developed and other established models available in the literature

In this subsection, a comparison is made between the values of Noise Reduction obtained from the modal model and the classical analytical methods. The latter namely the field and diffuse incidence mass laws [14] and Leppington's prediction [16]. Particularly in this subsection, an upper frequency of 450 Hz was considered for the calculation of the NR values.

Leppington's prediction may be considered an improvement on previous theories. In his formulation the transmission problem is described in terms of two distinct mechanisms, namely resonant and non-resonant. Therefore, below coincidence, the transmission efficiency is given by the resonant contribution averaged over a frequency band and the non-resonant contribution.

It is seen that strongly excited structural modes result in generating low values for the NR, which are determined by the structural-acoustic modal coupling coefficients as well as the damping factors.

Figures 2.24, 2.25 and 2.26 show the NR values for models 1, 2 and 3 respectively. Partitions with mass per unit area equal to 8.1 kg/m^2 and 78.5 kg/m^2 were considered. Critical frequencies equal to 3815 Hz and 1196 Hz were obtained for the light and heavyweight partitions respectively. The natural frequencies of the structural partitions are listed in Tables 2.3, 2.4 and 2.5.

In Figure 2.24-a and 2.24-b it is seen that at very low frequencies (below 100 Hz), differences of up to about 20 dB occurred between the modal model and the diffuse incidence Mass Law. In this situation, the dimensions of the subsystems were small in comparison with the wavelength of the sound. Thus, for this condition the motion of the

medium in the system is analogous to that of a mechanical system having lumped mechanical elements of mass, stiffness and damping.

The lowest NR values shown in Figures 2.24-a and 2.24-b are in the one third octave frequency bands with centre frequencies at 8 Hz and 12.5 Hz respectively. For the lightweight partition, this value approximately corresponds to the coupled frequency 9.02 Hz shown in Table 2.6. For the heavyweight partition (Figure 2.24-b), the lowest NR value corresponds to the coupled frequency equal to 12.53 Hz (see Table 2.7). It is seen that this frequency is the coupled version of the fundamental natural frequency of the heavyweight partition, which is equal to 12.08 Hz. It is well known that if a coupled system is excited acoustically and the acoustic volume responds predominantly as though the structure were infinitely rigid, this system is said to be weakly coupled. Therefore, the results confirmed the theory that 'weak coupling' effects occur in models with heavyweight partitions [80].

Moreover, at very low frequency the flexible partition behaves as a rigid-body and the resulting stiffness element is expressed by the acoustic bulk stiffness of the enclosed fluid in the room [4, 60]. The acoustic bulk stiffness is given by $k_A = \rho_o c_o S_A^2 / V_A$; where S_A is the room transverse area (height x width) and V_A is the volume of the acoustic room. In this case, the coupled frequency can be estimated by considering a one-degree-of-freedom mass-spring system. This simplified model consists of a structural mass connected to two 'springs' corresponding to both acoustic rooms. The natural frequency of free vibration of this simplified model was estimated and is approximately 15.5 Hz.

For the 1/3 octave bands with centre frequencies above 100 Hz, the NR values shown in Figure 2.24-a tend to those obtained via Leppington's prediction. In other words, the trend of the curve for the modal model approximates the established values, which consider the resonant and non-resonant contributions at higher frequencies. This is justified by the fact that the 'Schroeder frequencies' (see equation (2.1)) were approximately 298 Hz and 383 Hz for the source and receiving rooms respectively. Nevertheless, for the heavyweight partition Figure 2.24-b shows that the NR values are closer to the diffuse field Mass Law at higher frequencies.

Figure 2.25 shows the NR values obtained for model 2 (Figure 2.2b). In Figure 2.25-a, the variation of the modal model from the Mass Law and Leppington's formulation at low frequencies is less pronounced than that for model 1 shown in Figure 2.24-a. This is

due to the fact that model 1 (Figure 2.24) has exactly coincident resonance frequencies for the two rooms e.g. at 34, 68 and 85 Hz. In addition, there is geometric matching of modal distribution over the common partition. On the other hand, the NR results presented in Figure 2.25 show the effects of mismatch of modal properties of rooms having dissimilar geometrical characteristics. As the frequency increases, the results tend to the values calculated via the Leppington's approach.

By comparing Figures 2.24 and 2.25, it is also evident that at higher frequencies the effect of room shape on NR is not so significant. For instance, in the frequency band with centre frequency at 400 Hz, a difference of less than 2 dB is found between models 1 and 2.

Finally, it is seen that in both configurations (Figures 2.24 and 2.25) the values obtained via Leppington's formulation approximated to those using the field incidence Mass Law when the frequency increases. These results may be explained by the fact that the resonant contribution, which is taken into account in Leppington's formulae, was not significant within the frequency range considered, where the forced non-resonant vibration contribution is the dominant factor. Furthermore, for the heaviest partition the diffuse field Mass Law is about 3-6 dB lower than Leppington's or the field incidence Mass Law values at frequencies greater than 100 Hz.

Figure 2.26 shows a comparison of the NR levels between the values obtained using the modal model 3 and the classical methods. Similarly to the other models, it is seen that the lowest frequency structural mode is most affected by the coupling with the rooms for the lightweight partition. Comparing Figures 2.24 and 2.26 it can be seen that the presence of degenerate modes for the square partition and room of model 1 does not have a large effect on the results.

2.5.5 – Comparison of NR obtained via the modal model developed and another modal model available in the literature

The sound pressure level difference or Noise Reduction is also predicted via the modal model and the results in terms of frequency response are compared to those obtained by Osipov [12]. Figures 2.27 and 2.28 show the NR levels obtained via the modal model, Osipov's approach and the baffled plate model [12] for different partition properties. The simulations were based on a system comprising two rooms coupled by a single leaf partition with dimensions 5m x 3m. The source and receiving room depths were both equal to 3 m. It can be seen that the NR levels for Osipov's room-plate room prediction

and modal model followed the same trend over the whole frequency range and are generally in very good agreement. The small difference (about 3 dB) between Osipov's and the actual modal model herein used might be explained by the fact that the damping value used for the Osipov's model was unknown.

In addition, the baffled plate model, also presented by Osipov [12], shows less modulation in comparison with the modal model or Osipov's room-plate room model. Furthermore, the results obtained via the modal model and the Osipov's room-plate-room model also show very good agreement for all different partition densities considered over a wide range of cases ($\rho h = 28.8 kg/m^2$ to $\rho h = 460\ kg/m^2$).

2.6 – Conclusions

A comparison between numerical modal analysis and theoretical predictions has been performed. A maximum frequency of 450 Hz was used for the frequency response of the systems to a volume velocity point excitation in the source room. Above this frequency limit the computational storage requirements for variables as well as the operational running time on a personal computer became extremely problematic.

The effect of being selective in eliminating some modal contributions has not been reported here [14]. This is because the results are highly sensitive to the non-resonant modes in the frequency range considered. For instance, the non-resonant mass modes of the partition significantly contributed to the energy transmission between rooms. This is evident from the results, which approximates to those for the Mass Law as frequency increases.

Although there were many 'weak coupling coefficients', their summation was significant to the total coupling. Figures 2.5-2.8 show the contribution of certain modes to the fluid-structure interaction. It depends on the degree of spatial coupling between the modes at the common interface. Hence, all possible natural frequencies and their respective modes were included in this analysis. The results may also help in the understanding of the model, with the subsystems considered directly related to physical elements such as rooms and flexible partitions. They can also provide an initial discussion for the investigation of a SEA model, which can be useful for practical building acoustics.

Although this problem (the coupling between the panel and the acoustic fields) has been solved in previous work by several authors, the results obtained herein can also be used for guidance in real cases of architectural acoustic design. All the parameters, which

affected the modal composition of the sound field in the subsystems, were fundamental in the determination of the Sound Reduction Index. The results may also be used to interpret measurements made in-situ at low frequencies, e.g. where the classical definition of SRI in ISO140 for diffuse sound fields may not be appropriate or reliable.

Although the assumption of uncoupled 'rigid-walled' acoustic modes for the rooms [6] has been assumed for many years, the actual boundary condition, which is due to the velocity of the partition, cannot be replicated. The convergence problem may be rather sensitive at low frequencies and may require a significant summation of modes to provide accurate velocity and pressure predictions at the panel location. This is necessary for accurate predictions of the acoustic intensity and hence Sound Reduction Index.

Existing methodologies, i.e. the Mass Law and Leppington's formulation, similarly have difficulty at low frequencies. For instance, the assumption of diffuse field, etc., is no longer valid at very low frequencies, as few acoustic modes exist in the volumes. However, it has been shown that the SRI values obtained using the Modal model converge reasonably well to Leppington's prediction as the frequency increases.

Although the model will be validated experimentally later in this thesis, the good agreement between the modal model and Osipov's published room-plate-room model for the Noise Reduction indicated a good degree of reliability in the modal model. If one is interested in the Noise Reduction and hence requires spatially averaged acoustic pressures, then the methodology of using the modal method with 'rigid-walls' is acceptable and provides good results. This statement can be confirmed by the fact that the results obtained converged to the established and accepted analytical models as frequency increases.

Tables

The natural frequencies of the first 10 room modes Frequency range: 0 Hz-300 Hz					
Room dimension (5x2x2) m^3 Mode (l,m,n)	Frequency (Hz)	Room dimension (3x2x2) m^3 Mode (l,m,n)	Frequency (Hz)	Room dimension (3x2x5) m^3 Mode (l,m,n)	Frequency (Hz)
0 0 0	0.00	0 0 0	0.00	0 0 0	0.00
1 0 0	34.00	1 0 0	56.67	0 0 1	34.00
2 0 0	68.00	0 0 1	85.00	1 0 0	56.67
0 0 1	85.00	0 1 0	85.00	1 0 1	66.08
0 1 0	85.00	1 0 1	102.16	0 0 2	68.00
1 0 1	91.55	1 1 0	102.16	0 1 0	85.00
1 1 0	91.55	2 0 0	113.33	1 0 2	88.52
3 0 0	102.00	0 1 1	120.21	0 1 1	91.55
2 0 1	108.85	1 1 1	132.89	0 0 3	102.00
2 1 0	108.85	2 0 1	141.67	1 1 0	102.16

Table 2.1: Summary of the natural frequencies of 'rigid-wall' acoustic volumes used in Models 1 and 2.

The natural frequencies of the first 10 room modes Frequency range: 0 Hz-300 Hz			
Room dimension (5x2x1.8) m^3 Mode (l,m,n)	Frequency (Hz)	Room dimension (3x2x1.8) m^3 Mode (l,m,n)	Frequency (Hz)
0 0 0	0.00	0 0 0	0.00
1 0 0	34.00	1 0 0	56.67
2 0 0	68.00	0 0 1	85.00
0 1 0	85.00	0 1 0	94.44
1 1 0	91.55	1 0 1	102.16
0 0 1	94.44	1 1 0	110.14
1 0 1	100.38	2 0 0	113.33
3 0 0	102.00	0 1 1	127.03
2 1 0	108.85	1 1 1	139.12
2 0 1	116.38	2 0 1	141.67

Table 2.2: Summary of the natural frequencies of 'rigid-wall' acoustic volumes used in Model 3.

First 8 panel modes - Dimension: (1x1) m^2		First 8 panel modes - Dimension:(2x2) m^2	
Mode (p,q)	Frequency (Hz)	Mode (p,q)	Frequency (Hz)
1 1	15.15	1 1	3.79
1 2	37.88	1 2	9.47
2 1	37.88	2 1	9.47
2 2	60.61	2 2	15.15
1 3	75.76	1 3	18.94
3 1	75.76	3 1	18.94
2 3	98.48	2 3	24.62
3 2	98.48	3 2	24.62

Table 2.3: Summary of the *in vacuo* natural frequencies of partitions used in the models, assuming simply-supported boundary conditions and $\rho h = 8.1 kg/m^2$.

First 8 panel modes - Dimension: (2m x1.8m) – Model 3	
Mode (p,q)	Frequency (Hz)
1 1	4.23
2 1	9.91
1 2	11.25
2 2	16.93
3 1	19.38
1 3	22.94
3 2	26.39
2 3	28.62

Table 2.4: Summary of the *in vacuo* natural frequencies of partitions used in the models, assuming simply-supported boundary conditions and $\rho h = 8.1 kg/m^2$.

First 8 panel modes - Dimension: (2m x 2m) – Models 1 and 2		First 8 panel modes - Dimension: (2m x1.8m) – Model 3	
Mode (p,q)	Frequency (Hz)	Mode (p,q)	Frequency (Hz)
1 1	12.08	1 1	13.49
1 2	30.19	2 1	31.62
2 1	30.19	1 2	35.87
2 2	48.32	2 2	53.99
1 3	60.39	3 1	61.82
3 1	60.39	1 3	73.15
2 3	78.52	3 2	84.19
3 2	78.52	2 3	91.27

Table 2.5: Summary of the *in vacuo* natural frequencies of partition used in the models, assuming simply-supported boundary conditions and $\rho h = 78.5 kg/m^2$.

The first coupled frequencies (model 1)	The first coupled frequencies (model 2)	The first coupled frequencies (model 3)
Frequency (Hz)	Frequency (Hz)	Frequency (Hz)
0.00	0.00	0.00
9.02	8.92	9.54
9.02	8.98	10.86
10.98	9.04	10.95
14.72	14.64	16.64
18.57	18.45	19.36
19.04	18.51	22.79
19.04	18.51	24.22
24.26	24.08	28.43
24.26	24.08	32.44
31.98	31.58	35.66
31.98	31.58	38.13
33.86	34.07	39.06
33.86	34.07	39.54
36.03	36.56	44.85
36.03	36.56	49.46
37.87	37.44	51.28

Table 2.6: Summary of the first 10 coupled frequencies for models 1, 2 and 3 considering the whole interface flexible (2m x 2m) for models 1 and 2 and (2m x 1.8m) for model 3; The mass per unit area adopted was $\rho h = 8.1 kg/m^2$ for all models.

The first coupled frequencies (model 1)	The first coupled frequencies (model 2)	The first coupled frequencies (model 3)
Frequency (Hz)	Frequency (Hz)	Frequency (Hz)
0.00	0.00	0.00
12.53	12.28	13.88
30.01	30.00	31.47
30.01	30.00	34.19
34.17	33.99	35.72
34.17	34.25	53.87
48.12	48.13	56.71
56.56	56.62	61.83

Table 2.7: Summary of the first 10 coupled frequencies for models 1, 2 and 3 considering the whole interface flexible and $\rho h = 78.5 kg/m^2$.

First 10 coupled frequencies (model 1)	First 10 coupled frequencies (model 2)
Frequency (Hz)	Frequency (Hz)
0.00	0.00
15.52	15.03
34.46	33.99
37.32	34.64
37.32	37.32
56.97	37.34
60.25	56.79
68.01	60.25
75.45	66.14
75.81	68.01

Table 2.8: Summary of the first 10 coupled frequencies for model 1 and 2 considering a small flexible partition (1m x 1m and $\rho h = 8.1 kg/m^2$) in the middle of the common rigid wall.

Order		Plate (2x2) m^2	1	2	3	4	5	6
	Type		(1,1)	(1,2)	(2,1)	(2,2)	(1,3)	(3,1)
Source Room		Frequency (Hz)	3.79	9.47	9.47	15.15	18.94	18.94
1	(0,0,0)	0.00	1.0000	0.0000	0.0000	0.0000	0.3333	0.3333
2	(1,0,0)	34.00	1.0000	0.0000	0.0000	0.0000	0.3333	0.3333
3	(2,0,0)	68.00	1.0000	0.0000	0.0000	0.0000	0.3333	0.3333
4	(0,0,1)	85.00	0.0000	0.6667	0.0000	0.0000	0.0000	0.0000
5	(0,1,0)	85.00	0.0000	0.0000	0.6667	0.0000	0.0000	0.0000
6	(1,0,1)	91.55	0.0000	0.6667	0.0000	0.0000	0.0000	0.0000
7	(1,1,0)	91.55	0.0000	0.0000	0.6667	0.0000	0.0000	0.0000
8	(3,0,0)	102.00	1.0000	0.0000	0.0000	0.0000	0.3333	0.3333

Table 2.9: Summary of the first 8 natural frequencies and normalized geometric mode shape coupling coefficients (Cn_1p) for model 1.

Order		Plate (2x2) m^2	1	2	3	4	5	6
	Type		(1,1)	(1,2)	(2,1)	(2,2)	(1,3)	(3,1)
Receiving Room		Frequency (Hz)	3.79	9.47	9.47	15.15	18.94	18.94
1	(0,0,0)	0.00	1.0000	0.0000	0.0000	0.0000	0.3333	0.3333
2	(1,0,0)	56.67	1.0000	0.0000	0.0000	0.0000	0.3333	0.3333
3	(0,0,1)	85.00	0.0000	0.6667	0.0000	0.0000	0.0000	0.0000
4	(0,1,0)	85.00	0.0000	0.0000	0.6667	0.0000	0.0000	0.0000
5	(1,0,1)	102.16	0.0000	0.6667	0.0000	0.0000	0.0000	0.0000
6	(1,1,0)	102.16	0.0000	0.0000	0.6667	0.0000	0.0000	0.0000
7	(2,0,0)	113.33	1.0000	0.0000	0.0000	0.0000	0.3333	0.3333
8	(0,1,1)	120.21	0.0000	0.0000	0.0000	0.0000	0.4444	0.0000

Table 2.10: Summary of the first 8 natural frequencies and normalized geometric mode shape coupling coefficients (Cn_2p) for model 1.

Order		Plate (2x2) m^2	1	2	3	4	5	6
	Type		(1,1)	(1,2)	(2,1)	(2,2)	(1,3)	(3,1)
Receiving Room		Frequency (Hz)	3.79	9.47	9.47	15.15	18.94	18.94
1	(0,0,0)	0.00	1.0000	0.0000	0.0000	0.0000	0.3333	0.3333
2	(0,0,1)	34.00	0.7792	0.1799	0.0000	0.0000	0.2221	0.2597
3	(1,0,0)	56.67	1.0000	0.0000	0.0000	0.0000	0.3333	0.3333
4	(1,0,1)	66.08	0.7792	0.1799	0.0000	0.0000	0.2221	0.2597
5	(0,0,2)	68.00	0.2653	0.5384	0.0000	0.0000	0.0343	0.0884
6	(0,1,0)	85.00	0.0000	0.0000	0.6667	0.0000	0.0000	0.0000
7	(1,0,2)	88.52	0.2653	0.5384	0.0000	0.0000	0.0343	0.0884
8	(0,1,1)	91.55	0.0000	0.0000	0.5195	0.1200	0.0000	0.0000

Table 2.11: Summary of the first 8 natural frequencies and normalized geometric mode shape coupling coefficients (Cn_2p) for model 2.

Figures

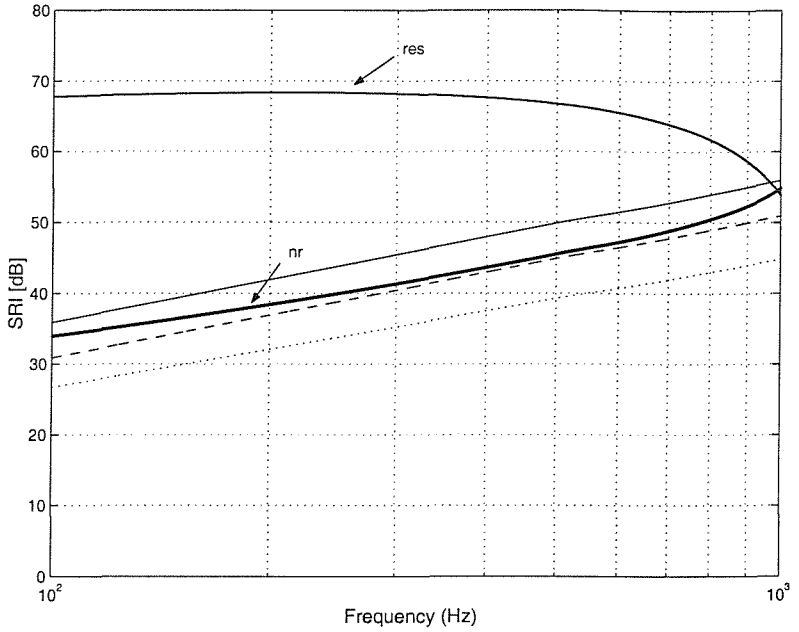

Figure 2.1: The Sound Reduction Index (for the various Mass Law expressions) for an infinite limp panel with nominal density equal to 78.5 kg/m^2. ____ normal incidence; ---- field incidence and ..... diffuse field incidence; res-Leppington's resonant transmission (see equation (2.8)); nr = Leppington's non-resonant transmission (see equation (2.9)).

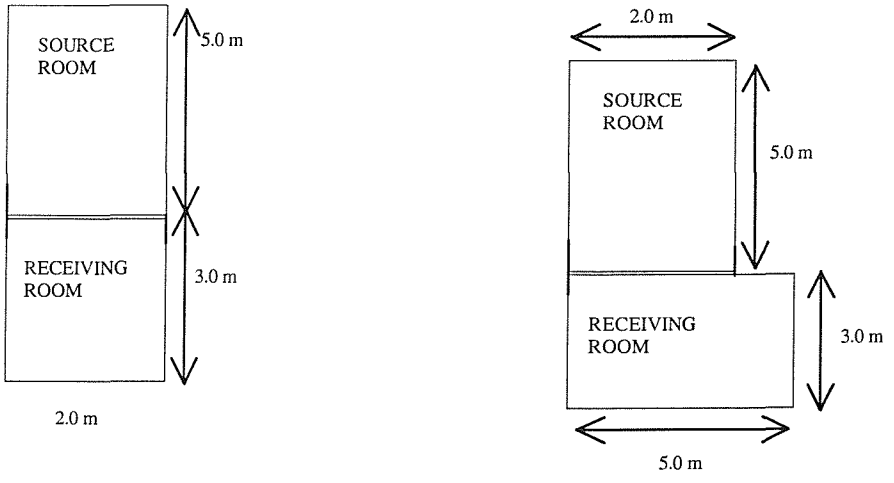

a) b)

Figure 2.2: Two rooms separated by a common wall (2m x 2m). Both rooms were of height equal to 2 m. a) Model 1; b) Model 2

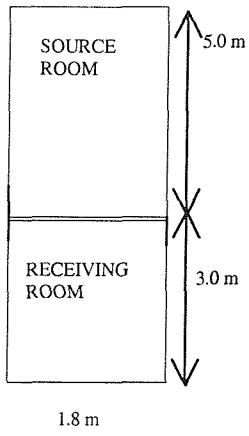

Figure 2.3: Two rooms separated by a common wall (2m x 1.8m). Both rooms were of height equal to 2 m – Model 3

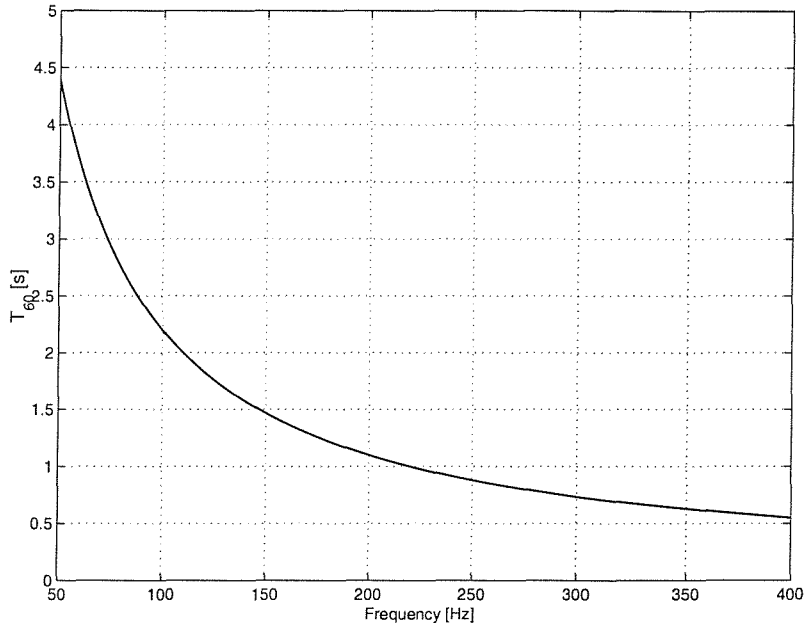

Figure 2.4: The corresponding T_{60} (s) that results using a constant loss factor $\eta = 0.01$.

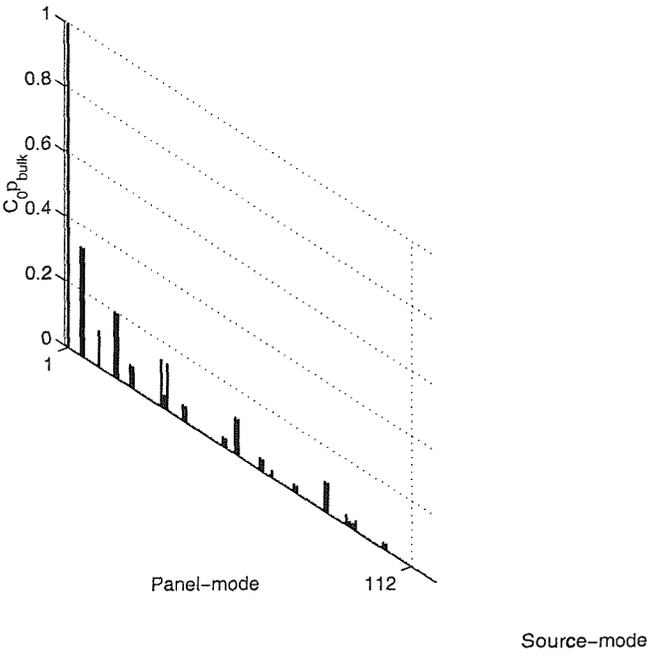

a)

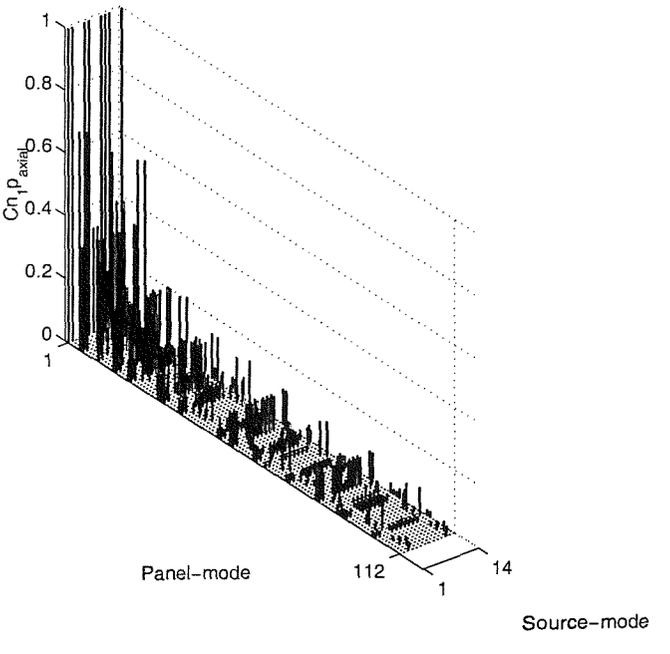

b)

Figure 2.5: The contribution of the bulk and axial modes of the source room to the normalized coupling coefficients $C_{n_1 p}$ considering a whole wall for model 1. a) bulk mode; b) axial modes (14 modes)

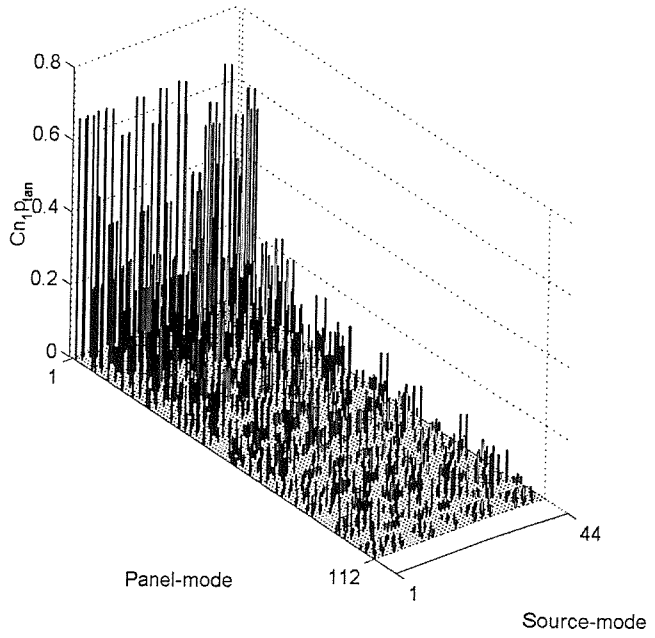

a)

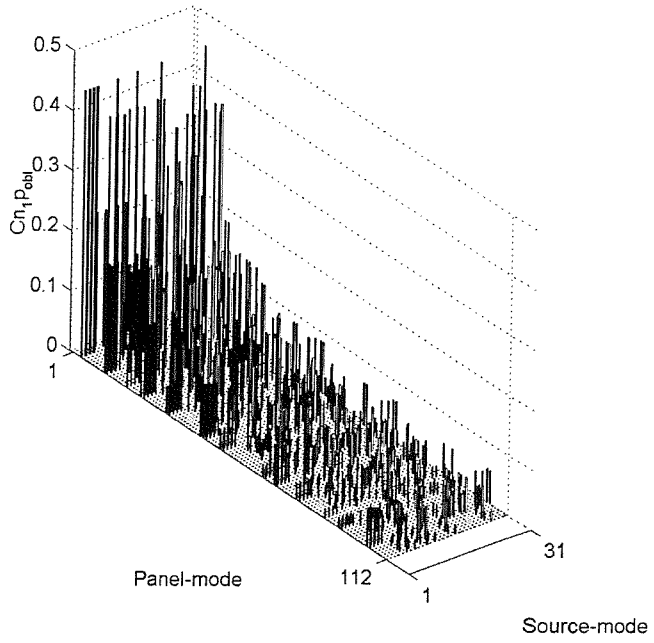

b)

Figure 2.6: The contribution of the tangential and oblique modes of the source room to the normalized coupling coefficients $C_{n_1 p}$ considering a whole wall for model 1. a) tangential modes (44 modes); b) oblique modes (31 modes)

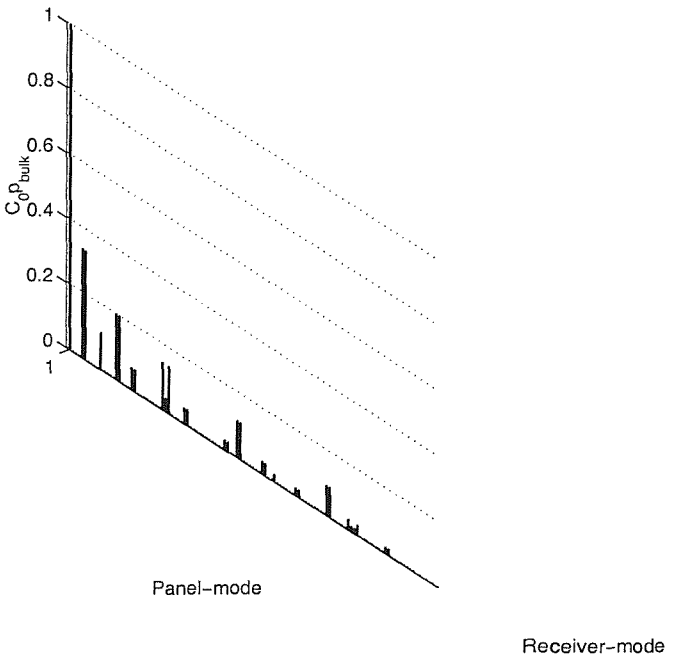

a)

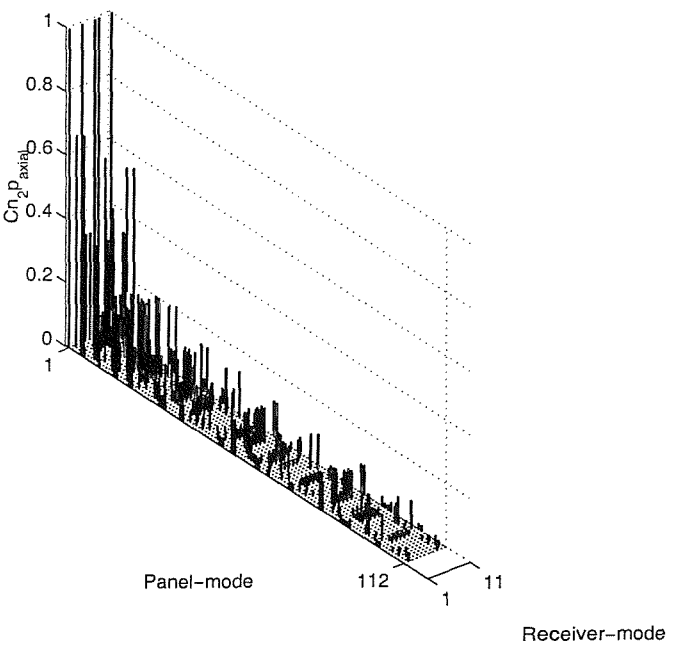

b)

Figure 2.7: The contribution of the bulk and axial modes of the receiving room to the normalized coupling coefficients $C_{n_2 p}$ considering a whole wall for model 1. a) bulk mode; b) axial modes (11 modes).

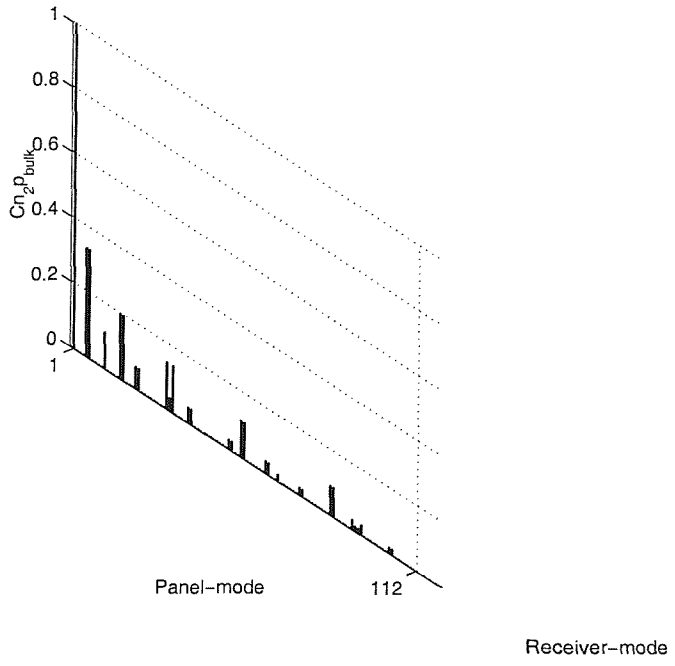

a)

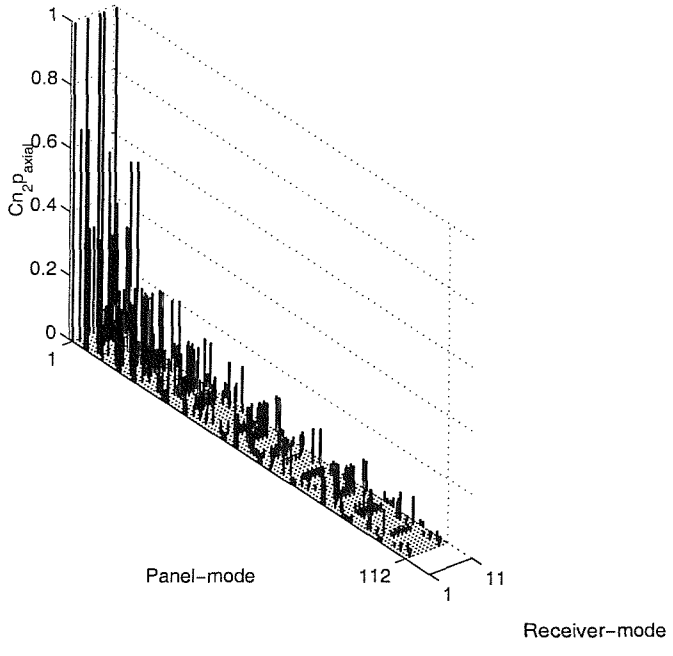

b)

Figure 2.8: The contribution of the tangential and oblique modes of the receiving room to the normalized coupling coefficients $C_{n_2 p}$ considering a whole wall for model 1. a) tangential modes (28 modes); b) oblique modes (19 modes)

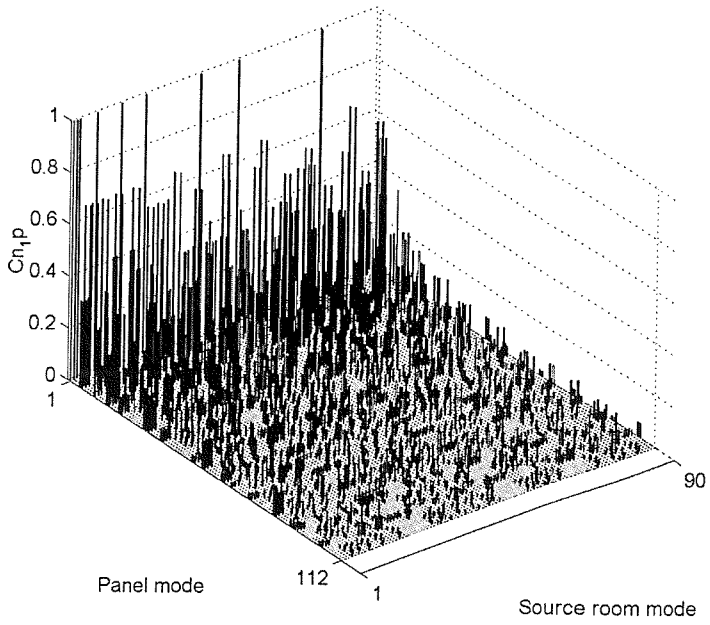

a)

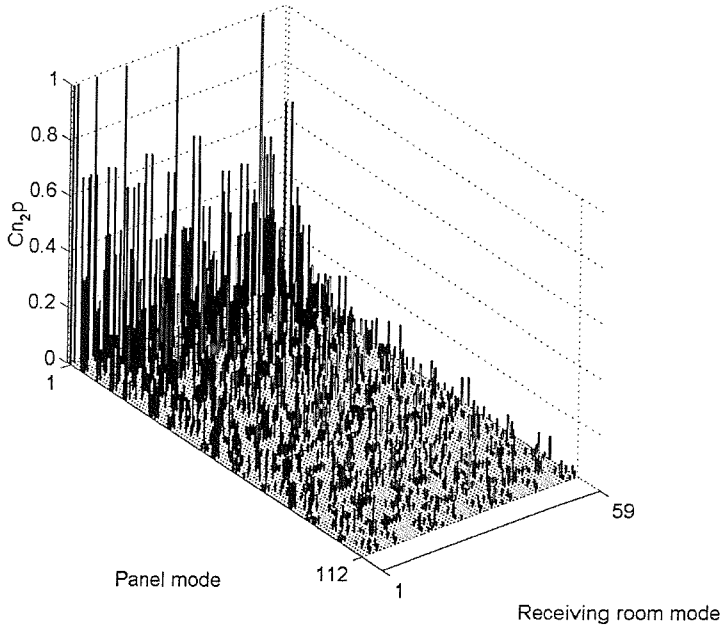

b)

Figure 2.9: Normalized coupling coefficients for model 1 considering a flexible panel over the whole common interface; a) panel and source room (112 panel modes and 90 room modes); b) panel and receiving room (112 panel modes and 59 room modes);

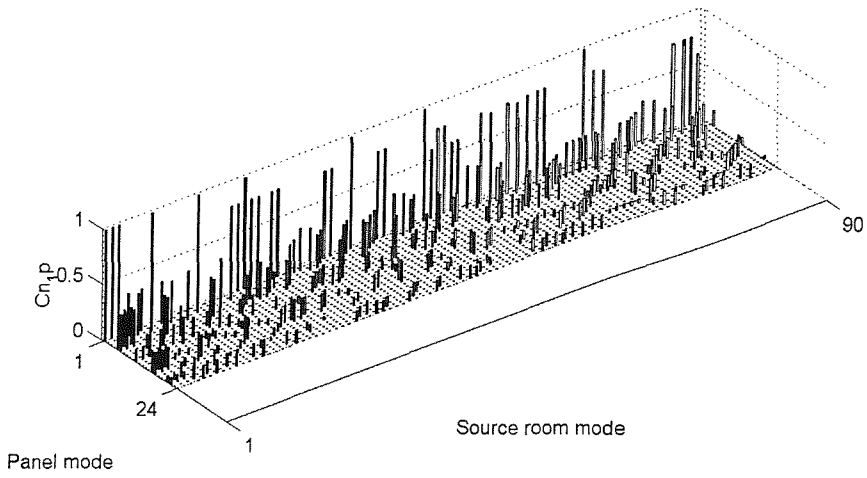

a)

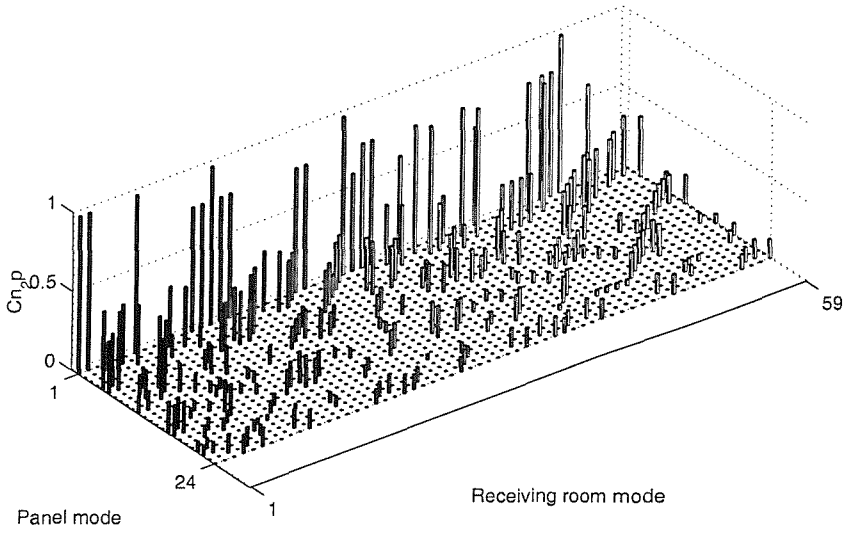

b)

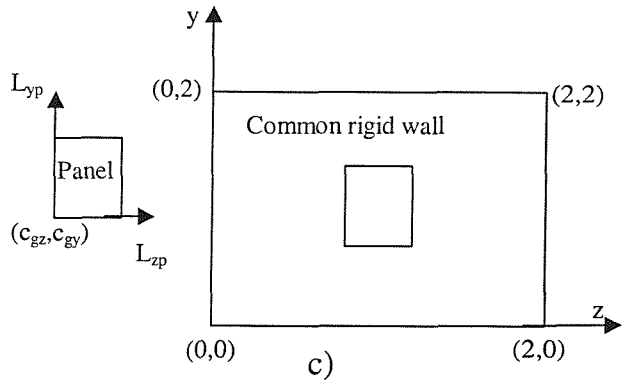

c)

Figure 2.10: Normalized coupling coefficients for model 1 considering a flexible panel (1m x 1m) in the middle of the common rigid wall (2m x 2m); a) panel and source room (24 panel modes and 90 room modes); b) panel and receiving room (24 panel modes and 59 room modes); c) panel location in the middle of the common wall ($c_{gy} = c_{gz} = 0.5$).

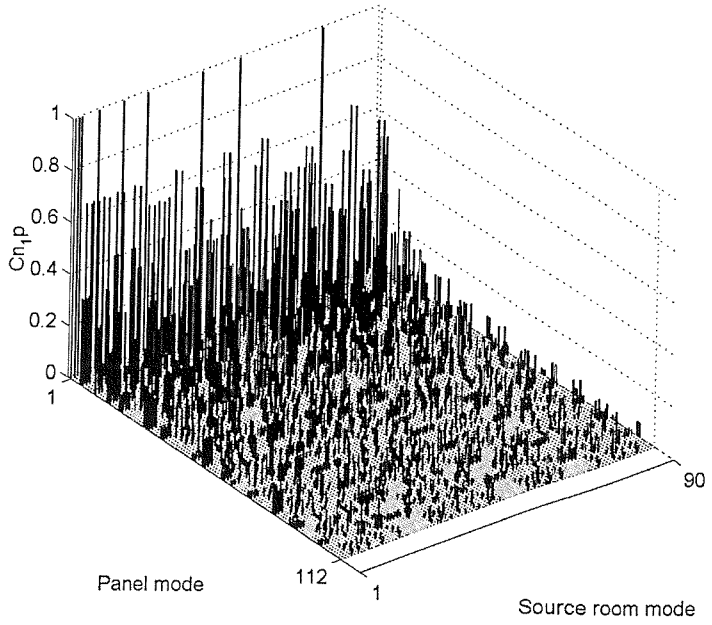

a)

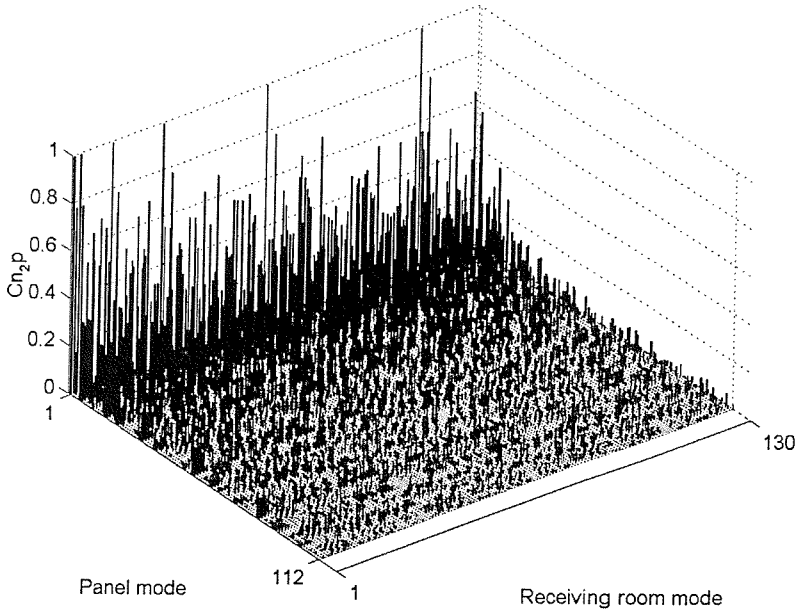

b)

Figure 2.11: Normalized coupling coefficients for model 2 considering a flexible panel over the whole common interface; a) panel and source room - (112 panel modes and 90 room modes); b) panel and receiving room (112 panel modes and 130 room modes);

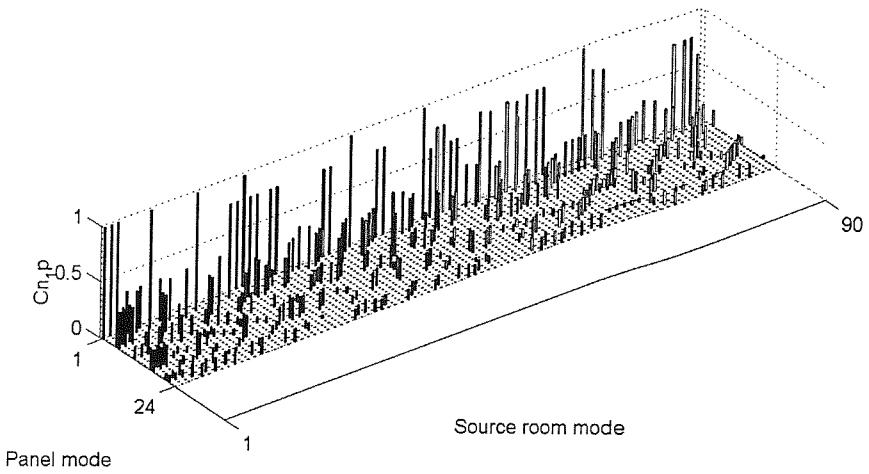

a)

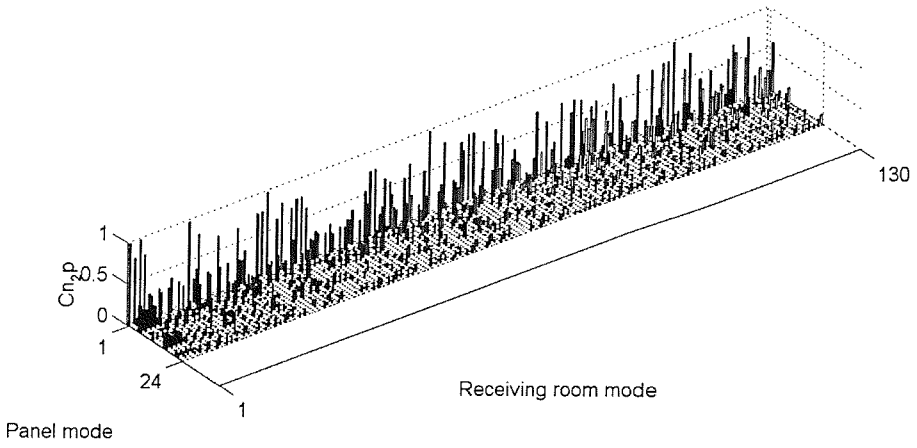

b)

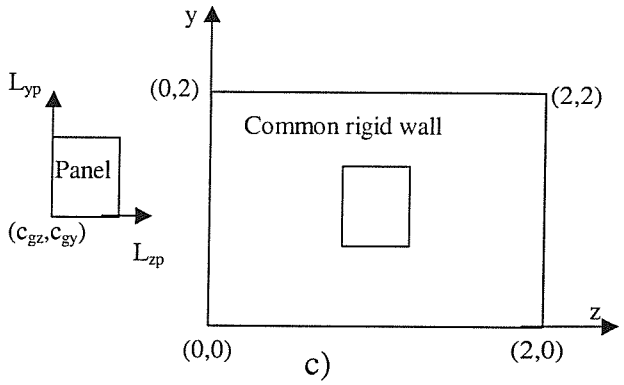

c)

Figure 2.12: Normalized coupling coefficients for model 2 considering a flexible panel (1m x 1m) in the middle of the common rigid wall (2m x 2m); a) panel and source room - (24 panel modes and 90 room modes); b) panel and receiving room (24 panel modes and 130 room modes); c) panel location in the middle of the common wall (c_{gy} = c_{gz} = 0.5).

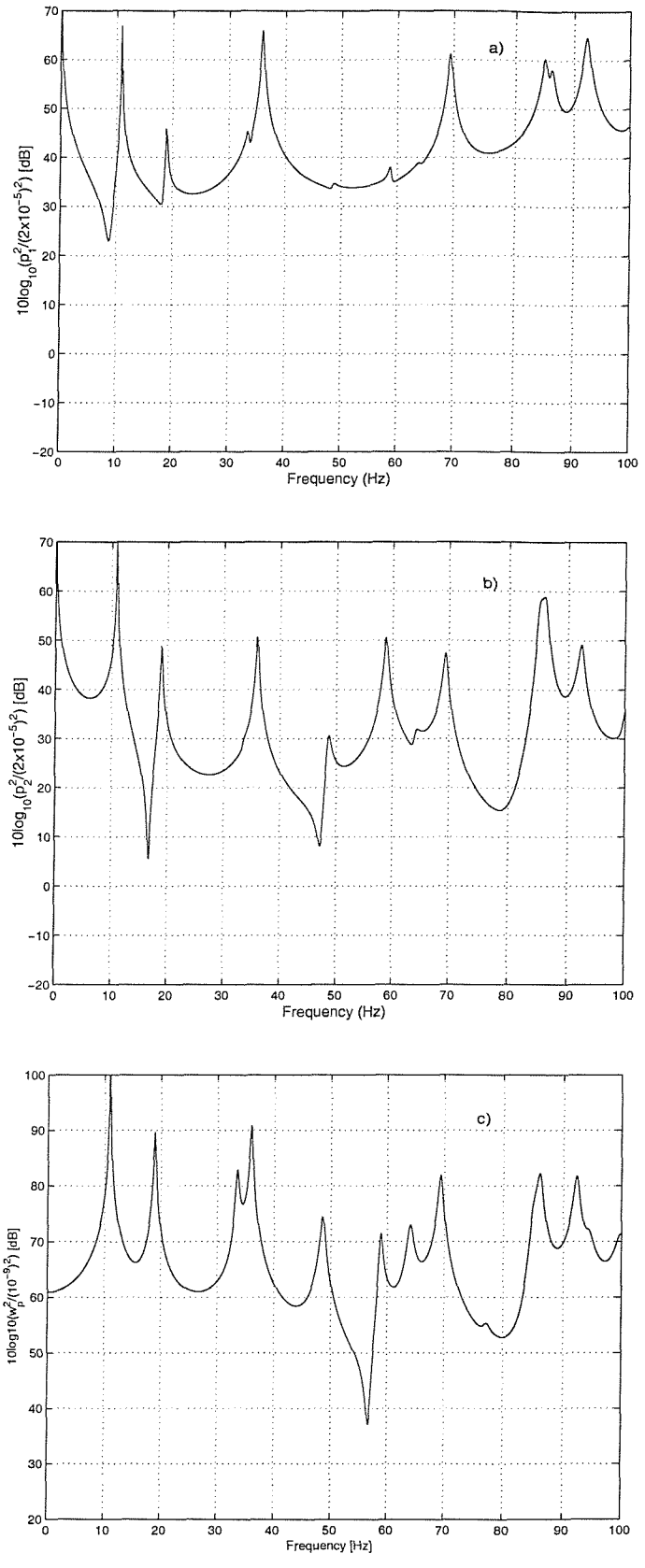

Figure 2.13: Predicted responses due to acoustic excitation of the structural-acoustic coupled system shown in Figure 2.2(a). $\rho h = 8.1 kg/m^2$. a) SPL in the source room (dB re 20 μ Pa); b) SPL in the receiving room (dB re 20 μ Pa); c) Structural velocity (dB re 10^{-9} m/s).

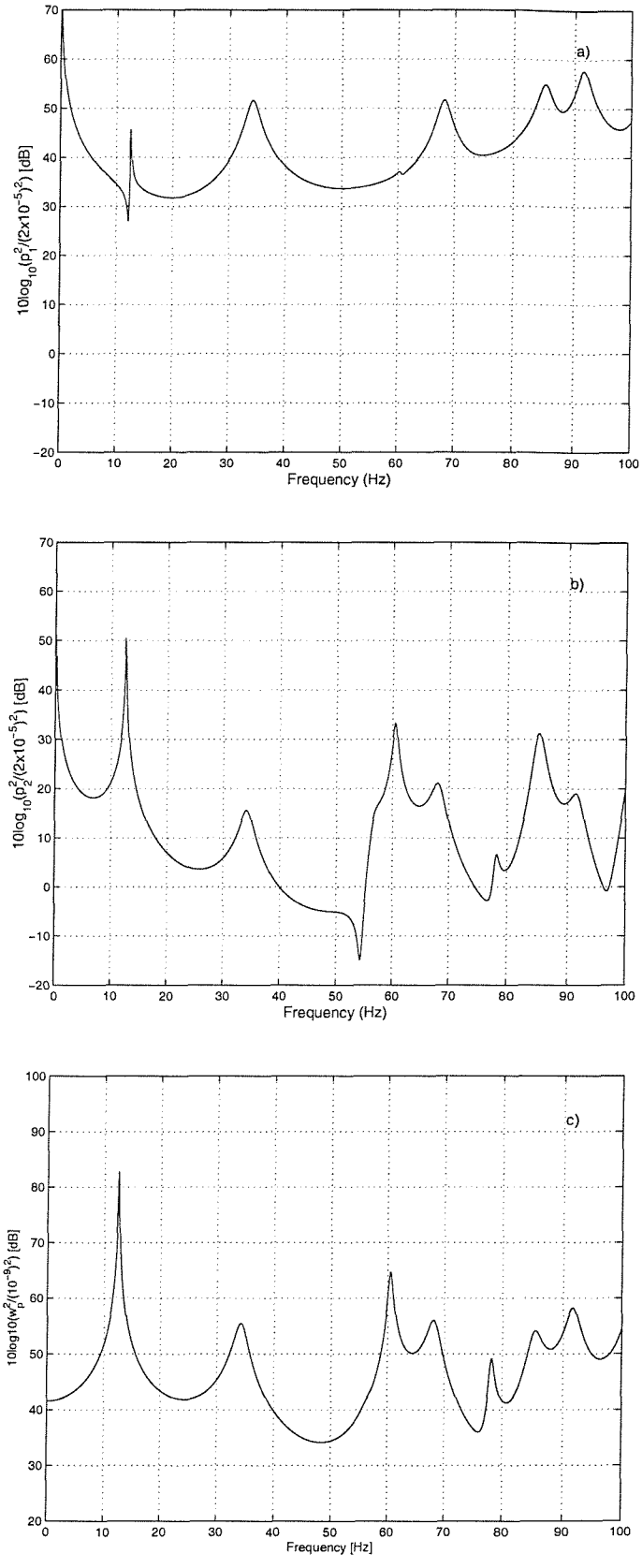

Figure 2.14: Predicted responses due to acoustic excitation of the structural-acoustic coupled system shown in Figure 2.2(a). The partition mass per unit area was 78.5 kg/m^2. a) Sound pressure level in the source room (dB re 20 μ Pa); b) Sound pressure level in the receiving room (dB re 20 μ Pa); c) Structural velocity (dB re 10^{-9} m/s).

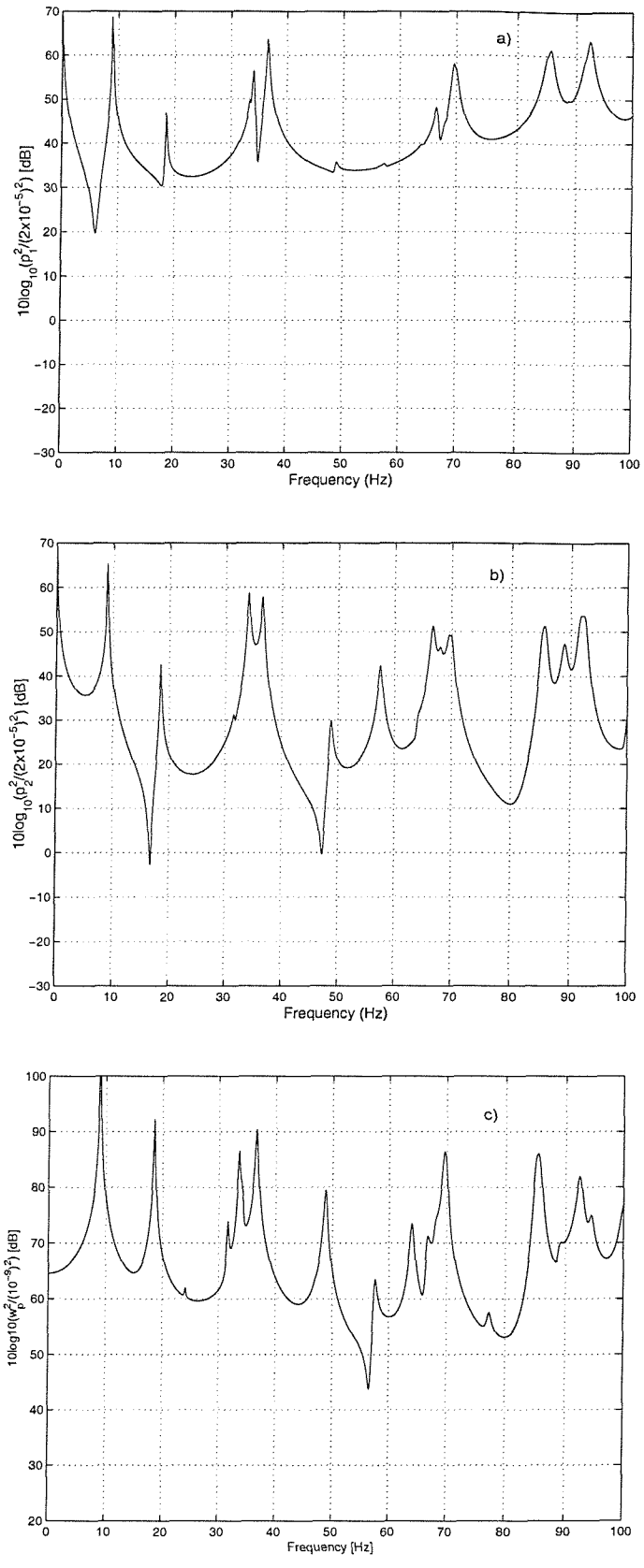

Figure 2.15: Predicted responses due to acoustic excitation of the structural-acoustic coupled system shown in Figure 2.2(b). The partition mass per unit area was 8.1 kg/m^2. a) Sound pressure level in the source room (dB re 20 μ Pa); b) Sound pressure level in the receiving room (dB re 20 μ Pa); c) Structural velocity (dB re 10^{-9} m/s).

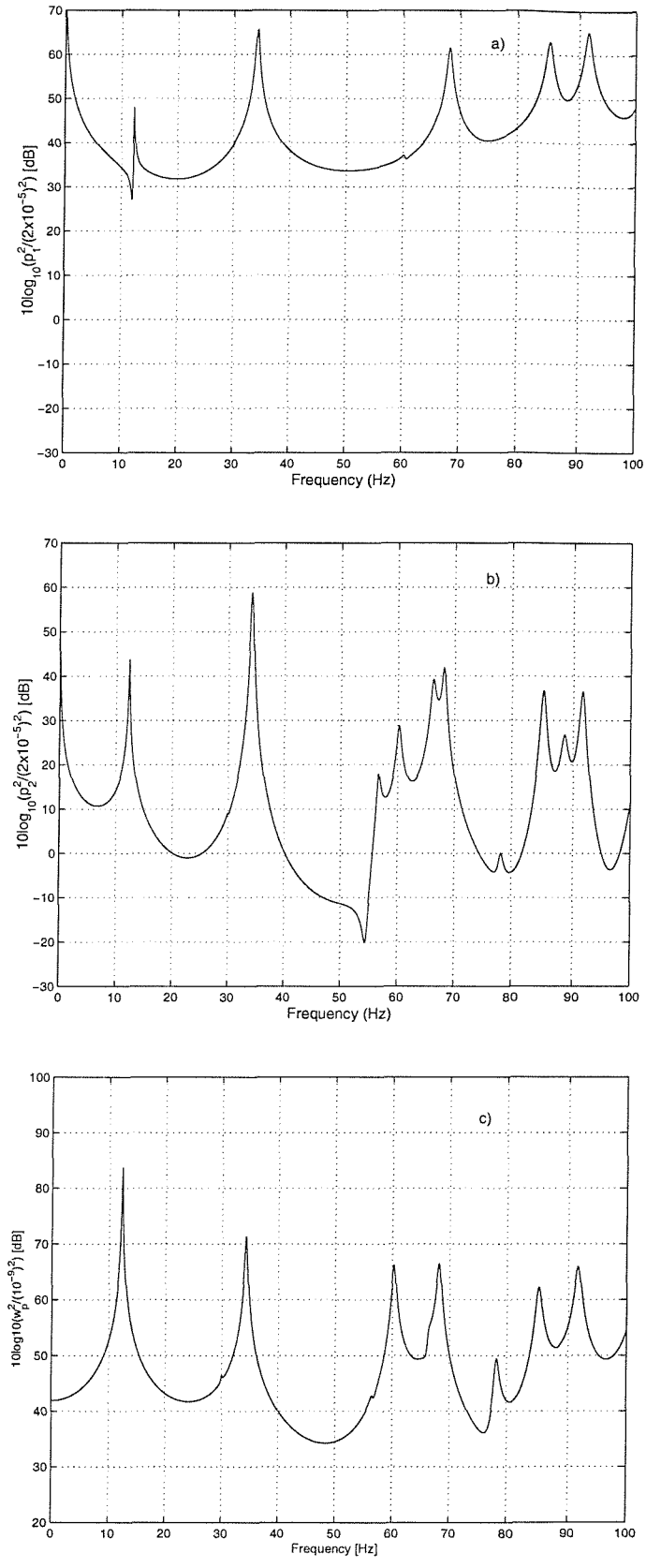

Figure 2.16: Predicted responses due to acoustic excitation of the structural-acoustic coupled system shown in Figure 2.2(b). The partition mass per unit area was 78.5 kg/m^2. a) Sound pressure level in the source room (dB re 20 μ Pa); b) Sound pressure level in the receiving room (dB re 20 μ Pa); c) Structural velocity (dB re 10^{-9} m/s).

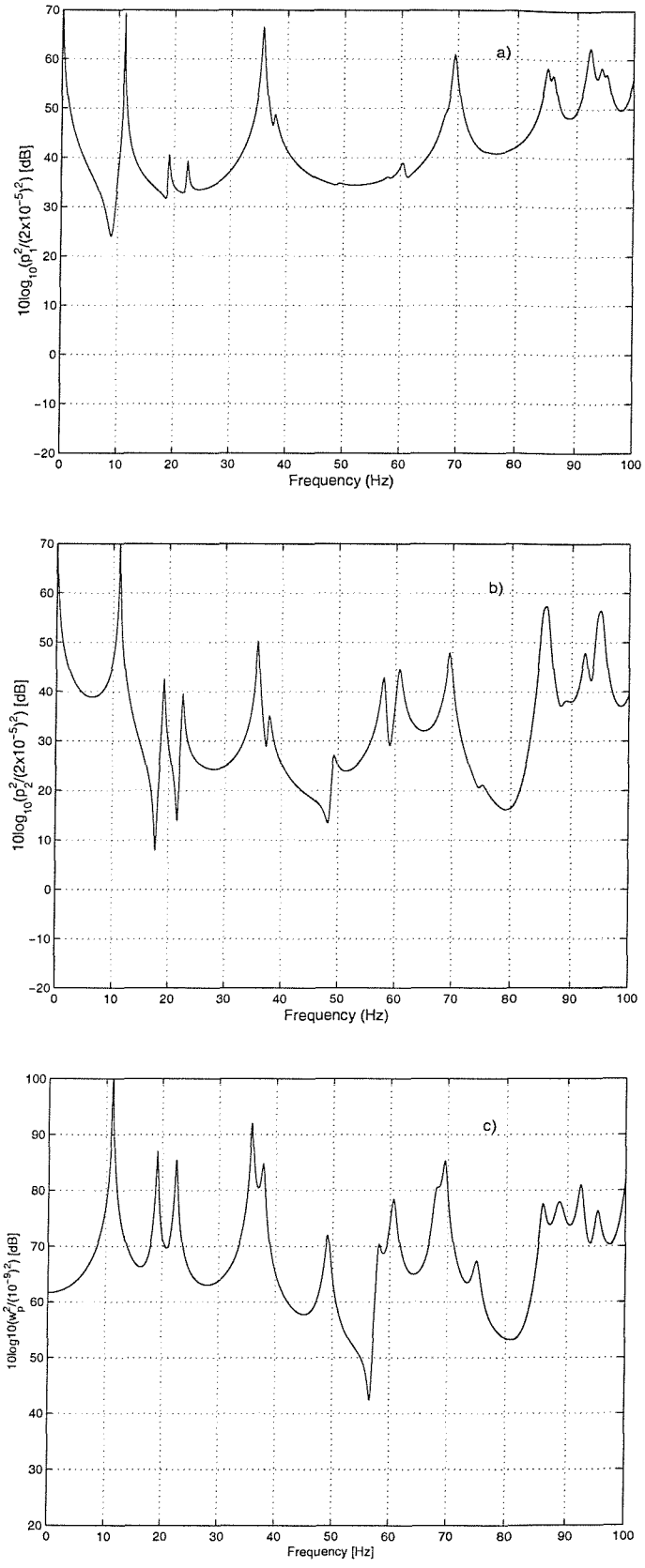

Figure 2.17: Predicted responses due to acoustic excitation of the structural-acoustic coupled system shown in Figure 2.3. The partition mass per unit area was 8.1 kg/m^2. a) Sound pressure level in the source room (dB re 20 μ Pa); b) Sound pressure level in the receiving room (dB re 20 μ Pa); c) Structural velocity (dB re 10^{-9} m/s).

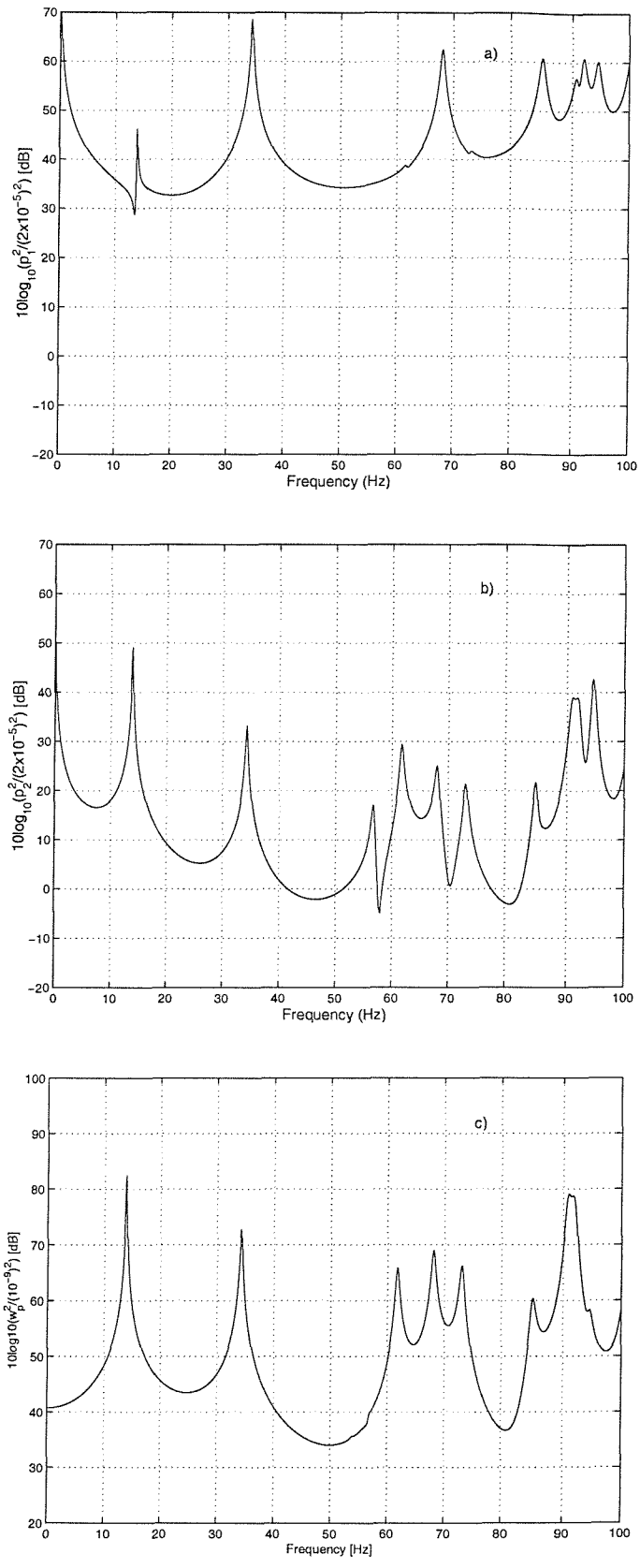

Figure 2.18: Predicted responses due to acoustic excitation of the structural-acoustic coupled system shown in Figure 2.3. The partition mass per unit area was 78.5 kg/m^2. a) Sound pressure level in the source room (dB re 20 μ Pa); b) Sound pressure level in the receiving room (dB re 20 μ Pa); c) Structural velocity (dB re 10^{-9} m/s).

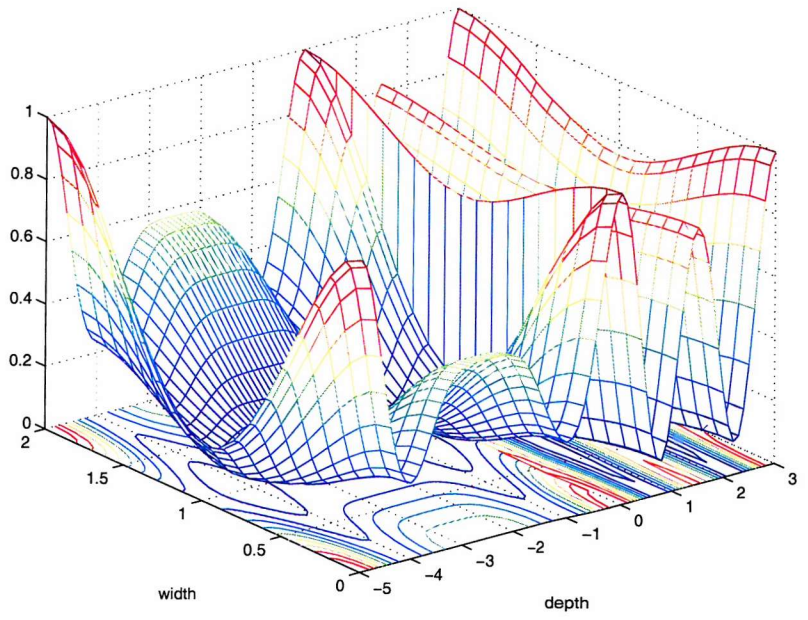

a)

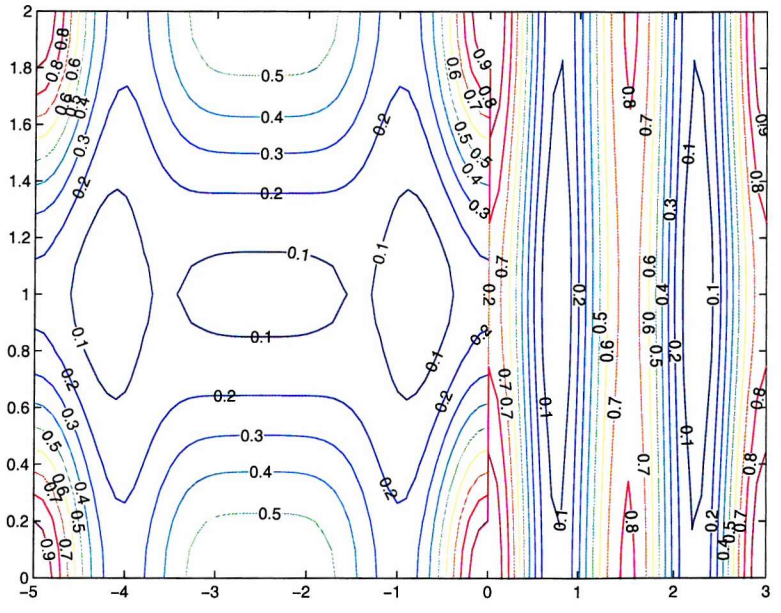

b)

Figure 2.19: Normalized mean square pressure distribution (model 1) with respect to the horizontal plane y = 1 m at 120 Hz. The partition dimensions and mass per unit area are 2m x2m and 8.1 kg/m^2 respectively. a) surface plot; b) Contour levels in (Pa^2/Pa^2);

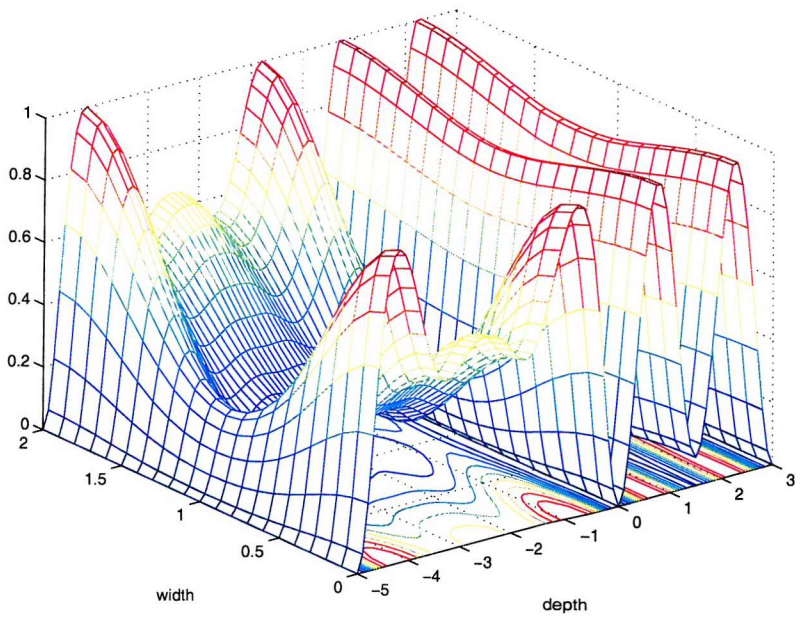

a)

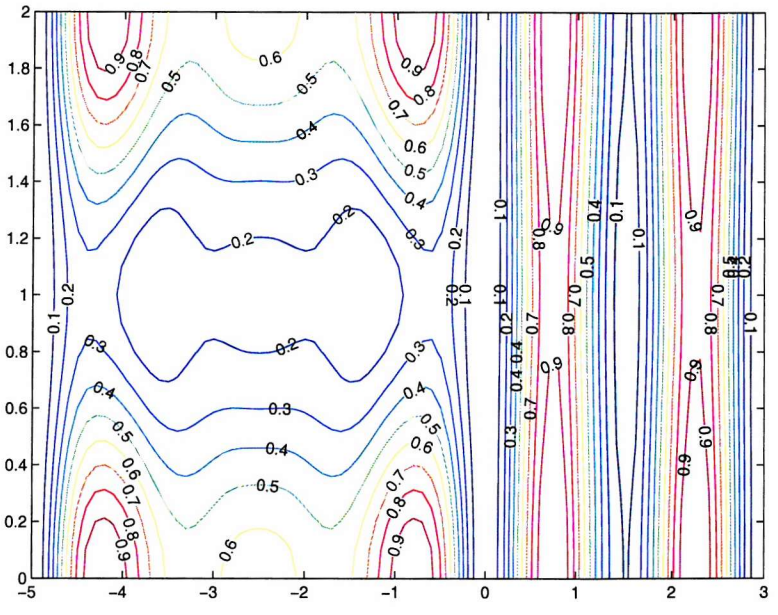

b)

Figure 2.20: Normalized mean square particle velocity distribution (model 1) in the x-direction with respect to the horizontal plane y = 1 m at 120 Hz. The nominal partition dimensions and mass per unit area are 2m x 2m and 8.1 kg/m^2 respectively. a) surface plot; b) Contour levels in (m/s)^2/(m/s)^2;

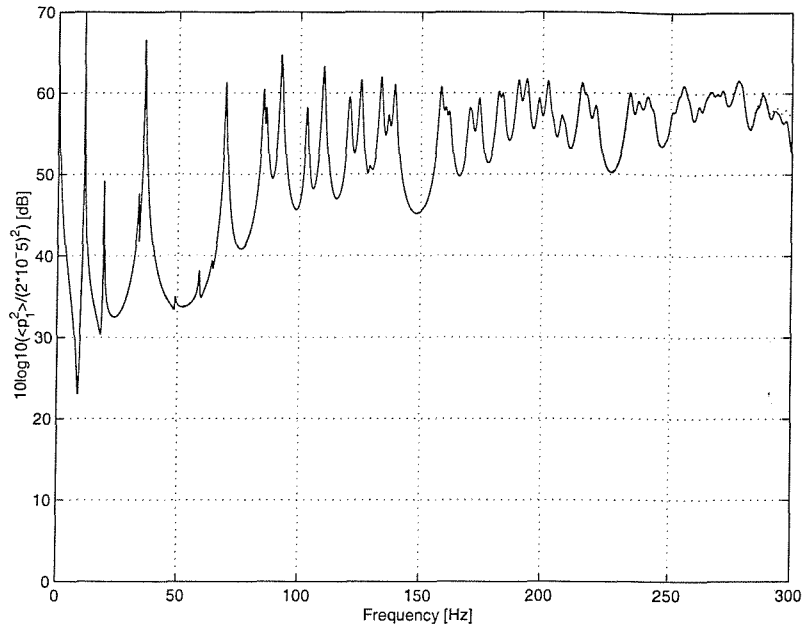

a)

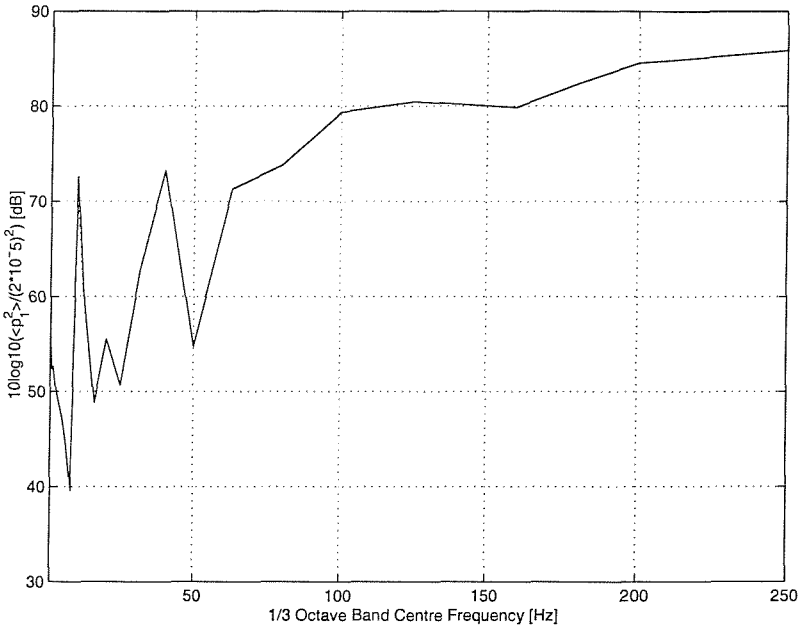

b)

Figure 2.21: Spatial averaged mean square pressure levels [dB re $2x10^{-5}$] in the source room as a function of the number of modes used in the calculation for the source room (model 1). The partition dimensions and mass per unit area are 2m x 2m and 8.1 kg/m^2 respectively. a) narrow bands; b) one third octave bands;_____90 modes; ------ 265 modes.

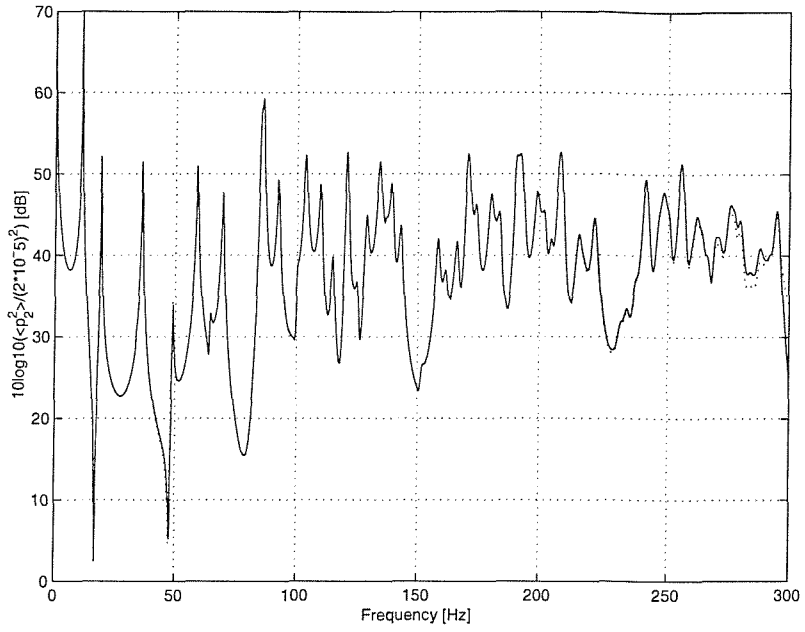

a)

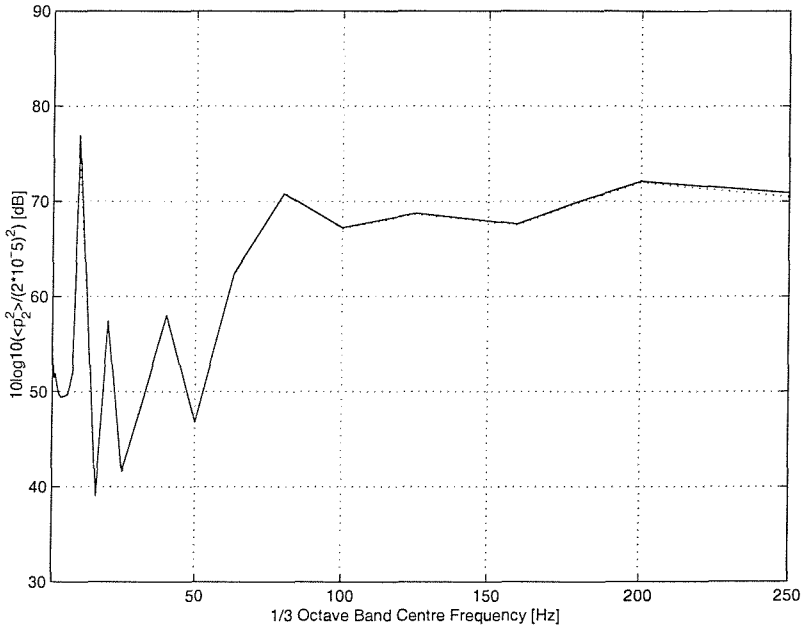

b)

Figure 2.22: Spatial averaged mean square pressure levels [dB re $2x10^{-5}$] in the receiving as a function of the number of modes used in the calculation for the receiving room (model 1). The partition dimensions and mass per unit area are 2m x 2m and 8.1 kg/m^2 respectively. a) narrow bands; b) one third octave bands;_____59 modes; ------ 166 modes.

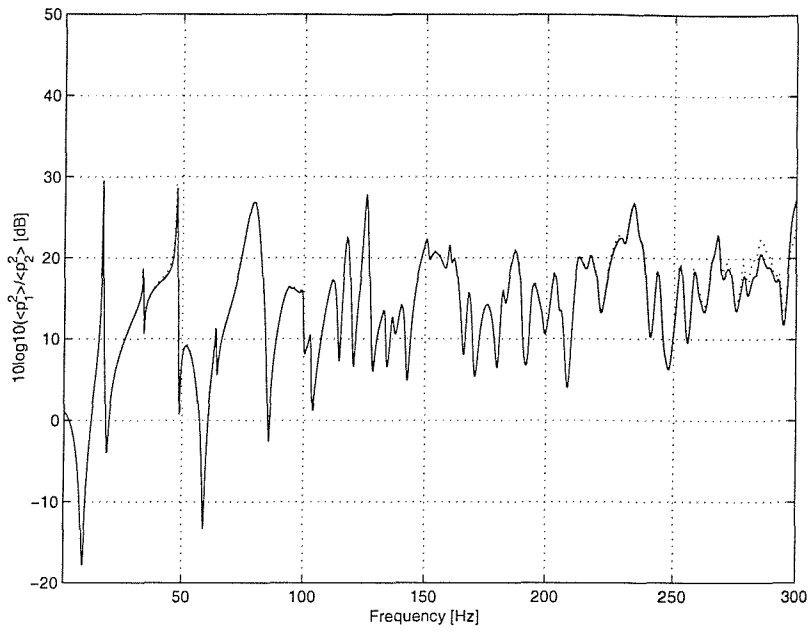

a)

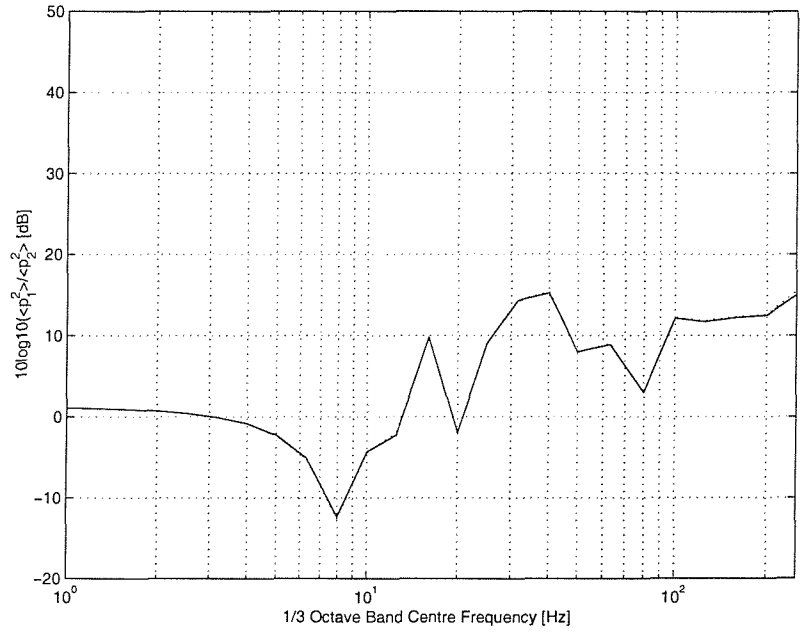

b)

Figure 2.23: Noise Reduction (NR) (model 1). The partition dimensions and mass per unit area are 2m x 2m and 8.1 kg/m^2 respectively. a) narrow bands; b) one third octave bands;_____ total number of modes used = 261; ------ total number of modes used = 606. There is negligible difference except above 200 Hz. The total number of modes consists of both acoustic and structural modes.

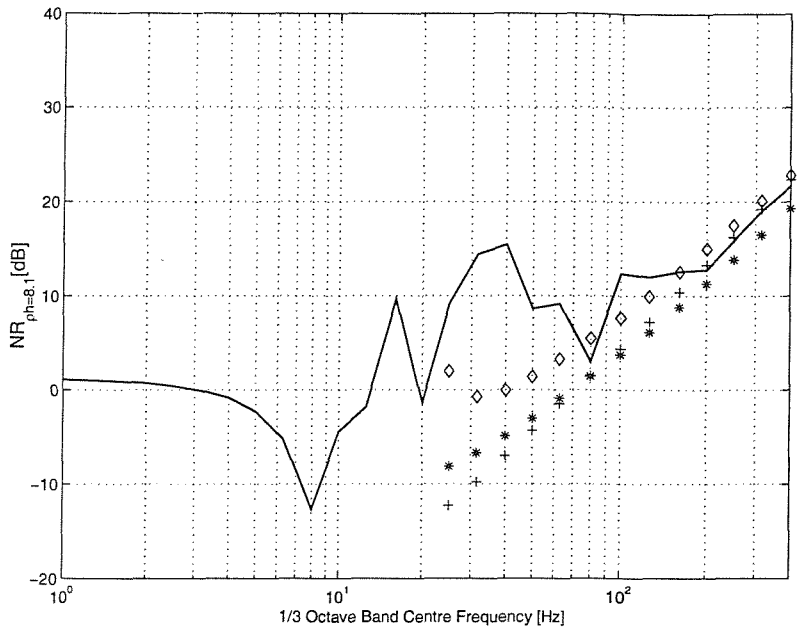

a)

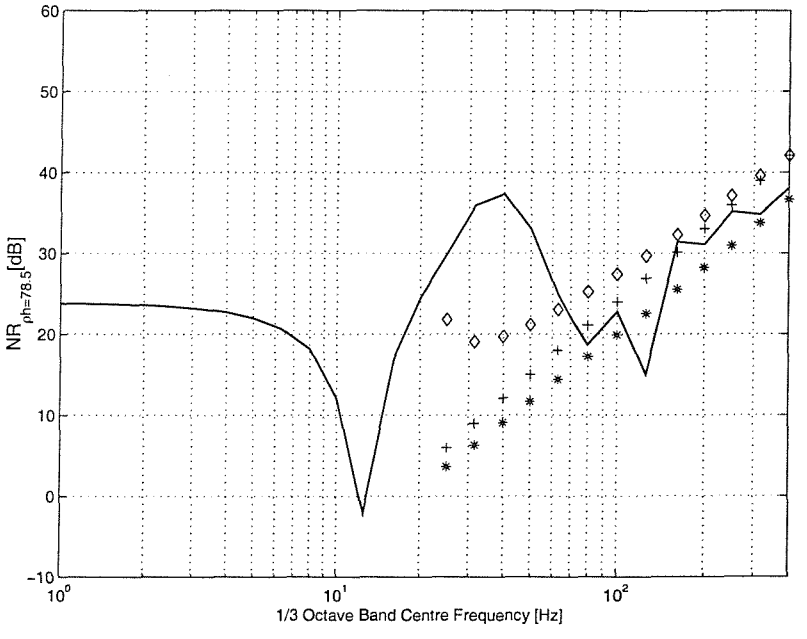

b)

Figure 2.24: Comparison of the Noise Reduction (NR) levels between the modal model 1 (see Figure 2.2a) and the classical methods. a) $\rho h = 8.1 kg/m^2$; b) $\rho h = 78.1 kg/m^2$; _____ Modal model; *** Diffuse incidence Mass Law; +++ Field incidence Mass Law; ◊◊◊ Leppington's prediction.

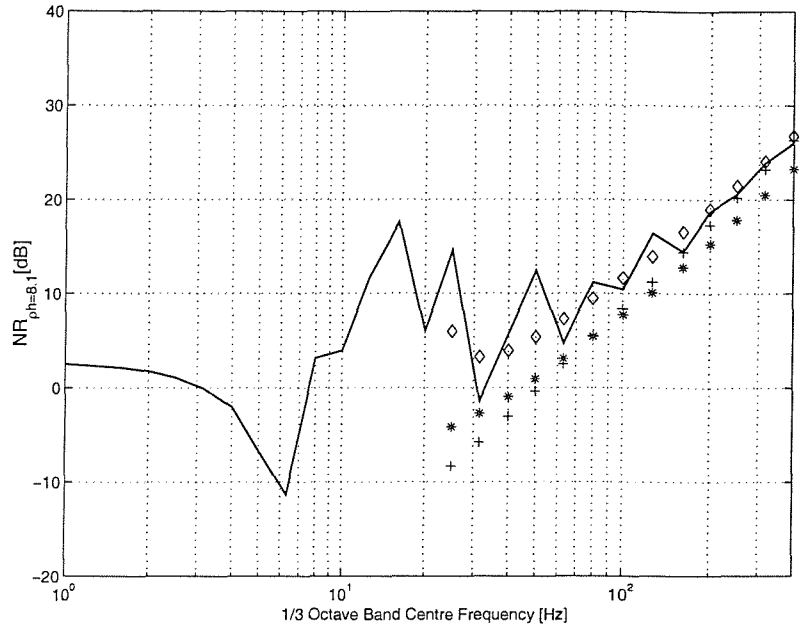

a)

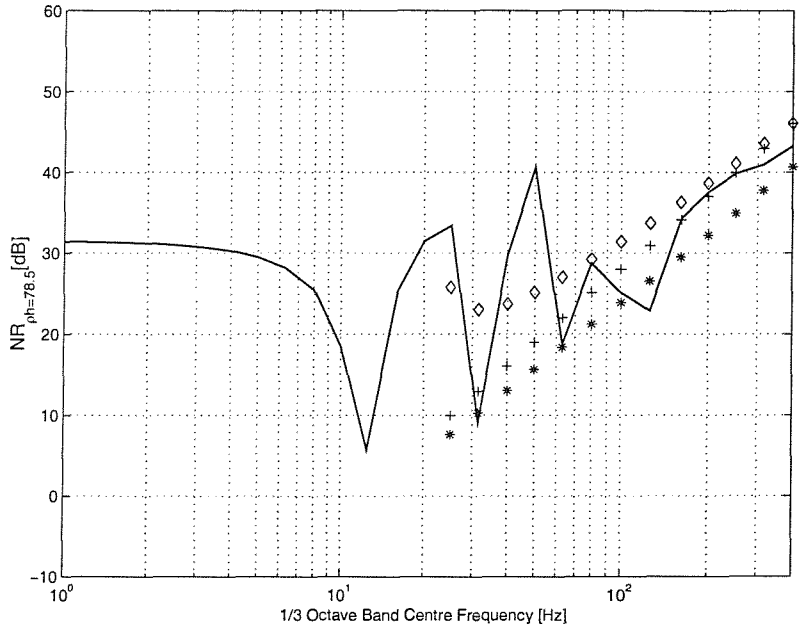

b)

Figure 2.25: Comparison of the Noise Reduction (NR) levels between the modal model 2 (see Figure 2.2-b) and the classical methods. a) $\rho h = 8.1 kg/m^2$; b) $\rho h = 78.1 kg/m^2$; _____ Modal model; *** Diffuse incidence Mass Law; +++ Field incidence Mass Law; ◊◊◊ Leppington's prediction.

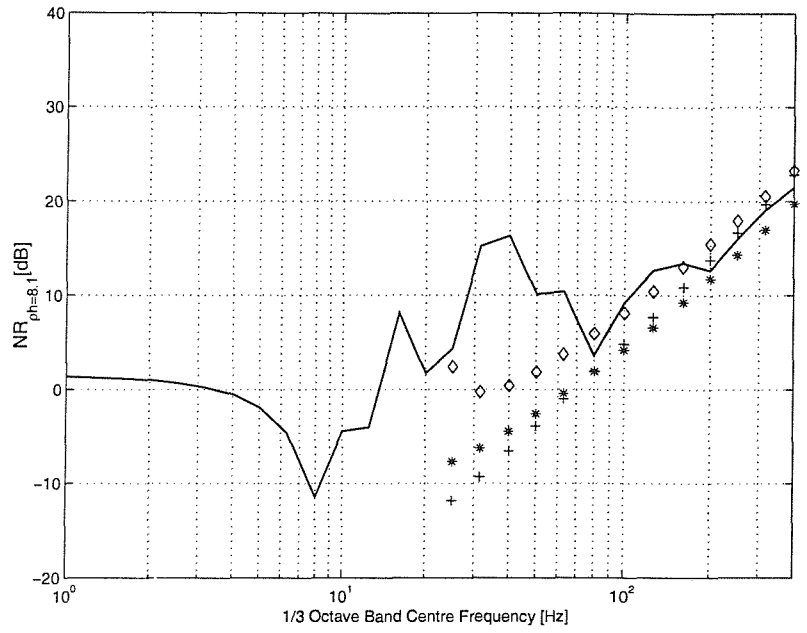

a)

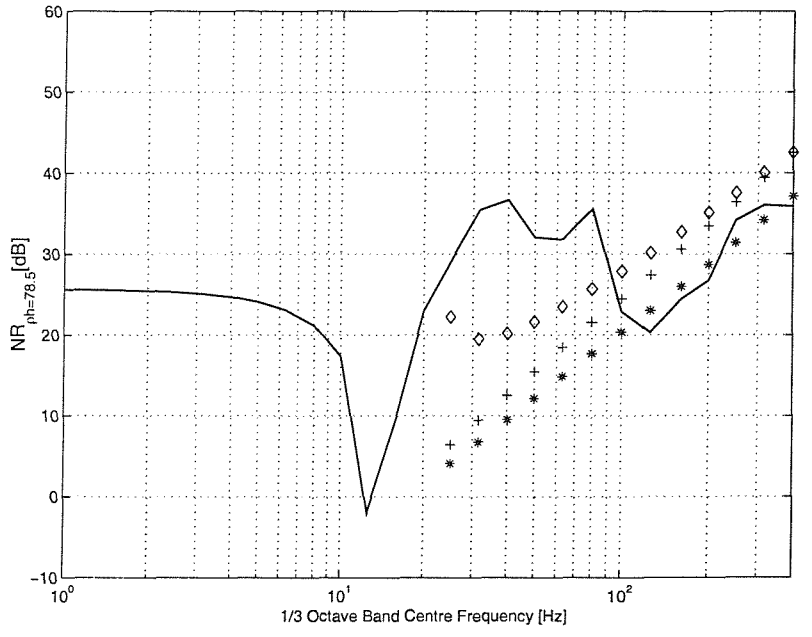

b)

Figure 2.26: Comparison of the Noise Reduction (NR) levels between the modal model 3 (see Figure 2.3) and the classical methods. a) $\rho h = 8.1 kg/m^2$; b) $\rho h = 78.1 kg/m^2$; _____ Modal model; *** Diffuse incidence Mass Law; +++ Field incidence Mass Law; ◊◊◊ Leppington's prediction.

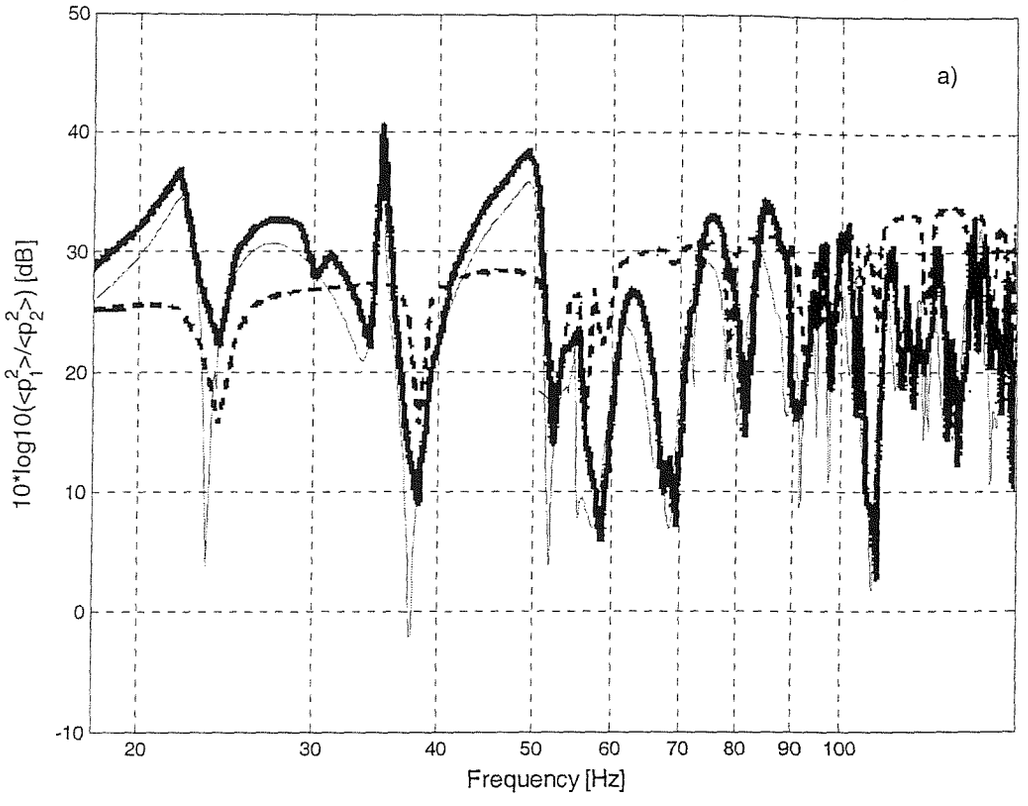

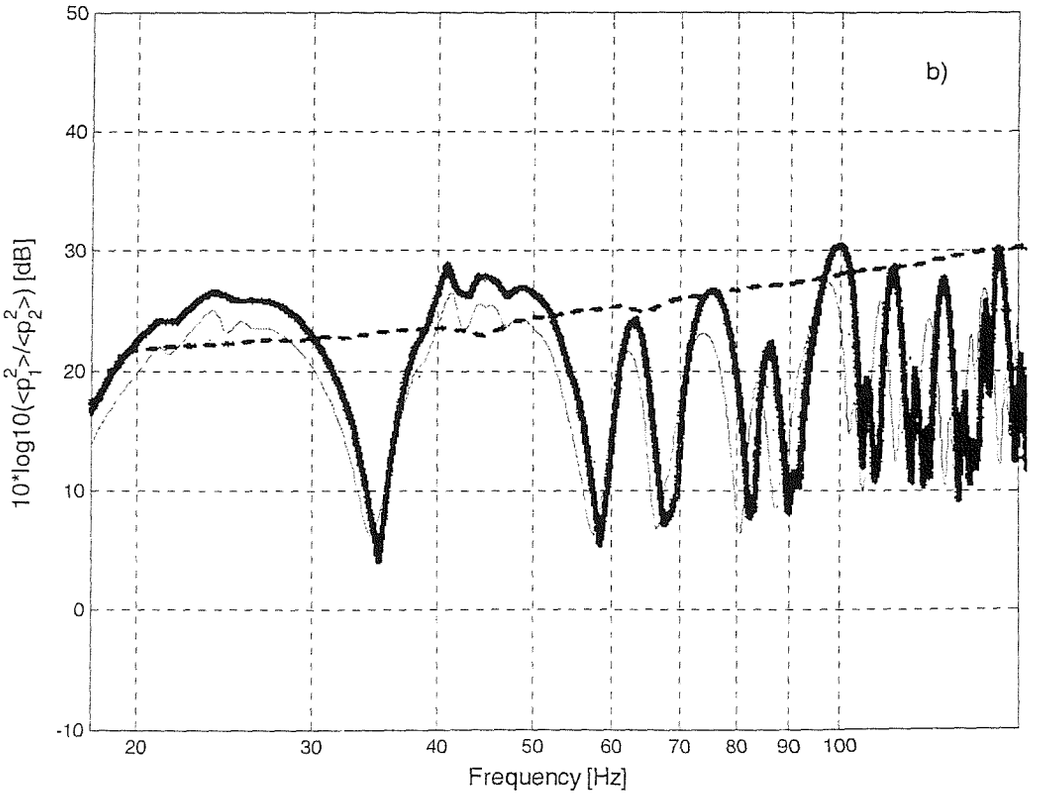

Figure 2.27: Comparison of the Noise Reduction (NR) levels. a) $\rho h = 49.8\,kg/m^2$; b) $\rho h = 28.8\,kg/m^2$; ——— Modal model; ------- Baffled Model [12]; ▬▬ results obtained by Osipov [12].

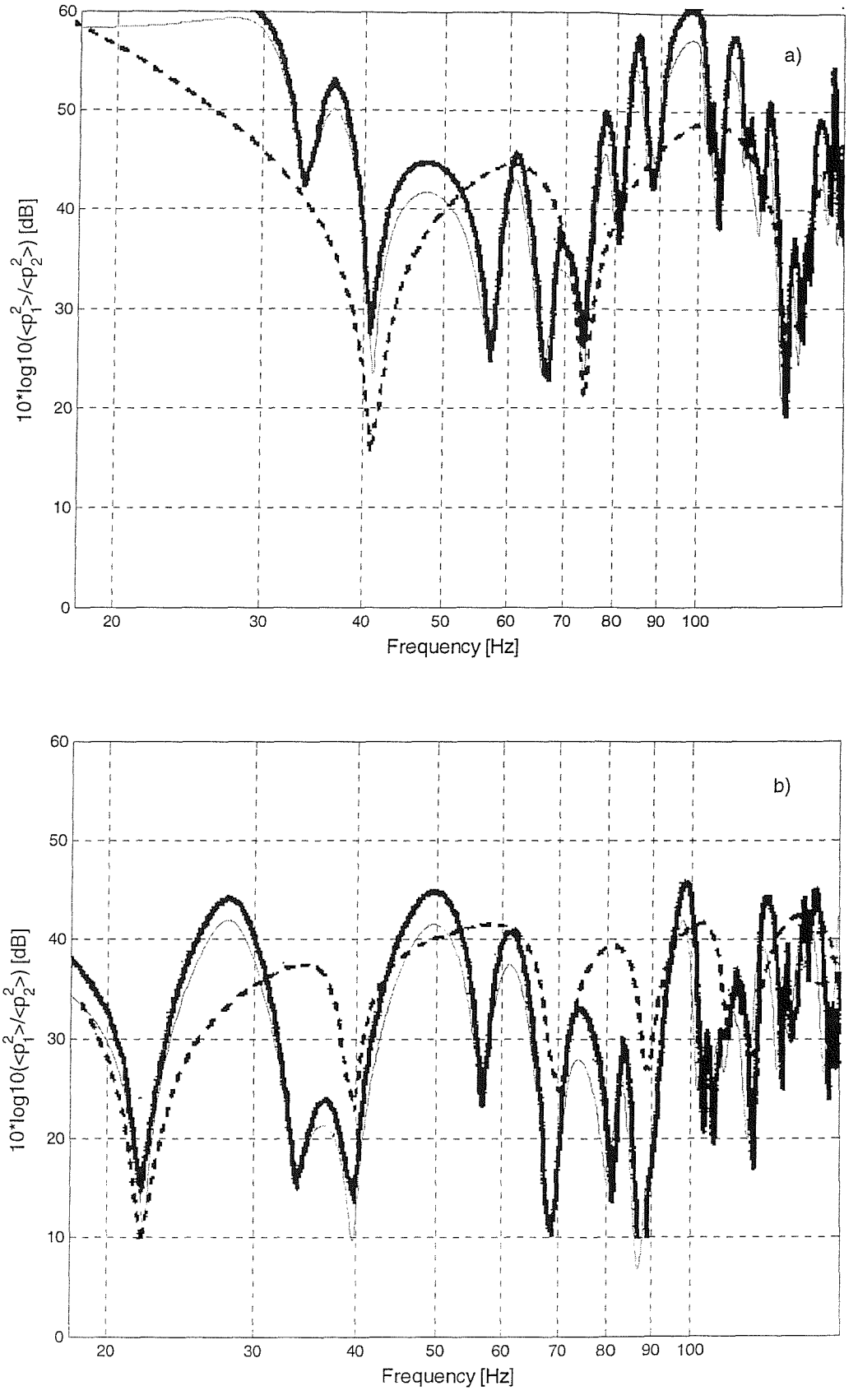

Figure 2.28: Comparison of the Noise Reduction (NR) levels. a) $\rho h = 460\,kg/m^2$; b) $\rho h = 240\,kg/m^2$; ———Modal model; --------Baffled Model [12]; ▬▬ results obtained by Osipov [12].

Chapter 3

EXPERIMENTAL INVESTIGATION OF ACOUSTIC TRANSMISSION

3.1 – Introduction

The focus of this chapter is on the aspects of experimental validation of the model for airborne sound transmission through partitions and data for validation of the predictive models.

The content of this chapter is described as follows. Firstly, the measurement of absorption of rooms, damping of the partition as well as the loudspeaker volume velocity are obtained experimentally. The test procedure and results are presented in section 3.2. In section 3.3, the acoustic behaviour of a single room is investigated by comparing measured results with those obtained analytically. The analysis was a preliminary exercise to the investigation of sound transmission discussed in the subsequent section.

Then, the validation of the transmission room model is presented in section 3.4. In section 3.5 the normal velocity of the panel is determined. Hence, the comparison of the measured result with the predicted is made. In appendix B, statistical analyses of the data are presented in terms of sample mean value and confidence intervals [46]. These statistical parameters are widely used in sound and vibration measurements. The frequency range considered here is based on that for which the previous modal model calculations were developed. Thus, the results presented apply for the frequency range 50 to 250 Hz, for the particular room dimensions and geometry. In order to avoid a signal contaminated by the background level in the very low frequency bands, a lower limit of the third octave with centre frequency 50 Hz was chosen. Finally, discussion and conclusions for the experimental tests are presented in section 3.6.

3.2 – Measurement of damping for the structural partition and rooms

The damping for the structural partition and rooms were obtained by using the Impulse Response Technique [44].

One comparison between the theoretical model and the experimental results is the response near resonance, which is itself mainly influenced by the damping either assumed in the model or that which actually exists in the experiment. Significant errors can be incurred due to poor damping estimates. For this reason, the damping for the structural partition was obtained using two different experimental techniques. In addition, the acoustic room absorption was obtained by measuring the reverberation time for each room. The overview of the experiments, procedures and results are presented below.

3.2.1 The measurement of structural damping

It is known that the total loss factor of a partition depends on the boundary condition of the specimen. In other words, the total loss factor is equal to the sum of the internal loss factor of the material, the coupling loss factor to the adjacent structures and the radiation loss factor to the surrounding media [31]. Therefore, two different techniques were used here namely on a free-free beam and on a panel in-situ. The former primarily gives an estimate of the material loss factor by examining the decay in the response of individual modes, normally restricted to just the fundamental bending mode. The latter is an in-situ approach where one measures the half power bandwidth of the resonances and requires the frequency response functions to be measured.

In the first method the duration of the response (vibration) due to impact excitation, which is characterized by the reverberation time (RT), was measured for the calculation of the structural damping. The reverberation time is defined as the time interval in which the vibration energy level decays by 60 dB. The tests were performed on a free-free beam sample taken from a plasterboard panel. Thus, these tests only measured the material loss factor since the radiation loss factor for the present case (free-free beam) is expected to be very low at low frequencies [5].

The measurement of the damping of the beam samples give a lower bound to damping in realistic configurations where plasterboard is used. The values taken when the plasterboard was tested *in situ* in the acoustic test rooms, with plasticine around the edges, may be higher than practical building configurations but is used in the simulations, which were performed to compare with the experimental results.

The supported span of the beam was 30 cm in length and its cross-section of dimensions 10cm x 1cm. A soft tip on the end of the hammer was used in order to provide the maximum input energy for the frequency range of interest. The position of the supports,

at 1/5 of the beam span in from the ends, were approximately at the nodal points of the fundamental mode of a free-free beam (see Figure 3.1). The force excitation and receiving points were located at opposite ends of the beam as shown in the figure.

The experimental procedure for determination of decay times is described as follows. On impacting a free-free plasterboard beam sample by a plastic headed hammer (type B&K 8202), the analyzer was triggered and started to record the response signal at the receiving point. At the receiving point an accelerometer was attached and connected to the acquisition equipment (a multi-channel HP real-time analyzer type 35650), which filtered the input signal by conveniently configuring the channel parameters.

The signal $s(t)$ received at a receiving point is given by [44]

$$s(t) = \int_{-\infty}^{t} f(\tau) h(t-\tau) d\tau \tag{3.1}$$

where $f(t)$ is input excitation force and $h(t)$ is the impulse response of the system. For an impulse at time t_i one has

$$f(\tau) = F_o \delta(\tau - t_i), \text{ then } s(t) = h(t-t_i) \tag{3.2}$$

The Hilbert transform H of a function $x(t)$ is used to produce the envelope of the signal and subsequently allows determination of the decay rate of the signal. It is given by [47]

$$H(x(t)) = -\frac{1}{\pi} \int_{-\infty}^{+\infty} x(\tau) \left(\frac{1}{t-\tau} \right) d\tau = \frac{1}{\pi} x(t) * \left(\frac{1}{t} \right) \tag{3.3}$$

where * means convolution.

Hence, the amplitude decay curves were obtained by taking the Hilbert transform of the received signal and then converting its absolute value to a logarithmic amplitude scale as follows

$$C(t) = 20 \log_{10} |H(x(t))| \quad \text{in dB} \tag{3.4}$$

A second technique, known as half-value or half-power bandwidth, was used to obtain the total loss factor of a plasterboard partition mounted *in situ* in the opening between the two acoustic reverberation chambers and is sealed around its periphery with plasticine. This does not provide a clamped edge, as it is dependent on the stiffness and adhesion

strength of the plasticine although it does provide a reasonable constraint on the flexural displacement but not slope. Also the values of damping found in this way are sometimes termed structural damping, to identify that the damping is dependent on both the damping inherent in the material and that which comes from other mechanisms including dissipation losses at the boundary which might be significant. First, the frequency response of the partition was obtained via a simple tap test (figure 3.2). The measurements were carried out at different positions, which were carefully chosen in order to avoid the difficulties associated with non-excited modes. Second, the total loss factor was then obtained by the relationship [48]

$$\eta = \frac{b}{f_n} \tag{3.5}$$

where f_n is the measured resonance frequency, approximately equal to the natural frequency for light damping, and b is the corresponding half-power point bandwidth, which is the bandwidth where the amplitude falls to $1/\sqrt{2}$ of its maximum value. This corresponds to a 3 dB reduction. The main limitation of applying equation (3.5) is that it is only valid for small values of damping and for low modal overlap. In other words, the frequency interval between resonance frequencies must be considerably greater than the half-power bandwidth.

The Young's modulus for the partition, which was used in the subsequent calculations, was obtained experimentally from [48]

$$k^4 = (2\pi f_B)^2 \frac{m'}{EI} \tag{3.6}$$

where m' is the mass per unit length of the test beam, which value was equal to 0.683 kg/m, kl is equal to 4.73 (where l is the length of the beam), and f_B is the measured resonance frequency (= 220 Hz) of the fundamental mode.

Therefore, the Young's modulus for the partition calculated using equation (3.6) was 2.53×10^9 N/m^2. This value was used in the subsequent calculations.

Figure 3.3.*a* presents the typical transient excitation obtained from hitting the beam using the hammer. The test was repeated several times in order to ensure that the input signal was free of multiple impacts. The detail of the impact is also shown using a zoomed time window.

The output signal response was acquired over a time duration of 1 *s*, which was long enough for recording the decay (see figure 3.3.*b*).

Figure 3.3.*c* shows the frequency response function (FRF) magnitude, which is the modulus of the ratio of the output signal spectrum to the excitation (input signal) spectrum, assuming no noise. Assuming that the first mode of vibration was dominant, the first resonance frequency of the beam was about f_B = 220 Hz.

Figure 3.3.*d* shows the Hilbert transform of the response in decibels. To determine damping, the T_{60}, which is the time necessary for the vibration level to decay 60 *dB*, was first obtained using the least square method [46] for fitting the best straight line to the data. The use of a best straight line fit to calculate T_{60} assumes diffuse field condition. Nevertheless, for non-diffuse field condition, it is recommended that an ensemble-average estimate of decay rates over a range of different excitation and receiver positions be obtained [18].

In other words, it is clear that at low frequencies a best straight line fit is not particularly appropriate, partly because the field is not diffuse and also few modes contribute and hence it is not normal to use equation (3.7). Nevertheless, as values were necessary in the model, the slopes of the lines were used to give estimates, albeit possibly very approximate, and these have been used in the simulations.

The value obtained was T_{60} = 0.6s. The loss factor parameter η, which is the ratio of energy lost to the reversible mechanical energy during one cycle of vibration, is related to T_{60} by [48]

$$\eta = \frac{\ln(10^6)}{2\pi f_B T_{60}} \tag{3.7}$$

For the free-free beam sample, the experimental value of the loss factor η, using the decay time technique, was hence found to be approximately 0.017.

Figure 3.4 shows the measured frequency response of a square plasterboard partition *in situ*. The first three predicted natural frequencies and modes of a simply-supported plasterboard were about 37.0 Hz, 92.5 Hz and 92.5 Hz, which correspond to the modes (1,1), (1,2) and (2,1) respectively. The panel dimensions were 0.69m x 0.69m and the formula for calculating the natural frequencies of a simply-supported panel is given by equation (2.11). For a clamped square plate, the natural frequencies of the first three

modes are 68 Hz, 139 Hz and 139 Hz. These values are obtained from formulae given in ref. [88]. According to the measured results, the first, second and third resonance frequencies were at approximately 41 Hz, 87 Hz and 96 Hz respectively.

This difference of within approximately 10 % between the values calculated assuming a simply-supported panel and measured results possibly indicates that a mixed boundary condition between free and simply-supported might have been realised experimentally due to the plasticine and fixture. In addition, some measurement errors actually occurred during the experimental test for measuring the total loss factor.

The loss factor obtained via the half-power point bandwidth technique was approximately 0.049 for the first resonance peak. This value was subsequently adopted in the theoretical modal model. It is significantly higher than the sample beam, and it is suspected that the origin of this is most likely to be the high damping and losses at the edges where the plasticine was situated.

3.2.2 The measurement of room absorption

The procedure used for the measurement of the absorption of the rooms was based on the reverberation time values obtained experimentally. In room acoustics, the duration of sound decay is usually characterized by the parameter T_{60}. It is defined by the time interval in which the sound pressure level decays by 60 dB. The amount of sound absorbed by the reverberation room walls can then be found from equation (3.7) using f instead of f_B where f is the centre frequency for the one-third octave bands.

The experimental setup is shown in Figure 3.5. A loudspeaker which had a minimum frequency response of $40Hz$ was driven by a random noise generator. This generator was connected in series with an adjustable analogue pass-band filter (KEMO type VBF8 with working range 0.01 Hz-100 kHz) and a decay time trigger box. The filtered noise was amplified by a power amplifier (type TPA50-D) directly connected to the loudspeaker. At the receiving point, sound pressure measurements were made using a B&K ½" microphone type 4191, connected to a B&K conditioning amplifier type 2609. Furthermore, a multi-channel HP real-time analyzer (type 35650) was used as the acquisition system.

The experiments were set up in an the ISVR acoustic laboratory, where two small reverberant rooms are connected by a common aperture. In order to measure the reverberation time of each room, the aperture was sealed by an isolating heavy stiff

panel. The source and receiving room internal dimensions (in the x, y and z directions) are 2.35m x 2.56m x 2.48m and 2.07m x 2.51m x 2.52m respectively. An aperture is located in the middle of the common wall which is in the (y-z) plane.

All test procedures were based on the International Standard ISO 354 [43] and on the method of integrated impulse response [44,47]. The reverberation time RT was measured for source and receiving rooms that are smaller than ISO 354 requirements. A loudspeaker, driven by a one-third octave band-pass filtered noise, excited the room until steady state condition was reached. The noise source radiated sound into the room for about 3 seconds before initializing the measurements. Nevertheless, a time interval of 2 seconds could be sufficient [44].

As the sound excitation was interrupted, the analyzer was triggered and started to record the signal at a receiving point. The microphone was connected to the acquisition equipment (HP analyzer), which filtered the input signal by conveniently configuring the microphone channel parameters. It was necessary to ensure that the filter pass-band range used in the noise source generator is not less than the one used in the microphone channel [28] and that the measurements were not unduly influenced by the response time of the filter.

Likewise in the procedure described previously, the decay curves here were obtained by taking the Hilbert transform of the received signal and converting its absolute value to a logarithmic amplitude scale. Previous work had shown that the decay rate of the acquisition system, including the filter, was shorter than the decay times being measured of the physical (acoustic) system and so would not interfere by producing artificially long decay times.

It has been recommended [28] that the reverberation time should be taken as three times the time necessary for the noise decay from 5 to 25 dB below the mean level. Therefore, spurious results that do not lie within this range were rejected. An acquisition time of two seconds was adopted.

Figures 3.6-3.9 show typical decay curve sets for the source and receiving rooms measured over one-third octave band centre frequencies. The reverberation time RT was then calculated from the best fitting straight line, obtained by the least-square method, from the Hilbert transform of the transient response. Figures 3.6 and 3.7 show typical decay curves obtained at one-third octave bands for the source room. For instance, in the one-third octave band with centre frequency at 63 Hz, only two modes (natural

frequencies equal to 65 Hz and 68 Hz) exist within the band. This situation is significant because it can produce spurious results. The presence of only two modes in a band might lead to irregular decays caused by beating between these two modes. For the one-third octave bands with centre frequencies 80 Hz and 100 Hz, one and three modes exist within these bands respectively. For instance, within the band with centre frequency 80 Hz the results are solely dependent on the modal characteristics of the mode (1,0,0) of the room.

Likewise, Figures 3.8 and 3.9 present the typical decay curves obtained in one-third octave bands for the receiving room.

According to ISO 354 [43] the recommended total number of measurements are twelve decays for one-third octave band centre frequencies ranging between 63 Hz and 250 Hz. As the reverberation time of a room, at very low frequencies, depends to a large extent on the position of the source and the receiving microphone, an ensemble averaging procedure, based on a combination of microphone positions was applied for each one-third octave band result.

Figures 3.10 and 3.11 show the T_{60} mean values, obtained from the decay rate measurements, for both rooms. According to equation (2.1) and considering an average T_{60} equal to 1.5s and 1.0s for the source and receiving rooms, the corresponding Schroeder frequencies are 634 Hz and 553 Hz. In addition, the upper and lower 95 % confidence limits (defined in Appendix B) are shown in the Figures. It appears that generally the variation in the RT lines is not too poor considering the difficulty in repeating the measurements and the variations introduced in the subsequent data processing and curve fitting. The reverberation time values are quoted in Table 3.4.

3.3 – Preliminary experimental test: sound field in a single room

3.3.1 –Measurement of the source volume velocity

In order to compare the measured and predicted results, the source volume velocity used in the experimental test has to be known *a priori*. Thus, a loudspeaker placed in the corner of a room was chosen. The loudspeaker position was (-211 cm, 20 cm, 20 cm) using a (x,y,z) coordinate system. The sound source and its volume velocity was then obtained using a laser vibrometer. It could not be assumed that the source acted as a

simple monopole with its output directly related to the voltage supplied. Figure 3.12 shows the experimental set-up for the measurements.

The source volume velocity was obtained by measuring the instantaneous surface velocity of the loudspeaker , which was driven with steady broadband noise, using a Scanning Laser Doppler Velocimeter (SLDV). It consists of a scanning head and a vibrometer controller.

The measurement was made as a beam of laser light was directed to the target point and the Doppler-shifted wavelength of the reflected light measured automatically [49]. A sequence of single point measurements across the surface of the loudspeaker was made by defining the scan points to be targeted by the laser.

Figure 3.13 shows the coherence for the transfer function H_1, which relates the velocity of the speaker to the voltage fed to it. It can be seen that at frequencies less than 50 Hz and greater than 300 Hz, the coherence function indicated poor correlation between the input voltage and the output velocity signal. This was partly due to the size of the loudspeaker design, making it difficult to obtain significant response at low frequencies. Likewise, poor coherence was also observed at frequencies greater than about 350 Hz, which might either be due to the loudspeaker response or optical difficulties in obtaining a good laser reflection.

Figure 3.14 shows the transfer function H_1 in terms of its amplitude and phase. According to the results, a peak value occurred at about 100 Hz. This was due to the mechanical resonance of the loudspeaker.

Figure 3.15 shows the measured power spectrum of the loudspeaker vibration volume velocity. The volume velocity of the loudspeaker was calculated by multiplying its spatially averaged vibration velocity amplitude by its circular surface area. The result also illustrates the increased values at about 100 Hz.

Alternatively, the source sound power could have been determined using the power balance equations [8] involving the reverberation time measurements and average mean square sound pressure in the room.

Figures 3.16 and 3.17 show the variation of vibration velocity amplitude over the loudspeaker cone at 100 Hz and 200 Hz respectively. A circular grid was defined over the loudspeaker contour. At low frequencies, a cone loudspeaker mounted in a cabinet vibrates and radiates as a monopole source [18]. Figure 3.16 shows the non-uniform

velocity distribution over the loudspeaker at the one-third octave band centre frequency equal to 100 Hz. The spatial variation of the surface velocity was certainly not uniform, due to the mechanical resonance of the loudspeaker at approximately 100 Hz. On the other hand, Figure 3.17 shows a more uniform velocity distribution over the scanned area in the one third octave band centred at 200 Hz.

3.3.2 – Overview of the experimental test and measurement procedures

Although the experimental validation of a single-room modal model using frequency response measurements was difficult and time consuming, it was appropriate to consider this simpler generally accepted case first in order to obtain an overview for the two-room modal model used later in section 3.4.

The mean square sound pressure was measured at six different positions inside the room using B&K $^1/_2$ inch microphones (type 4165). The microphone positions in the room are illustrated in Figure 3.18. Their coordinates inside the room are listed in table 3.1. Although acoustic transducers (microphones and microphone pre-amplifiers) and microphone conditioning amplifiers are calibrated during their manufacture, small adjustments for the sensitivity factors are still necessary. Therefore, a sound level calibrator was used to check the sensitivity of each microphone before each measurement. After executing all measurements, another calibration procedure was repeated.

The separating distances between microphones and microphone position and room boundaries were less than the minimum values required by the ISO 140 standard [41]. It is recommended that an averaging time of at least six seconds be used for measurements made at frequencies below 500 Hz. However, a minimum value of fifteen seconds, which is the time required for the 50 Hz centred third-octave band, was used [41].

It is known that the measurement of sound pressure at low frequencies in a room is complicated due to a distinct spatial predominance of some modes in a specific bandwidth driven at resonance. Thus, a spatial average value for sound pressure level in a small room is difficult to obtain experimentally.

The sound source operated at a corner opposite to the test partition, in order to increase the contribution of the oblique modes [50]. A generated signal equivalent to 'white' noise was used. The noise was filtered by using a pass band which corresponds to the one used in the microphone channel. The mean square sound pressure was measured

with a resolution of 0.5 Hz and the data was acquired from 0 Hz to about 500 Hz. In addition the microphone conditioning amplifiers provided additional gain in order to optimise or improve the signal to noise ratios. This ensured that the frequency range for the analysis was covered with extra information if required.

Alternatively, forms of frequency response functions or FRFs could also have been used in order to characterize the system dynamic behaviour [51].

3.3.3 –Results

The predicted results were obtained using a modal model based on equation (2.39) shown in Chapter 2 without the term containing the generalized coordinate $\dot{w}_p$, which is on the right-hand side of the equation. A total of 278 modes for the room were considered for the prediction of the frequency response. The first three predicted natural frequencies and modes of the room are 65 Hz, 68 Hz and 74 Hz, which correspond to the modes (0,1,0), (0,0,1) and (1,0,0) respectively.

Figure 3.19 shows a comparison between the spatially averaged measurements of SPL in a single room (dB re $2x10^{-5}$ Pa) and the background noise in the room. It is seen the higher peaks in the background noise occurred at frequency multiples of 50 Hz (e.g. 100 Hz, 150 Hz, etc.). This phenomenon was due to the background mains interference noise picked up by the microphone conditioning amplifiers. Nevertheless, this fact did not invalidate the measurements, as all peak values were at least 30 dB below the measured signal.

Figures 3.20-3.25 show comparisons between the levels of measured and predicted sound pressure levels, for different measurement positions inside the room. The measured source volume velocity was used as the source excitation in the modal model. It was determined from the measurements of the voltage PSD to the loudspeaker and the relationship between this and the volume velocity of the loudspeaker itself, determined from the spatially averaged surface velocity. The results are presented in narrow and one third octave bands.

For the results in narrow bands, it is seen that fair agreement between the measured and predicted values occurred over most of the frequency range. For the results presented in one third octave bands, a maximum difference of less than 5dB occurred in most of the frequency bands.

In general, the peaks and dips displayed in the results correspond to the contribution and the interaction of the individual room modes. Although the predicted and the measured values at the corner positions show good agreement at very low frequencies, a shift in level between the measurements and simulations occurred as the frequency increases. Such differences may be explained by the sensitivity of the results to the measurement errors on estimating the actual loss factor. However, the PSDs followed similar trends over most of frequency range.

Figure 3.26-a and 3.26-b present the variation of the SPL values (dB re $2x10^{-5}$ Pa) from the mean value at positions P_1-P_6 for the predicted and measured values respectively. The mean value was determined by averaging the squared pressure amplitudes. It is seen that at 50 Hz the values diverge from the mean for both the measured and predicted results. For frequencies ranging from 63 Hz to 100 Hz, the measured values show greater variation in comparison with the theoretical results. However, as the frequency increases, the variation tends to decrease for both set of results.

Finally, Figure 3.27 shows a comparison between the measured and predicted spatial averaged mean squared sound pressure levels (dB re $2x10^{-5}$ Pa). The averaged values were obtained by calculating the arithmetic mean value over all positions. Within the usual tolerance of acoustic measurements the agreement is quite good.

3.4 – Experimental validation of the modal model - two rooms coupled by a single-leaf partition

3.4.1 –Test facilities and equipment

The sound transmission experiments performed and reported herein were made in the ISVR teaching laboratory. A plasterboard single leaf partition was fitted in the test opening located in the middle of the common wall. The square partition dimensions were 0.69m x 0.69m and thickness 0.01 m respectively. The partition surface was recessed by 43 cm from the wall in the receiving room. It was flush with the source room surface.

A laser vibrometer (SLVD) was used to measure the instantaneous velocity of a loudspeaker with a minimum frequency response of 40 Hz. The loudspeaker, driven by a random noise generator, was connected in series with a band pass filter (type KEMO VBF8 covering 0.01 Hz-100 kHz). In addition, a power amplifier type TPA50-D was

directly connected to the loudspeaker. The sound pressure measurements were made using B&K free-field ½'' inch microphones (type 4191), connected to B&K microphone conditioning amplifiers (type 2609). A multi-channel HP real-time analyzer (type 35650) was used for simultaneously recording sound pressure signals filtered in both rooms. Before each measurement, the entire arrangement was checked and calibrated using a B&K calibrator.

A general diagram of the test facilities, including transducers and instrumentation for noise measuring is shown in Figure 3.28.

3.4.2 – Test Procedure

The separating distances between microphones, microphone positions and room boundaries did not agree with the values recommend in ISO 140 [41] due to the small dimensions of the rooms. The coordinates of microphone positions are listed in Tables 3.2 and 3.3. Figure 3.29 shows the configuration of the microphones inside both rooms. Eight and two microphone positions were selected for the source and receiving rooms respectively.

Figures 3.30 and 3.31 show the comparison between the typical measurements of SPL and the background noise for the source and receiving rooms respectively. Figure 3.30 shows that the noise floor level (background noise) in the source room was at least 20 dB below the spatially averaged sound pressure level measured. On the other hand, Figure 3.31 shows that the background noise level measured in the receiving room was relatively high in comparison with the measured signal (spatially averaged sound pressure level). In addition, the loudspeaker system was not powerful enough in order to generate higher sound pressure levels in the source room.

Therefore, due to the poor signal-to-noise response in the receiving room, only two different positions were selected for the receiving room, specifically at the corners, in order to increase the contribution from the oblique modes. As in the single room test, a generated random signal was used. The noise was also filtered by using a pass band which corresponds to the one used for the microphone channels. The frequency response spectra were measured with a resolution of 0.5 Hz.

3.4.3 –Results

The measured and predicted results were estimated in narrow and one third octave bands varying from 50 to 250 Hz. A total of 278 and 254 modes were used in the modal

analysis for source and receiving rooms respectively. The first three predicted natural frequencies and modes for the source room were 65 Hz, 68 Hz and 74 Hz, which correspond to the modes (0,1,0), (0,0,1) and (1,0,0) respectively. For the receiving room, the first three predicted natural frequencies and modes were 68 Hz, 68 Hz and 81 Hz, which correspond to the modes (0,0,1), (0,1,0) and (1,0,0) respectively. For the partition, a total of 8 modes were incorporated. As mentioned previously, the first three natural frequencies and modes, considering a simply-supported partition, were about 37 Hz, 92 Hz and 92 Hz, which corresponded to the modes (1,1), (1,2) and (2,1) respectively. The critical frequency for the partition was approximately 3190 Hz.

One of the most important checks for any experimental test is the one which tests the repeatability of a set of measurements. Repeatability is defined as the closeness of agreement between uncorrelated test results obtained under the same laboratory, equipment set-up and methodology [34]. Although the repeatability parameter defined in ref. [34] has not been directly calculated here, confidence intervals derivable from a set of 10 measurements were considered for each one-third octave frequency band (see Figures 3.32-3.34). It is seen that the confidence interval for the SPL measured in the source and receiving room indicates that greater variations from the mean value occur in the receiving room. This higher variance may be due to variations in temperature and/or changes in the setup conditions in order to measure the response at different points. In addition, lower signal levels are generally difficult to measure accurately because of the contribution of background noise.

The sound pressure was measured using microphones in the source (at positions P_1-P_8) and receiving rooms (at positions P''_1 and P''_2). Figures 3.35-3.42 show a comparison between the measured and predicted sound pressure levels (dB re $2x10^{-5}$ Pa) at eight different positions in the source room.

For the narrow band results, a reasonable agreement is obtained between the curves at very low frequencies. Although the predicted and the measured values at the corner positions in the source room show good agreement, especially at very low frequencies, a shift in level between the measurements and simulations occurred as the frequency increases. In general, the curves followed similar trends over most of the frequency range, similar to the single room model. The resonance peaks can be reasonably well identified within the frequency range considered. On the other hand, at frequencies greater than about 250 Hz, the resonance peaks begin to overlap.

For instance, at position 6 (Figure 3.40) the first resonance peak is at about 68 Hz, which corresponds to second acoustic mode (0,0,1) in the source room. The second peak is at about 75 Hz, which corresponds to the third acoustic mode (1,0,0). At position 7 (Figure 3.41), which is in the middle of the room, the pronounced peak at 131 Hz corresponds to the first acoustic symmetric mode (0,2,0).

In summary, for the results in one-third octaves, it is seen that between 50 Hz and 100 Hz, a variation of about 10 dB is obtained between the curves. On the other hand, above 150 Hz, a maximum difference of 5 dB is obtained for most positions.

Figures 3.43 and 3.44, which present the Power Spectrum in terms of sound pressure for the receiving room, show poor agreement between the predicted and measured responses for some parts of the spectrum. It appears that those discrepancies are closely related to the structural response of the partition. The generally weak measured response of the acoustic field in the receiving room can be explained by the fact that the antisymmetric modes have not been sufficiently excited due to the partition position in the middle of the separating wall, which corresponds to a pressure node of those modes.

The deviation of the predicted values from those obtained experimentally may also be due to the poor signal-to-noise ratio values obtained. Moreover, the difficulty in assessing the absorption and the flanking paths for the vibration transmission might have contributed to the poor agreement between the measured and predicted response in the receiving room. For the results in one third octave bands, it is shown that a maximum difference of about 15 dB was found between the measured and predicted results in frequency bands above 100 Hz.

Figures 3.45 and 3.46 present the variation of the sound pressure level values averaged over all microphone positions for the source and receiving rooms respectively. A reasonable agreement between the measured and predicted values can be observed over most of the higher frequency range in the source room. Conversely, below 100 Hz, significant variations were obtained. Comparing Figures 3.45 and 3.26, it is seen that better agreement between measured and predicted values are evident for the single room model (Figure 3.26). It can be explained by the fact that it is a simpler model, so that no structural coupling or damping effects are involved into the calculations.

Figure 3.47 shows a comparison between the predicted and measured Noise Reduction. A maximum difference of 15 dB occurs between the measured and predicted results. Between 63 Hz and 100 Hz, a difference of less than about 2 dB is noted in one-third

octaves. It is seen that between 100 Hz and 150 Hz a maximum difference of about 5 dB is found. On the other hand, between 150 Hz and 250 Hz, a maximum difference of about 9 dB is obtained. The main reason for discrepancy within the frequency range considered was due to the poor signal-to-noise ratio in the receiving room, which limited the highest levels of NR that could be observed compared to the predicted values.

3.5 – Experimental determination of the partition normal velocity

Craik [31] theoretically investigated the influence of the partition boundary conditions on the sound transmission. It was found that the resonant transmission contribution below the critical frequency was substantially affected by the partition boundary conditions. In addition, the larger the panel surface area, the lower the transmission due to resonant vibration [54].

3.5.1–Description of the test set-up

Measurements of the frequency response of the partition were made in order to compare it with the theoretical results available from the modal model. As the partition was excited at frequencies below its critical frequency, the response mechanism was characterized by the propagation of forced-bending waves. In other words, the non-resonant forced vibration dominates the sound transmission mechanism. Moreover, the partition was acoustically excited rather than being excited by mechanical forces. Therefore, the radiation efficiency of a partition is greater than that when mechanical excitation is considered [5]. Thus, the mass of the partition was the most important parameter affecting the sound transmission.

The vibration measurements of the surface velocity were made by using a Polytec Scanning Laser Doppler Velocimeter (SLDV). The SLDV measurement set-up consisted of a scanning head and a vibrometer controller as shown in Figure 3.48. The whole area of the loudspeaker and partition were scanned in a relatively short time.

3.5.2 –Results

A total of 8 modes were selected for the simulation of the partition response. The partition critical frequency was about 3190 Hz. Figure 3.49 shows the location of the scanning points at which the partition normal velocity was measured. Figure 3.50 shows the mean square normal velocity distribution over the partition in the one-third octave

band with centre frequency equal to 100 Hz. According to the figure, it appears to represent the second mode of the partition. Figure 3.51 shows the partition normal velocity spectral amplitude over the whole frequency band and the clear dominance of the 80 Hz and 100 Hz contributions.

Figure 3.52 shows a comparison between the measured and predicted mean square normal velocity levels (in dB re 10^{-9} m/s). It is seen that the resonance frequencies obtained experimentally are slightly shifted from those obtained via theoretical simulation at low frequencies. In addition to that, it is clear that the measured frequency response curve shows the contribution due to the resonance frequencies of the room modes. For instance, Figure 3.52 shows a peak at 74 Hz, mode (1,0,0) of the source room. The degree of coupling between the partition velocity and the acoustic pressure modes in the rooms reflects the amount of energy that can be exchanged between these subsystems. Additionally, Figure 3.53 shows the results in one-third octave bands. It is seen that there is generally good agreement between the predicted and measured velocities.

The partition edge condition considered in the modal model was simply supported, which allows rotation of the edges. However, the plasterboard panel used in the experimental test was mounted in the opening using a thick layer of plasticine (± 10 mm) for sealing the edges at the perimeter of the partition. Thus, by analyzing the results obtained, an effect could be due to the change of edge conditions from simply-supported to any other condition, perhaps a mixed edge condition, as it is suspected that the plasticine provides less constraint than the simply-supported case.

It is also known that if the edges were clamped the radiation efficiency would be higher at frequencies below the panel critical frequency. This is equivalent to an enhancement factor of four for the resonant contribution of the power flow [16]. The influence of the recessed depth, which depends on the position of the test specimen in the opening, is an important factor that has not been considered on the simulations (for the measurements made in the ISVR teaching laboratory, this depth was equal to 40 cm). Nevertheless, in the frequency range considered it is unlikely that the partition edges or recess has had any significant effect on the results. Alternatively, the problem with poor signal to noise ratio in the SLVD might have influenced the actual accuracy of the structural response measurements.

3.6 – Conclusions

Experimental test data has been compared with the predictions of the theoretical modal model developed previously for assessing the sound transmission mechanism between two rectangular rooms at low frequencies. The material properties of the partition and sound absorption for the rooms were measured within reasonable experimental accuracy. The values obtained were subsequently taken into account in the simulations. In addition, preliminary sound field measurements in a single-room were made before tests on the coupled two-room model. Good agreement between the modal model and measurements were found for this case. Finally, the experimental investigation considered a room-plate-room configuration, for measuring sound transmission through a plasterboard partition and partition response at low frequency.

According to the findings, it is evident that the partition response was strongly affected by the modal characteristics of the rooms. For instance, Figure 3.52 shows a peak at 74 Hz, which is the natural frequency corresponding to the mode (1,0,0) for the source room. In addition, it seems that the partition edge condition, in particular the mounting of the specimen and the test aperture, might have affected the noise reduction.

It appears that the comparison and validation of the sound transmission model has been clearly influenced by other factors such as a poor signal-to-noise ratio for measurements made in the receiving room, the difficulty of measuring absorption at low frequencies, etc. According to Lang [24], when a random noise source and a real-time analyzer are both used for sound pressure measurements, the background noise can significantly influence the results, especially in the cases of high sound insulation.

At low frequencies (below 125 Hz), the NR values in one-third octaves show reasonable agreement between the measured and predicted results. However, when a direct comparison of the sets of data is made at frequencies greater than 150 Hz, differences of up to 9 dB are found in terms of the NR results.

Therefore, despite the poor signal to noise ratio for practical purposes, the results of this chapter have shown that the conventional theoretical model, developed in chapter 2 gives acceptable results for further investigation of sound transmission in buildings, for example the effect of panel size, position and room geometries.

Tables

Coordinates	X (cm)	Y (cm)	Z (cm)
Mic. position 1 (P_1)	-70.0	70.0	181.0
Mic. position 2 (P_2)	-70.0	70.0	70.0
Mic. position 3 (P_3)	-70.0	192.0	70.0
Mic. position 4 (P_4)	-168.0	70.0	181.0
Mic. position 5 (P_5)	-168.0	192.0	70.0
Mic. position 6 (P_6)	-168.0	192.0	181.0

Table 3.1: Coordinates of the microphone positions inside the source room where the sound pressure levels were measured – (One-room modal model). The origin of the coordinate system (x,y,z) is defined in Figure 3.5.

Coordinates	X (cm)	Y (cm)	Z (cm)
Mic. position 1 (P_1)	-70.0	70.0	70.0
Mic. position 2 (P_2)	-70.0	186.0	70.0
Mic. position 3 (P_3)	-70.0	186.0	181.0
Mic. position 4 (P_4)	-168.0	70.0	181.0
Mic. position 5 (P_5)	-168.0	186.0	70.0
Mic. position 6 (P_6)	-168.0	186.0	181.0
Mic. position 7 (P_7)	-115.0	129.0	125.0
Mic. position 8 (P_8)	-35.0	129.0	125.0

Table 3.2: Coordinates of the microphone positions inside the source room, where the PSDs of sound pressure were obtained – (Two-rooms modal model)

Coordinates	X (cm)	Y (cm)	Z (cm)
Mic. position 1 (P''_1)	70.0	70.0	70.0
Mic. position 2 (P''_2)	168.0	70.0	70.0

Table 3.3: Coordinates of the microphone positions inside the receiving room where the PSDs of sound pressure were obtained – (Two-rooms modal model)

1/3 octave frequency bands – (Hz)	RT_1 (s)	RT_2(s)
63	1.6	1.1
80	2.9	0.9
100	1.5	0.9
125	1.4	1.1
160	1.9	0.8
200	2.4	1.1
250	1.9	1.1
315	2.4	1.6

Table 3.4: Reverberation time RT_1 and RT_2 for the source and receiving rooms respectively. The values are quoted in 1/3 octave bands.

Figures

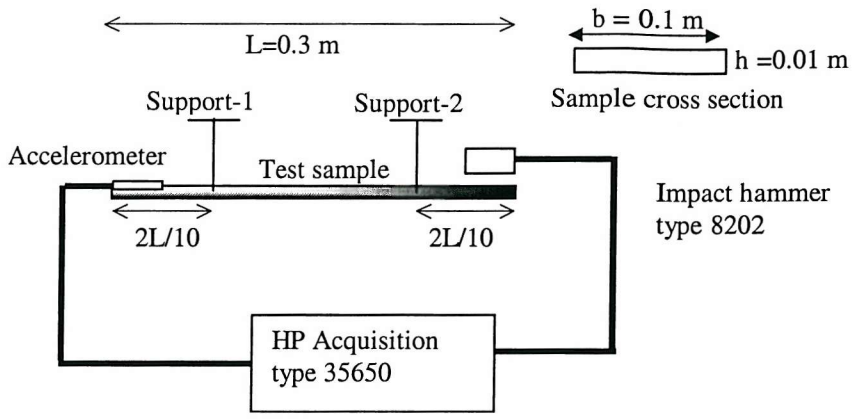

Figure 3.1: Instrumentation used to measure damping constant and the Young's modulus on a freely suspended beam using the decay time technique [48].

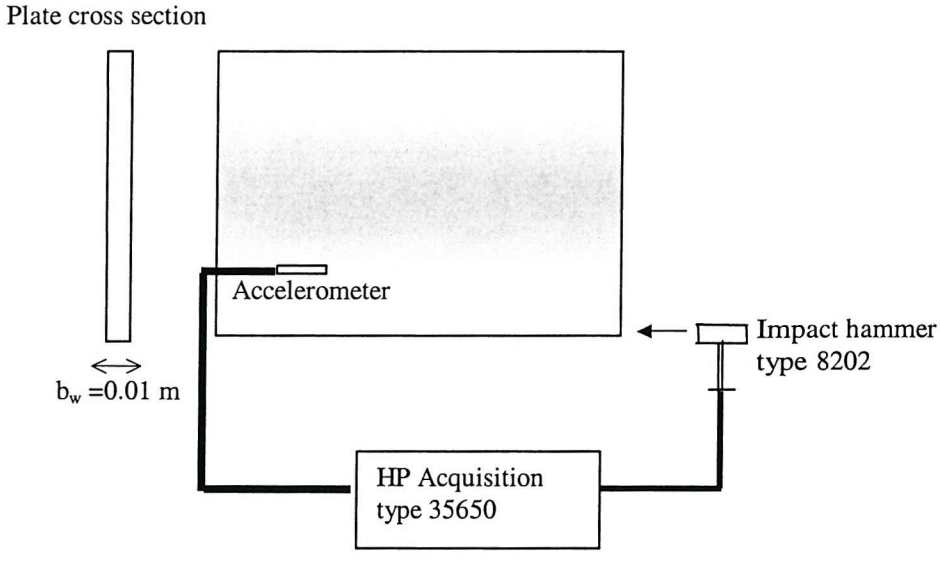

Figure 3.2: Instrumentation used to measure the frequency response of the partition *in-situ* via a simple tap test. The total loss factor is obtained by using the half-power bandwidth technique [48].

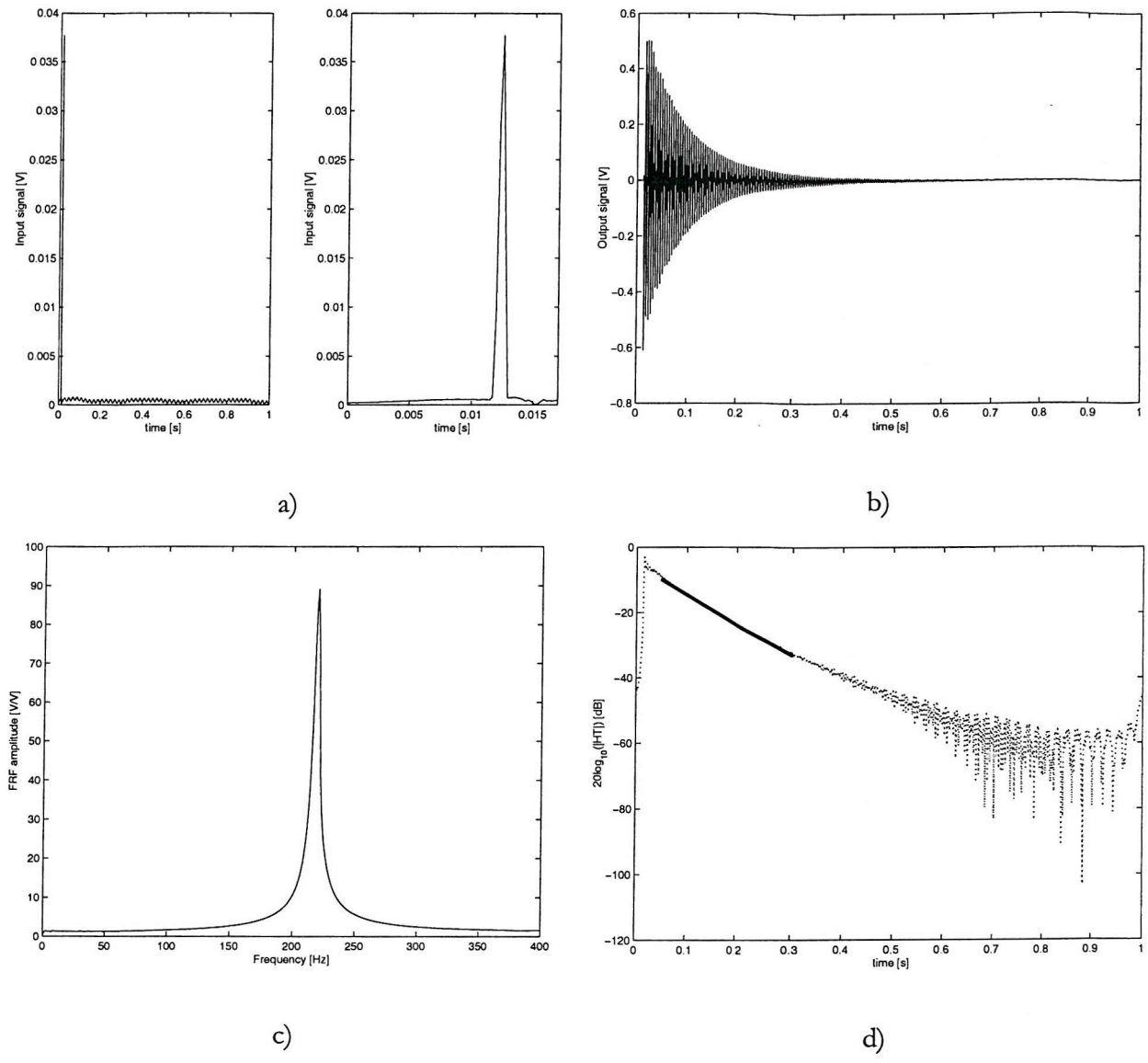

Figure 3.3: Measurement of structural damping for a plasterboard beam. Typical transient excitation (a), response time history (b) and a transfer function (TF) derived from them using Fast Fourier Transform (FFT) ratio (c). The Hilbert Transform (HT) of the response is also presented (d).

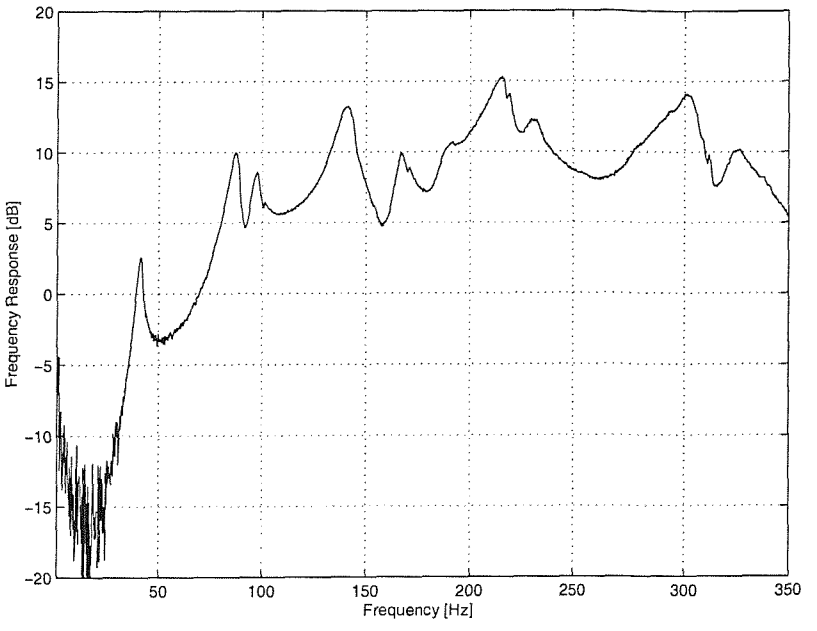

Figure 3.4: Frequency response of the plasterboard (in situ) due to an impact excitation.

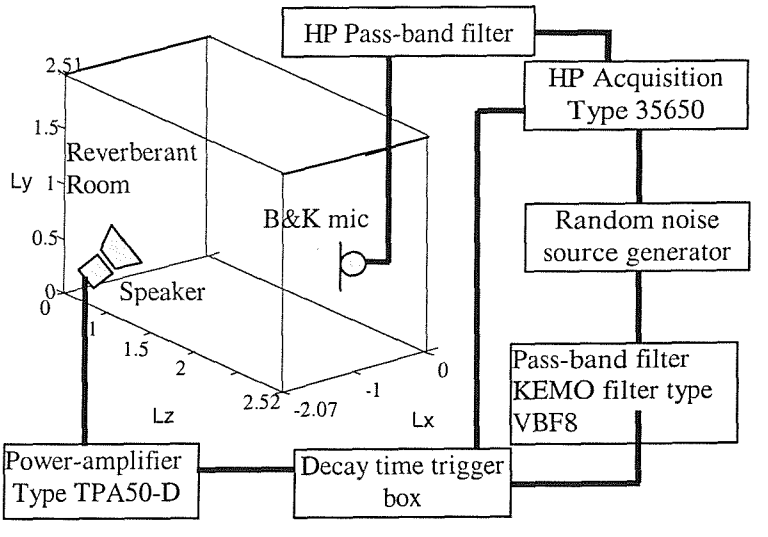

Figure 3.5: Instrumentation used to measure the Reverberation Time of rooms.

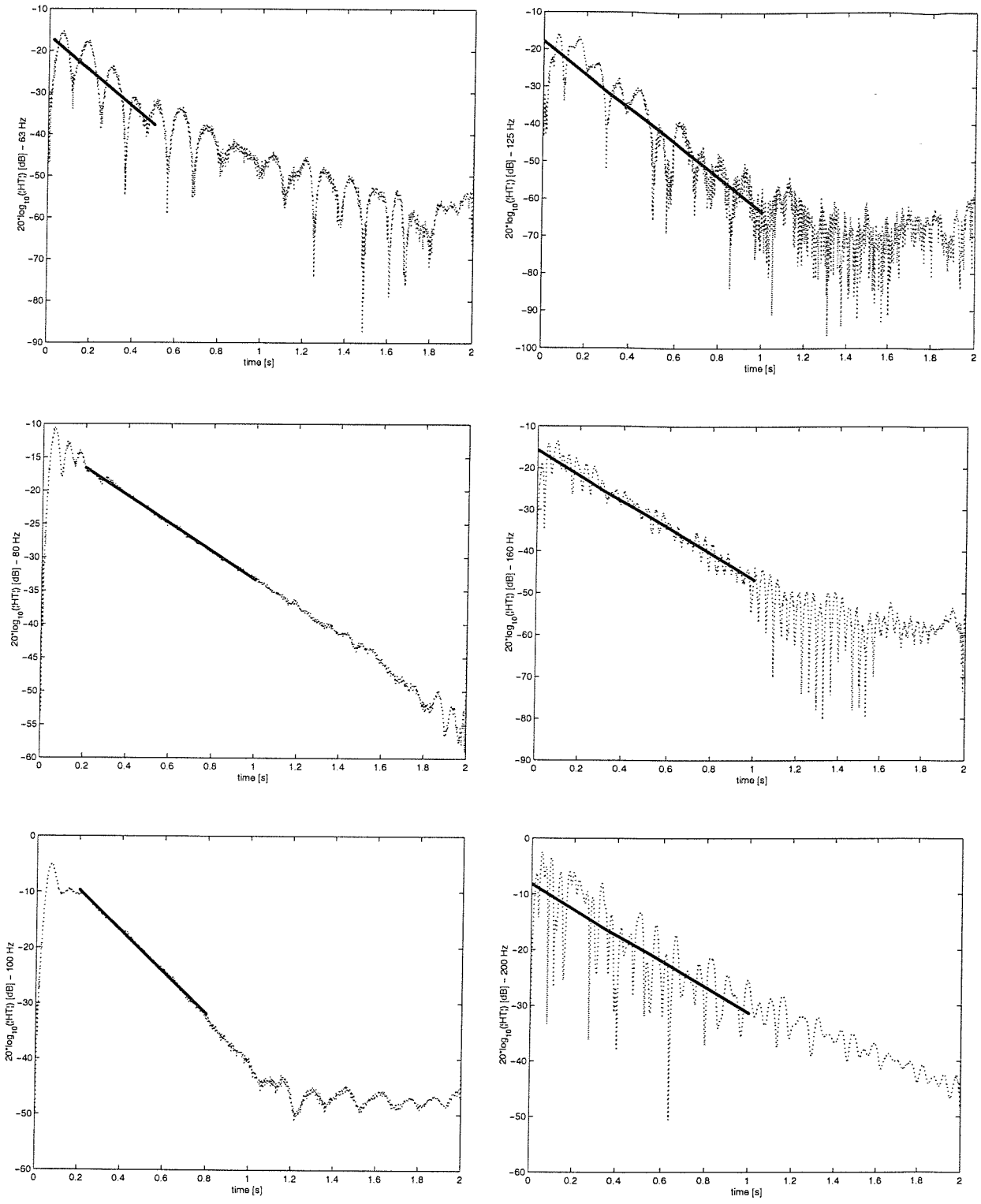

Figure 3.6: Typical decay curves obtained at the one-third octave band centre frequencies 63 Hz , 80 Hz , 100 Hz, 125 Hz, 160 Hz, and 200 Hz for the source room. Hilbert Transform (HT) of the Impulse Response is subjected to the best fitting straight line.

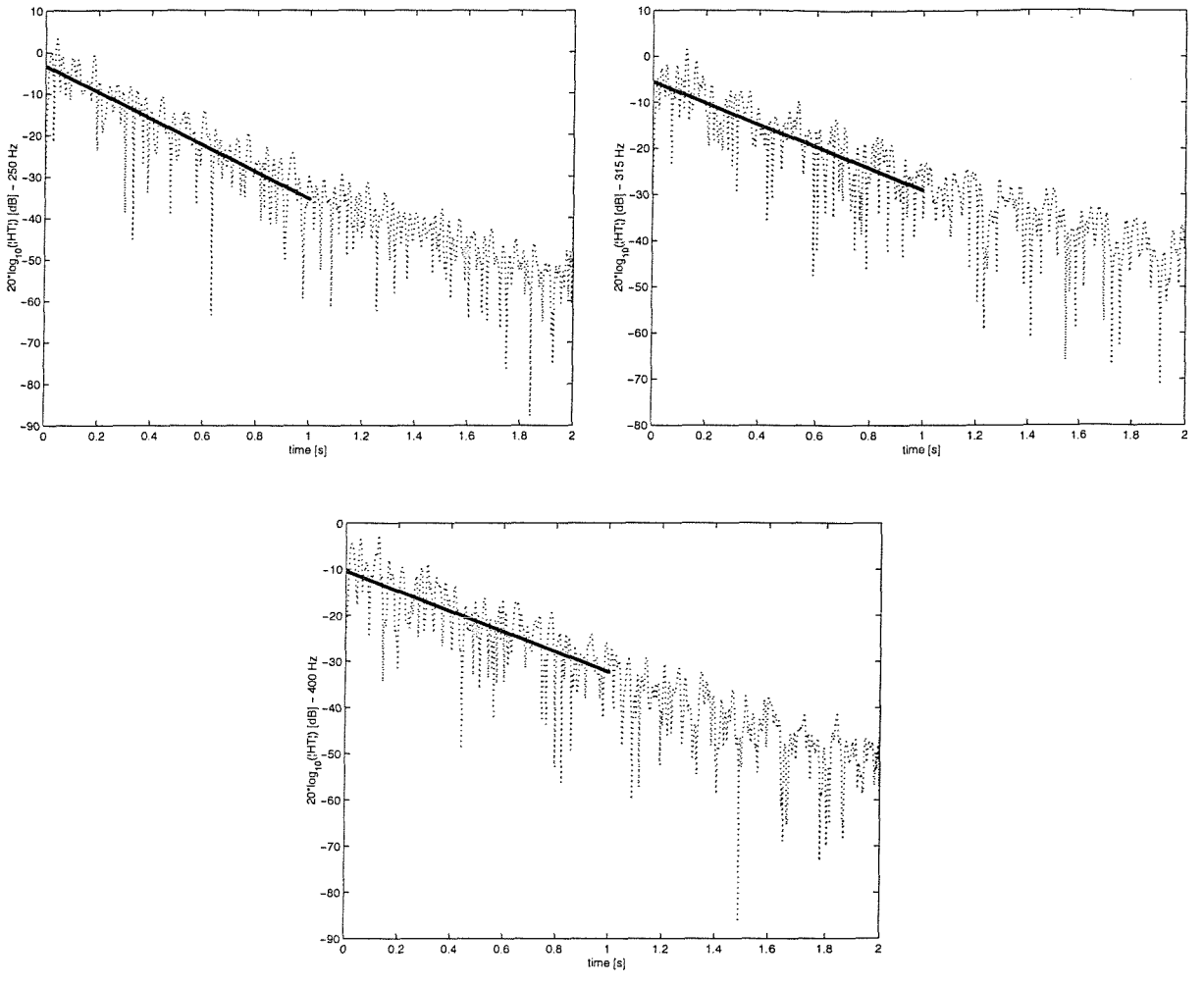

Figure 3.7: Typical decay curves obtained at the one-third octave band centre frequencies 250 Hz, 315 Hz and 400 Hz for the source room. Hilbert Transform (HT) of the Impulse Response is subjected to the best fitting straight line.

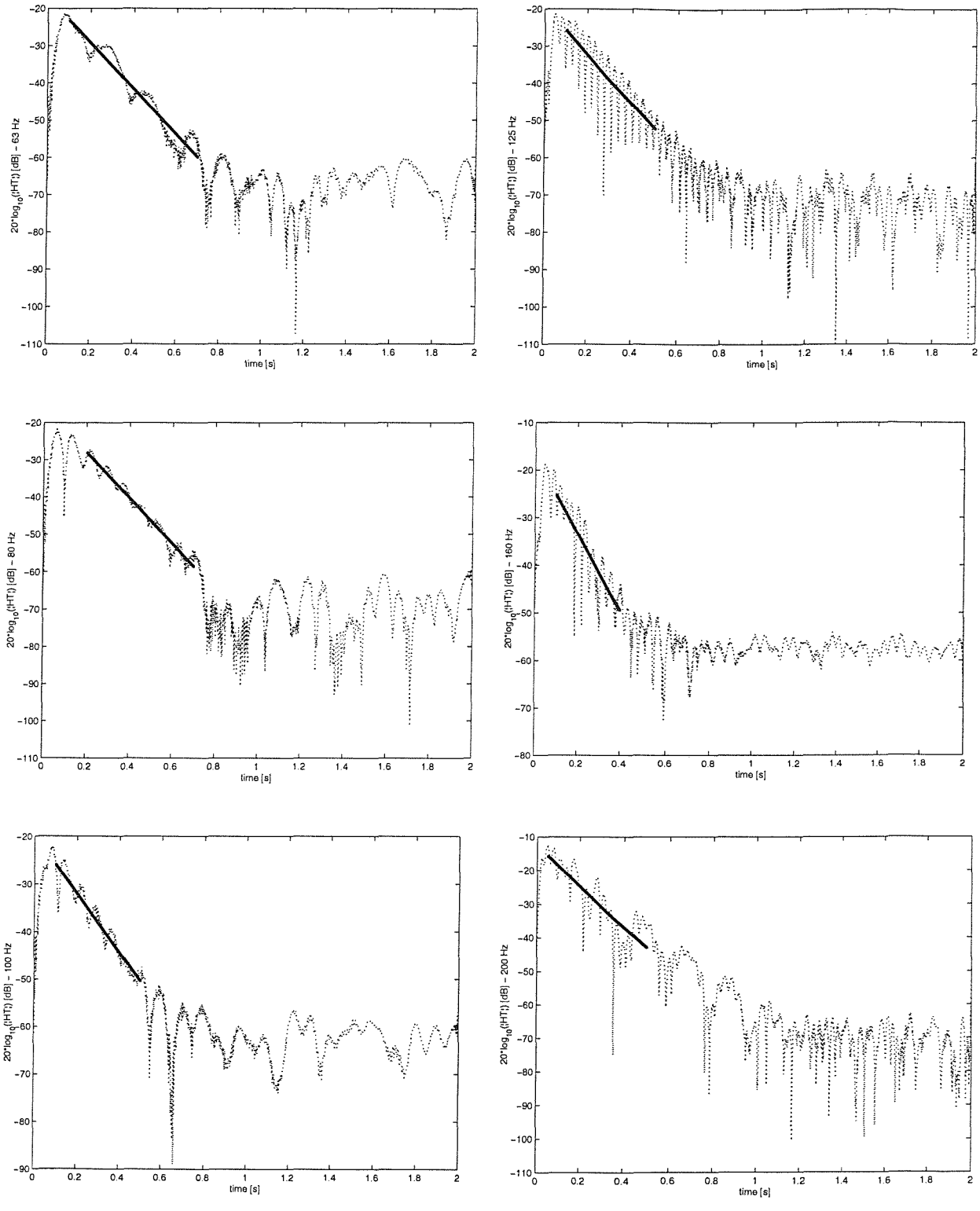

Figure 3.8: Typical decay curves obtained at the one-third octave band centre frequencies 63 Hz, 80 Hz, 100 Hz, 125 Hz, 160 Hz, and 200 Hz for the receiving room. Hilbert Transform (HT) of the Impulse Response is subjected to the best fitting straight line.

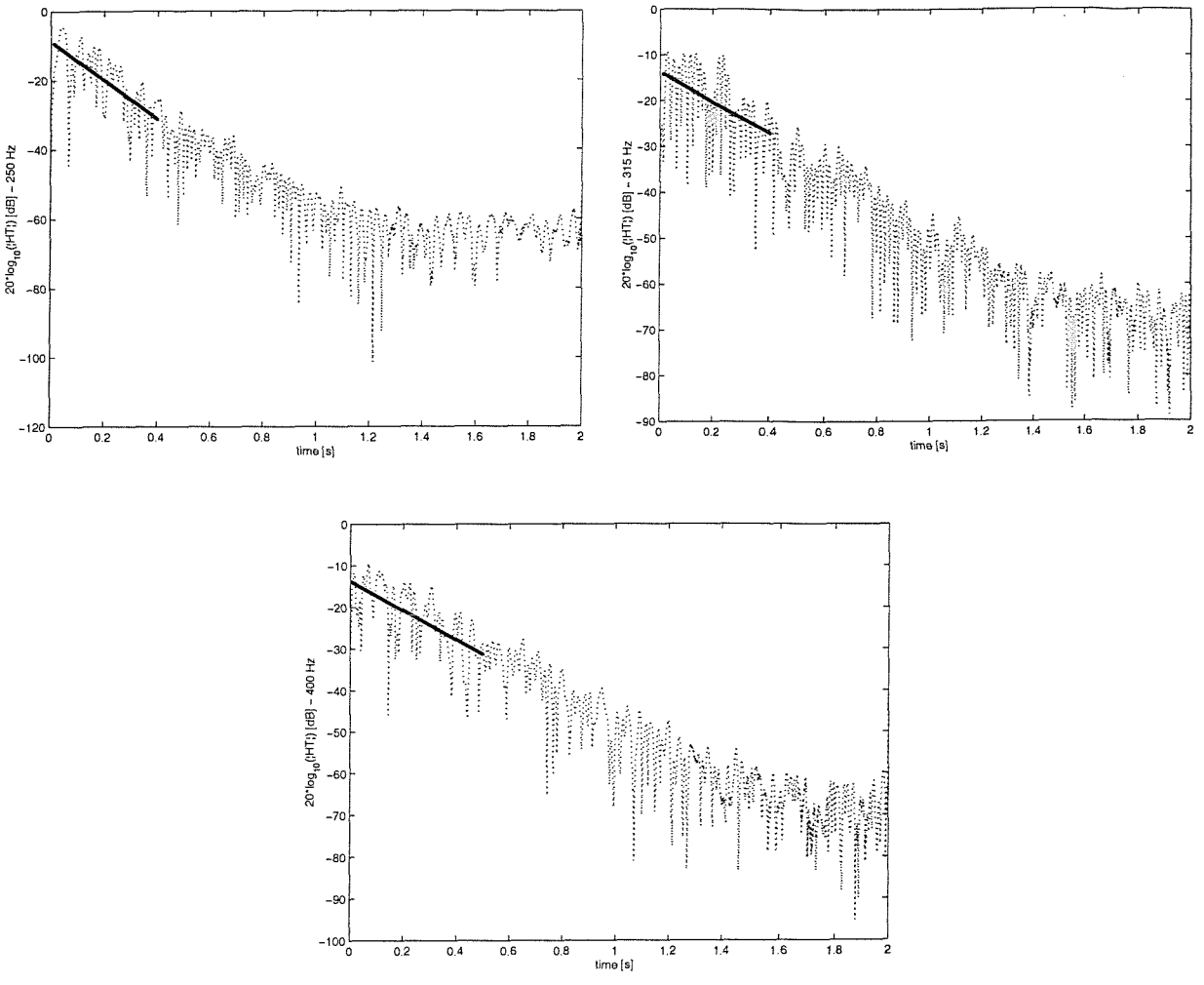

Figure 3.9: Typical decay curves obtained at the centre frequencies 250 Hz, 315 Hz and 400 Hz for the receiving room. Hilbert Transform (HT) of the Impulse Response is subjected to the best fitting straight line.

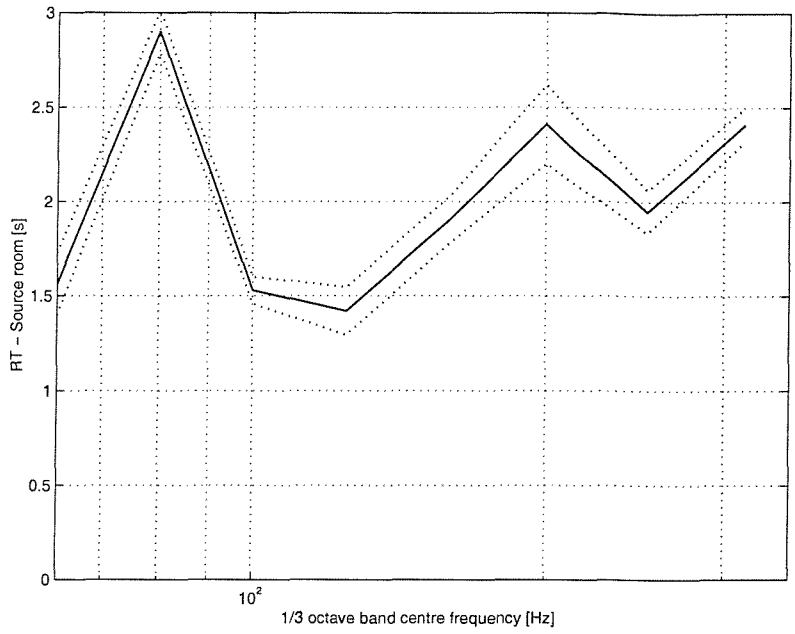

Figure 3.10: Reverberation Time data obtained from the decay rate measurements in the source room; ____ Mean value; .....Upper and Lower 95% confidence limits.

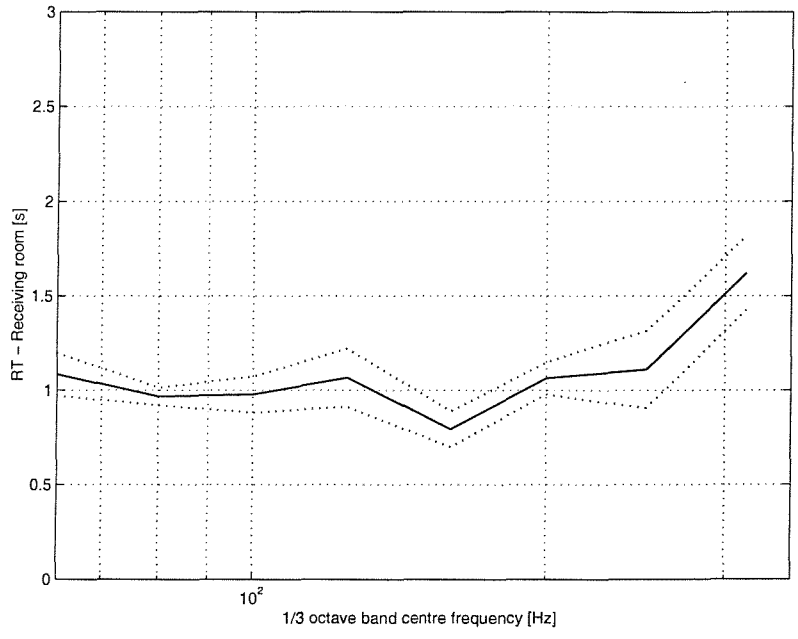

Figure 3.11: Reverberation Time data obtained from the decay rate measurements in the receiving room; —— Mean value; .....Upper and Lower 95% confidence limits.

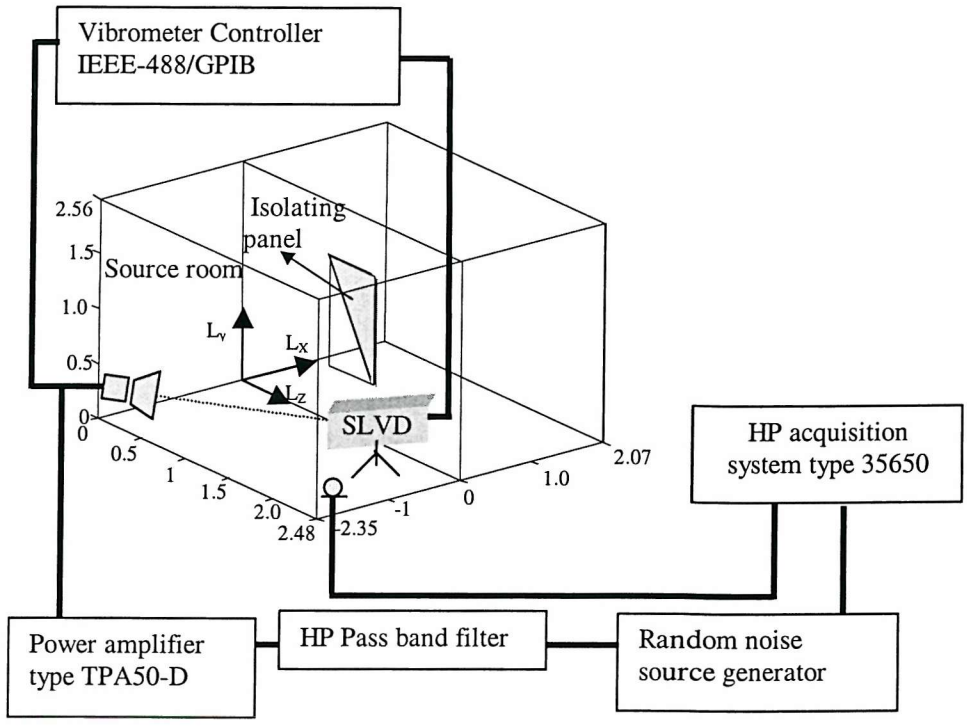

Figure 3.12: Experimental setup for the laboratory measurements of source volume velocity, Sound Pressure Level (SPL) and acoustic transfer impedance (single-room model).

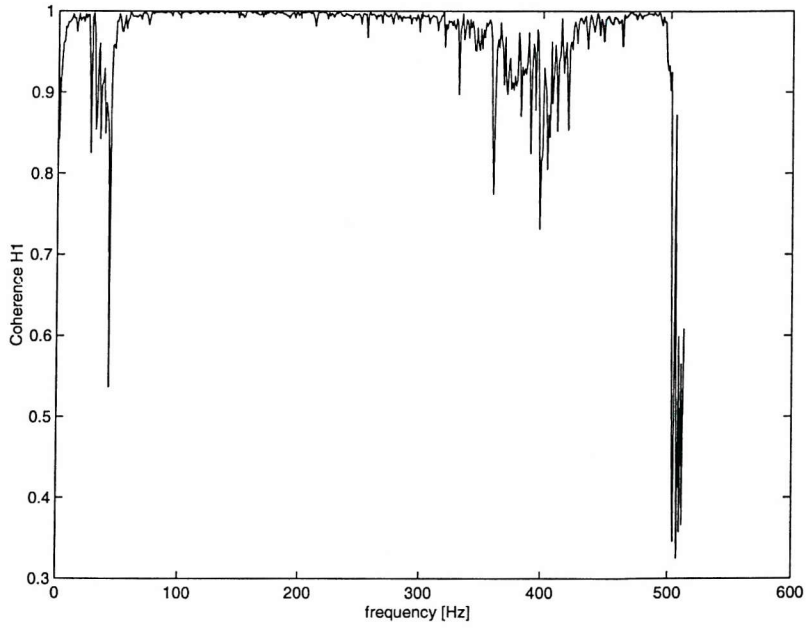

Figure 3.13: Coherence for the transfer function H_1, which relates the velocity of the speaker to the voltage fed to it.

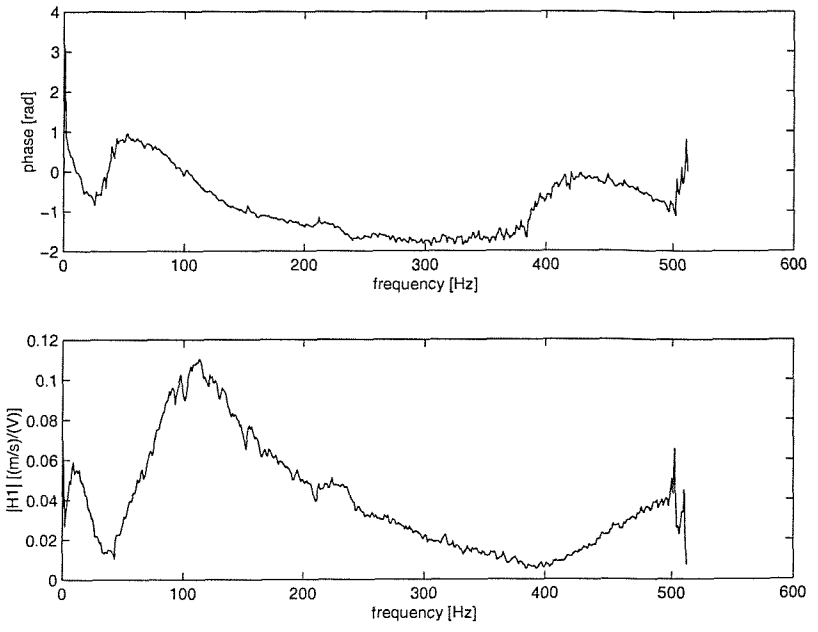

Figure 3.14: Experimentally measured transfer function H_1, which relates the velocity of the speaker to the voltage fed to it.

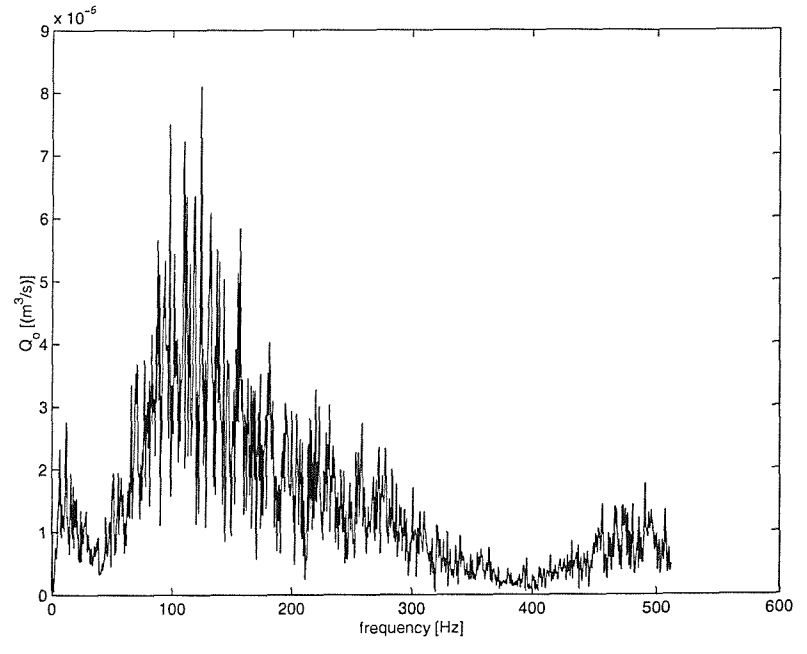

Figure 3.15: Experimentally measured vibration volume velocity of the loudspeaker.

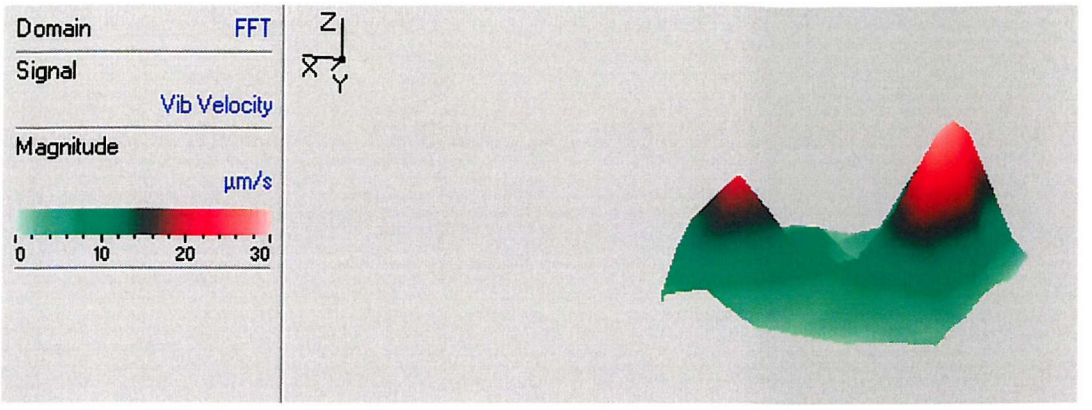

Figure 3.16: Variation of the velocity over the loudspeaker cone at 100 Hz frequency band (picture obtained from the Polytec Scanning Vibrometer software 7.1).

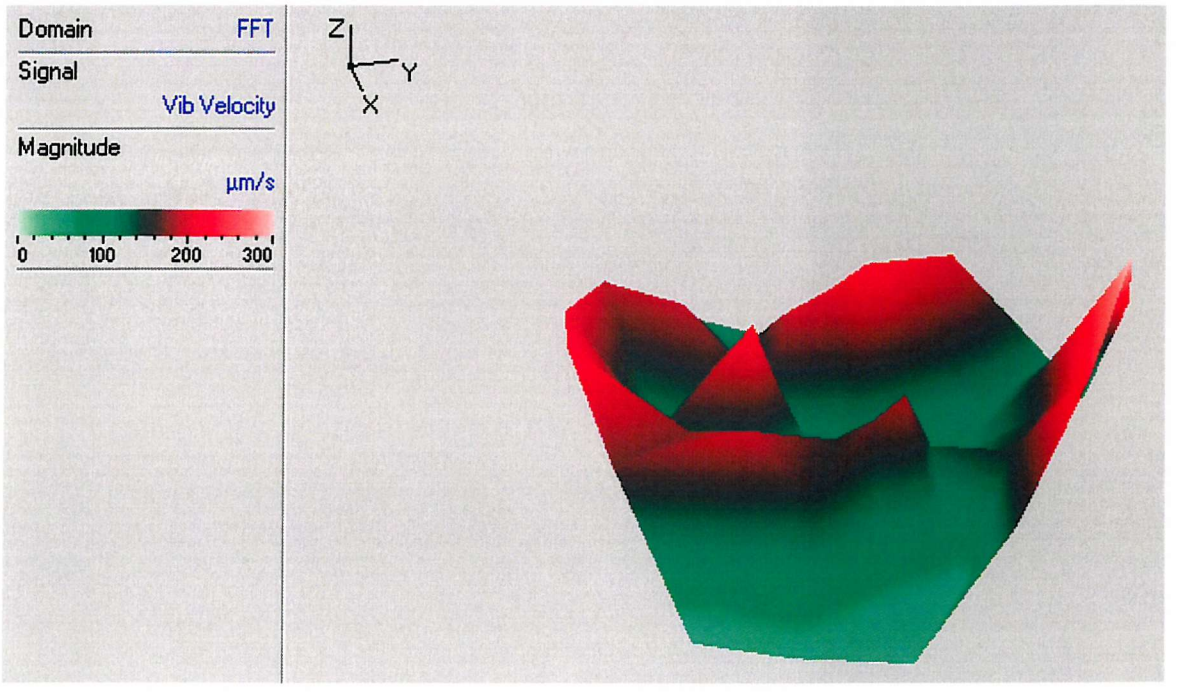

Figure 3.17: Variation of the vibration velocity amplitude over the loudspeaker cone at 200 Hz frequency band. (picture obtained from the Polytec Scanning Vibrometer software 7.1).

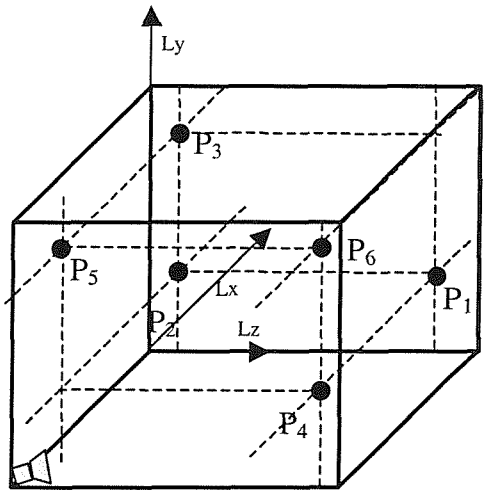

Figure 3.18 Microphone positions in the room

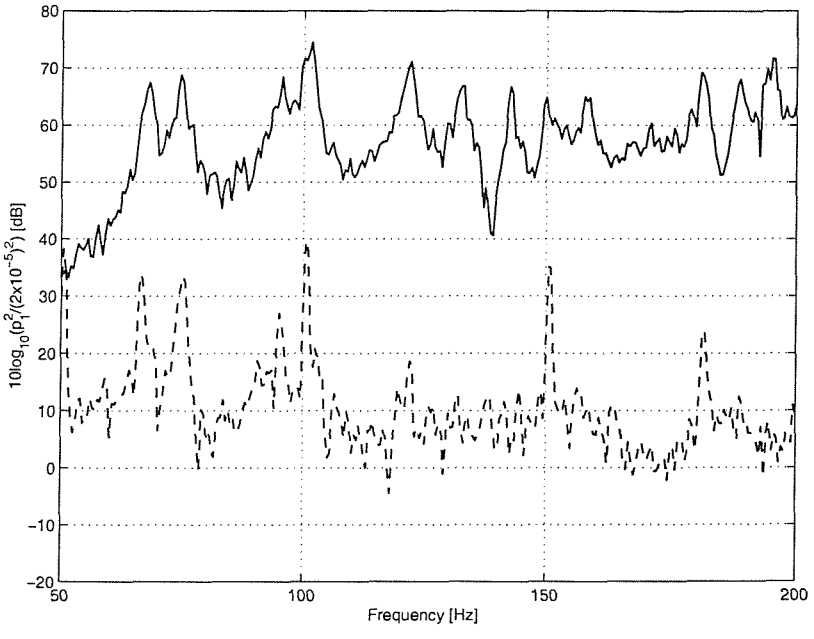

Figure 3.19 Typical measurements of the SPL in a single room (dB re $2x10^{-5}$) compared to the measurement of the background noise in the room. _____ Spatially averaged measurement; ----- noise

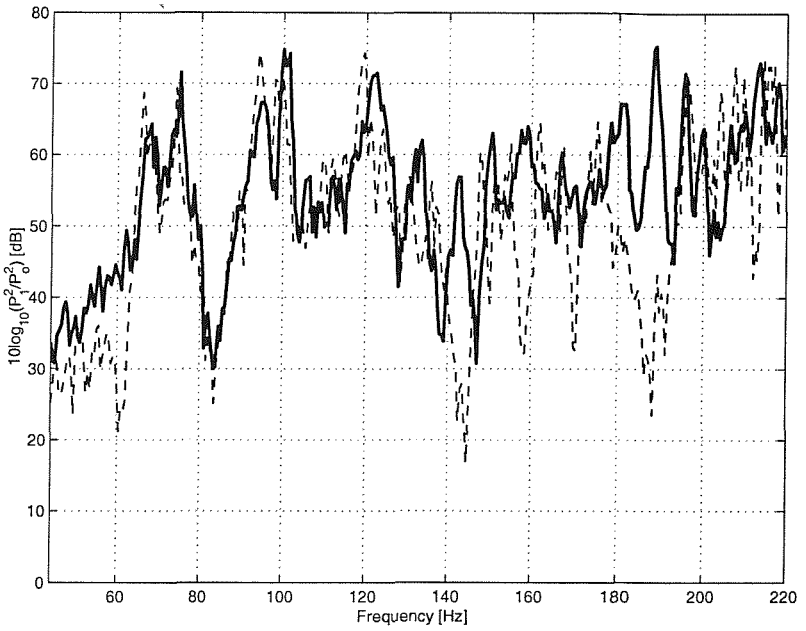

a)

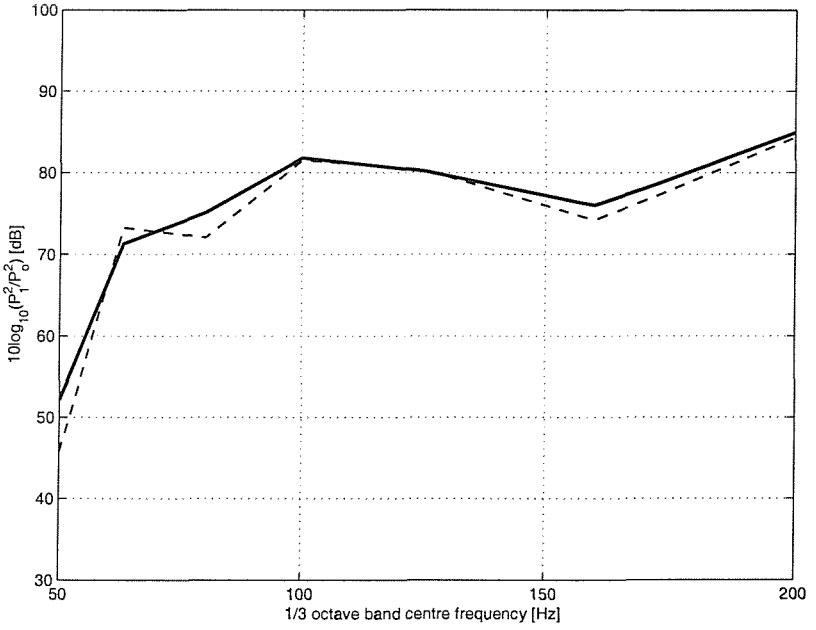

b)

Figure 3.20: Comparison between measured and predicted sound pressure levels (dB re $2x10^{-5}$ Pa) at position 1 for the single-room model; a) narrow bands; b) one third octave bands; _____ measured; ----- predicted

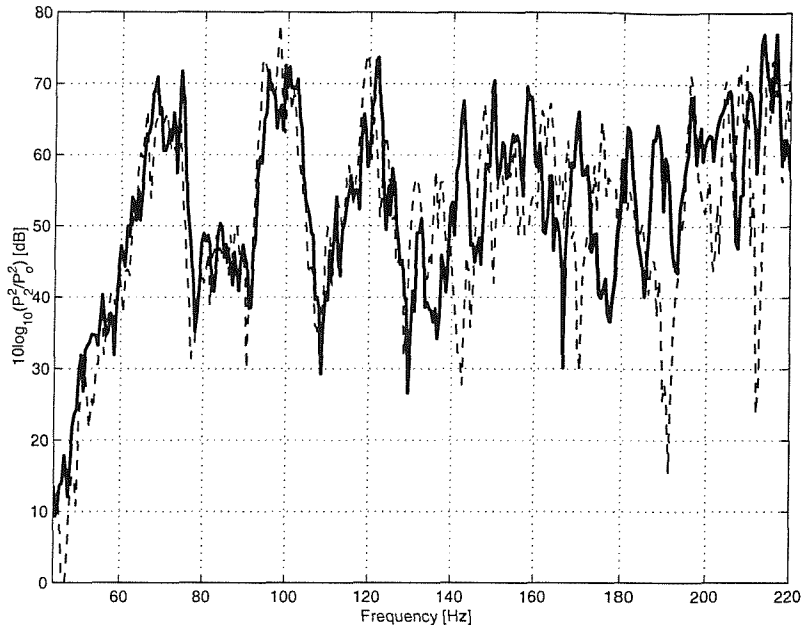

a)

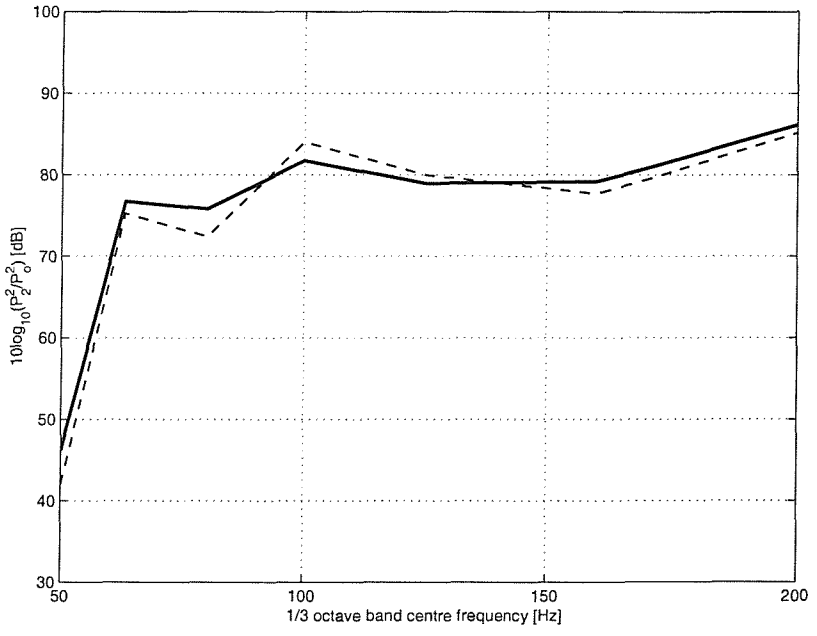

b)

Figure 3.21: Comparison between measured and predicted sound pressure levels (dB re $2x10^{-5}$ Pa) at position 2 for the single-room model; a) narrow bands; b) one third octave bands; _____ measured; ----- predicted

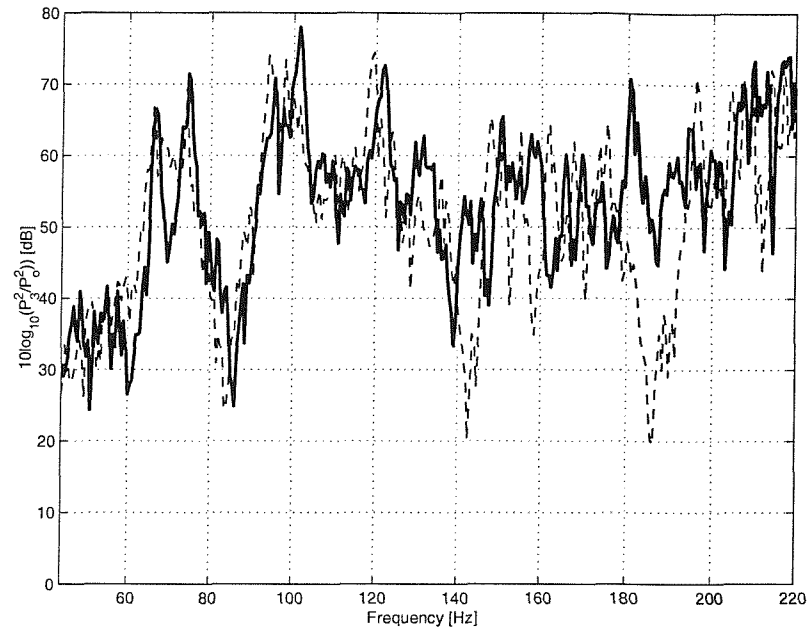

a)

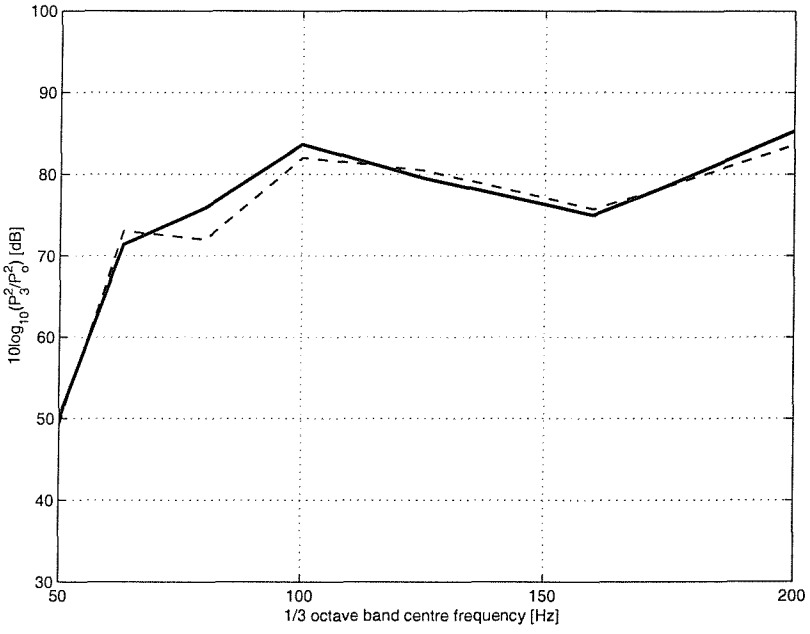

b)

Figure 3.22: Comparison between measured and predicted sound pressure levels (dB re $2x10^{-5}$ Pa) at position 3 for the single-room model; a) narrow bands; b) one third octave bands; _____ measured; ----- predicted

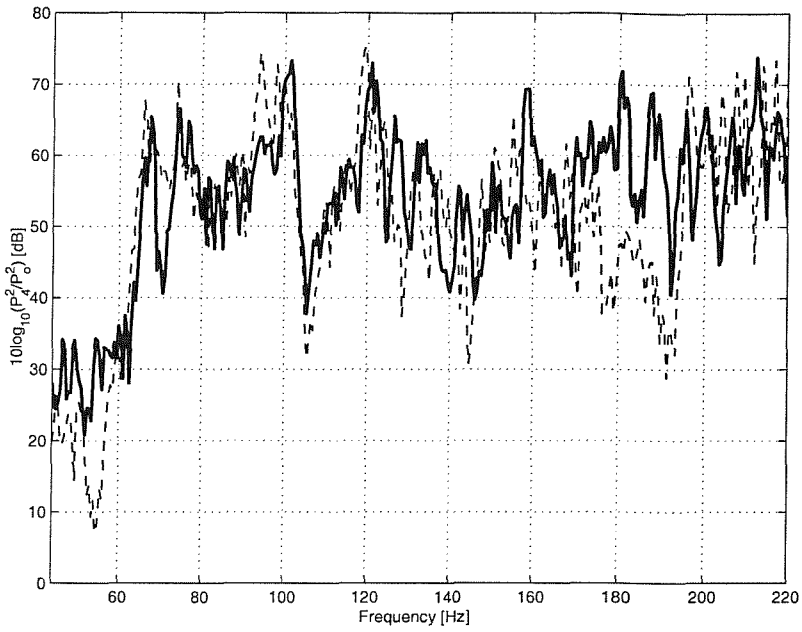

a)

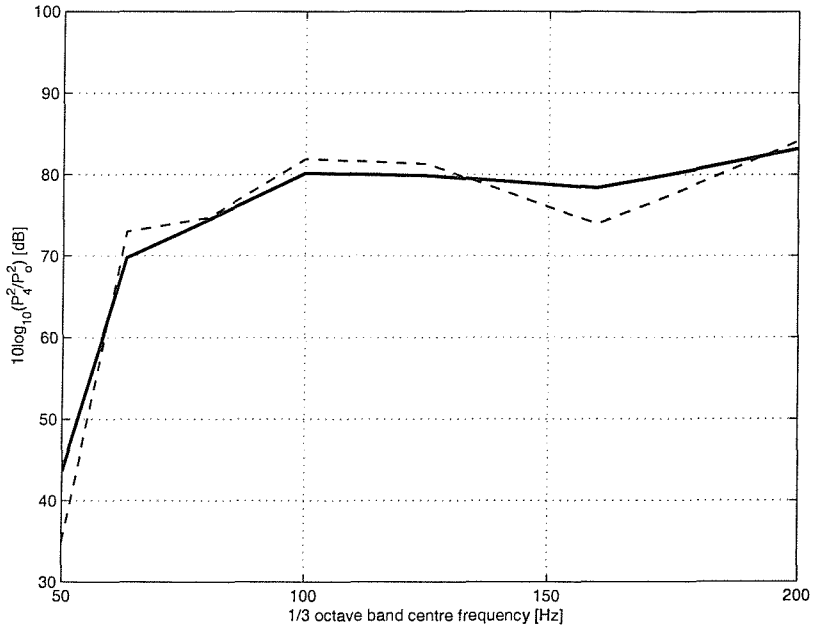

b)

Figure 3.23: Comparison between measured and predicted sound pressure levels (dB re $2x10^{-5}$ Pa) at position 4 for the single-room model; a) narrow bands; b) one third octave bands; _____ measured; ----- predicted

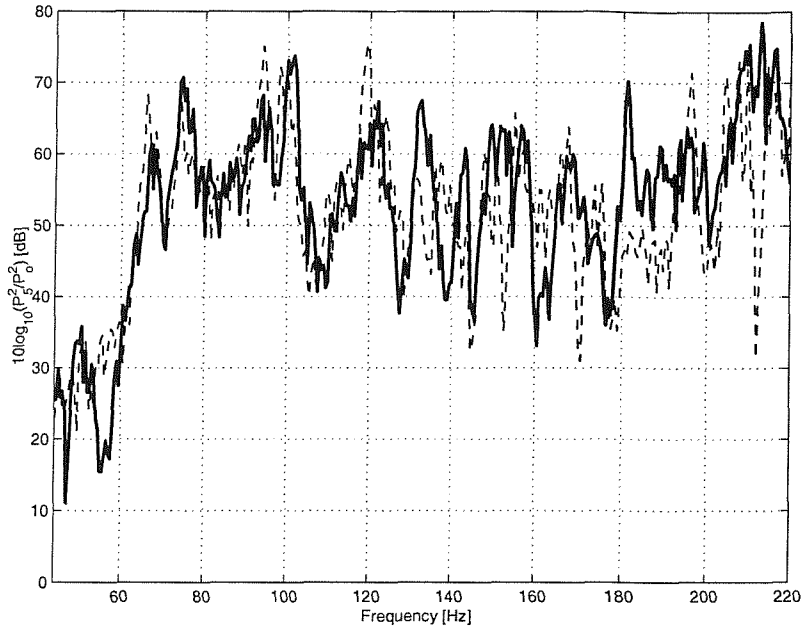

a)

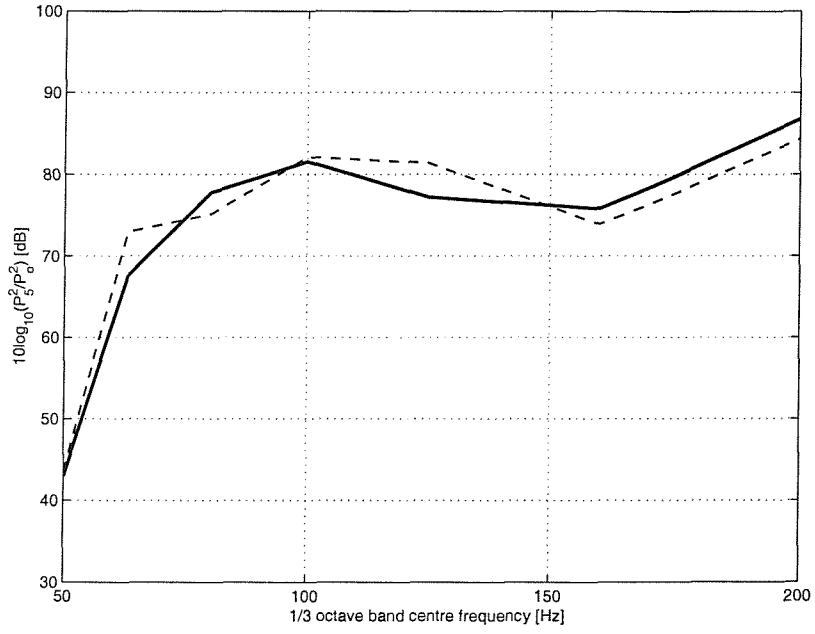

b)

Figure 3.24: Comparison between measured and predicted sound pressure levels (dB re $2x10^{-5}$ Pa) at position 5 for the single-room model; a) narrow bands; b) one third octave bands; _____ measured; ----- predicted

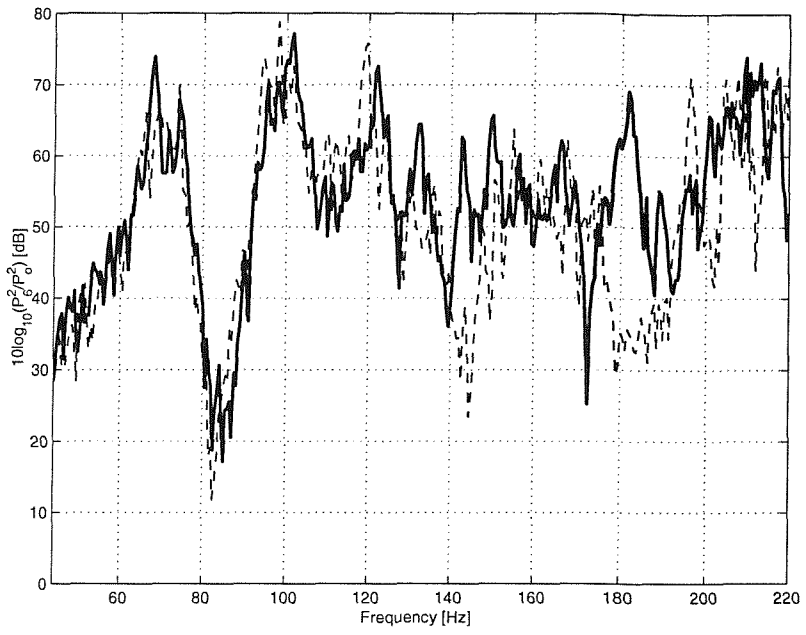

a)

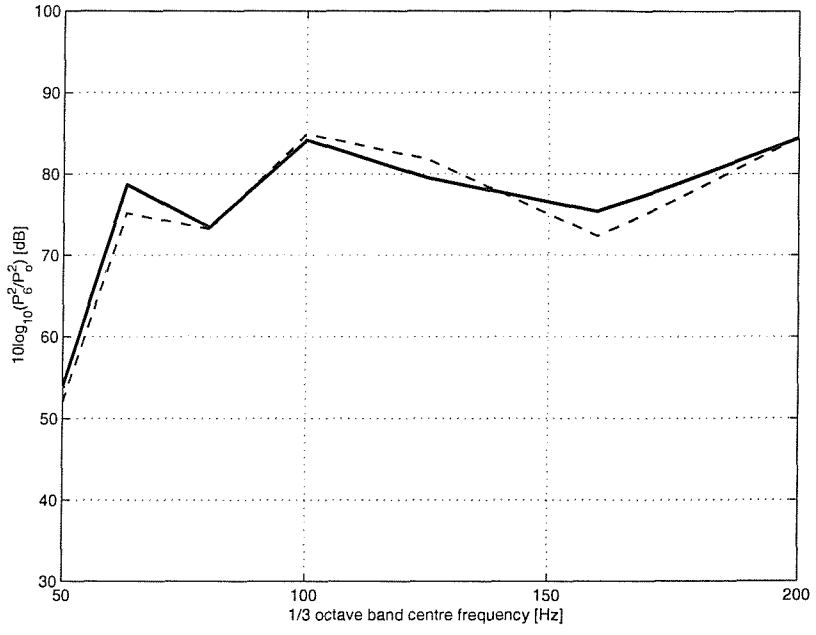

b)

Figure 3.25: Comparison between measured and predicted sound pressure levels (dB re $2x10^{-5}$ Pa) at position 6 for the single-room model; a) narrow bands; b) one third octave bands; _____ measured; ----- predicted

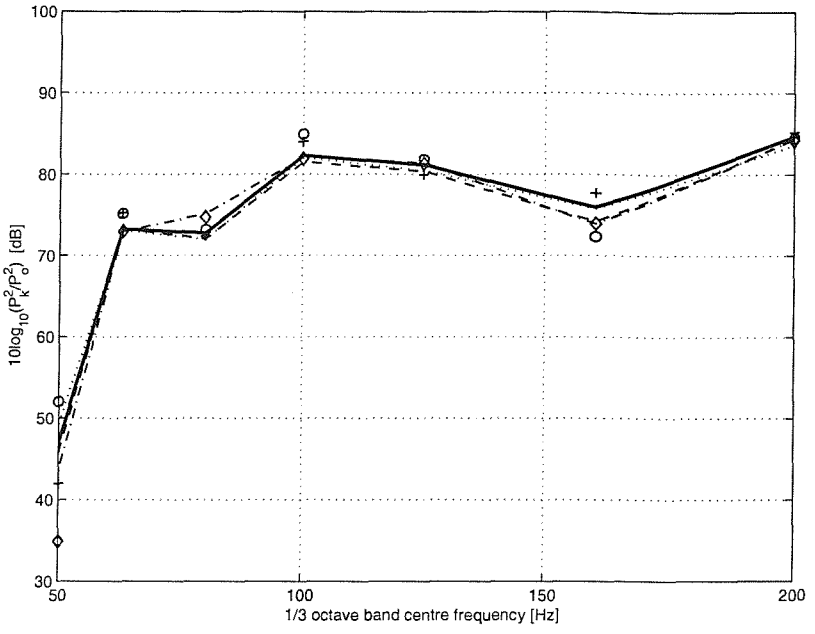

a)

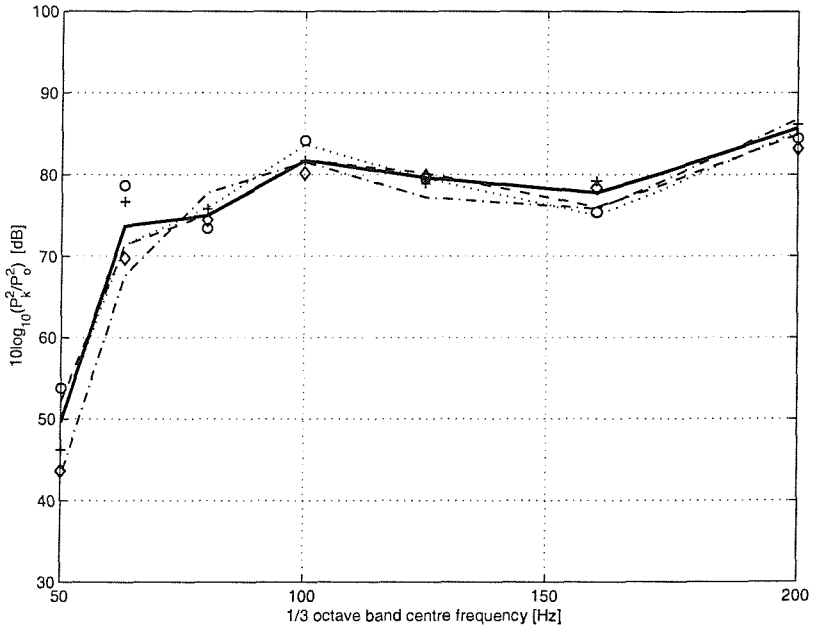

b)

Figure 3.26: Summary of the SPL (dB re $2x10^{-5}$ Pa) at six different positions and the mean value averaged over all positions; a) predicted results; b) measured results; ---- P_1 ; +++ P_2 ; ..... P_3 ; ◊◊◊ P_4 ; -.- P_5 ; -o- P_6 ; The solid line in graph (a) and (b) represents the spatially averaged pressure taken from the predicted and measured values respectively.

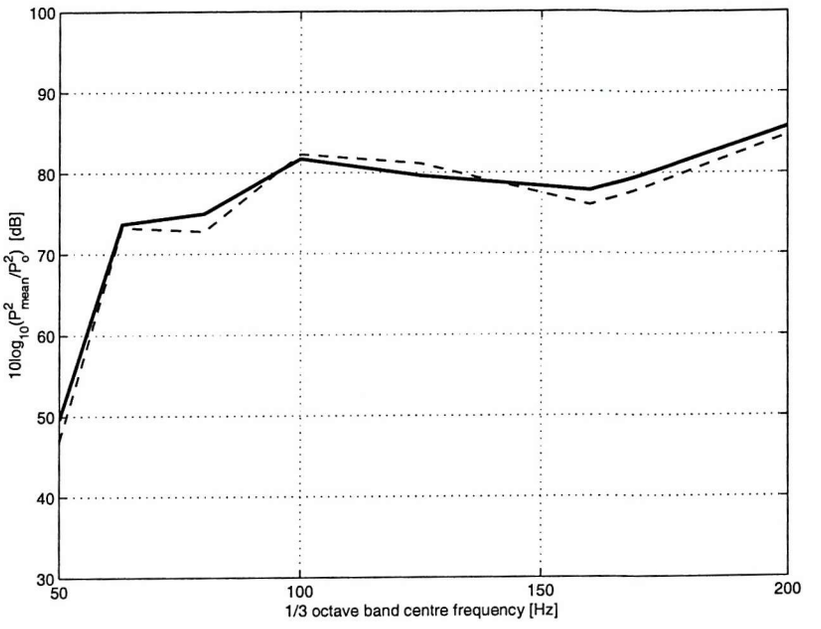

Figure 3.27: Comparison between measured and predicted spatial-averaged sound pressure levels (dB re $2x10^{-5}$ Pa)._____ measured; ------ predicted

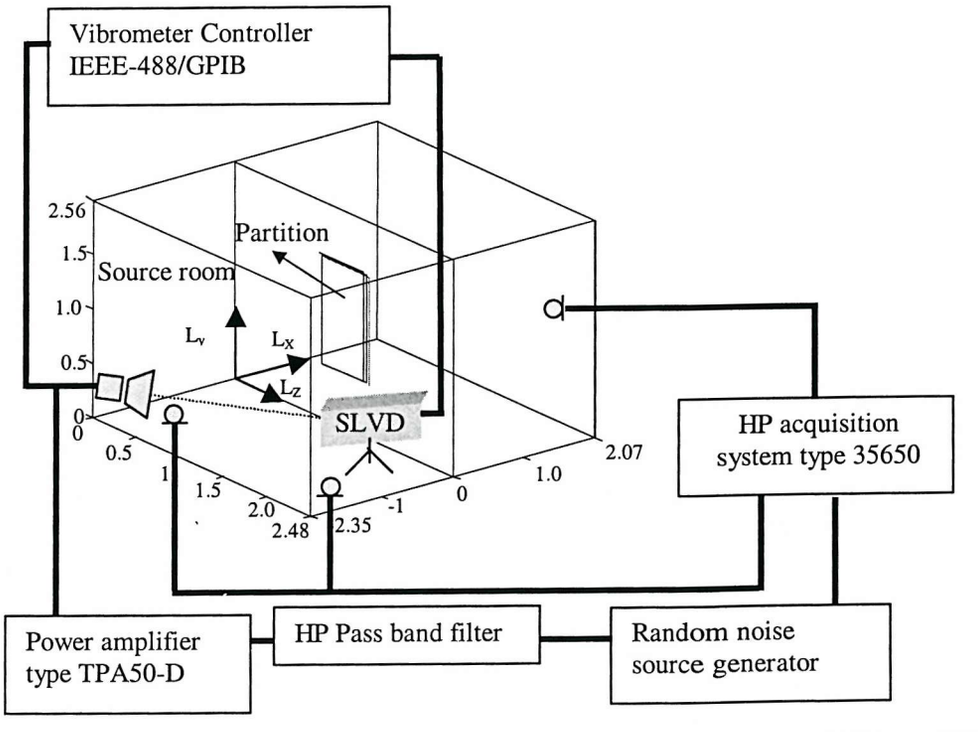

Figure 3.28: Experimental setup for the laboratory measurements of FRFs and Noise Reduction (NR).

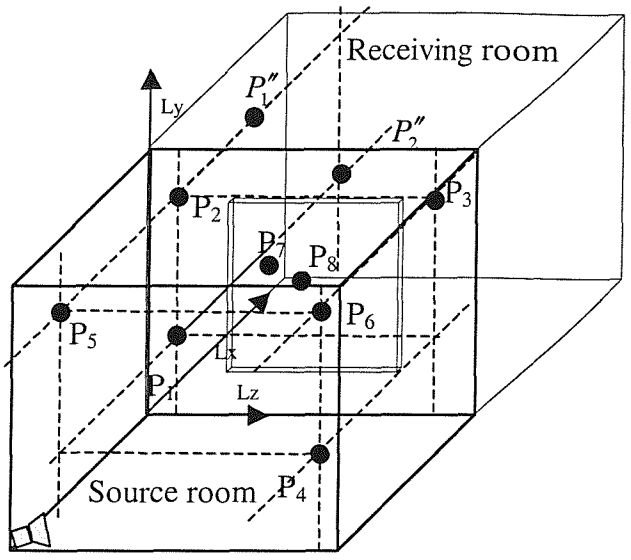

Figure 3.29 Microphone positions in the source and receiving room

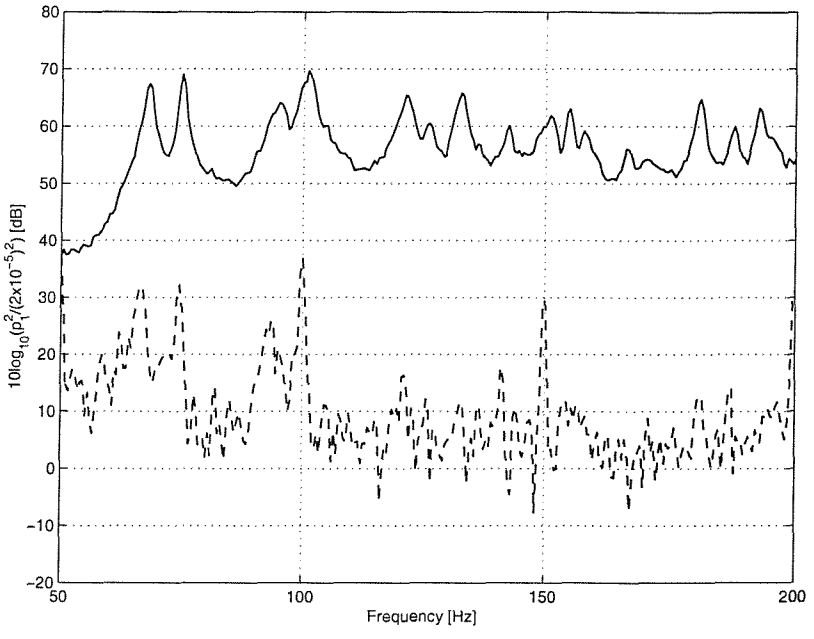

Figure 3.30: Typical measurement of the SPL in the source room (dB re $2x10^{-5}$) compared to the measurement of the background noise in the room. _____ Spatially averaged measurement; ----- noise

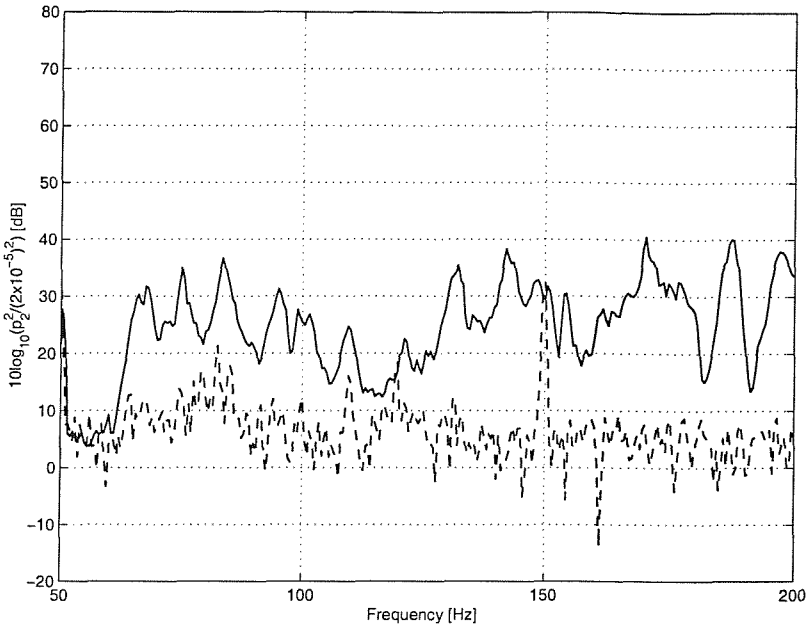

Figure 3.31: Typical measurement of the SPL in the receiving room (dB re $2x10^{-5}$) compared to the measurement of the background noise in the room. _____ Spatially averaged measurement; ----- noise

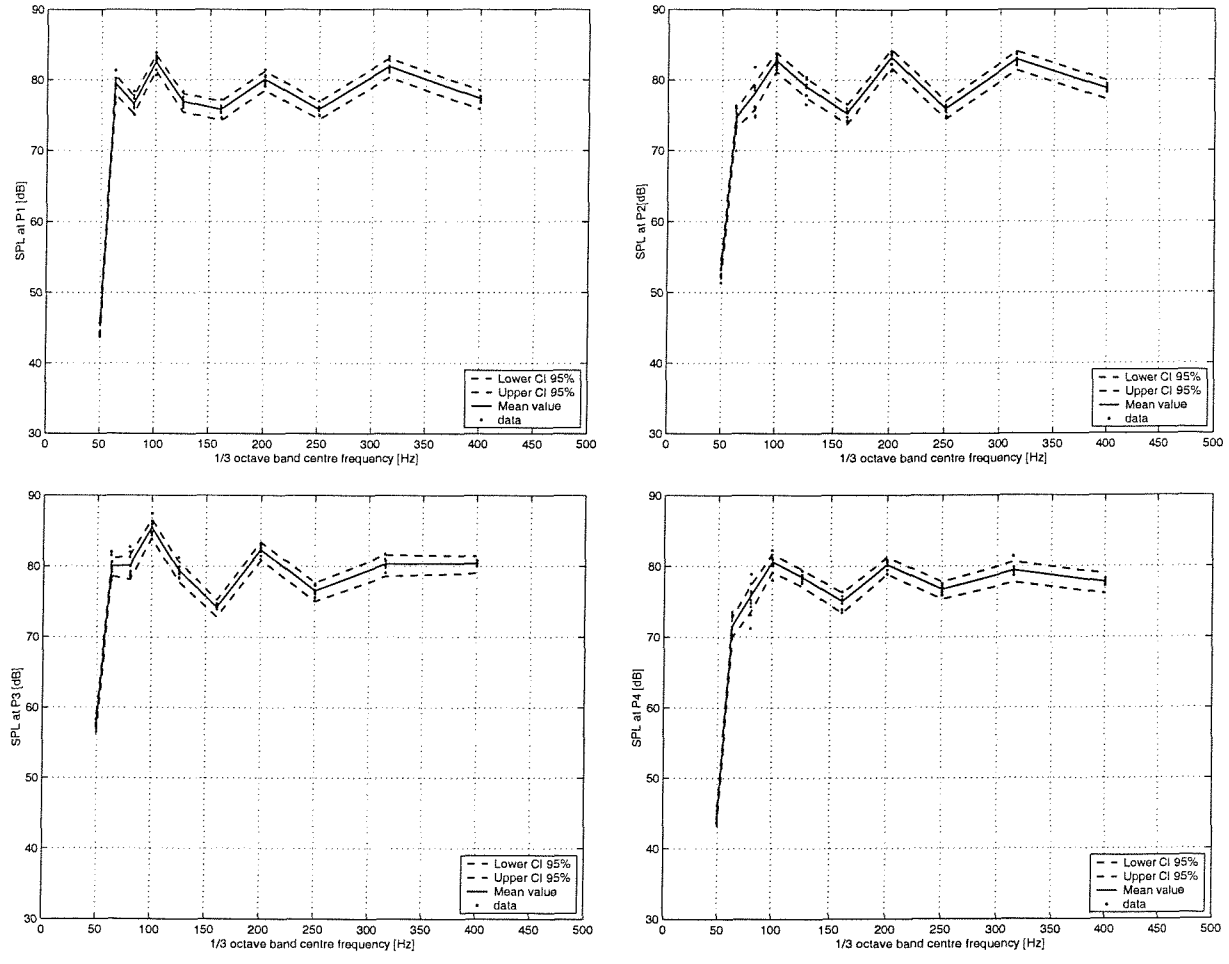

Figure 3.32: Confidence interval for SPL measured at different positions in the source room

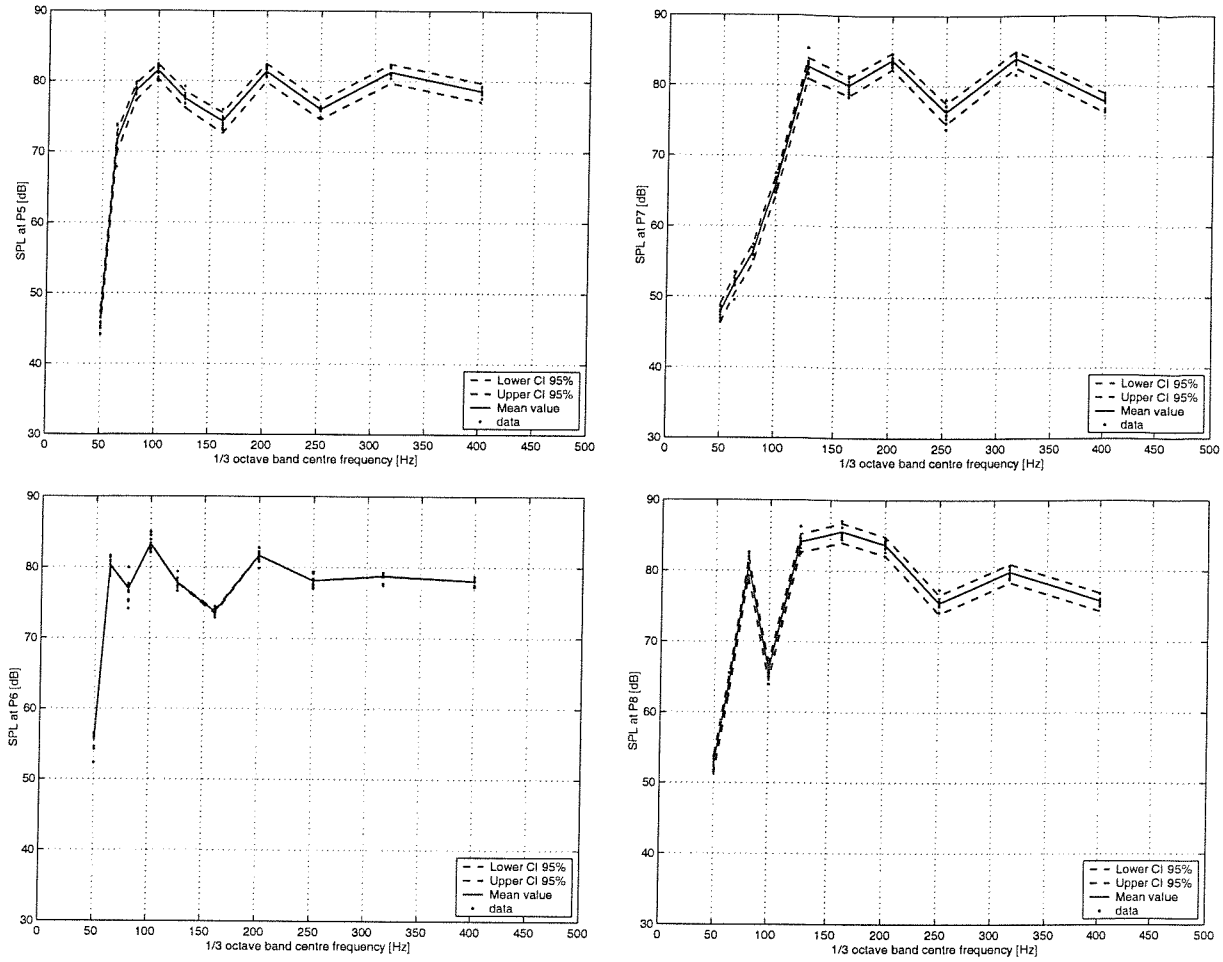

Figure 3.33: Confidence interval for SPL measured at different positions in the source room

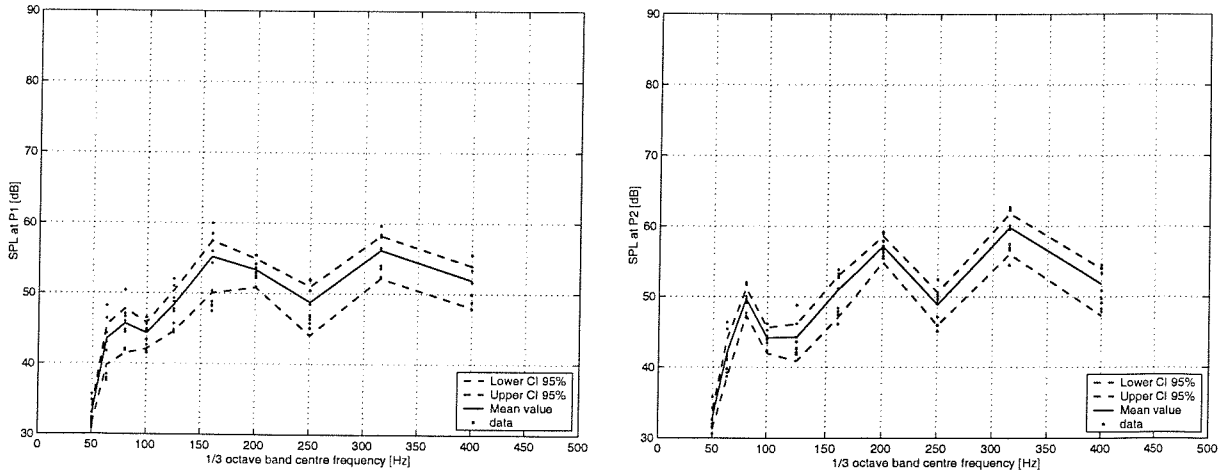

Figure 3.34: Confidence interval for SPL measured at position 1 and position 2 in the receiving room.

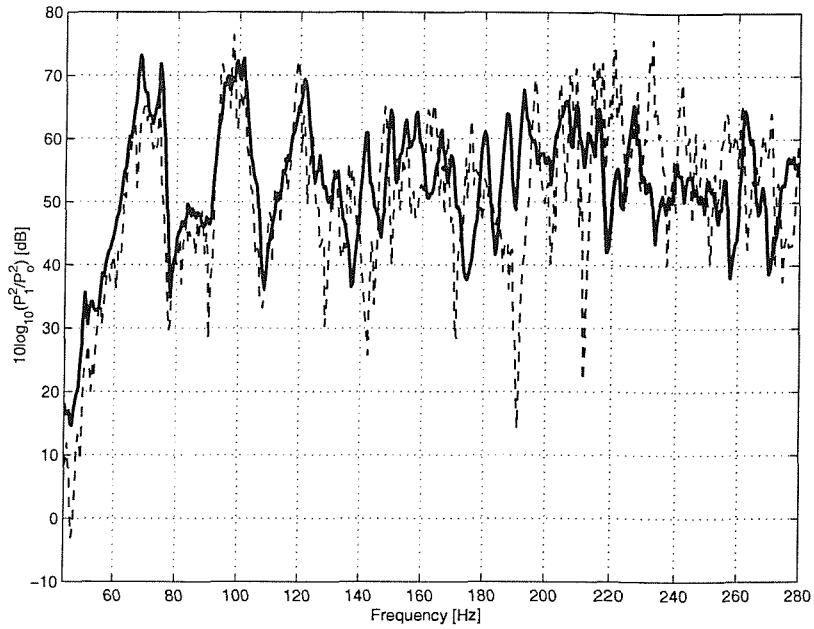

a)

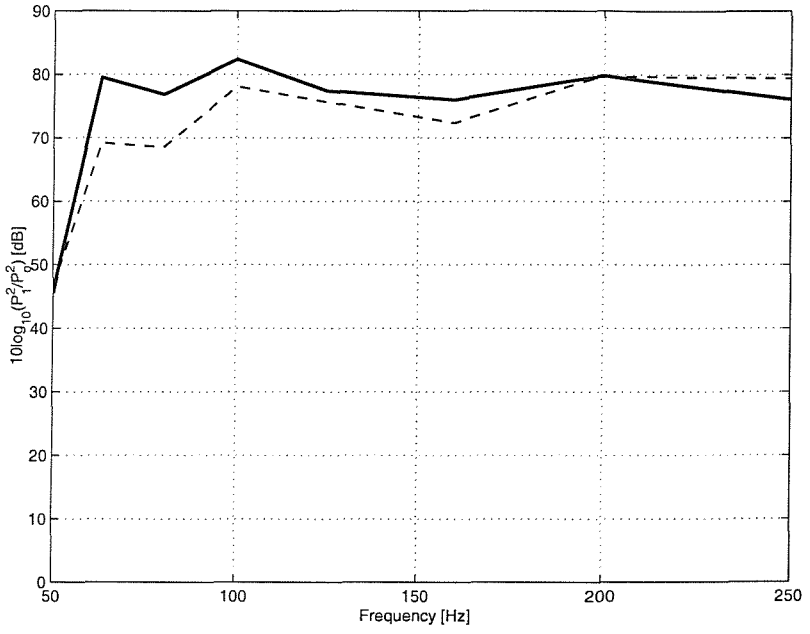

b)

Figure 3.35: Comparison between measured and predicted sound pressure levels (dB re $2x10^{-5}$ Pa) at position 1 for the source room; a) narrow bands; b) one third octave bands; _____ measured; ----- predicted

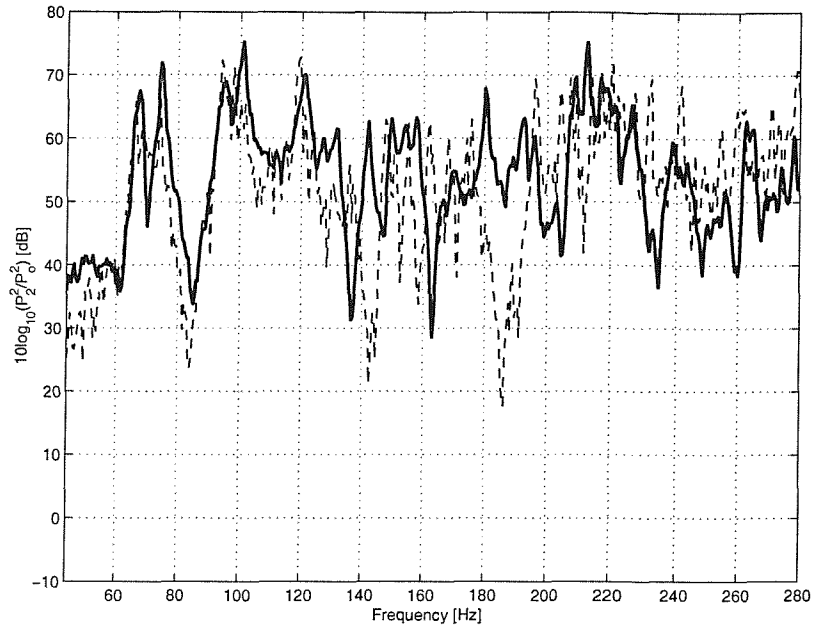

a)

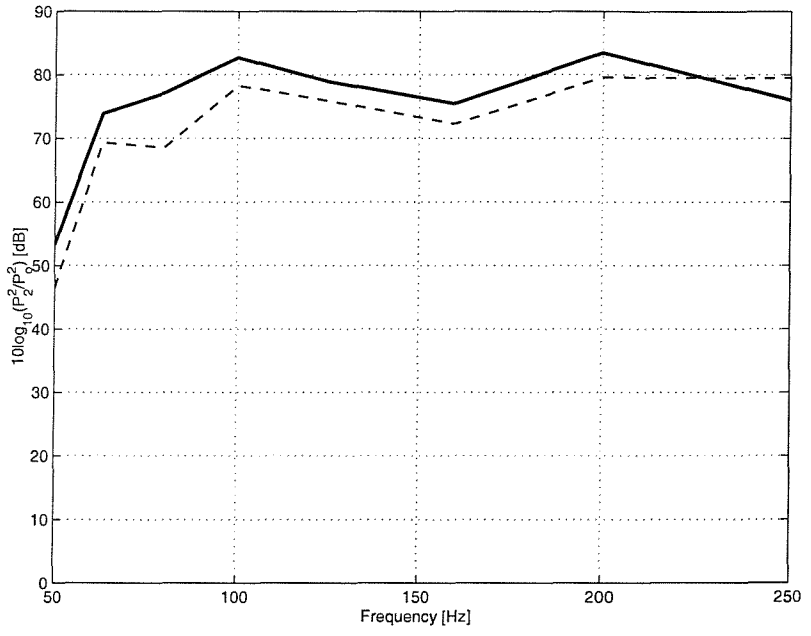

b)

Figure 3.36: Comparison between measured and predicted sound pressure levels (dB re $2x10^{-5}$ Pa) at position 2 for the source room; a) narrow bands; b) one third octave bands; _____ measured; ----- predicted

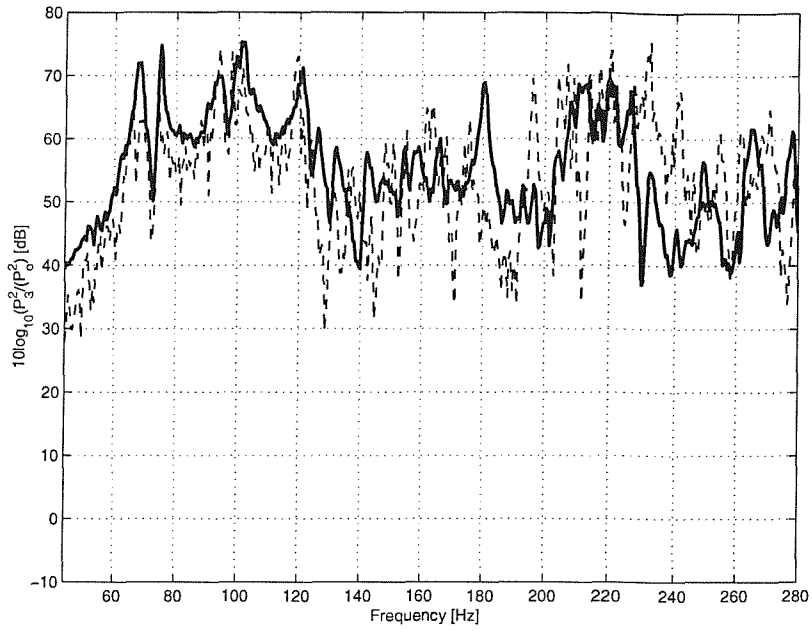

a)

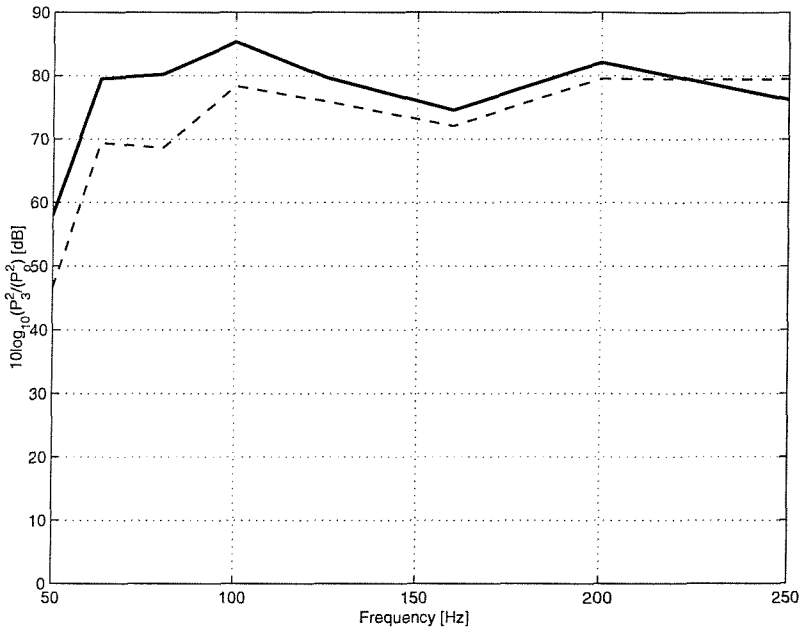

b)

Figure 3.37: Comparison between measured and predicted sound pressure levels (dB re $2x10^{-5}$ Pa) at position 3 for the source room; a) narrow bands; b) one third octave bands; _____ measured; ----- predicted

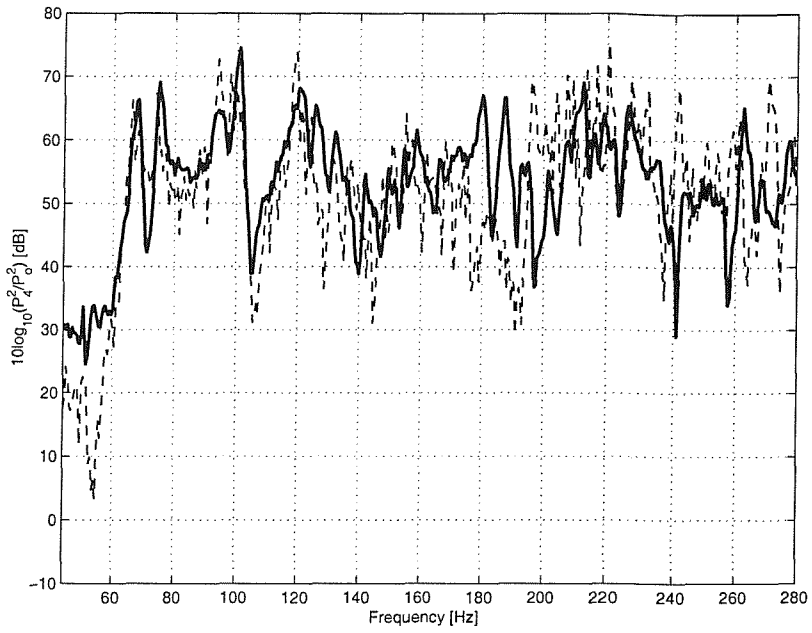

a)

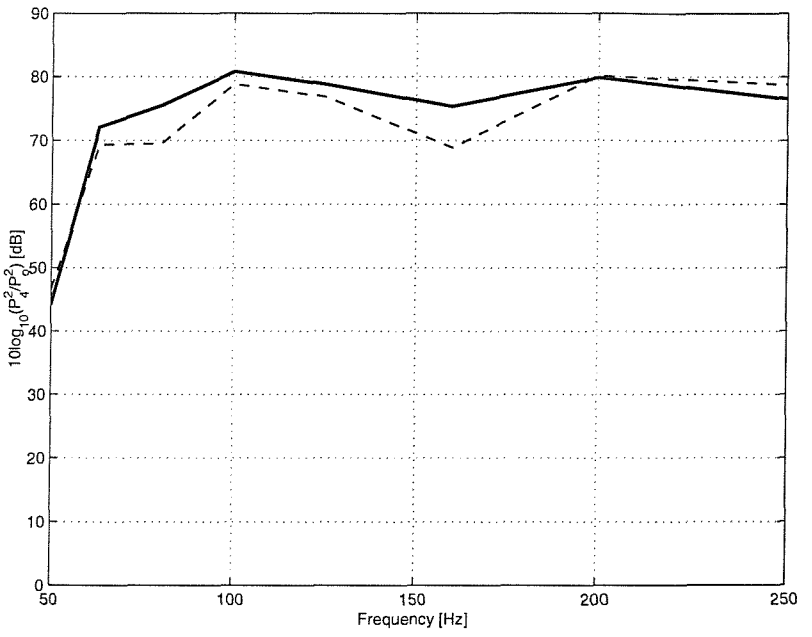

b)

Figure 3.38: Comparison between measured and predicted sound pressure levels (dB re $2x10^{-5}$ Pa) at position 4 for the source room; a) narrow bands; b) one third octave bands; _____ measured; ----- predicted

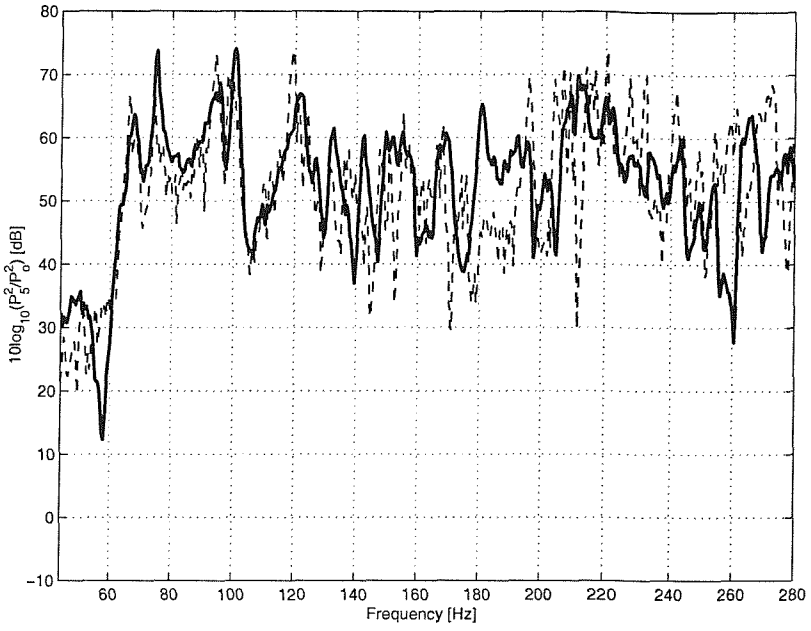

a)

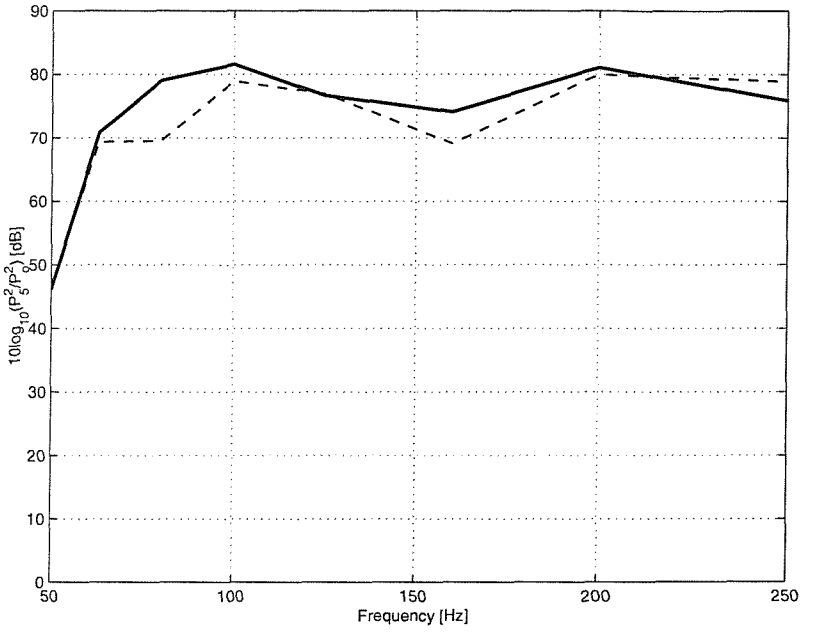

b)

Figure 3.39: Comparison between measured and predicted sound pressure levels (dB re $2x10^{-5}$ Pa) at position 5 for the source room; a) narrow bands; b) one third octave bands; _____ measured; ----- predicted

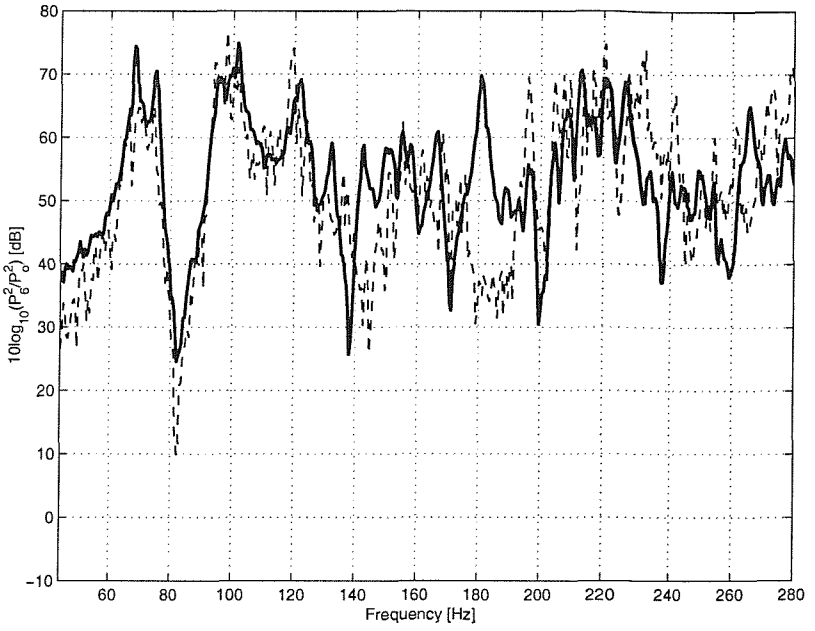

a)

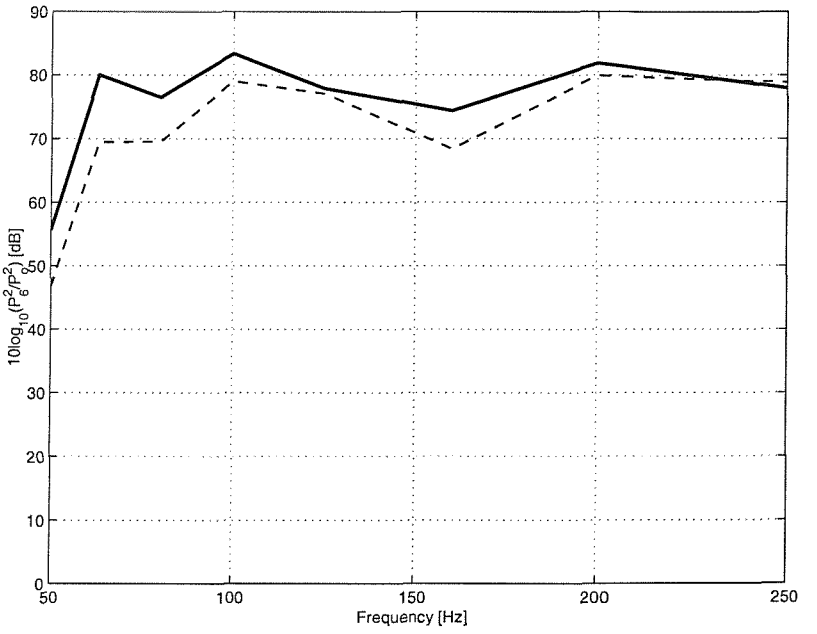

b)

Figure 3.40: Comparison between measured and predicted sound pressure levels (dB re $2x10^{-5}$ Pa) at position 6 for the source room; a) narrow bands; b) one third octave bands; _____ measured; ----- predicted

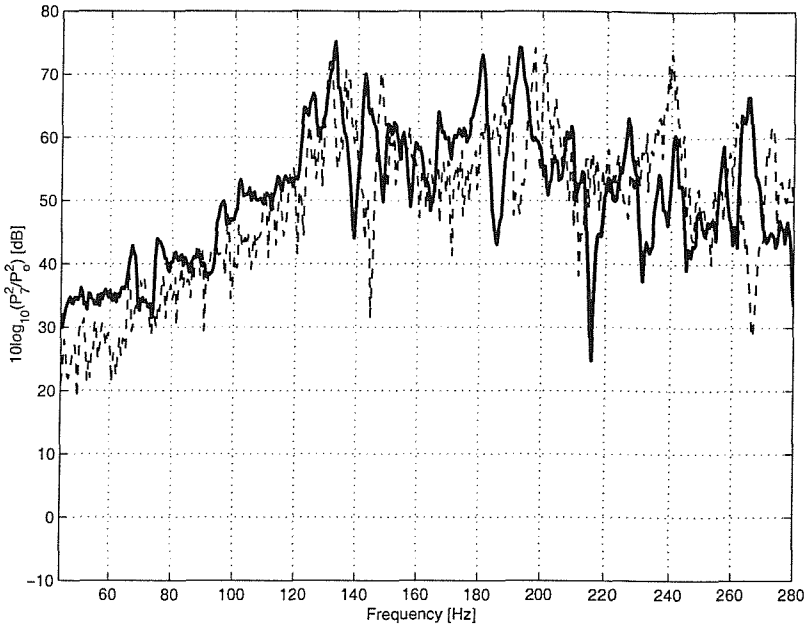

a)

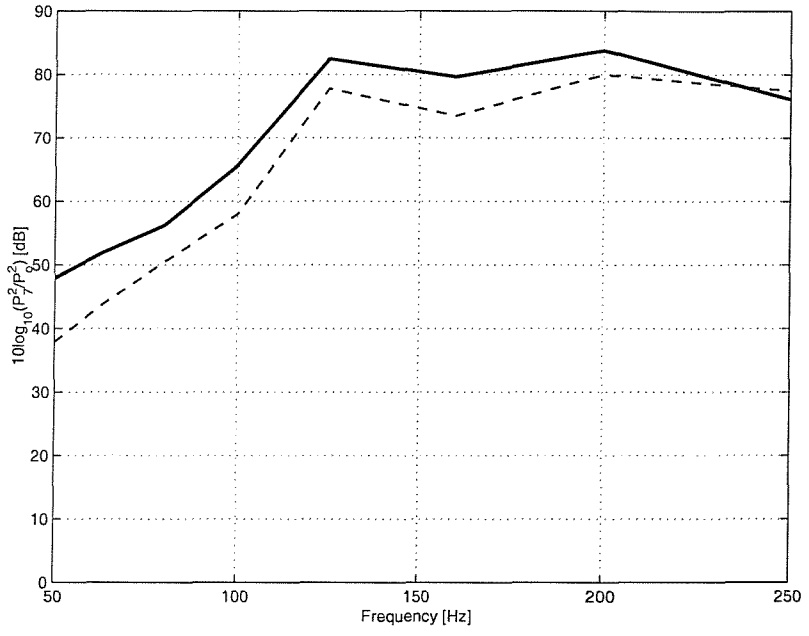

b)

Figure 3.41: Comparison between measured and predicted sound pressure levels (dB re $2x10^{-5}$ Pa) at position 7 for the source room; a) narrow bands; b) one third octave bands; _____ measured; ----- predicted

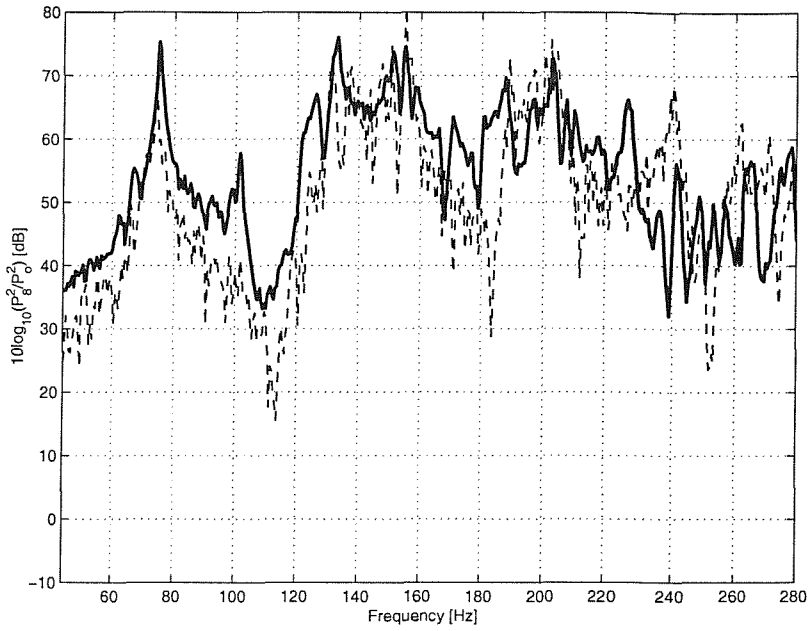

a)

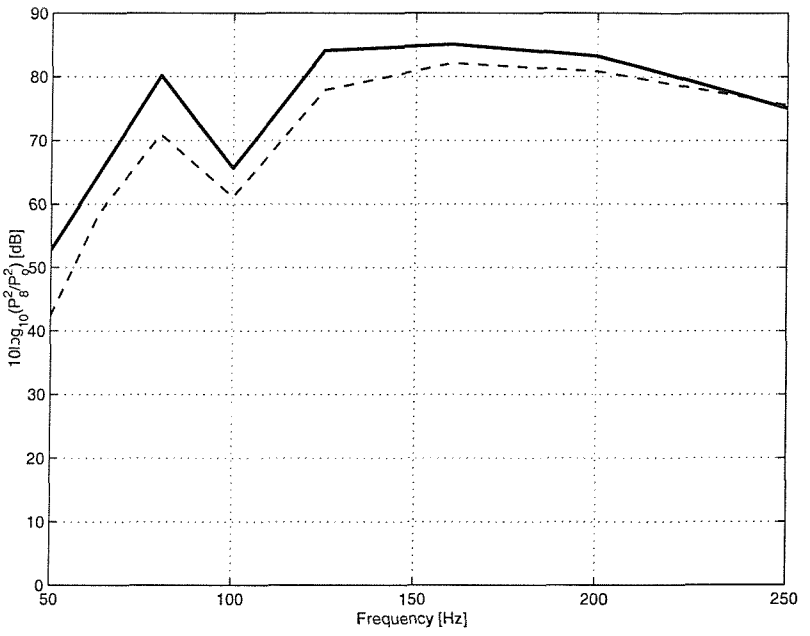

b)

Figure 3.42: Comparison between measured and predicted sound pressure levels (dB re $2x10^{-5}$ Pa) at position 8 for the source room; a) narrow bands; b) one third octave bands; _____ measured; ----- predicted

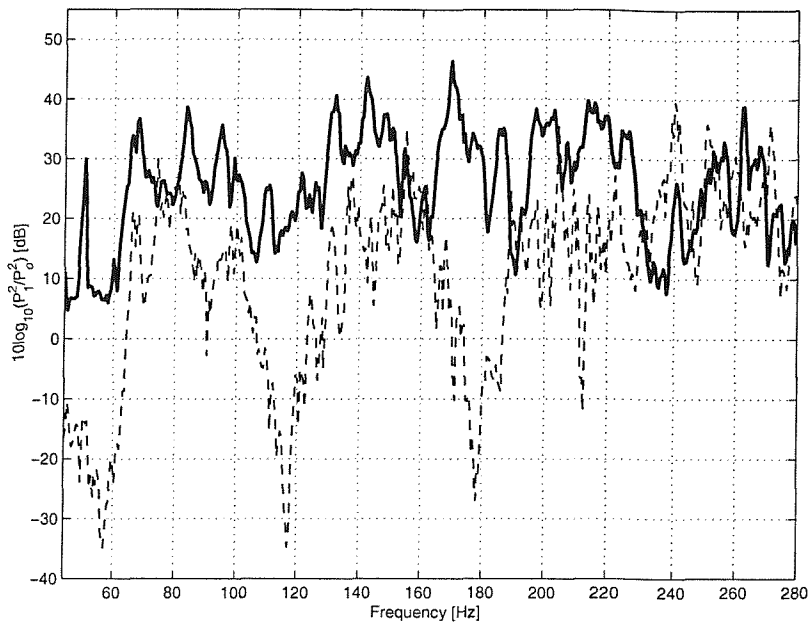

a)

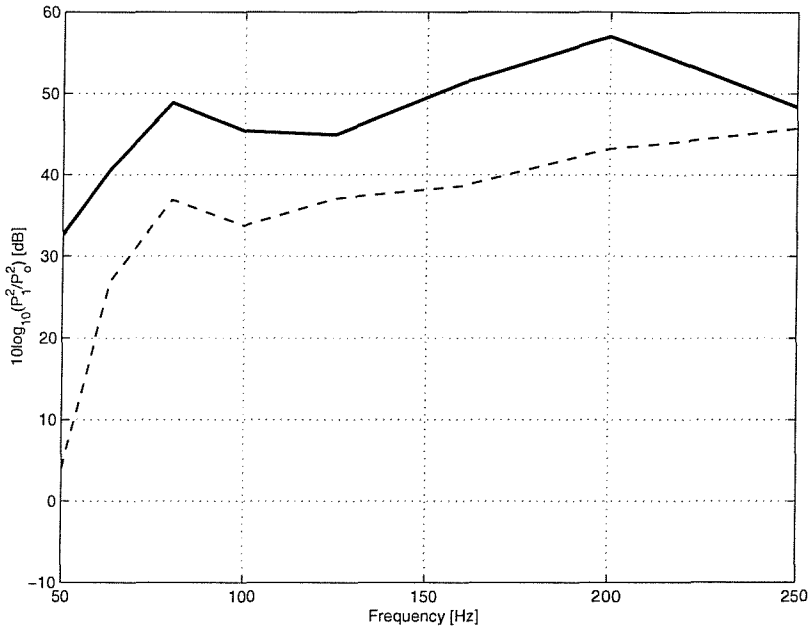

b)

Figure 3.43: Comparison between measured and predicted sound pressure levels (dB re $2x10^{-5}$ Pa) at position 1 for the receiving room; a) narrow bands; b) one third octave bands; _____ measured; ----- predicted

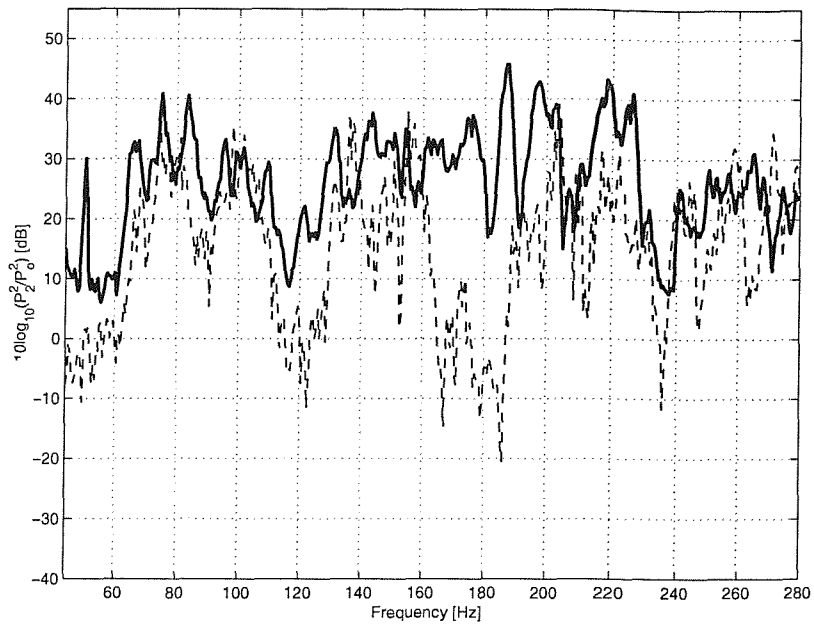

a)

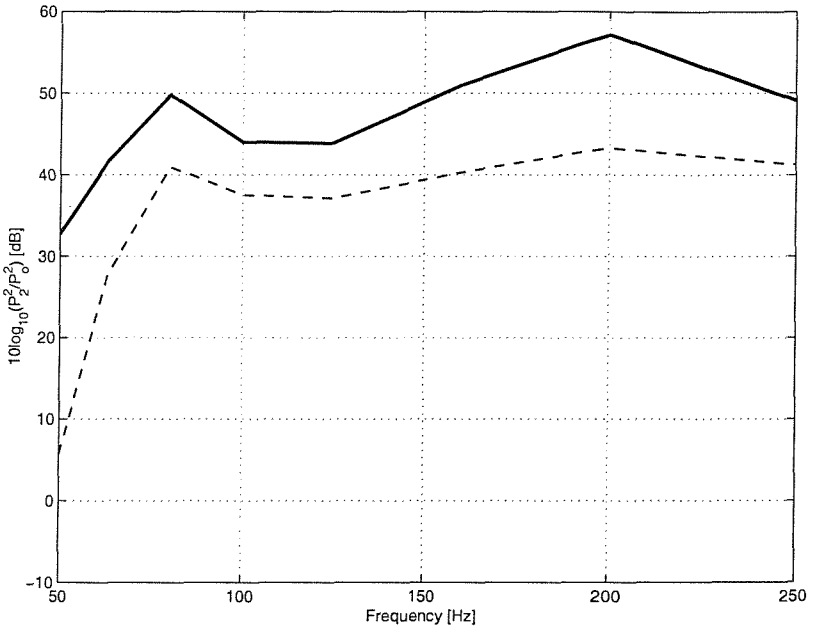

b)

Figure 3.44: Comparison between measured and predicted sound pressure levels (dB re $2x10^{-5}$ Pa) at position 2 for the receiving room; a) narrow bands; b) one third octave bands; _____ measured; ----- predicted

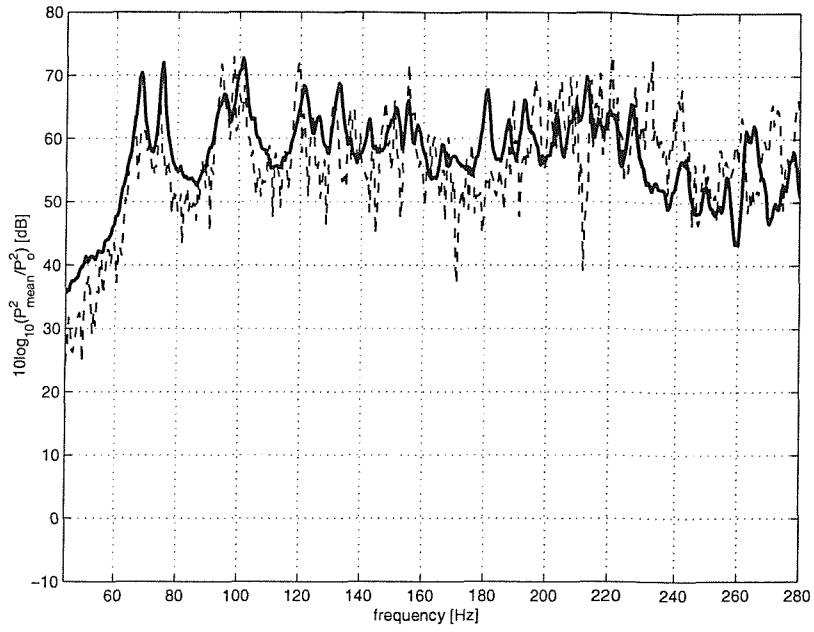

a)

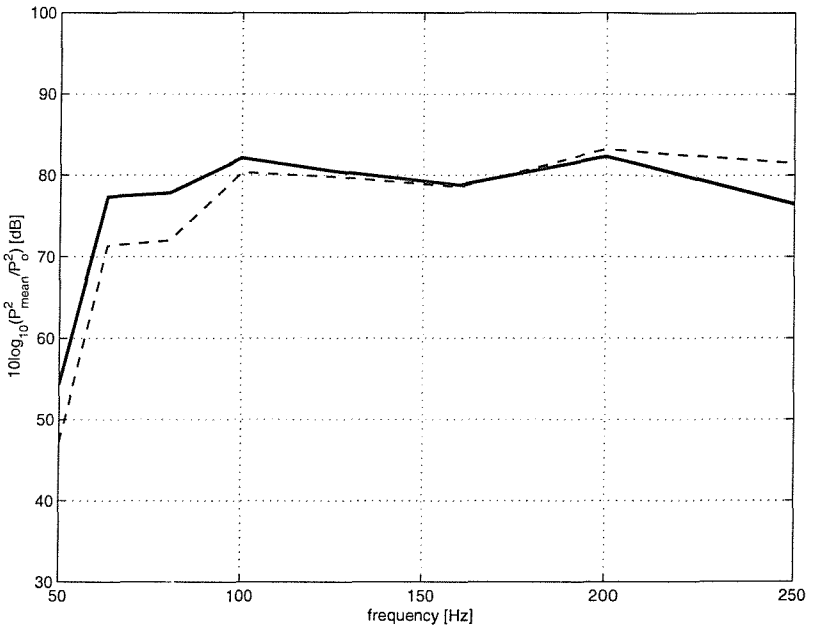

b)

Figure 3.45: Comparison between measured and predicted sound pressure levels (dB re $2x10^{-5}$ Pa) averaged over all positions for the source room; a) narrow bands; b) one third octave bands; _____ measured; ----- predicted

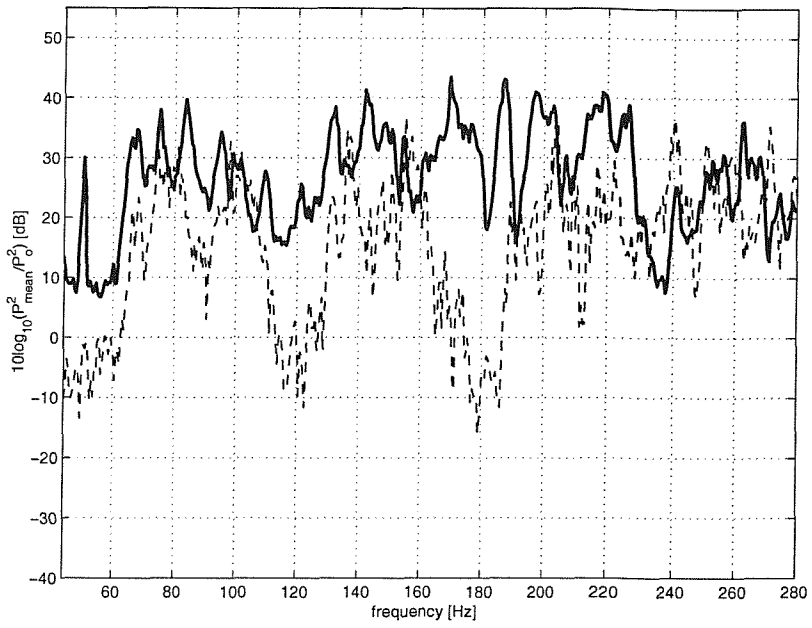

a)

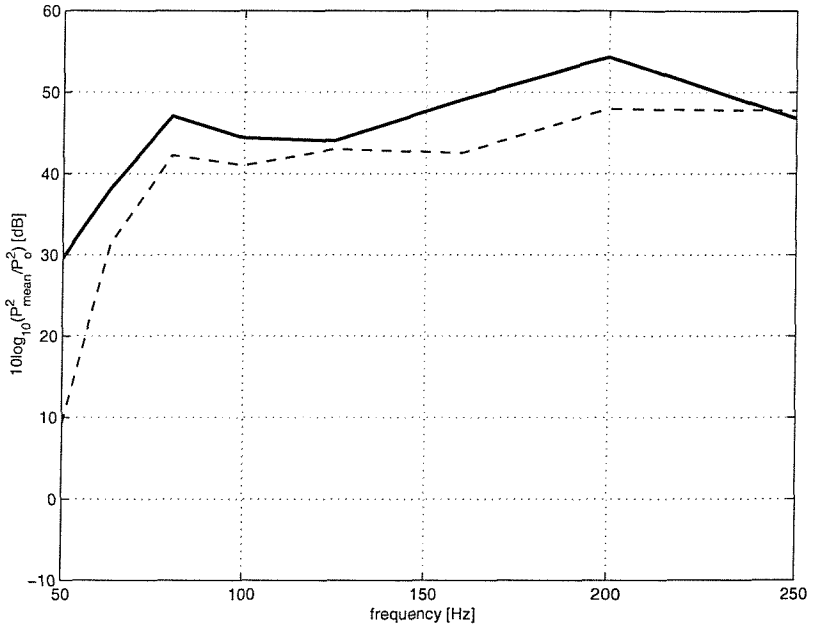

b)

Figure 3.46: Comparison between measured and predicted sound pressure levels (dB re $2x10^{-5}$ Pa) averaged over all positions for the receiving room; a) narrow bands; b) one third octave bands; _____ measured; ----- predicted

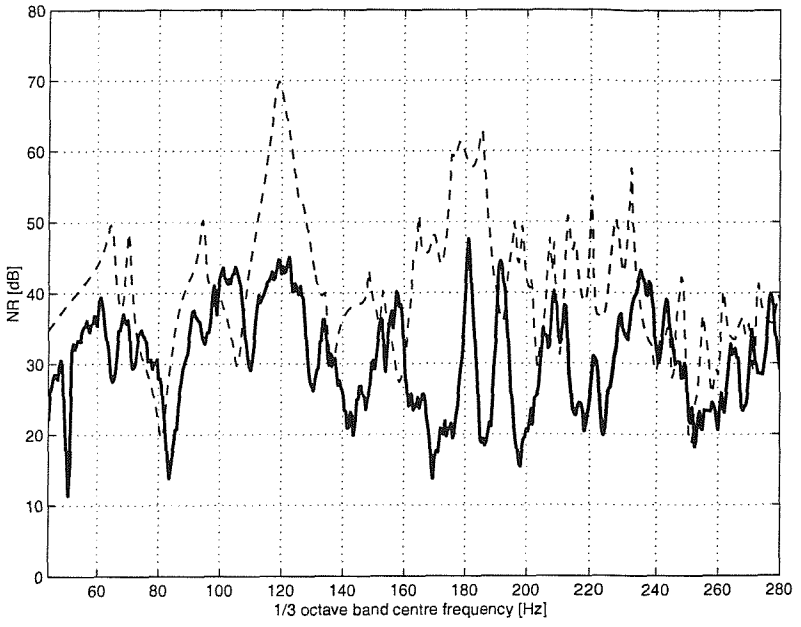

a)

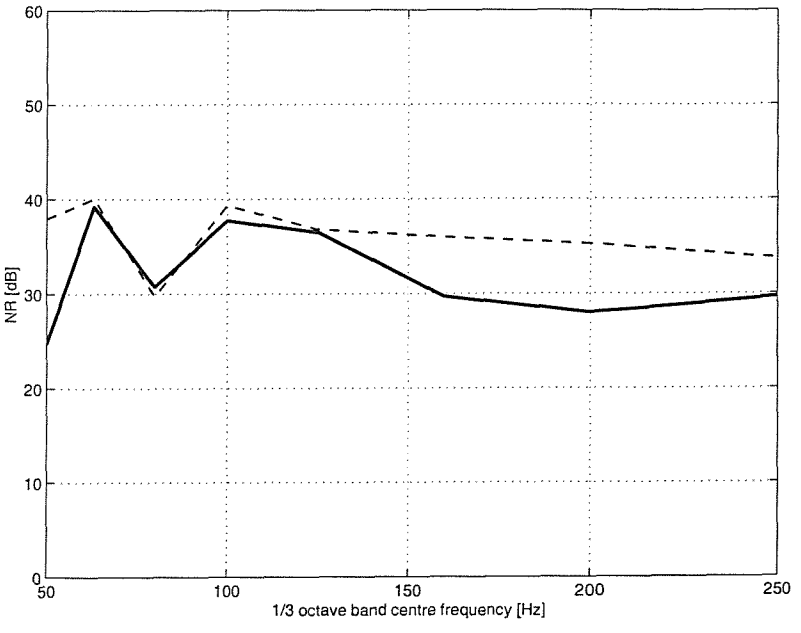

b)

Figure 3.47: Comparison between measured and predicted NR levels; a) narrow bands; b) one third octave bands; _____ measured; ----- predicted

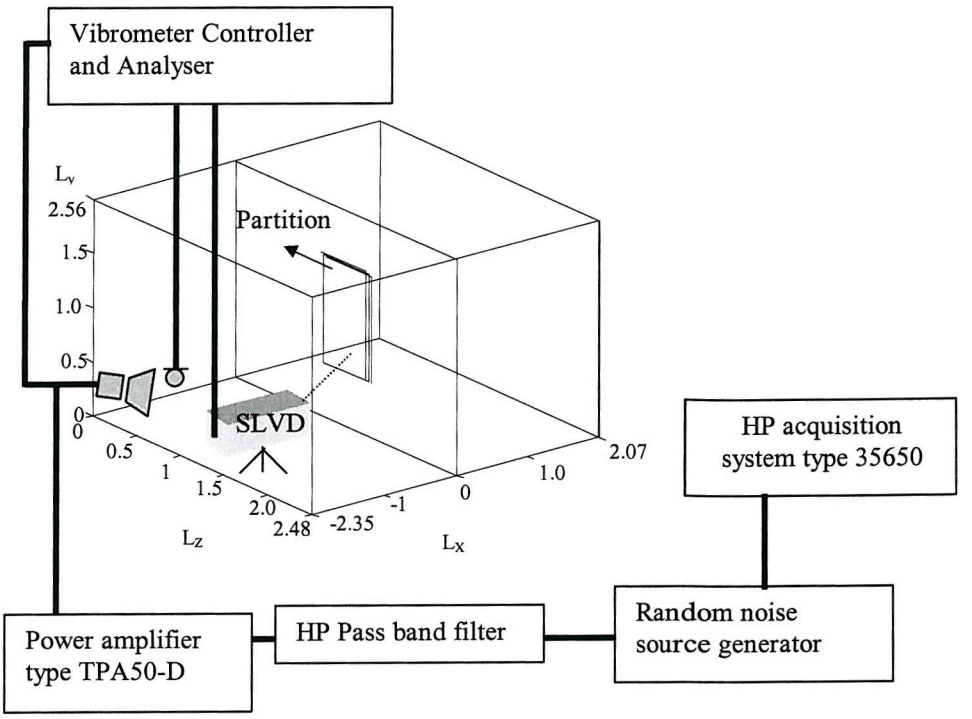

Figure 3.48: Experimental setup for the laboratory measurement of partition velocity.

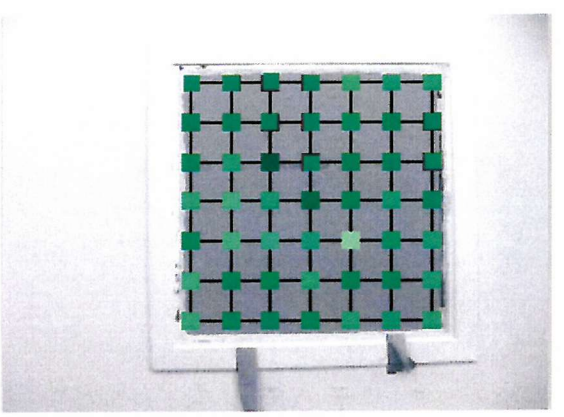

Figure 3.49: Definition of the scanning points over the partition

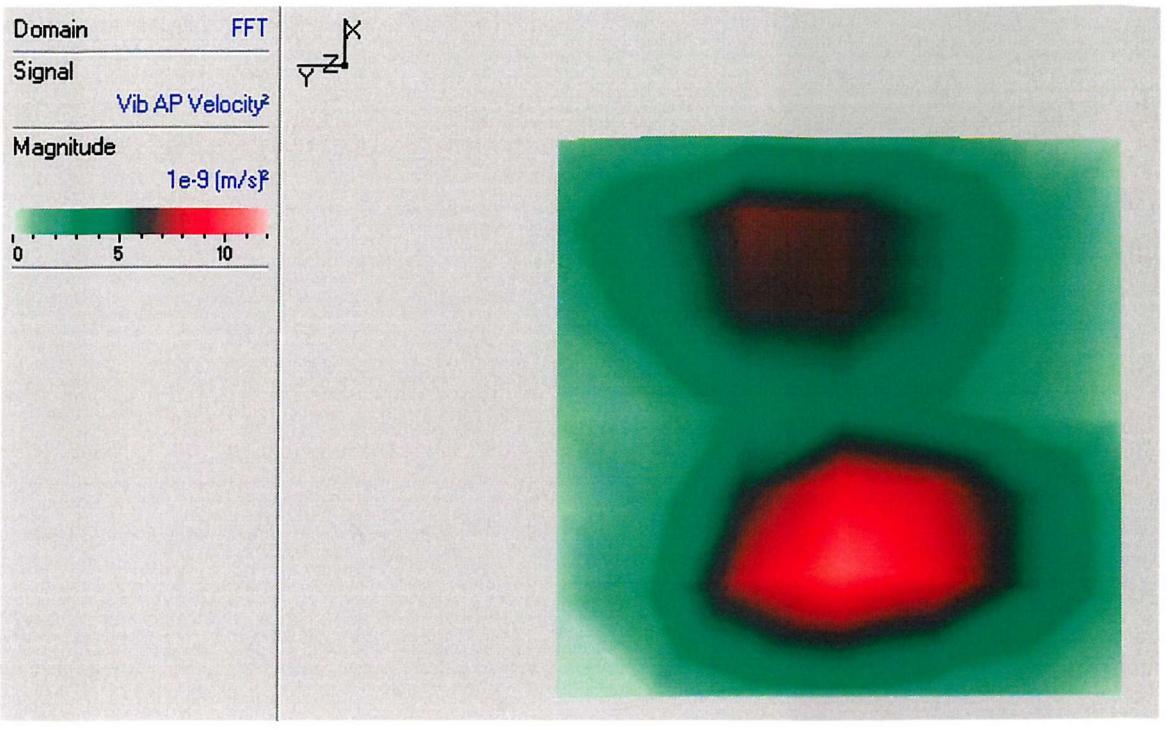

Figure 3.50: Mean square normal velocity distribution over the partition at the frequency band equal to 100 Hz

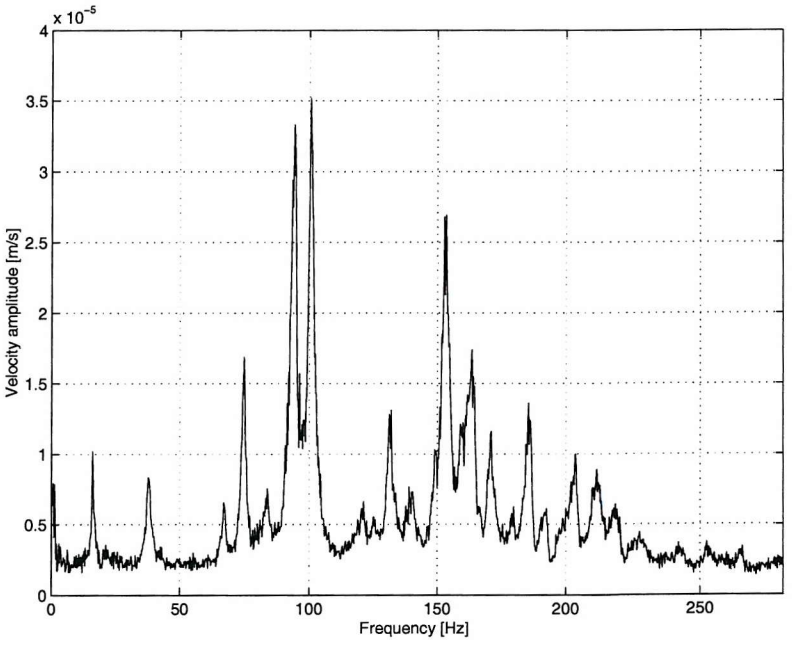

Figure 3.51: Partition normal velocity amplitude over the frequency band 0-280 Hz.

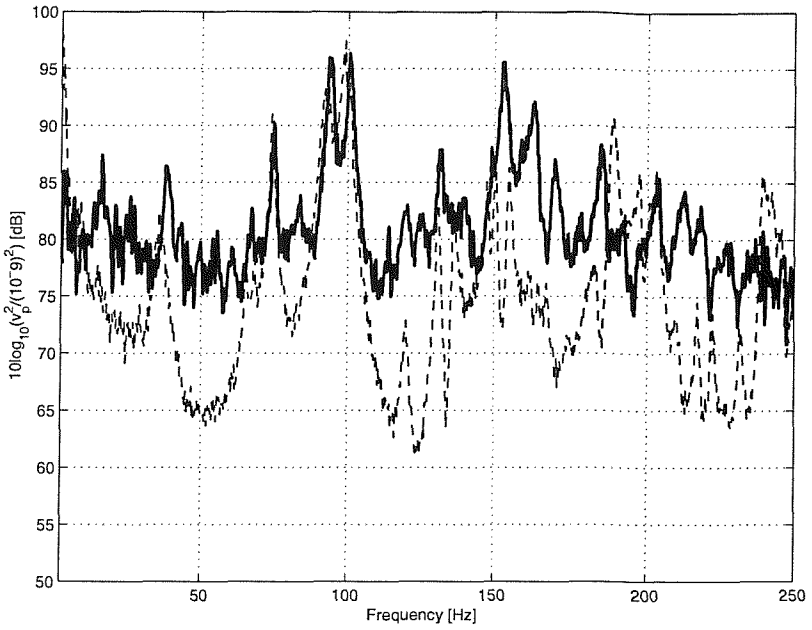

Figure 3.52: Mean square normal velocity of the test partition [dB re 10^{-9} m/s] in narrow frequency bands.

measured; -------- predicted

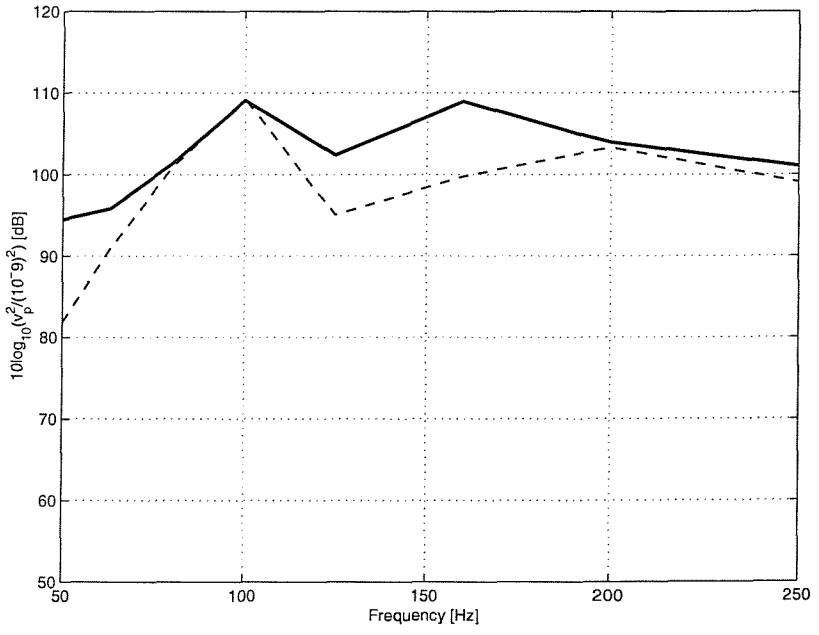

Figure 3.53: Mean square normal velocity of the test partition [dB re 10^{-9} m/s] in one-third octave bands.

measured; -------- predicted

Chapter 4

SOUND TRANSMISSION SENSITIVITY AND VARIABILITY USING THE MODAL MODEL

4.1 – Introduction

Whilst most predictions in building acoustics and design invariably use published and readily available models, some attempt to quantify confidence limits that cover most cases would be invaluable. For instance, the parameters (e.g. room dimensions, panel position, room absorption, etc.) are shown to have a substantial effect on the Noise Reduction (NR) and Coupling Loss Factor, the latter being a very important factor for predicting sound transmission using Statistical Energy Analysis (SEA) [8]. These considerations are discussed in detail in the following sections.

The main goal of this Chapter is to examine the variability of the Noise reduction difference and CLF to some architectural parameters via a parametric study. This study is aimed at providing not only a better understanding of the sound transmission mechanism in itself but also to produce a useful set of data which for instance can be used by acousticians as input data for a SEA analysis. This data might be useful for optimizing sound insulation in buildings at low frequencies, where the modal behaviour of rooms strongly influences the transmission.

This Chapter is organized as follows. Firstly, a parametric study of the influence of the source and receiving room dimensions on the Noise Reduction (NR) is investigated in section 4.2 (see Figures 4.1, 4.2 and 4.3). Next, the effects of room absorption on transmission is considered and discussed in section 4.3. Then, the influence of different panel positions in the common wall between rooms (see Figure 4.4) on NR is considered in section 4.4. Finally, in section 4.5, the equivalent CLF is evaluated on the basis of SEA assumptions and the influence of modal density and modal overlap is considered.

The results that are discussed in this Chapter were obtained via simulations using the modal model developed in Chapter 2. The analysis is based on considering the influence of some variations in the 'input' parameters, which are required in the pre-processing

stage of a numerical experiment, and on the subsequent sound transmission mechanisms of typical building configurations.

4.2 – The influence of room dimensions on sound transmission

In this section, the influence of the room dimensions on the NR has been considered. Numerical experiments were made using sets of simulations, which follow a pre-established analysis pattern. In other words, this analysis was based on the variation of a particular geometrical parameter whilst keeping the others unaltered. Thus, the assessment of the variability and sensitivity of transmission efficiencies to a chosen parameter can be made. In general, there will be some inter-dependence but this is outside of the scope of this initial investigation.

Firstly, the variation of NR with the ratio of the receiving room height to the source room height is considered. In order to perform the simulations, usually an initial model ought to be defined *a priori*. The baseline model was defined as two dissimilar rooms separated by a common elastic partition over the whole interface. The thickness of the partition was 0.01m. The density and Young's Modulus of Elasticity were 806 kg/m^3 and 2.12x10^9 N/m^2 respectively. The critical frequency of the partition was 3815 Hz. The reverberation time for the source and receiving room surfaces was chosen as an averaged value of $T_{60} = 1.0s$. In terms of damping values this represents a total loss factor equal to $\eta = 2.2/fT_{60}$; where f is the corresponding centre frequency of a particular one third octave band. A source of unit volume velocity was located at position (-L_{x1}, 0,0) where L_{x1} is the depth of the source room.

The continuous solid and dashed lines (shown in Figures 4.1, 4.2 and 4.3) represent the initial and modified configurations respectively. A total number of 11 iterations were made in order to simulate the original (solid line) and modified models in each case. The models were obtained by logarithmically varying one dimension at a time (height, width or depth of room 2) whilst keeping the others unaltered. For the baseline model, a total number of 48, 35 and 97 modes were used for room 1, room 2 and partition respectively. The frequency range and volume sizes considered dictated the choice of the number of modes used.

Figures 4.5 (a) and (b) show the variation of the difference between the diffuse incidence Noise Reduction NR_{ML} (obtained from the Mass Law Theory - equation (2.6)) for an infinite panel with frequency for distinct heights of room 2 (see Figure 4.1) and the 'actual' Noise Reduction NR^{ij}_{modal}. The analysis was performed in one-third octave bands (from 20 to 250 Hz). In this frequency range, a total number of 287 modes were used for the greatest height of room 2, i.e. L_{y2} =18 m. The Noise Reduction values NR^{12}_{modal} and NR^{21}_{modal} were calculated for constant volume velocity source located in room 1 (where the height was kept fixed) and room 2 respectively. The variation of the parameters with the receiving room height is given in Table 4.1.

The 'actual' Noise Reduction NR^{ij}_{modal} was obtained by predicting the sound pressure level difference between the source and receiving rooms. The diffuse field Noise Reduction NR_{ML} is defined in refs. [2,18], and likewise it was obtained using equations (1.1) and (2.6). The mean calculated normalized levels lie below 0 dB within most of the frequency range for all room configurations. This fact was predictable at low frequencies, where the diffuse incidence Mass Law overestimated the transmission efficiency due to the assumption of diffuse field behaviour in the source room. Hence, both results that are referenced to the Mass Law show convergence being achieved in the frequency range under investigation, especially at high frequencies where the agreement is fair.

The calculated 'Schroeder' frequency (see equation (2.1)) given in Table 4.1 was greater than the highest 1/3 octave band centre frequency considered in all model configurations. Therefore, the predicted system response in all cases was strongly influenced by individual modes of the rooms.

At very low frequencies, a significant variation in the NR differences occurred between the configurations. On the other hand, as the frequency increased the differences were significantly reduced. As it is known, the influence of room dimensions on sound transmission is generally less significant when the acoustic wavelengths are in the order of or smaller than the room dimensions. Consequently, the pressure variation tends to become smaller over the whole acoustic volume of both source and receiving rooms.

By comparing Figures 4.5 (a) and (b), it is seen that the variation of the height of the receiving room had a significant effect on the sound transmission primarily at low frequencies. On the other hand, in general the variation of the height of the source room

(room 2) did not alter the Noise Reduction NR^{21}_{modal} substantially. This result is consistent with the findings on structure-borne sound transmission proposed by Craik *et al* [61]. It was hypothesized that the Coupling Loss Factor (CLF) varies with the mobility of the receiving subsystem, not that of the source subsystem. In other words, the modal properties of the source subsystem do not seem to have as much influence on the sound transmission mechanism. If one examines the results above 80 Hz, where modes of both rooms exist, then the variation in the transmission is similar and it is not so obvious that the source subsystem can be neglected when examining the variability.

In Figure 4.5 (a), there is a significant variation of the NR differences in the frequency range 31.5-80 Hz. It is also seen that above 80 Hz, which is also the fundamental natural frequency of the room 2 for the baseline model, the differences between configurations were sharply reduced. The acoustic wavelength assumed values smaller than the room heights. In this situation, the geometry of room 2 had no influence on the interaction between modes and therefore the system behaved like two similar rooms. Figure 4.5 (b) shows that the highest value of the NR difference (and consequently the lowest value for NR^{21}_{modal}) is in the 63 Hz band centre, which is approximately the fundamental frequency of room 1. It is also evident that for identical rooms, which have similar resonance frequencies and eigenfunctions, the NR difference is much higher.

Likewise, Figures 4.6 (a) and (b) show the variation of the NR differnece obtained when considering Leppington's approach [16]. The results are on average higher than those using the Mass Law approach (Figures 4.5 (a) and 4.5 (b)). This indicates that the effect of considering panel dimensions on predicting the results, as considered in ref. [16], was significant in the low frequency ranges.

Figures 4.7 (a) and (b) show the variation of the NR difference values predicted using the modal model to those obtained via the Mass Law whilst varying the width of room 2 from 2.0 to 20.0 m (see Table 4.3). A total number of 290 modes were selected for the greatest width, which was equal to 20.0 m. For all cases the depths and heights of rooms were kept constant (see Figure 4.2). Different configurations of the receiving room were important on predicting NR^{12}_{modal} at frequencies below 100 Hz. Above 100 Hz, there was not much change from Figure 4.7 (a) to 4.7 (b) in terms of NR levels. A maximum difference of 5 dB is found as frequency increases.

Figure 4.8 presents the variation of the results using Leppington's approach. As mentioned above, the results (in terms of the NR differences) using Leppington's approach tended to be greater than those obtained via the diffuse incidence Mass Law theory.

Figure 4.9 and 4.10 show the variation of the NR differences for different values of depth ratio (see Table 4.4) compared to the 'Mass Law' and Leppington's formula respectively. For the greatest value for the depth, a total number of 290 modes was used in the calculations. It is seen that below about 80 Hz, the results for NR^{12}_{modal} present differences up to about 20 dB. Above 80 Hz, the differences are reduced to less than 10 dB. At the higher frequencies, the acoustic wavelengths were less than the room depths. In this situation, the geometry of the 'corridor', which is usually used as a mean of connecting rooms in a real building, did not have such a strong influence on the interaction between the modes and therefore the system behaved like two similar rooms. Furthermore, the variation of the results in terms of the Noise Reduction NR^{21}_{modal} was less than about 10 dB over the whole frequency range. This fact indicates once again that the power transmission between subsystems is most dependent on the characteristics of the receiver for the low frequencies.

In summary, the predicted values depend on how well the modes of both subsystems are coupled to each other. This can be justified by some examples presented in Chapter 2 where higher NR values were obtained for poor coupling between the subsystem modes at the interface. As mentioned previously, similar room volumes yield identical natural frequencies and mode shapes, which lead to a strong geometrical coupling in addition to frequency matching. For instance, in Figure 4.5 poorer sound insulation is clearly observed when $L_{y2} = L_{y1}$ at 250 Hz. Conversely, higher sound insulation is obtained when mismatching of modes occurs in the case of considering two geometrically different rooms coupled together.

4.3 – The influence of room absorption on sound transmission

In this section, the influence of room absorption on sound transmission is investigated using the same baseline model defined previously.

Figures 4.11 and 4.12 present the variation of the NR differences for the baseline model when the Reverberation Time of room 2 (T_2) took different constant values from 1.0 s to 0.2 s over all frequencies. In Figure 4.11 (a), the normalized transmission ratio levels increase with absorption at frequencies below 80 Hz. Variations of less than 10 dB are found. However, there is no significant variation at higher frequencies.

At high frequencies (above the Schroeder frequency) when the reverberation time is decreased, the modal overlap factor is increased and vice-versa. This results in a higher probability of better coupling between individual modes and therefore lower sound insulation. However, the first natural mode for the receiving room is at 85 Hz, so that below 85 Hz the variation of the NR difference with frequency was mainly due to the use of equation (2.49) in which a diffuse field condition is assumed. It relates the damping for the receiving room to the SRI values.

The variation in the absorption of the source room did not have significant influence on the sound insulation (see Figure 4.11 (b)). Whilst the modal damping of the source room was increased, the modal properties of the receiving room remained practically unaltered. Although higher absorption exists in the source room, resulting in lower sound intensity on the partition, the proportion of this power transmitted appears to be unaffected.

Figures 4.12 (a) and (b) show the variation of the NR difference with frequency for different values of T_2 compared to Leppington's formula. Although the plots show similar trends compared to those presented in Figure 4.11, higher values of the NR difference are found when frequency increases.

4.4 – The influence of panel position on sound transmission

The sensitivity of the NR relative to a flexible panel position, with the rest of the common wall rigid, is shown in Figure 4.13 and 4.14 compared to the diffuse incidence Mass Law [14,18] and Leppington's prediction [16] respectively. A total number of 10 structural modes were considered for the simply-supported panel with dimensions 0.6m x 0.8m. The thickness of the partition was *0.01*m. The density and Young's modulus of elasticity were *806* kg/m^3 and 2.12×10^9 N/m^2 respectively. The reverberation time for both the source and receiving room were constant and equal to 1.0 s. The predicted fundamental natural frequency for the simply supported panel was 32.9 Hz.

The results presented in Figures 4.13 and 4.14 show similar trends over the frequency range considered. Nevertheless, the results shown in Figure 4.14 are on average about 6 dB higher than those presented in Figure 4.13 over most of the frequency range. It might be explained by the influence of the panel surface area on the transmission efficiency which is taken into account in the Leppington's formulation. The first distinct peak in the NR difference levels was observed at about the fundamental natural frequency of the panel. It is known that at a panel-controlled resonance, the transmission efficiency is not dependent on the room acoustic impedance, but upon geometrical coupling factors.

At low frequencies, the spatial distribution of room modes varies mainly along preferential directions (e.g. the x axis direction perpendicular to the panel). Below 80 Hz, the NR difference curve (Figures 4.13 (a) and 4.14 (a)) does not exhibit distinct differences whilst varying the panel position. This is understandable as the fundamental frequency of room 2 is 85 Hz. When panel-controlled modes are excited below the room-controlled modes, the Mass Law behaviour may tend to dominate the transmission. However, for the opposite situation, when the panel-controlled resonance frequency is higher than the room-controlled resonance frequency, non-resonant panel stiffness behaviour may then dominate [60].

For the panel at the corner (position P_4), where the tangential modes in the receiving room were fully excited, higher values of transmission occurred. As mentioned in Chapter 2, it is dependent on the degree of geometric coupling between the structural and acoustic modes. When the frequency increased, oblique modes tended to be dominant in the rooms and the difference between the panel positions became less important on the sound insulation.

Figure 4.15 shows the contribution of a particular mode 'n' to the total spatially averaged mean square pressure in the receiving room for different values of panel position on the common wall. The results are presented in terms of the ratio of the spatially averaged mean square pressure of mode 'n' to the total spatially averaged mean square pressure. Figures 4.15a and 4.15b show the results obtained using 1/3 octave bands with centre frequencies at 125 Hz and 200 Hz respectively. Figure 4.15a shows that the uncoupled modes (1,0,1), (0,1,1) and (1,1,0) have the most significant contribution to the spatially averaged mean square pressure in the receiving room in the lower of the two bands. For instance, the greatest contribution is due to the (0,1,1) mode when the panel is at position

P_1. On the other hand, Figure 4.15b shows that for the panel at position P_8, the uncoupled (1,2,0) mode is the main contributor in the one-third octave band centred at 200 Hz.

In summary, transmission behaviour becomes complex and dependent on panel position. With the panel located at the centre of the common wall, only few structural modes were excited. However, as the panel location was moved into the corner of wall, most of its even and odd modes were excited. This occurred because of the response of a large number of *in vacuo* panel modes to oblique fields excited by the point source. Similarly, the reduction or increase of the coupling between the source room and panel, depending upon panel location, is also replicated in the coupling between the panel and the receiving room.

4.5 – Comparison of the transmission variability with published results on Coupling Loss Factor variability

4.5.1 – Introduction

Generally, the sound transmission mechanism in a real building involves a great number of different and complex transmission paths. In Statistical Energy Analysis (SEA) these paths are classified as direct and flanking paths [62]. In this section, only the direct transmission is considered in the implemented SEA model, so that the problem was described as one room emitting noise and another room receiving it. Thus, in this section a limp panel model with nominal density equal to 8.1 kg/m^2 is considered. The thickness of the partition was *0.01*m. A Reverberation Time T_{60} =1s was considered herein.

The spatial averaged, time averaged energy for each acoustic subsystem was evaluated from this baseline model, which consisted of two rooms coupled by a limp partition. Later on this Chapter, one can see that it was necessary to use a limp panel model, so that some parameters (in terms of CLF variability) defined in the literature could be used herein for comparison.

The performance of a building can be predicted by a basic SEA technique, which is described in refs. [8] and [63]. The power flow between SEA subsystems can be described by the coupling between them that takes places at their boundaries. For instance, the fraction of maximum stored energy of subsystem 1 transmitted to subsystem 2 per cycle is $2\pi\eta_{12}$, where η_{12} is the Coupling Loss Factor (CLF). This is

defined in the similar way to the definition of the loss factor η of a subsystem, namely $2\pi\eta$ is the fraction of the maximum stored energy which is lost or dissipated per cycle. This can be lost through mechanical and thermal means or can take into account losses due to other subsystems, which have not been explicitly defined.

4.5.2 – The SEA model

The aim of this section is to make an initial parametric investigation for the CLFs and then compare their variability with theoretical upper and lower bound curves previously presented in the literature [58]. Thus, the usefulness of SEA as a framework of analysis can be assessed by the estimation of variance and confidence intervals.

The simplest method of estimating the CLFs is presented here for the sake of simplicity and in order to provide results that can be compared with published data [58]. Therefore, the main assumption here is that there are only two subsystems in the SEA model, which correspond to the source and receiving rooms. It seems that this assumed condition is reasonable, as the non-resonant transmission or forced transmission is the most important contribution to the transmission mechanism.

In SEA modelling, one of the most important parameters is the modal density. It is defined as the number of modes that lie in an increment of frequency. For instance, the modal density for a standard room is given by [8]

$$n(f) = \frac{4\pi f^2 V}{c_o^3} + \frac{\pi f S'}{2c_o^2} + \frac{L'}{8c_o} \tag{4.1}$$

where V is the room volume, S' is the total surface area of the room and L' is the total perimeter of the room. Table 4.1 shows the variation of the modal density for room 2 in the one-third octave band with centre frequency at 250 Hz. The modal density for room 1 was equal to 0.419 in the same frequency band.

According to Figure 4.16, the power balance equations for the two coupled rooms (which are represented by the subscripts 1 and 2) and excited one at a time are then given by [64]

$$P_{1,in}^1 = P_{1,diss}^1 + P_{12}^1 = \omega\left(\eta_1 E_1^1 + \eta_{12}^1 E_1^1 - \eta_{21}^1 E_2^1\right) \tag{4.2}$$

$$0 = P_{2,diss}^1 + P_{21}^1 = \omega\left(\eta_2 E_2^1 + \eta_{21}^1 E_2^1 - \eta_{12}^1 E_1^1\right) \tag{4.3}$$

$$P_{2,in}^2 = P_{2,diss}^2 + P_{21}^2 = \omega\left(\eta_2 E_2^2 + \eta_{21}^2 E_2^2 - \eta_{12}^2 E_1^2\right) \tag{4.4}$$

$$0 = P_{1,diss}^2 + P_{12}^2 = \omega\left(\eta_1 E_1^2 + \eta_{12}^2 E_1^2 - \eta_{21}^2 E_2^2\right) \tag{4.5}$$

where η_i is the Internal Loss Factor for each subsystem, E_i is the spatial averaged, time averaged energy in subsystem i. η_{ij} is the Coupling Loss Factor from subsystem i to subsystem j. ω is the angular frequency in radians per second. P_{diss} and P_{in} are the time averaged dissipated and input powers respectively. P_{ij} is the power transmitted from subsystem i to subsystem j. The superscripts 1 and 2 indicate in which subsystem the excitation is applied separately one at a time.

Therefore, by assuming that $\eta_{ij}^1 = \eta_{ij}^2$ and according to the concept of power injection method [65], the 'effective' Coupling Loss Factor η_{ij} for two conservatively coupled subsystems 1 and 2 can be obtained by rearranging the equations (4.3) and (4.5) as

$$\begin{Bmatrix} \eta_{12} \\ \eta_{21} \end{Bmatrix} = \frac{1}{\omega}\begin{bmatrix} E_1^1 & -E_2^1 \\ -E_1^2 & E_2^2 \end{bmatrix}^{-1} \begin{Bmatrix} \omega\eta_2 E_2^1 \\ \omega\eta_1 E_1^2 \end{Bmatrix} \tag{4.6}$$

The spatial average time averaged energy for an acoustic subsystem i can be obtained according to the general expression [8]

$$E_i = \left(\frac{\left\langle \overline{p}_i^2 \right\rangle V_i}{\rho_o c_o^2}\right) \tag{4.7}$$

where V_i is the volume of subsystem i and $\left\langle \overline{p}_i^2 \right\rangle$ is the spatial averaged mean square pressure in subsystem i. This has been obtained by using the modal model derived in Chapter 2, which was modified to calculate the coupling between the volumes by a limp panel. The calculations were run with no dissipation in the limp panel.

Likewise, the damping Loss Factor of a particular acoustic subsystem i may be approximated by the expression [8]

$$\eta_i = \frac{13.8}{\omega T_{60,i}} \tag{4.8}$$

where $T_{60,i}$ is the Reverberation Time for subsystem i. For the SEA simulations $T_{60,i}$ was constant and equal to 1.0 s. Equation (4.8) is a general expression for the total loss factor

which only gives the damping loss factor for weakly coupled systems (i.e. CLFs << internal loss factor) as measurements for the Reverberation Time will normally include some effect of dissipation from other subsystems connected to the volume. Therefore, a value of T_{60} was set and then used to infer the damping loss factor.

Although the CLFs are only defined for finite systems, an expression for the CLF of 'semi-infinite' acoustic subsystems can be obtained by assuming diffuse field conditions in both rooms. In addition, it is assumed that there is direct transmission between rooms, where forced transmission is the most important contribution. Thus, the CLF η_{12} from subsystem 1 to subsystem 2, is given approximately by [8]

$$\eta_{ML} \approx \frac{c_o S \tau_\infty}{4\omega V_1} \tag{4.9}$$

where τ_∞ is the diffuse transmission efficiency obtained via Mass Law theory described previously. V_1 is the volume of the source room and S is the partition area.

The Coupling Loss Factor η_{21} can also be obtained from η_{12} by the consistency relationship [64]

$$n_1 \eta_{12} = n_2 \eta_{21} \tag{4.10}$$

where n_1 and n_2 are the modal densities (see equation (4.1)) for subsystems 1 and 2 respectively.

The variability of the CLFs with the subsystem properties in SEA models have been recently studied by Park et al [58]. A sensitivity analysis was performed using an analytical model for two coupled plates. The Dynamic Stiffness Method was used in the evaluation of their model. Thus, an 'empirical model' for the variability of CLF (σ^2) was derived for two coupled finite plates according to the expression [58]

$$\sigma^2 = \frac{6}{M_{comb} + N_{comb}^2/16} \tag{4.11}$$

$$M_{comb} = \frac{2M_1M_2}{M_1 + M_2} \tag{4.12}$$

$$N_{comb} = \frac{2N_1N_2}{N_1 + N_2} \tag{4.13}$$

where σ^2 is the variance of the dB values; M_{comb} and N_{comb} are the combined modal overlap factor and number of modes respectively. M_1 and M_2 are the modal overlap factors for subsystems 1 and 2 respectively. They are defined as the ratio of the modal bandwidth to the average frequency spacing between modes [8]. Similarly, N_1 and N_2 are the mode counts for subsystem 1 and 2.

4.5.3 – Results

Results were obtained in terms of the variation of the CLF ratio with the combined modal overlap factor M_{comb} for different room configurations. The numerical frequency range covered was 0 to 300 Hz, although the results are only plotted at values where at least one non bulk mode exists in either room. Firstly, the CLF ratio, in Figures 4.17-4.21, was defined as the ratio of the 'effective' coupling loss factor (equation (4.6)), obtained for a particular system configuration, to the averaged 'effective' CLF, which was obtained by considering the mean value over all of the different configurations of a particular parameter, e.g. the height ratio of the rooms. The results were calculated in sets of one-third octave bands.

Secondly, the CLF ratio, in Figures 4.22 and 4.23, was calculated as the ratio of the 'effective' CLF to the one obtained using equation (4.9). Although an average result was used for reference, it did not converge to the diffuse incidence Mass Law.

Figures 4.17-4.19 show the variation of CLF ratio with M_{comb} whilst varying the height, width and depth ratio of the rooms. In Figure 4.17, the source room height was fixed and equal to 1.8 m. The receiver height varied from 1.8 to 18 m. It is seen that the results lay within the bounds for most of the M_{comb} range. At higher frequencies, the CLF ratio values vary within the range +/- 1dB.

Likewise, Figures 4.18 and 4.19 also show that the convergence of the results rapidly increases with the combined Modal Overlap factor. Figure 4.18 shows that at higher Modal Overlap factors, the CLF ratio values tend to be less than +/- 0.5 dB. Similarly, Figure 4.19 shows a fairly good convergence rate with increasing Modal Overlap.

Figure 4.20 shows the variation of CLF ratio with M_{comb} for different values of the Reverberation Time ratio (T_2/T_1). The Reverberation Time of the source room was fixed and equal to 1.0 s. However, for the receiving room it was varied from 1.0 s to 0.2 s. It

appears that the most significant variations in terms of the CLF ratios occurred for the case of varying the RT of the source room whilst keeping the RT of the receiving room constant.

Figure 4.21 shows the variation of CLF ratio with M_{comb} for different values of panel position on the common rigid wall. Very small variation is observed at the lower values of M_{comb}, i.e. at lower frequencies for the source and receiving rooms where there are few if any acoustic modes and transmission is low. On the other hand, significant variations occur in the range where acoustic modes exist. These variations indicate very high spatial coupling sensitivity.

Finally, Figures 4.22 and 4.23 show the variation of CLF ratio, which is defined here as the ratio of the actual transmission to the diffuse incidence Mass Law transmission, with M_{comb} whilst varying the height and width of the rooms respectively. In Figure 4.22, the source room height was fixed and equal to 1.8 m. The receiver height varied from 1.8 to 18 m. It is seen that the results approximately lay on the upper bound for most of the M_{comb} range. However, they tend to diverge from the Mass Law results η_{ML} as the combined modal overlap increases. Likewise, Figure 4.23 shows that the Mass Law results η_{ML} are lower than the 'effective' Coupling Loss factor at low frequencies. However, the 'effective' CLF tends to be lower than the η_{ML} when frequency increases.

4.6 – Conclusions

Firstly, the variation of the NR differences with frequency whilst varying one of the room dimensions has been presented in this chapter. It was shown that at very low frequencies, the variation of the room dimensions affected the transmission substantially. These results are similar with those of Craik [61], which showed that for transmission between plates it is the receiving subsystem that affects the power flow. At the higher frequencies there is an increasing contribution from the source room though.

In addition, the results in terms of convergence to the Mass Law predictions have shown poor agreement at low frequencies. This is because of the strong modal behaviour of the chosen subsystems, which have obviously low mode count due to their small volumes. Nevertheless, it is seen that at higher frequencies a fairly good agreement is achieved, as

the sound field tended to become more 'diffuse'. In general, the results show a difference of less than 3 dB in the frequency band with centre frequency at 250 Hz, for example.

Finally, numerical simulations for the investigation of the variation of CLF ratio with the combined Modal Overlap Factor were obtained for a limp panel model. Hence, there was no resonance contribution of the panel on the frequency response of the system. Even though there was no stiffness term in the equation of motion of the panel, i.e. the panel was limp, its mass term was allowed to contribute.

The sound transmission results thus had no resonant panel behaviour and the variation of results were mainly due to the panel position and also the matching or separation of the room natural frequencies (i.e. modal overlap).

The results were then compared to previously published envelope results given for structure to structure coupling limits (Park *et al* in reference [58]). It is seen that most of the results, which are presented in terms of CLF ratio, fit reasonably well within the published envelope results [58] for the frequency range investigated. Only the results due to variation of the panel position are not in such good agreement and it is suspected that this might be due to extreme sensitivity of the modal model to the spatial coupling terms.

The actual fluid-structure interaction problem considered herein was evaluated at very low frequencies. In addition, small acoustic volumes were considered for the baseline models. Consequently, small values of Modal Overlap Factors were obtained. The envelope results presented by Park *et al* [58] were developed on the basis of only two coupled subsystems, namely two coupled rectangular plates. Hence, there was no 'intermediate' connection between them, such as a beam. In other words, the modal model formulated here was equivalent to the structure-to-structure coupling problem published in ref. [58], as the model herein considered the contribution of a limp partition with no modes on the transmission mechanism. No attempt has been made here to produce alternative limits for the acoustic-structural problem, as it does not appear to be particular easy to solve or generalize.

Tables

L_{y2}/L_{y1}	L_{y1}(m)	L_{y2}(m)	L_{x1}(m)	L_{x2}(m)	$L_{z1}=L_{z2}$	n_1 (f)	n_2 (f)	$f_{1,Schroed}$	$f_{2,Schroed}$
1.000	1.800	1.800	3.000	2.000	2.000	0.419	0.290	430.3	527.0
1.259	1.800	2.266	3.000	2.000	2.000	0.419	0.356	430.3	469.7
1.585	1.800	2.853	3.000	2.000	2.000	0.419	0.438	430.3	418.6
1.995	1.800	3.591	3.000	2.000	2.000	0.419	0.542	430.3	373.1
2.512	1.800	4.522	3.000	2.000	2.000	0.419	0.673	430.3	332.5
3.162	1.800	5.692	3.000	2.000	2.000	0.419	0.837	430.3	296.4
3.981	1.800	7.166	3.000	2.000	2.000	0.419	1.045	430.3	264.1
5.012	1.800	9.022	3.000	2.000	2.000	0.419	1.305	430.3	235.4
6.309	1.800	11.356	3.000	2.000	2.000	0.419	1.634	430.3	209.8
7.943	1.800	14.297	3.000	2.000	2.000	0.419	2.047	430.3	187.0
10.000	1.800	18.000	3.000	2.000	2.000	0.419	2.567	430.3	166.6

Table 4.1: Variation of room parameters with the height ratio L_{y2}/L_{y1}. L_x, L_y and L_z are room depth, height and width respectively. n (f) is the modal density in the highest 1/3 octave band with centre frequency equal to 250 Hz and $f_{Schroed}$ is the *Schroeder* frequency (Hz) above which the acoustic field is assumed to be diffuse. The subscripts 1 and 2 represent the source and receiving rooms respectively.

f_1(Hz)	f_2(Hz)	f_p(Hz)
0.0	0.0	4.2
56.7	85.0	9.9
85.0	85.0	11.2
94.4	94.4	16.9
102.2	120.2	19.4
110.1	127.1	22.9
113.3	127.1	26.4
127.1	152.9	28.6
139.1	170.0	32.6
141.7	170.0	38.1

Table 4.2: The first ten natural frequencies of the uncoupled rigid walled rooms and partition for the height ratio L_{y2}/L_{y1} =1. 'f' is the natural frequency of the uncoupled rooms and partition. The subscripts 1, 2 and 'p' represent the source, receiving and partition respectively.

L_{z2}/L_{z1}	L_{z1}(m)	L_{z2}(m)	L_{x1}(m)	L_{x2}(m)	$L_{y1}=L_{y2}$	n_1 (f)	n_2 (f)	$f_{1,Schroed}$	$f_{2,Schroed}$
1.000	2.000	2.000	3.000	2.000	1.800	0.419	0.290	430.3	527.0
1.259	2.000	2.518	3.000	2.000	1.800	0.419	0.357	430.3	469.7
1.585	2.000	3.170	3.000	2.000	1.800	0.419	0.440	430.3	418.6
1.995	2.000	3.990	3.000	2.000	1.800	0.419	0.546	430.3	373.1
2.512	2.000	5.024	3.000	2.000	1.800	0.419	0.678	430.3	332.5
3.162	2.000	6.324	3.000	2.000	1.800	0.419	0.845	430.3	296.4
3.981	2.000	7.962	3.000	2.000	1.800	0.419	1.055	430.3	264.1
5.012	2.000	10.024	3.000	2.000	1.800	0.419	1.319	430.3	235.4
6.309	2.000	12.618	3.000	2.000	1.800	0.419	1.652	430.3	209.8
7.943	2.000	15.886	3.000	2.000	1.800	0.419	2.071	430.3	187.0
10.000	2.000	20.000	3.000	2.000	1.800	0.419	2.598	430.3	166.6

Table 4.3: Variation of room parameters with the width ratio L_{z2}/L_{z1}. L_x, L_y and L_z are room depth, height and width respectively. n (f) is the modal density in the highest 1/3 octave band with centre frequency equal to 250 Hz and $f_{Schroed}$ is the *Schroeder* frequency (Hz) above which the acoustic field is assumed to be diffuse. The subscripts 1 and 2 represent the source and receiving rooms respectively.

L_{x2}/L_{x1}	L_{x1}(m)	L_{x2}(m)	$L_{y1}=L_{y2}$	$L_{z1}=L_{z2}$	n_1 (f)	n_2 (f)	$f_{1,Schroed}$	$f_{2,Schroed}$
1.000	3.000	3.000	1.800	2.000	0.419	0.419	430.3	430.3
1.259	3.000	3.777	1.800	2.000	0.419	0.518	430.3	383.5
1.585	3.000	4.755	1.800	2.000	0.419	0.644	430.3	341.8
1.995	3.000	5.985	1.800	2.000	0.419	0.801	430.3	304.7
2.512	3.000	7.536	1.800	2.000	0.419	1.000	430.3	271.5
3.162	3.000	9.486	1.800	2.000	0.419	1.250	430.3	242.0
3.981	3.000	11.943	1.800	2.000	0.419	1.565	430.3	215.7
5.012	3.000	15.036	1.800	2.000	0.419	1.962	430.3	192.2
6.309	3.000	18.927	1.800	2.000	0.419	2.461	430.3	171.3
7.943	3.000	23.829	1.800	2.000	0.419	3.089	430.3	152.7
10.000	3.000	30.000	1.800	2.000	0.419	3.881	430.3	136.1

Table 4.4: Variation of room parameters with the depth ratio L_{x2}/L_{x1}. L_x, L_y and L_z are room depth, height and width respectively. n (f) is the modal density in the highest 1/3 octave band with centre frequency equal to 250 Hz and $f_{Schroed}$ is the *Schroeder* frequency (Hz) above which the acoustic field is assumed to be diffuse. The subscripts 1 and 2 represent the source and receiving rooms respectively.

T_2/T_1	T_1	T_2	L_{x1}	L_{x2}	$L_{y1}=L_{y2}$	$L_{z1}=L_{z2}$	n_1 (f)	n_2 (f)
1.0	1.0	1.0	3.000	2.000	1.800	2.000	0.419	0.290
0.8	1.0	0.8	3.000	2.000	1.800	2.000	0.419	0.290
0.6	1.0	0.6	3.000	2.000	1.800	2.000	0.419	0.290
0.4	1.0	0.4	3.000	2.000	1.800	2.000	0.419	0.290
0.2	1.0	0.2	3.000	2.000	1.800	2.000	0.419	0.290

Table 4.5: Variation of room parameters with the Reverberation Time ratio (T_2/T_1). L_x, L_y and L_z are room depth, height and width respectively. n (f) is the modal density in the highest 1/3 octave band with centre frequency equal to 250 Hz. The subscripts 1 and 2 represent the source and receiving rooms respectively. For the source and receiving rooms the Schroeder frequencies are 430 Hz and 527 Hz respectively.

Position	c_{gy} (m)	c_{gz} (m)	L_{yp} (m)	L_{zp} (m)
1	0.6	0.6	0.6	0.8
2	0.4	0.4	0.6	0.8
3	0.2	0.2	0.6	0.8
4	0.0	0.0	0.6	0.8
5	0.4	0.6	0.6	0.8
6	0.2	0.6	0.6	0.8
7	0.0	0.6	0.6	0.8
8	0.6	0.4	0.6	0.8
9	0.6	0.2	0.6	0.8
10	0.6	0.0	0.6	0.8

Table 4.6: List of 10 different panel positions on the common wall separating source and receiving rooms. (c_{gy}, c_{gz}) is the coordinate of the panel left-bottom corner in the y and z directions respectively. The surface area of the elastic panel is equal to (L_{yp} x L_{zp}). The dimensions of the rigid common wall is 1.8m x 2.0m.

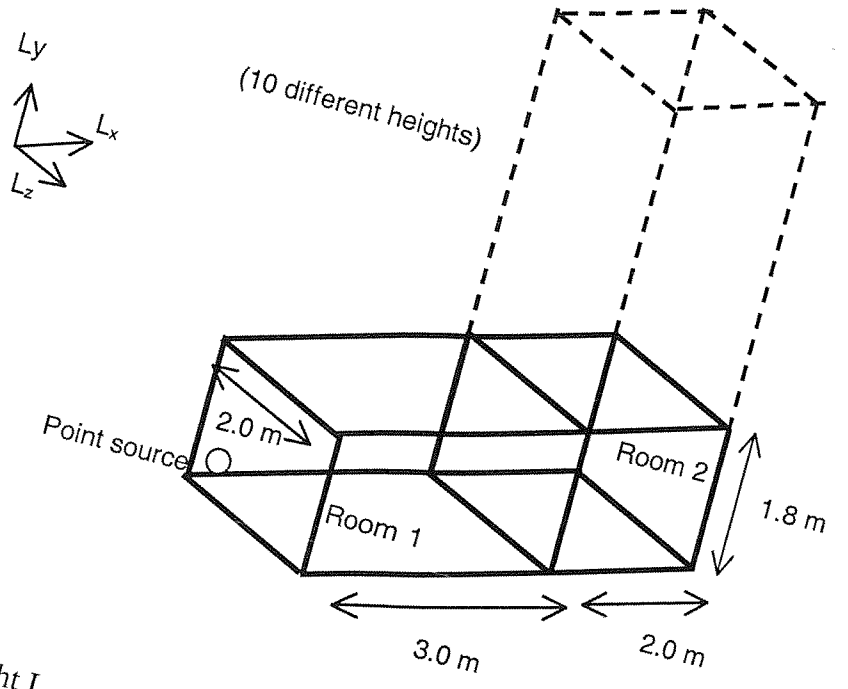

Figure 4.1: Variation of the height L_{y2} of Room 2 (see Table 4.1). A monopole source with volume velocity equal to $3x10^{-5}$ m^3/s was located at the corner of the room.

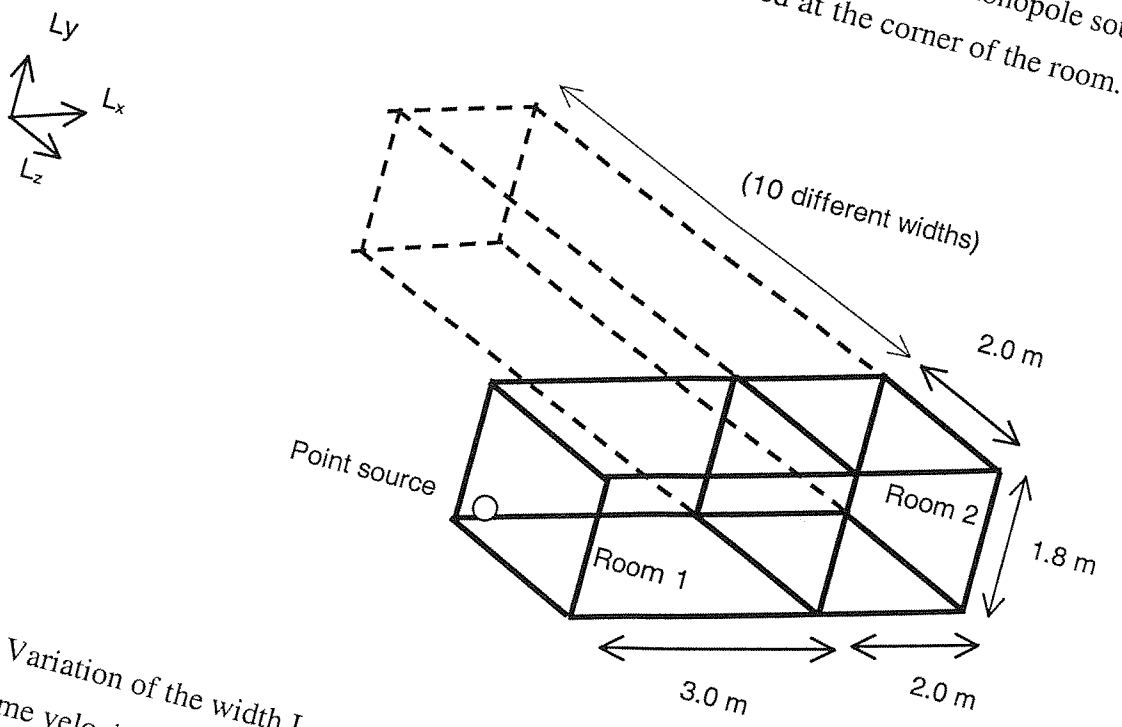

Figure 4.2: Variation of the width L_{z2} of Room 2 (see Table 4.3). A Monopole source with volume velocity equal to $3x10^{-5}$ m^3/s was located at the corner of the room.

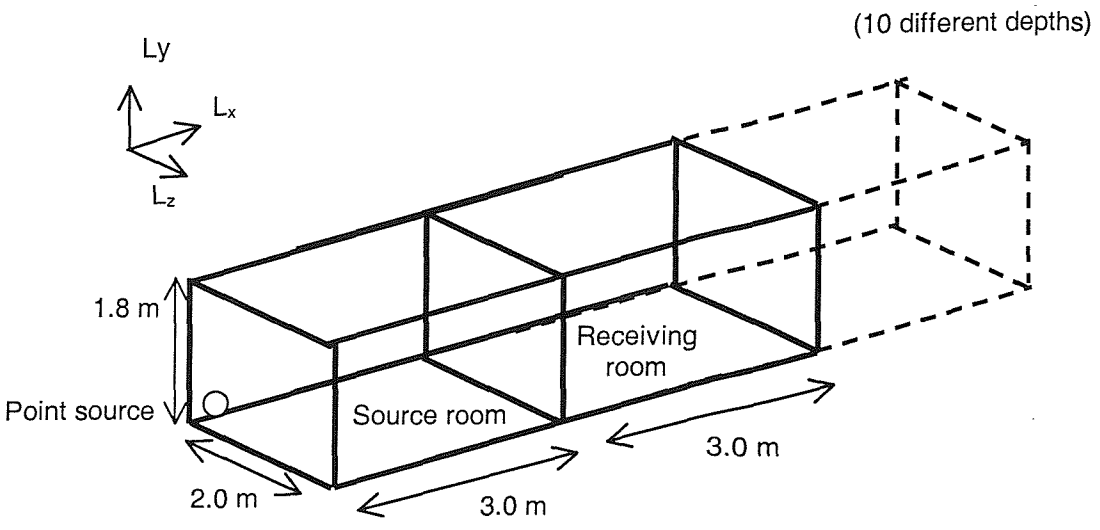

Figure 4.3: Variation of the depth L_{x2} of Room 2 (see Table 4.4) A Monopole source with volume velocity equal to $3x10^{-5}$ m^3/s was located at the corner of the room

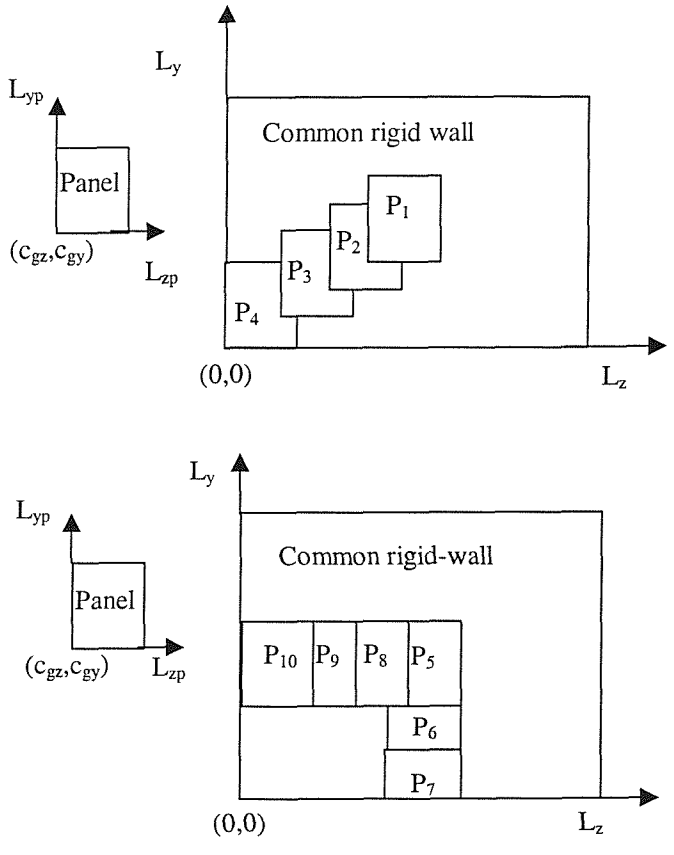

Figure 4.4: Variation of panel positions on the common wall; The coordinates c_{gy} and c_{gz} for each panel position are defined in Table 4.6

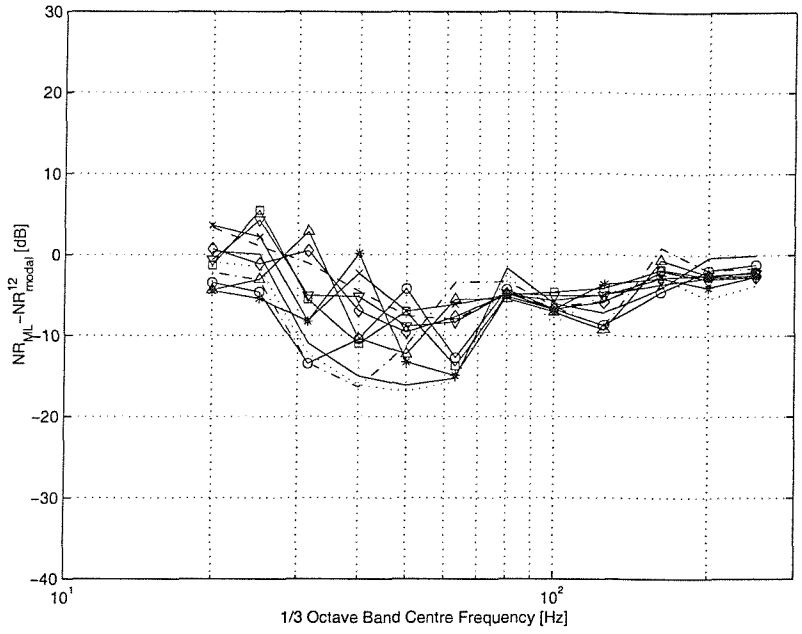

a)

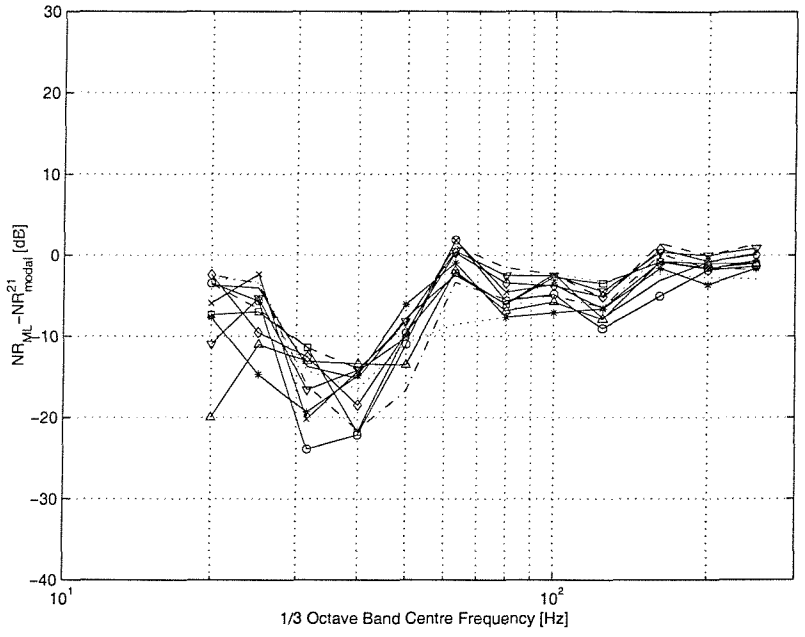

b)

Figure 4.5: Variation of the NR differences with frequency for different values of height ratio (L_{y2}/L_{y1}) compared to the diffuse incidence Mass Law (ML). (a): $NR_{ML} - NR^{12}_{modal}$ [dB]; (b): $NR_{ML} - NR^{21}_{modal}$ [dB]. The height of the room 1 (L_{y1}) is fixed and equal to 1.8 m. The height of room 2 (L_{y2}) varies from 1.8 to 18.0 m; — 1.80; ····· 2.27; -·- 2.85; -o- 3.59; -*- 4.52; -Δ- 5.69; - - 7.16; -x- 9.02; -◊- 11.36; -∇- 14.29; ---- 18.00.

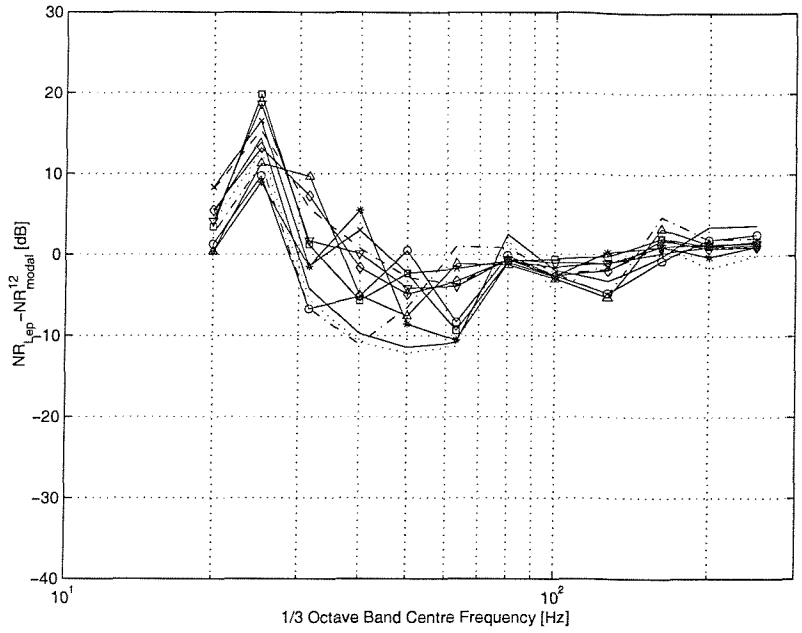

a)

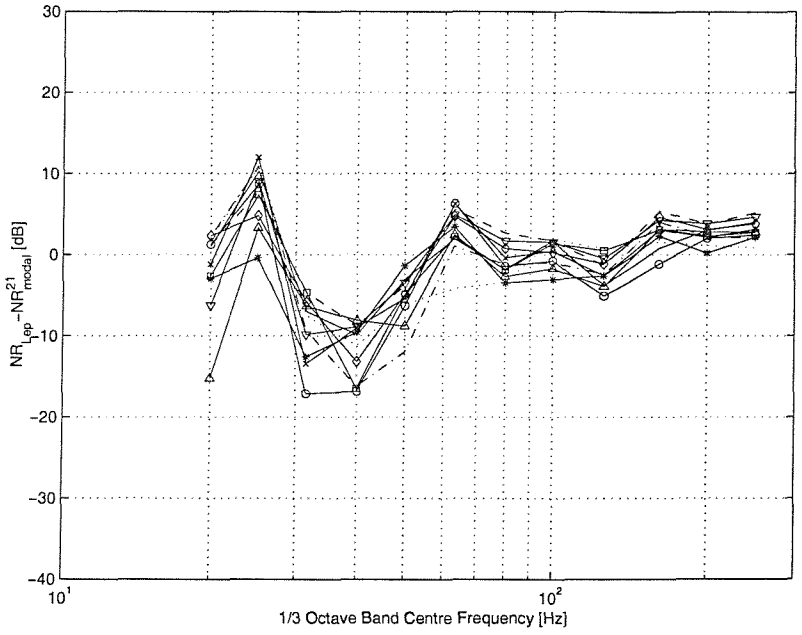

b)

Figure 4.6: Variation of the NR differences with frequency for different values of height ratio (L_{y2}/L_{y1}) compared to Leppington's formula [16]. (a): $NR_{ML} - NR^{12}_{modal}$ [dB]; (b): $NR_{ML} - NR^{21}_{modal}$ [dB]. The height of room 1 (L_{y1}) is 1.8 m. The height of the room 2 (L_{y2}) varies from 1.8 to 18.0 m; — 1.80; ····· 2.27; -·- 2.85; -o- 3.59; -*- 4.52; -Δ- 5.69; - - 7.16; -x- 9.02; -◊- 11.36; -∇- 14.29; ---- 18.00.

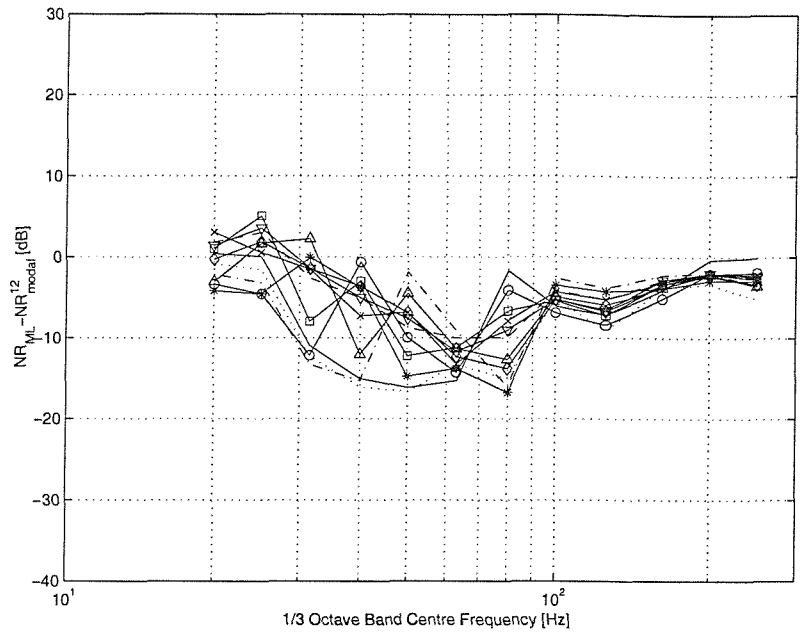

a)

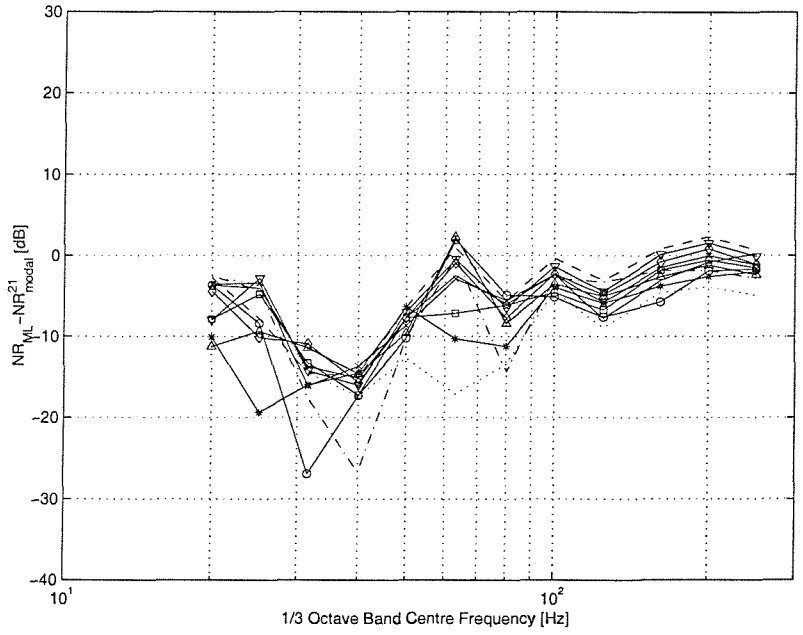

b)

Figure 4.7: Variation of the NR differences with frequency for different values of width ratio (L_{z2}/L_{z1}) compared to the diffuse incidence Mass Law (ML). (a): $NR_{ML} - NR^{12}_{modal}$ [dB]; (b): $NR_{ML} - NR^{21}_{modal}$ [dB]. The width of room 1 (L_{z1}) is 2.0 m. The width of the room 2 (L_{z2}) varies from 2.0 to 20.0 m; — 2.00; ····· 2.52; -·- 3.17; -o- 3.99; -*- 5.02; -Δ- 6.32; - - 7.96; -x- 10.02; -◊- 12.62; -∇- 15.89; ---- 20.00.

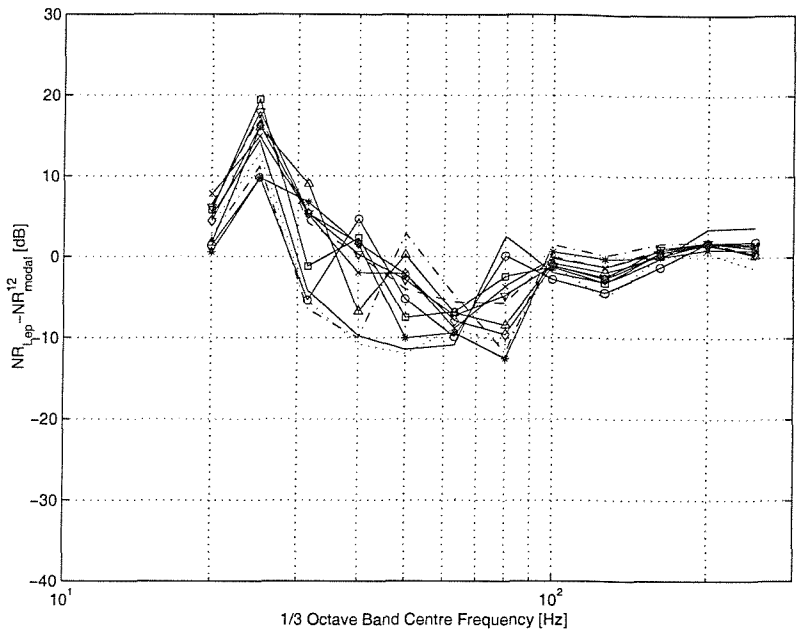

a)

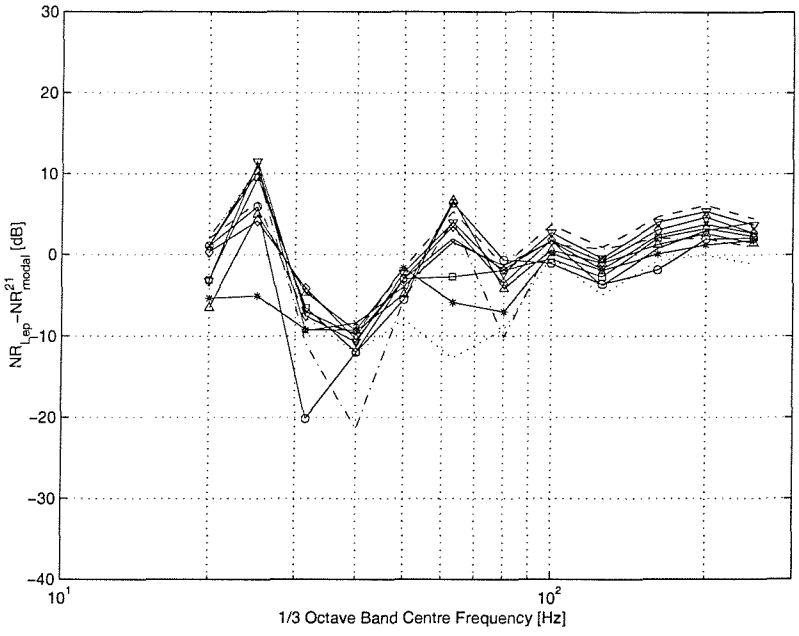

b)

Figure 4.8: Variation of the NR differences with frequency for different values of width ratio (L_{z2}/L_{z1}) compared to Leppington's formula [16]. (a): $NR_{Lep} - NR^{12}_{modal}$ [dB]; (b): $NR_{Lep} - NR^{21}_{modal}$ [dB]. The width of the room 1 (L_{z1}) is 2.0 m. The width of the room 2 (L_{z2}) varies from 2.0 to 20.0 m; — 2.00; ····· 2.52; -·- 3.17; -o- 3.99; -*- 5.02; -Δ- 6.32; -- 7.96; -x- 10.02; -◊- 12.62; -∇- 15.89; ---- 20.00.

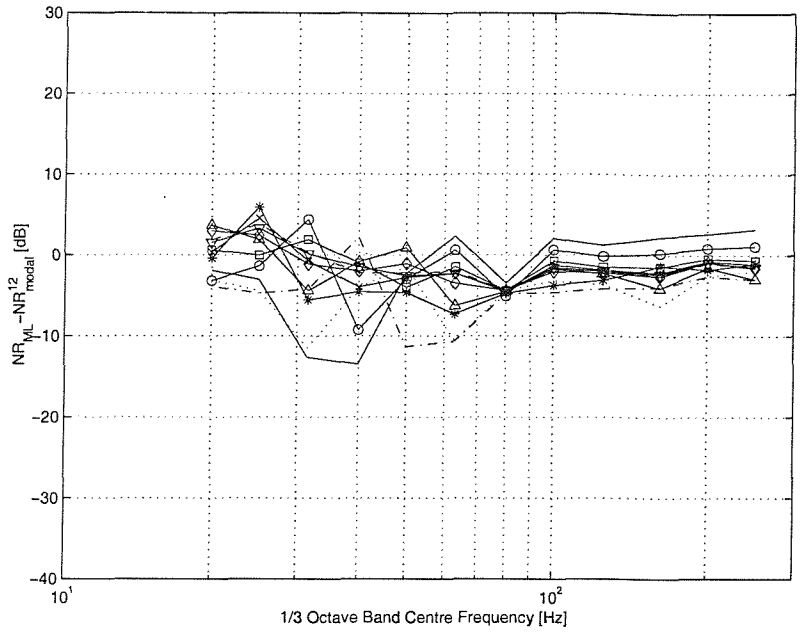

a)

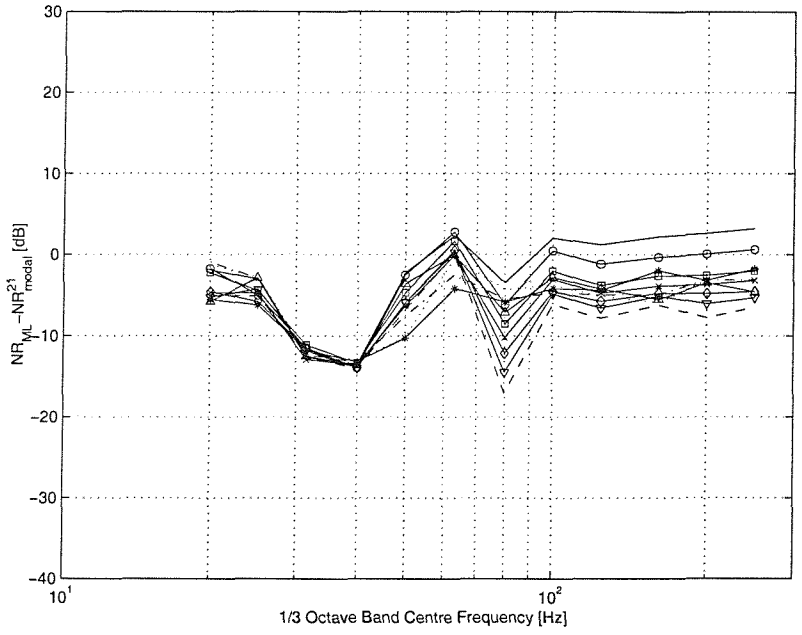

b)

Figure 4.9: Variation of the NR differences with frequency for different values of depth ratio (L_{x2}/L_{x1}) compared to the diffuse incidence Mass Law (ML). (a): $NR_{ML} - NR^{12}_{modal}$ [dB]; (b): $NR_{ML} - NR^{21}_{modal}$ [dB]. The depth of the room 1 (L_{x1}) is 3.0 m. The depth of the room 2 (L_{z2}) varies from 3.0 to 30.0 m; — 3.00; ····· 3.77; -·- 4.76; -o- 5.99; -*- 7.54; -Δ- 9.49; - - 11.94; -x- 15.04; -◊- 18.93; -∇- 23.83; ---- 30.00.

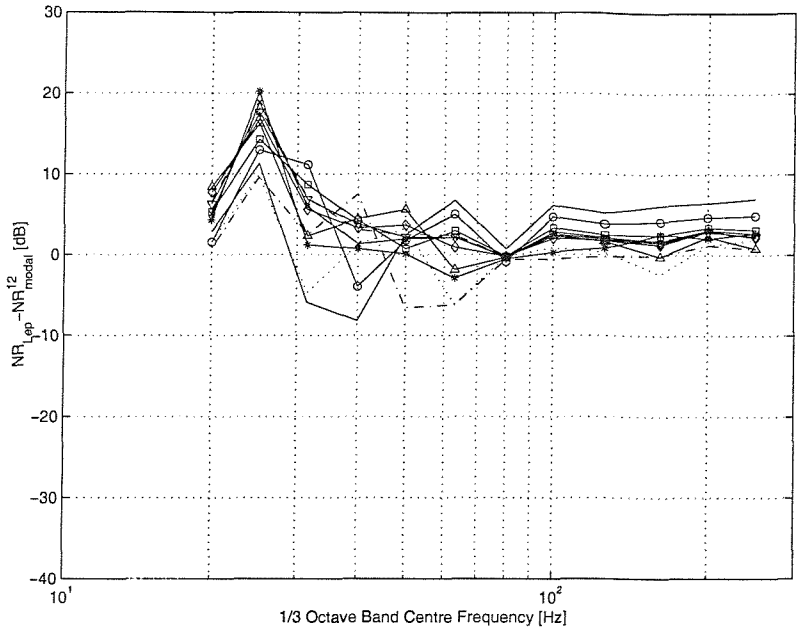

a)

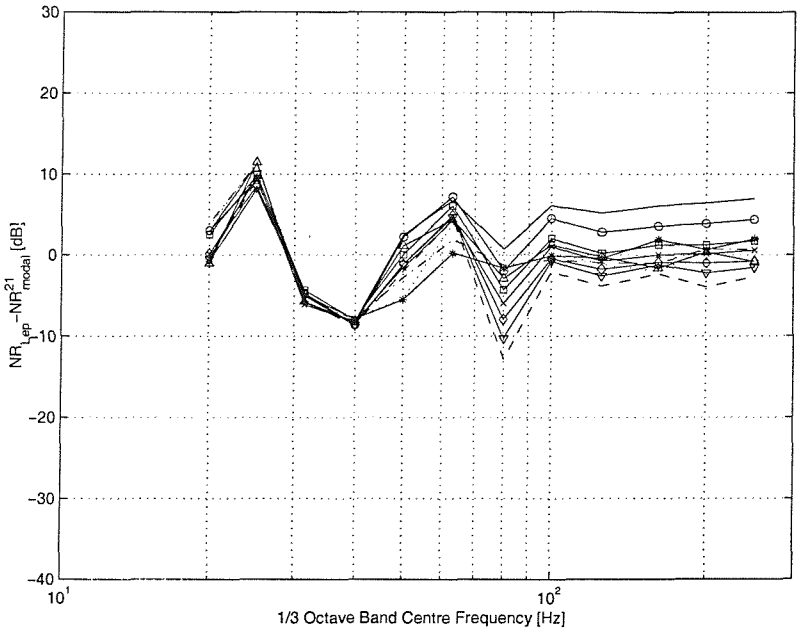

b)

Figure 4.10: Variation of the NR differences with frequency for different values of depth ratio (L_{x2}/L_{x1}) compared to Leppington's formula [16]. (a): $NR_{Lep} - NR^{12}_{modal}$ [dB]; (b): $NR_{Lep} - NR^{21}_{modal}$ [dB]. The depth of the room 1 (L_{x1}) is 3.0 m. The depth of the room 2 (L_{z2}) varies from 3.0 to 30.0 m; — 3.00; ····· 3.77; -·- 4.76; -o- 5.99; -*- 7.54; -Δ- 9.49; -- 11.94; -x- 15.04; -◊- 18.93; -∇- 23.83; ---- 30.00.

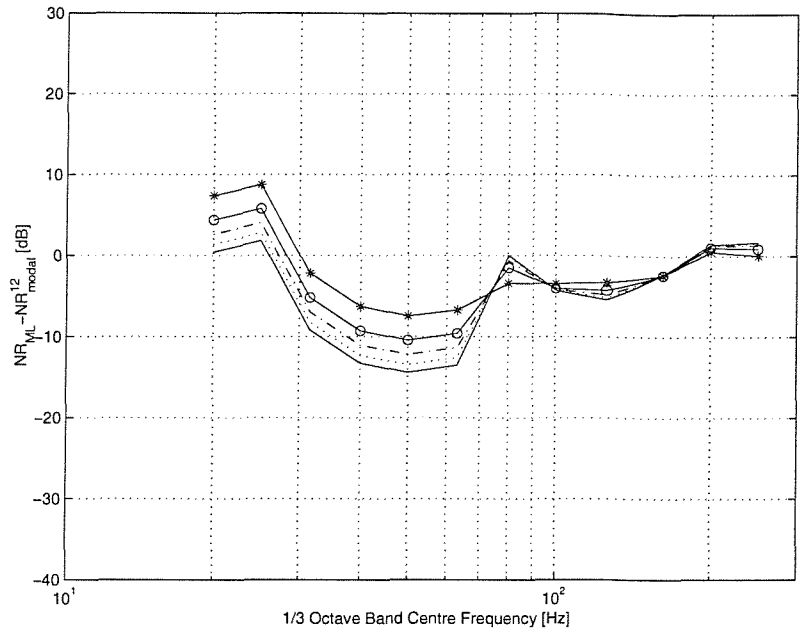

a)

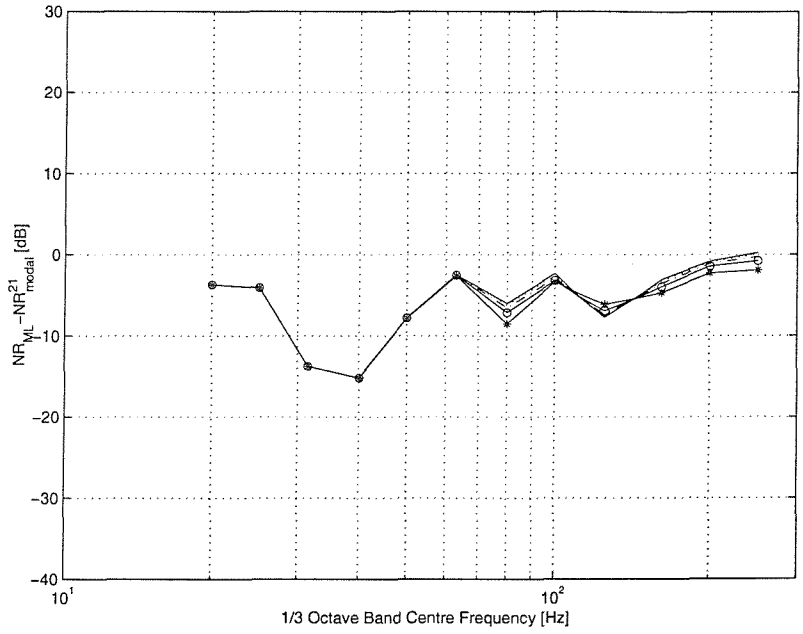

b)

Figure 4.11: Variation of the NR differences with frequency for different values of reverberation time ratio (T_2/T_1) compared to Mass Law (ML). (a): $NR_{Lep} - NR^{12}_{modal}$ [dB]; (b): $NR_{Lep} - NR^{21}_{modal}$ [dB]. The reverberation time of room 1 (T_1) is 1.0 s. The reverberation time of room 2 (T_2) varies from 1.0 to 0.2 s; — 1.0; ····· 0.8; -·- 0.6; -o- 0.4; -*- 0.2.

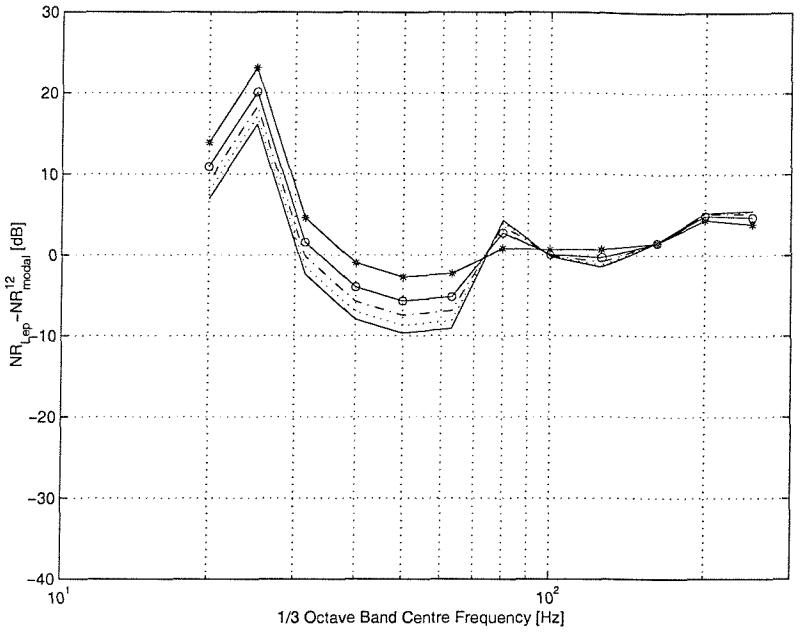

a)

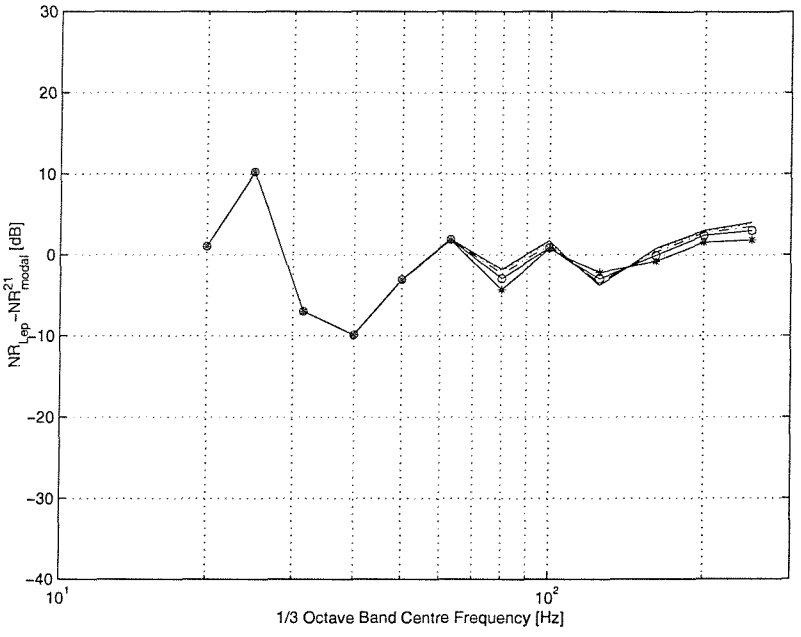

b)

Figure 4.12: Variation of the NR differences with frequency for different values of reverberation time ratio (T_2/T_1) compared to Leppington's formula [16]. (a): $NR_{Lep} - NR^{12}_{modal}$ [dB]; (b): $NR_{Lep} - NR^{21}_{modal}$ [dB re 1]. The reverberation time of room 1 (T_1) is 1.0 s. The reverberation time of the room 2 (T_2) varies from 1.0 to 0.2 s; — 1.0; ····· 0.8; -·- 0.6; -o- 0.4; -*- 0.2.

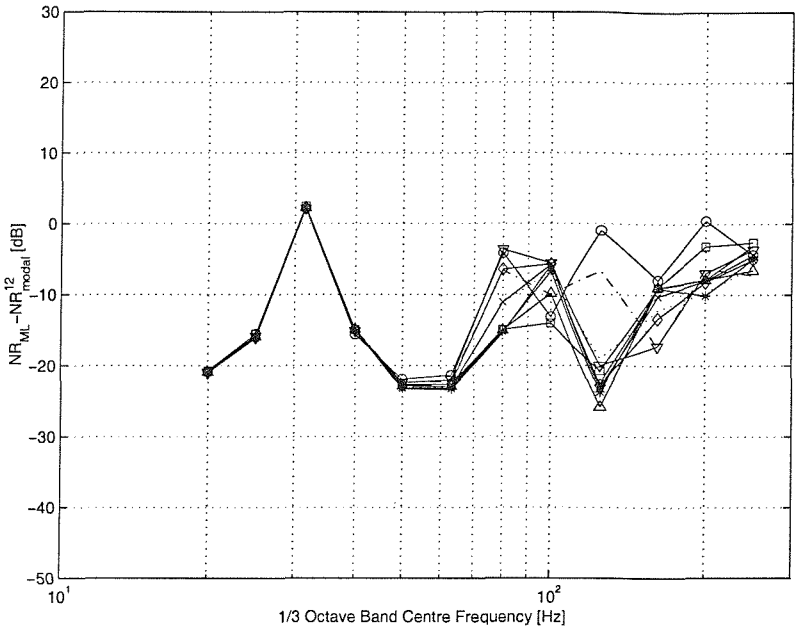

a)

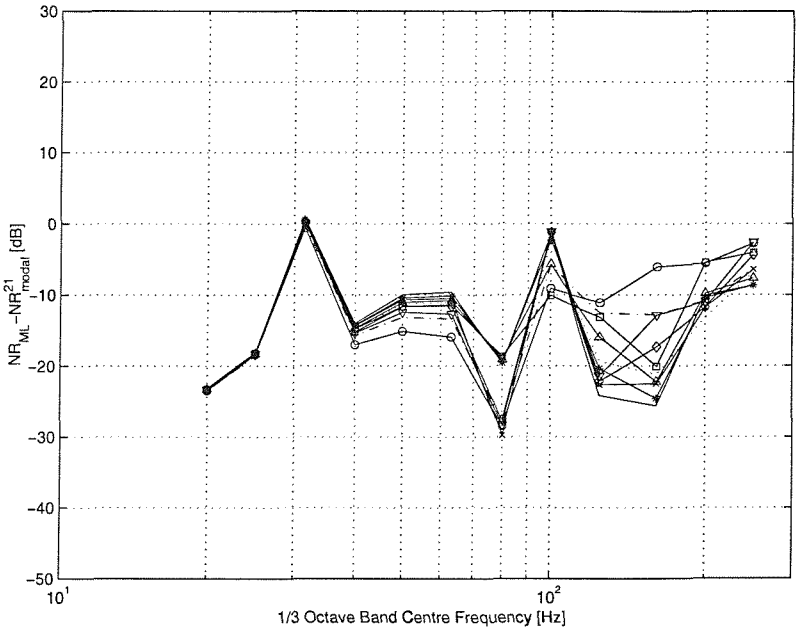

b)

Figure 4.13: Variation of the NR differences with frequency for different values of panel positions on the common wall compared to the diffuse incidence Mass Law (ML). (a): $NR_{Lep} - NR^{12}_{modal}$ [dB]; (b): $NR_{Lep} - NR^{21}_{modal}$ [dB]. The panel positions (see Figure 4.4) are ; — P_1; ····· P_2; -·- P_3; -o- P_4; -*- P_5; - - P_6; -x- P_7; -◊- P_8; -▽- P_9.

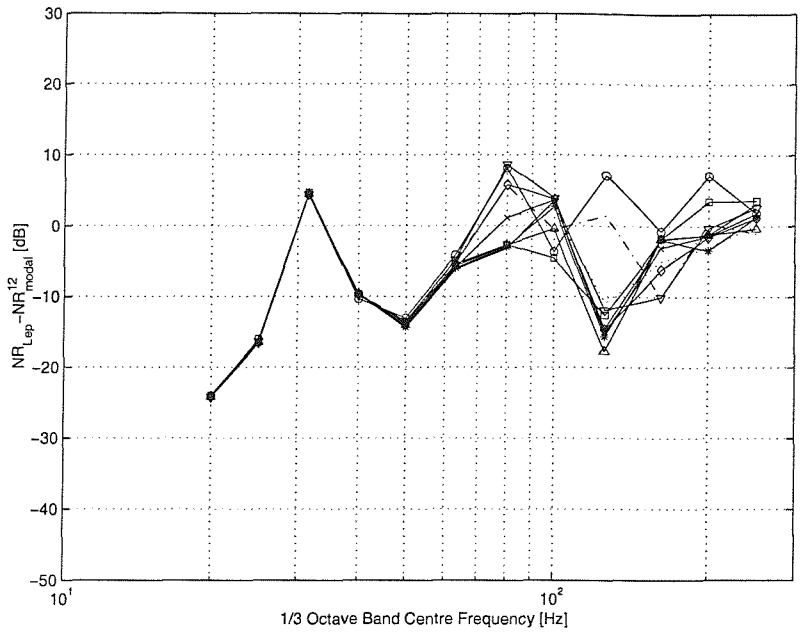

a)

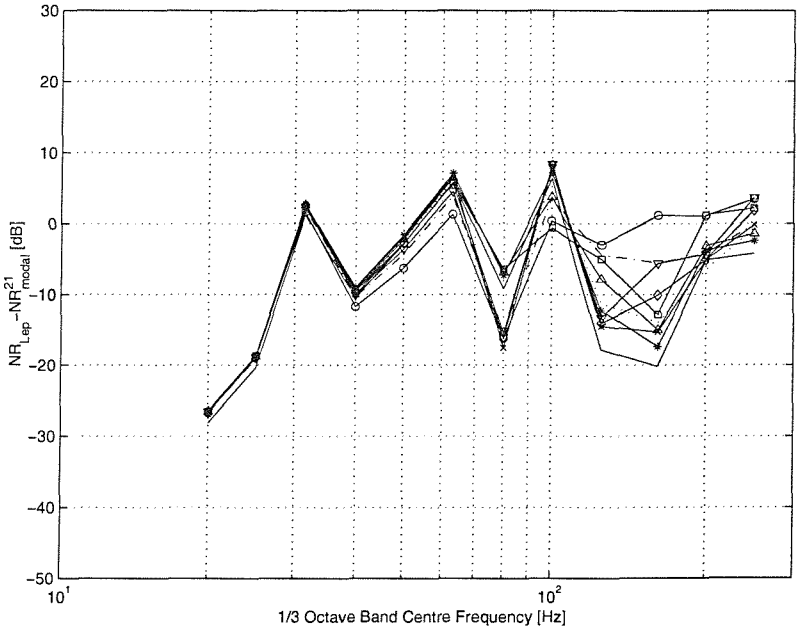

b)

Figure 4.14: Variation of the NR differences with frequency for different values of panel positions on the common wall compared to Leppington's formula. (a): $NR_{Lep} - NR^{12}_{modal}$ [dB]; (b): $NR_{Lep} - NR^{21}_{modal}$ [dB]. The panel positions (see Figure 4.4) are ; — P_1; ····· P_2; -·- P_3; -o- P_4; -*- P_5; - - P_6; -x- P_7; -◊- P_8; -∇- P_9.

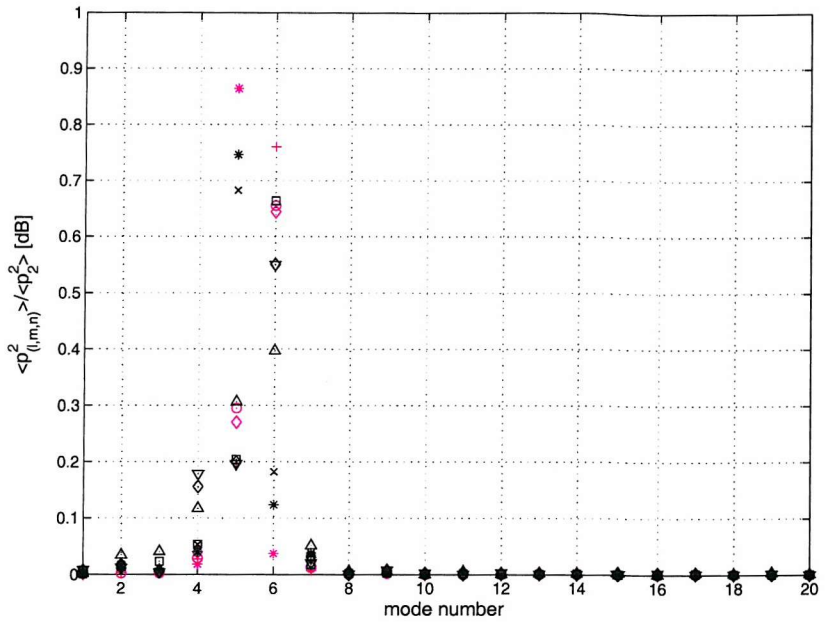

a)

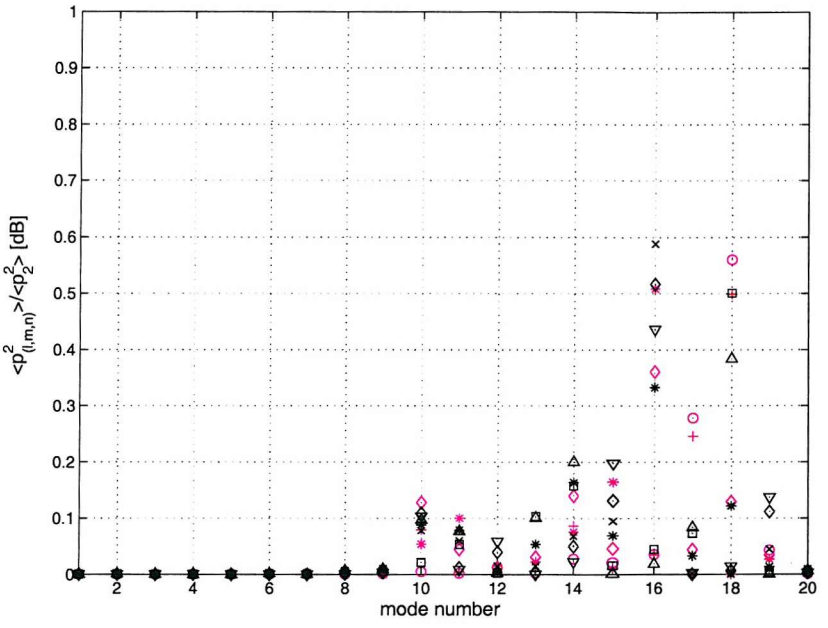

b)

Figure 4.15: Variation of the ratio of the spatially averaged mean square pressure of mode '(l,m,n)' to the total mean square pressure (in the receiving room) with mode number for different values of panel position on the common wall. (a):1/3 octave band with centre at 125 Hz; (b):1/3 octave band with centre at 200 Hz. The panel positions (see Figure 4.4) are ; -*- P_1; -◊-P_2; -+- P_3; -o- P_4; -*- P_5; -Δ- P_6; - - P_7; -x- P_8; -◊- P_9; -∇- P_{10}. The corresponding mode numbers are: 1-(0,0,1); 2-(1,0,0); 3-(0,1,0); 4-(1,0,1); 5-(0,1,1); 6-(1,1,0); 7-(1,1,1); 8-(0,0,2); 9-(2,0,0); 10-(0,2,0); 11-(1,0,2); 12-(2,0,1); 13-(0,1,2); 14-(2,1,0); 15-(0,2,1); 16-(1,2,0); 17-(1,1,2); 18-(2,1,1); 19-(1,2,1); 20-(2,0,2).

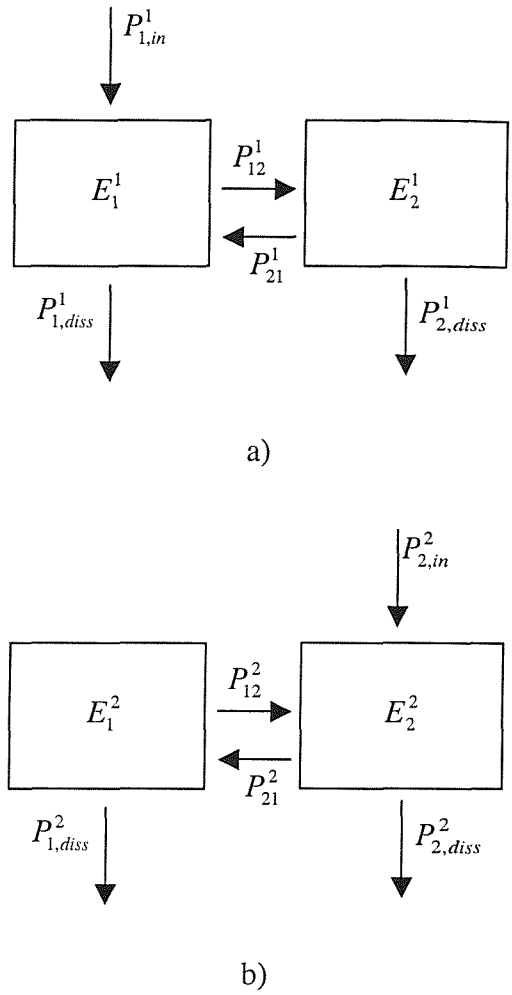

Figure 4.16: SEA models of two rooms separated by a single-leaf partition approximated by a two subsystem model. Therefore, only the non-resonant transmission path is considered. a) Power is injected into subsystem 1; b) Power is injected into subsystem 2. The subscripts 'i j' denote the power flow from subsystem 'i' to subsystem 'j' and the superscript indicates which subsystem is under direct excitation.

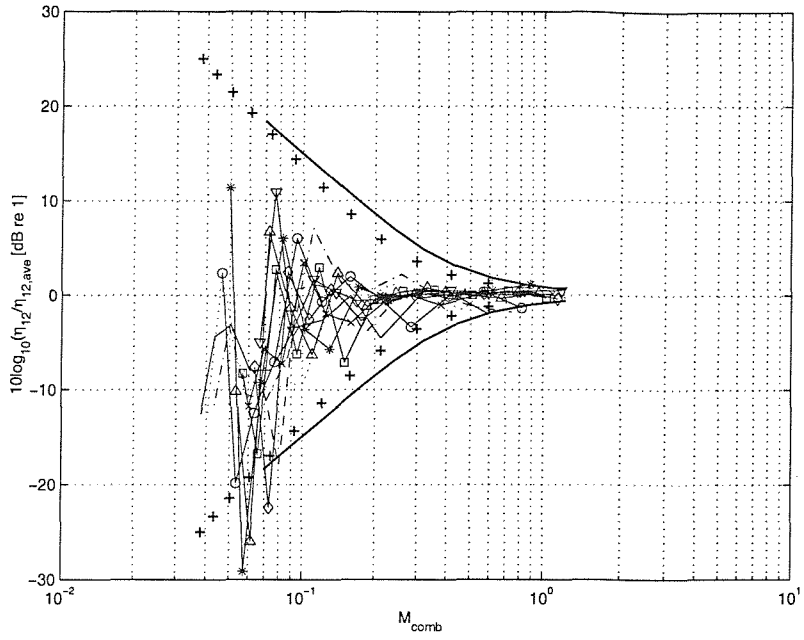

a)

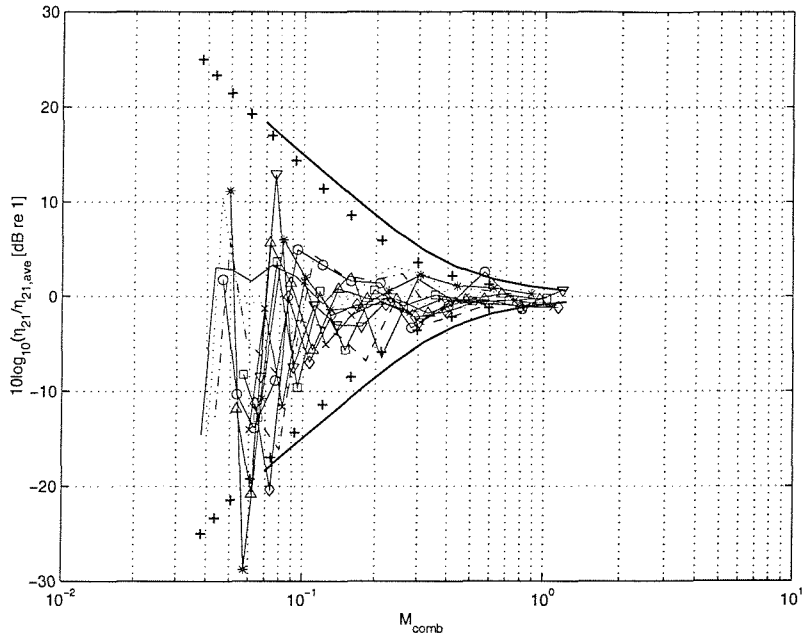

b)

Figure 4.17: Variation of CLF ratio with the combined Modal Overlap factor M_{comb} for different values of height ratio (L_{y2}/L_{y1}) compared to the average over all of the height variations. (a):$10\log_{10}(\eta_{12}/\eta_{12,ave})$ [dB re 1]; (b):$10\log_{10}(\eta_{21}/\eta_{21,ave})$ [dB re 1]. The height of room 1 (L_{y1}) is 1.8 m. The height of room 2 (L_{y2}) varies from 1.8 to 18.0 m; — 1.80; ····· 2.27; -·- 2.85; -o- 3.59; -*- 4.52; -Δ- 5.69; - - 7.16; -x- 9.02; -◊- 11.36; -∇- 14.29; ---- 18.00; +++ bounds ($\pm 2\sigma$) for $L_{y2} = 1.8$; — bounds ($\pm 2\sigma$) for $L_{y2} = 18.0$.

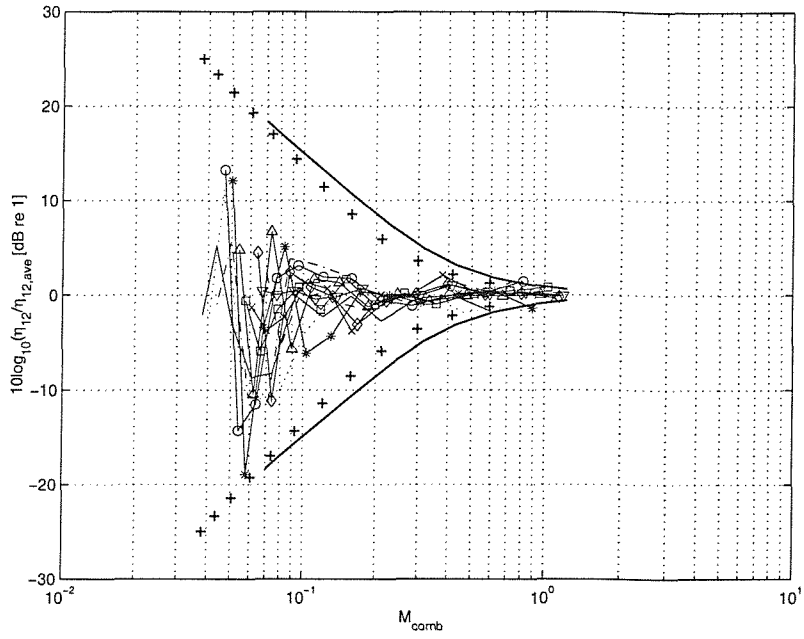

a)

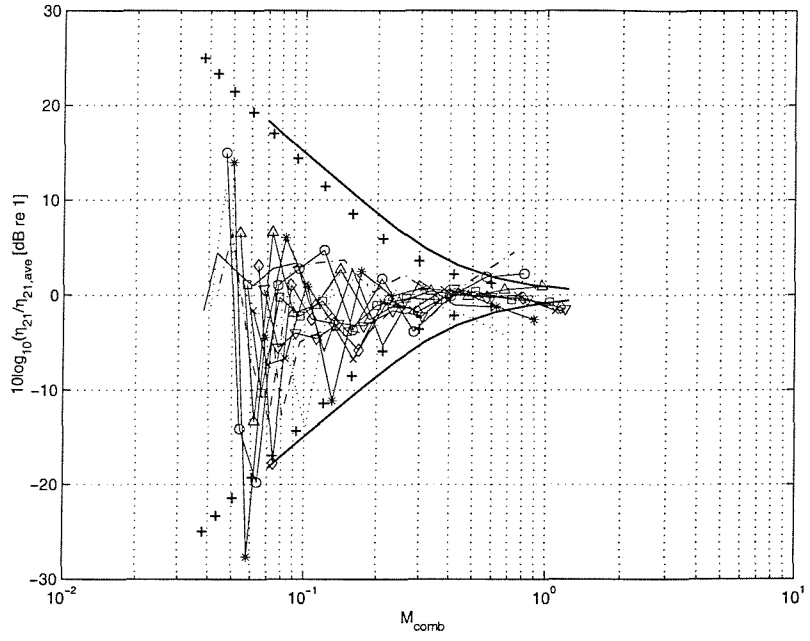

b)

Figure 4.18: Variation of CLF ratio with combined Modal Overlap factor M_{comb} for different values of width ratio (L_{z2}/L_{z1}) compared to the average over all of the width variations. (a):$10\log_0(\eta_{12}/\eta_{12ave})$ [dB re 1]; (b):$10\log_0(\eta_{21}/\eta_{21ave})$ [dB re 1]. The width of room 1 (L_{z1}) is 2.0 m. The width of the room 2 (L_{z2}) varies from 2.0 to 20.0 m; — 2.00; ····· 2.52; -·- 3.17; -o- 3.99; -*- 5.02; -Δ- 6.32; - - 7.96; -x- 10.02; -◊- 12.62; -∇- 15.89; -- -- 20.00. +++ bounds ($\pm 2\sigma$) for $L_{z2} = 2.0$; — bounds ($\pm 2\sigma$) for $L_{z2} = 20.0$.

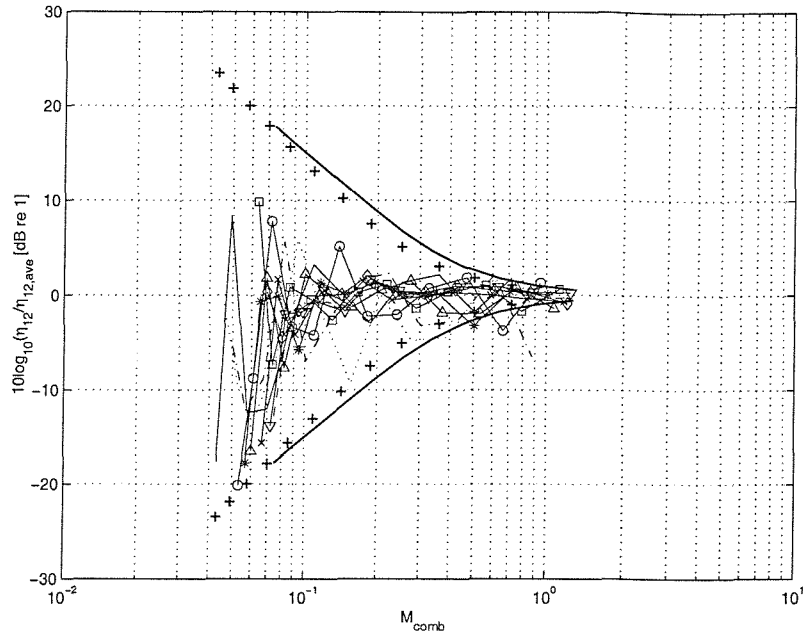

a)

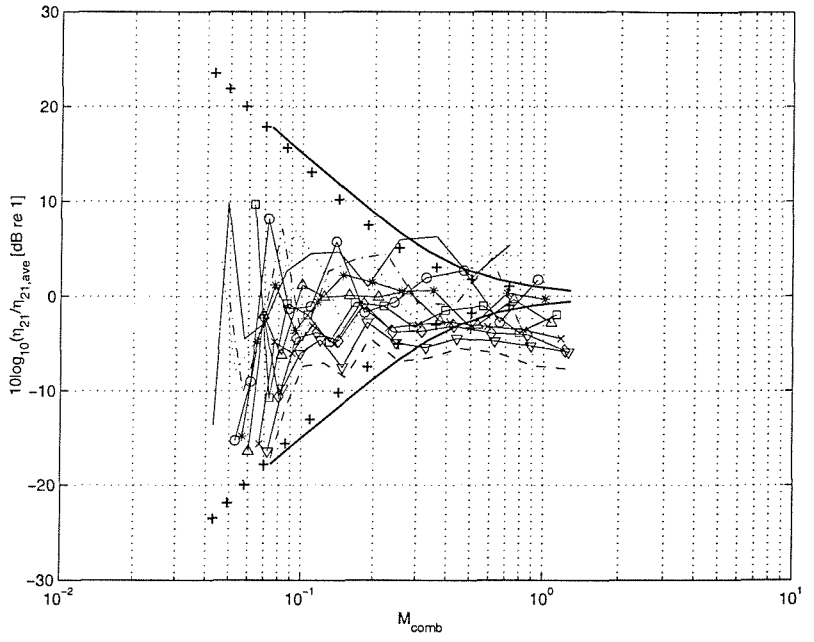

b)

Figure 4.19: Variation of CLF ratio with the combined Modal Overlap factor M_{comb} for different values of depth ratio (L_{x2}/L_{x1}) compared to the average over all of the depth variations. (a): $10\log_0(\eta_{12}/\eta_{12ave})$ [dB re 1]; (b): $10\log_0(\eta_{21}/\eta_{21ave})$ [dB re 1]. The depth of room 1 (L_{x1}) is 3.0 m. The depth of the room 2 (L_{x2}) varies from 3.0 to 30.0 m; — 3.00; ····· 3.77; -·- 4.76; -o- 5.99; -*- 7.54; -Δ- 9.49; - - 11.94; -x- 15.04; -◊- 18.93; -∇- 23.83; ---- 30.00. +++ bounds ($\pm 2\sigma$) for $L_{x2} = 3.0$; — bounds ($\pm 2\sigma$) for $L_{x2} = 30.0$.

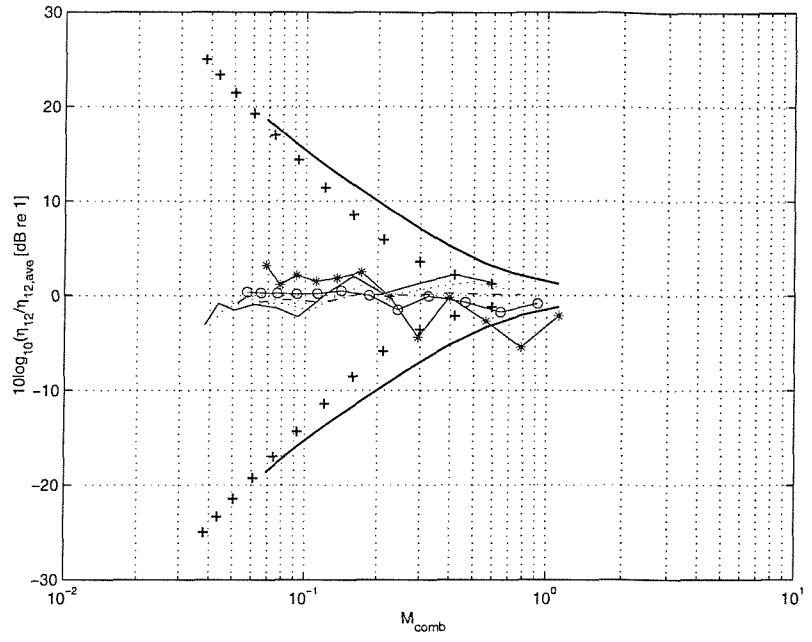

a)

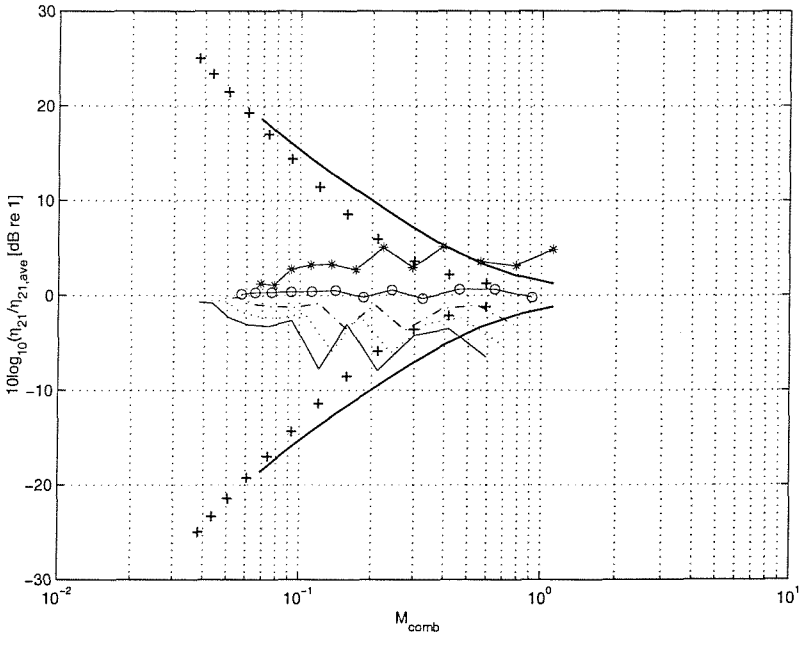

b)

Figure 4.20: Variation of CLF ratio with the combined Modal Overlap factor M_{comb} for different values of reverberation time ratio (T_2/T_1) compared to the average over all of the reverberation time variations. (a): $10\log_0(\eta_{12}/\eta_{12ave})$ [dB re 1]; (b): $10\log_0(\eta_{21}/\eta_{21ave})$ [dB re 1]. The reverberation time of the room 1 (T_1) is 1.0 s. The reverberation time of room 2 (T_2) varies from 1.0 s to 0.2s; — 1.0; ····· 0.8; -·- 0.6; -o- 0.4; -*- 0.2. +++ bounds ($\pm 2\sigma$) for $T_2 = 1.0$; — bounds ($\pm 2\sigma$) for $T_2 = 0.2$.

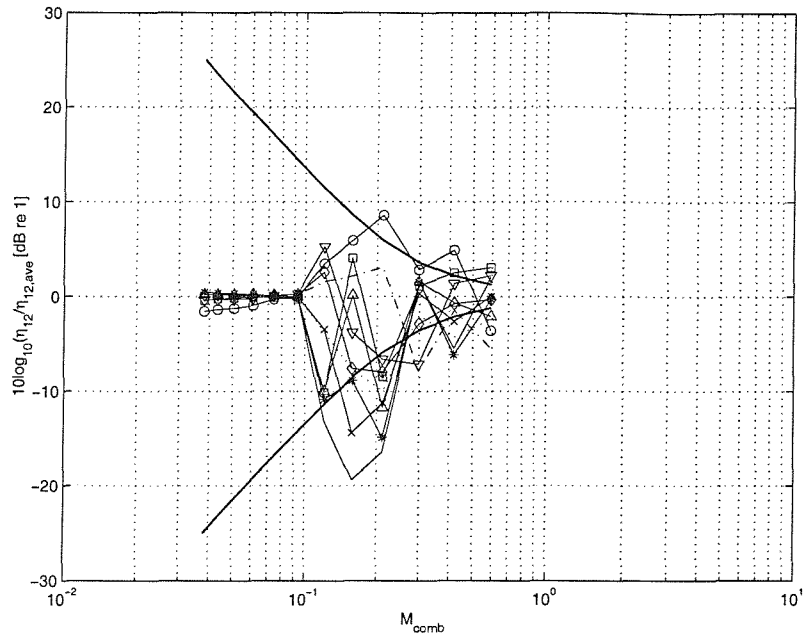

a)

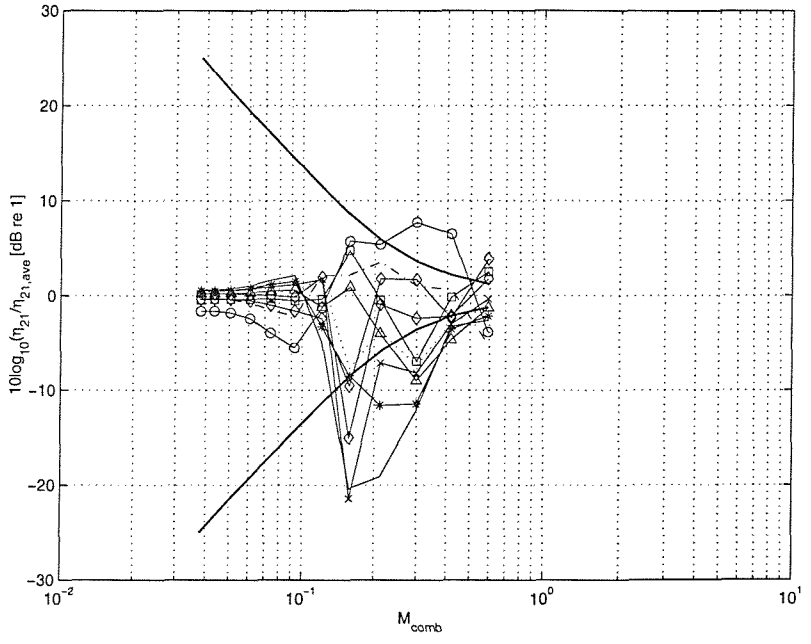

b)

Figure 4.21: Variation of CLF ratio with the combined Modal Overlap factor M_{comb} for different values of panel position on the common wall compared to the average over all of the panel positions. (a):$10\log_{10}(\eta_{12}/\eta_{12,ave})$ [dB re 1]; (b):$10\log_{10}(\eta_{21}/\eta_{21,ave})$ [dB re 1]. The panel positions are (see Figure 4.4): —P_1; ····· P_2; -·- P_3; -o- P_4; -*- P_5; -Δ- P_6; - - P_7; -x- P_8; -◊- P_9; -∇- P_{10}. — upper and lower bounds ($\pm 2\sigma$) obtained from equation (4.12).

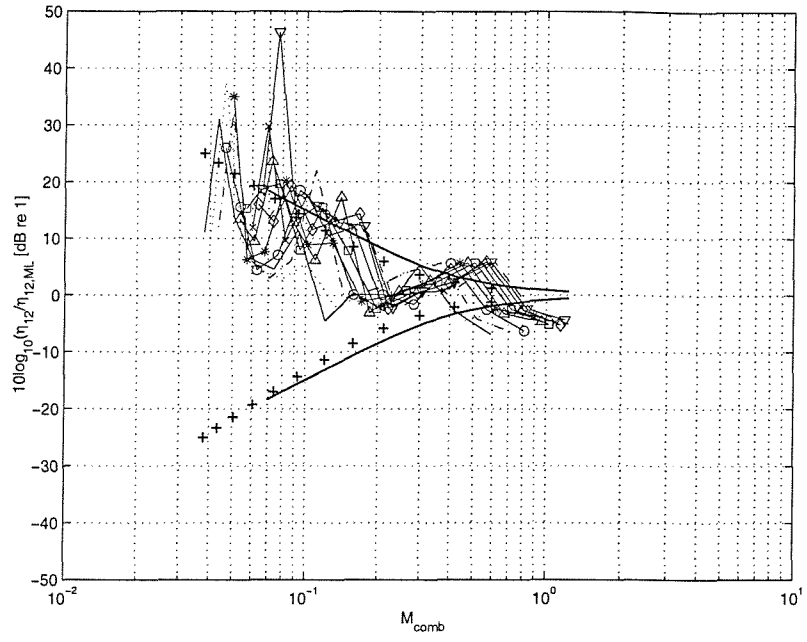

a)

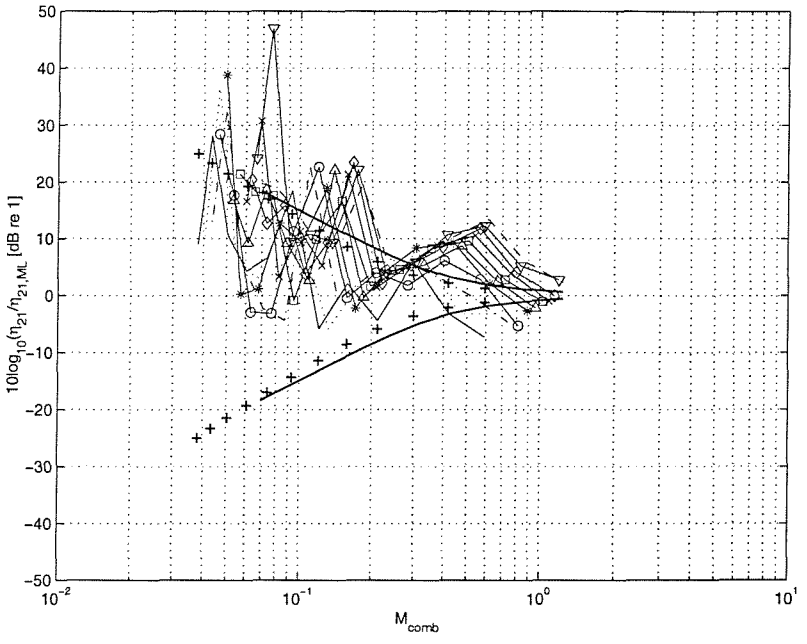

b)

Figure 4.22: Variation of CLF ratio with the combined Modal Overlap factor M_{comb} for different values of height ratio (L_{y2}/L_{y1}) compared to the diffuse incidence Mass Law. (a): $10\log_0(\eta_{12}/\eta_{ML})$ [dB re 1]; (b): $10\log_0(\eta_{21}/\eta_{ML})$ [dB re 1]. The height of room 1 (L_{y1}) is 1.8 m. The height of room 2 (L_{y2}) varies from 1.8 to 18.0 m; — 1.80; ····· 2.27; -·- 2.85; -o- 3.59; -*- 4.52; -Δ- 5.69; - - 7.16; -x- 9.02; -◊- 11.36; -∇- 14.29; ---- 18.00; +++ bounds ($\pm 2\sigma$) for L_{y2} = 1.8; — bounds ($\pm 2\sigma$) for L_{y2} = 18.0.

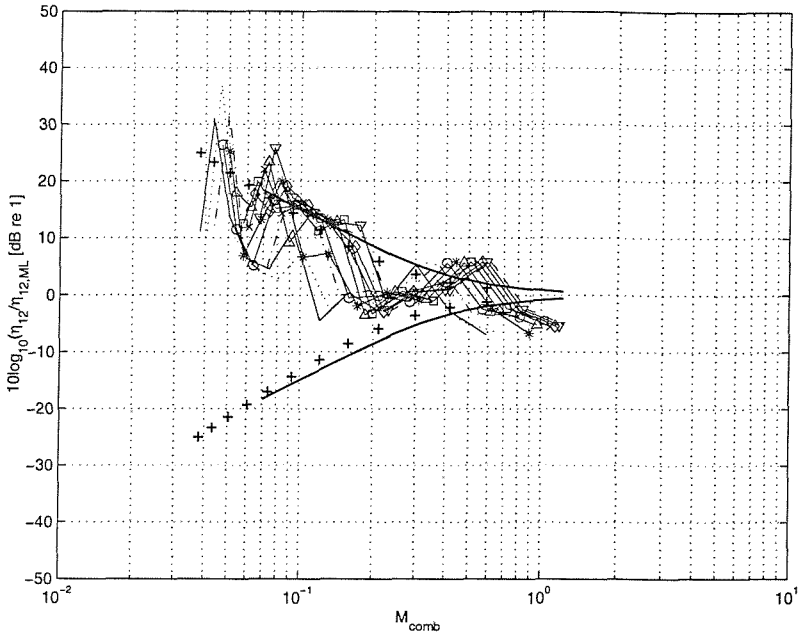

a)

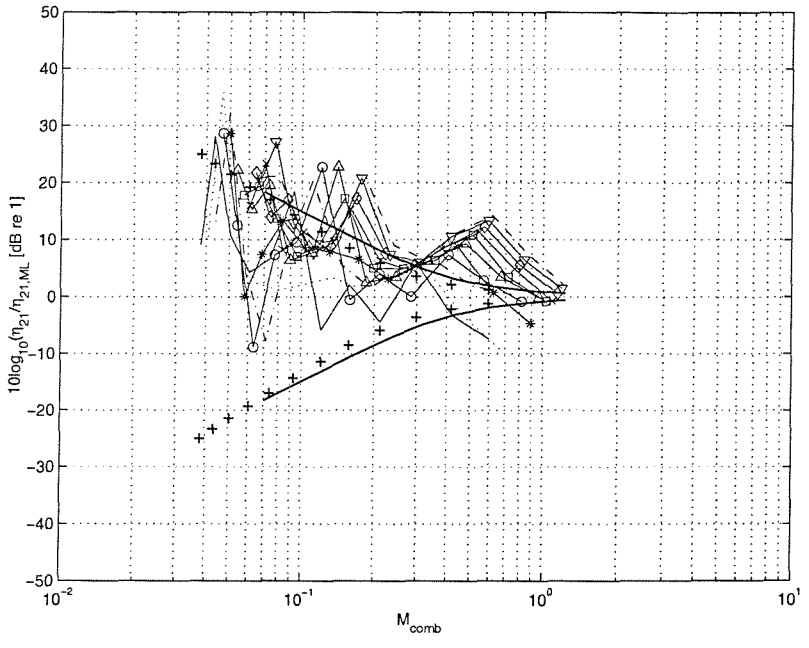

b)

Figure 4.23: Variation of CLF ratio with combined Modal Overlap factor M_{comb} for different values of width ratio (L_{z2}/L_{z1}) compared to the diffuse incidence Mass Law. (a): $10\log_0(\eta_{12}/\eta_{ML})$ [dB re 1]; (b): $10\log_0(\eta_{21}/\eta_{ML})$ [dB re 1]. The width of room 1 (L_{z1}) is 2.0 m. The width of the room 2 (L_{z2}) varies from 2.0 to 20.0 m; — 2.00; ····· 2.52; -·- 3.17; -o- 3.99; -*- 5.02; -Δ- 6.32; - - 7.96; -x- 10.02; -◊- 12.62; -∇- 15.89; ---- 20.00. +++ bounds ($\pm 2\sigma$) for L_{z2} = 2.0; — bounds ($\pm 2\sigma$) for L_{z2} = 20.0.

Chapter 5

ACOUSTIC-STRUCTURAL INTERACTION ANALYSIS USING THE COMPONENT MODE SYNTHESIS METHOD

5.1 – Introduction

The literature survey has revealed that a significant amount of work has concentrated on analysing sound transmission using uncoupled 'rigid-walled' acoustic modes for the acoustic volumes. In this case the boundary condition at the interface between acoustic volumes, which is due to the velocity of the partition, cannot be replicated. Hence, the aim of this chapter is to develop an alternative model for the prediction of noise transmission in terms of the Component Mode Synthesis (CMS) method. It is developed and applied here initially to acoustic-structural coupled volumes possessing one-dimensional wave propagation to verify the accuracy and applicability of the approach. The following chapter extends the work to the three-dimensional case.

The CMS method requires the user to model separate components of a problem in terms of a summation over constraint modes and component normal modes and has previously been applied in structural dynamics. A constraint mode is defined as the static deformation of a subsystem when a unit displacement or velocity is applied to one coordinate of a specific set of 'interface' coordinates. The number of constraint modes considered is equal in number to the number of redundant interface degrees of freedom. The component normal modes are eigenvectors of the component and may be classified according to their boundary conditions either as fixed-interface modes or free-interface modes. The number of normal modes chosen depends upon the frequency range of the calculations and convergence requirements.

The main objective here is to analyse the effects of the imposition of common velocity on the acoustic-structural interface via the Component Mode Synthesis Method (CMS). This original development for the problem provides an improved analytical approach which also shows analytically the importance of including kinematic compatibility in structural-acoustic problems. Some background information about the method is provided as a basis for assisting the understanding of the process. Following this, the

formulation of the structural-acoustic problem in terms of 'components' is described. The results obtained using CMS are compared to those obtained using both a one dimensional exact wave approach explained below and standard modal analysis. Finally, conclusions are drawn based on the analysis of the results and the extension to three-dimensional acoustic systems is discussed which is subsequently implemented in chapter 6.

5.2 – The One-Dimensional Wave Approach

Firstly, consider the one-dimensional acoustic system given in Figure 5.1 as it provides a basis for comparison with the CMS and modal models. Components 1 and 2 are respectively the source and receiver volumes separated by a limp partition of mass per unit area m. An incoming harmonic plane sound wave with amplitude A_s is incident upon the partition from the region $x < 0$. As a result, a 'reflected' plane wave with amplitude B_s propagates in the negative x direction. Thus, the total pressure field p_1 inside the *source component* is given by

$$p_1 = A_s e^{-jkx} + B_s e^{jkx} \tag{5.1}$$

where k is the complex wavenumber of the propagating plane waves, which for light damping is $(\omega/c_o)(1-j\eta/2)$ and η is the loss factor. The time dependence $e^{j\omega t}$ is assumed throughout. The wave amplitudes A_s and B_s in equation (5.1) are the total amplitudes of the travelling waves in the two directions incorporating all multiple reflections from the ends.

Likewise, the acoustic pressure field transmitted through and incident upon the partition from the region $x > 0$ is defined by the coefficients C_r and D_r respectively. Therefore, the total pressure field p_2 in the *receiving component* may also be represented in terms of propagating solutions as follows

$$p_2 = C_r e^{-jkx} + D_r e^{jkx} \tag{5.2}$$

From equations (5.1) and (5.2), it is evident that there are four unknowns to be determined. Thus, the appropriate boundary conditions can be expressed by the set of equations below, where velocity continuity and force equilibrium are applied.

$$A_s e^{jkL_{x1}} + B_s e^{-jkL_{x1}} = \frac{F_o}{S} \text{ at } x = -L_{x1} \text{ for the force acting on the source volume} \quad (5.3)$$

$$\frac{C_r e^{-jkL_{x2}} - D_r e^{jkL_{x2}}}{\rho_o c_o} = 0 \text{ i.e. rigid termination at } x = L_{x2} \quad (5.4)$$

$$(A_s - B_s) - (C_r - D_r) = 0 \text{ i.e. velocity continuity at } x = 0 \quad (5.5)$$

$$(A_s + B_s) - (C_r + D_r) = mj\omega\left(\frac{A_s - B_s}{\rho_o c_o}\right) \text{ at } x = 0 \quad (5.6)$$

The last equation is Newton's second law of motion, relating the net pressure on the limp panel and its resulting acceleration.

In summary, equations (5.3) and (5.4) are constraint equations that impose pressure equilibrium at the source end, $x = -L_{x1}$, and zero velocity at $x = L_{x2}$ respectively. Equation (5.5) relates the particle velocities at the interface ($x = 0$) between the acoustic volumes (kinematic compatibility), assuming an incompressible mass. Finally, equation (5.6) is for a force equilibrium constraint when a 'limp panel' of mass m per unit area separates the acoustic volumes, relating the force on the panel and its acceleration. Equations (5.3)-(5.6) were set up as a matrix system of equations. For any frequency there is an exact solution for the two volumes and the pressure and particle velocity can be found explicitly.

5.3 – The Component Mode Synthesis Method - CMS

5.3.1 - The definition for the sets of component modes

Despite the fact that any number of components can be used to form a system, only two components are to be considered to illustrate the method. Figure 5.1 illustrates a uniform rigid-walled duct, which will be divided into two CMS components. By choice the limp mass was considered connected to and its effect incorporated in the first volume, but in principle the choice of volume is arbitrary. Therefore, the first component consists of the fluid column plus a *limp mass* partition, being defined for $x = -L_{x1}$ to $x = 0$. The receiving component is defined by the fluid volume which varies from $x = 0$ to $x = L_{x2}$. A sliding rigid piston, which undergoes harmonic oscillation, is fitted to one end of the duct. The other end of the duct (at $x = L_{x2}$) is a rigid termination. It is assumed that the fluid

displacement function $\varepsilon(x,t)$ at position x and time t over the length of the duct can be written in terms of component modes and the corresponding modal generalized coordinates $\bar{\varepsilon}$ by the modal transformation

$$\varepsilon = \Psi\bar{\varepsilon} \tag{5.7}$$

where Ψ is the normalized modal matrix (transformation matrix) of assumed modes defined below.

The modal matrices Ψ_1 and Ψ_2 for the source and receiving components are defined and partitioned as follows

$$\Psi_1 = [\psi_{n1} \quad \psi_{c1}] \tag{5.8}$$

$$\Psi_2 = [\psi_{n2} \quad \psi_{c2}] \tag{5.9}$$

where ψ_c and ψ_n are the constraint and the normal modes respectively. The normal modes are taken to be those of the volumes with a fixed interface (i.e. rigid wall at the interface). The selected normal modes were defined as shape functions satisfying the geometric boundary conditions for each acoustic component. The normal mode ψ_n and the constraint mode ψ_c used in the modal matrices above are classified according to the boundary conditions specified for each component. They are normalized and given by

$$\psi_n = \frac{\phi_n}{\sqrt{\mathrm{m}_n}} \tag{5.10}$$

$$\psi_c = \frac{\phi_c}{\sqrt{\mathrm{m}_c}} \tag{5.11}$$

$$\mathrm{m}_n = \int_{L_x} \rho S \phi_n^2 \mathrm{dx} \text{ and } \mathrm{m}_c = \int_{L_x} \rho S \phi_c^2 \mathrm{dx} \tag{5.12}$$

where ϕ_n is the set of free-fixed interface normal modes which satisfy the condition of unit velocity applied to a moving wall in the source component. For the receiving component they are a set of fixed-fixed interface normal modes. ϕ_c is the constraint mode which satisfies zero velocity on x = -L_{x1} and unit velocity on x = 0 for the source component or unit velocity on x = 0 and zero velocity on x = L_{x2} for the receiving component respectively. These are best visualized by inspection of Figure 5.2, which

shows the corresponding normal and constraint modes for the two volumes. The matrices for the generalized coordinates $\bar{\varepsilon}_1$ and $\bar{\varepsilon}_2$ for the *source* and *receiving* components are then given by

$$\bar{\varepsilon}_1 = [\bar{\varepsilon}_{n1} \quad \bar{\varepsilon}_{c1}]^T \tag{5.13}$$

$$\bar{\varepsilon}_2 = [\bar{\varepsilon}_{n2} \quad \bar{\varepsilon}_{c2}]^T \tag{5.14}$$

where the coordinates $\bar{\varepsilon}_c$ and $\bar{\varepsilon}_n$ relate to the constraint and the normal modes respectively.

5.3.2 - Constraint Equations

A constraint equation, which imposes particle velocity compatibility at the interface (x=0), is then given by

$$C_{ct} = \int_S \left(\frac{\partial \varepsilon_1(x,t)}{\partial t}\bigg|_{x=0} - \frac{\partial \varepsilon_2(x,t)}{\partial t}\bigg|_{x=0} \right)^2 dS = 0 \tag{5.15}$$

where S is the area of the limp partition and this equation is most general to allow the partition to cover only part of the common interface.

It is implicit in equation (5.15) that the same reference coordinate (see Figure 5.1(a)) is used for both component 1 and component 2. Using the Least Squares Method to minimize the function C_{ct} with respect to each unknown variable in equation (5.15) and considering equation (5.7), the following linear sets of equations can be obtained in matrix form as

$$\frac{\partial C_{ct}}{\partial \bar{\varepsilon}_{c1}} = \frac{\partial C_{ct}}{\partial \bar{\varepsilon}_{c2}} = 0 \quad \Rightarrow \quad R_c \bar{G} = 0 \tag{5.16}$$

where $\bar{\mathrm{G}} = [\bar{\varepsilon}_{\mathrm{n1}} \quad \bar{\varepsilon}_{\mathrm{c1}} \vdots \ \bar{\varepsilon}_{\mathrm{n2}} \quad \bar{\varepsilon}_{\mathrm{c2}}]^{\mathrm{T}}$ (5.17)

and $\mathrm{R_c} = [\mathrm{R}_1 \vdots \mathrm{R}_2]$ (5.18)

where R_1 and R_2 are the sub-matrices containing the terms, i.e. the component modes evaluated at the interface, $\Psi_1|_{x=0}$ and $-\Psi_2|_{x=0}$ for components 1 and 2 respectively.

5.3.3 - System Synthesis

The equations of motion for component 1 and component 2, with the former including the approximate dynamic effects from the *limp* partition in the generalized modal mass [69], are expressed using Lagrange's equations in terms of their generalized coordinates $\bar{\varepsilon}$ as

$$\left(M_1 + M_p\right)\ddot{\bar{\varepsilon}}_1 + C_{d1}\dot{\bar{\varepsilon}}_1 + K_1\bar{\varepsilon}_1 - \lambda R_1 = F_1 \tag{5.19}$$

where $F_1 = \left(F_o^S \Psi_1(x)\right)_{x=-L_{x1}}$

and $$M_2\ddot{\bar{\varepsilon}}_2 + C_{d2}\dot{\bar{\varepsilon}}_2 + K_2\bar{\varepsilon}_2 - \lambda R_2 = 0 \tag{5.20}$$

where λ is in general a vector of Lagrange multipliers to apply the interface constraints. M, C_d, and K are the modal mass, damping and stiffness matrices for the components respectively; and F_1 is the generalized force on the acoustic component 1 [70]. F_o^S is the imposed force amplitude.

The modal mass M_p of the partition is used to simulate the interface loaded modes of component 1 [69]. The corresponding eigenproblem for the component 1 is then of the form

$$\left[K_1 - \omega_n^2\left(M_1 + M_p\right)\right]\bar{\varepsilon}_1 = 0 \tag{5.21}$$

The set of equations for the entire system is then given by

$$\mu\ddot{\bar{G}} + \varsigma\dot{\bar{G}} + \chi\bar{G} - \lambda R_c^T = F_T \tag{5.22}$$

where $\mu = \begin{bmatrix} M_1 + M_p & 0 \\ 0 & M_2 \end{bmatrix}$; $\varsigma = \begin{bmatrix} C_1 & 0 \\ 0 & C_2 \end{bmatrix}$; $\chi = \begin{bmatrix} K_1 & 0 \\ 0 & K_2 \end{bmatrix}$; $F_T = \begin{Bmatrix} F_1 \\ 0 \end{Bmatrix}$.

μ, ς and χ are the system modal mass, damping and stiffness matrices respectively. F_T is the column vector containing the generalized forces exerted on the fluid components.

It can also be seen that the coordinates $\bar{G}$ defined in equation (5.17) are not linearly independent in the set of equations (5.22), due to the constraint equations (5.16), i.e.

there are more equations than unknowns. Alternatively, a linear modal transformation T_r can be used to solve the set of equations (5.22) in terms of generalized independent coordinates $\overline{q}_i$, which allows for a reduction of the number of variables due to the constraint equations available. The transformation is then given by

$$\overline{G}^s = T_r \overline{q}_i \tag{5.23}$$

where $$\overline{G}^s = [\overline{\varepsilon}_{c1} \vdots \overline{\varepsilon}_{n1} \quad \overline{\varepsilon}_{n2} \quad \overline{\varepsilon}_{c2}]^T \tag{5.24}$$

and $$\overline{q}_i = [\overline{\varepsilon}_{n1} \quad \overline{\varepsilon}_{n2} \quad \overline{\varepsilon}_{c2}]^T \tag{5.25}$$

The matrix $\overline{G}^s$ is the rearranged matrix of $\overline{G}$ in terms of dependent and independent coordinates. Equation (5.16) can be rearranged and also rewritten as

$$R_c^s \overline{G}^s = 0 \tag{5.26}$$

and $$\mathrm{R}_c^s = [\mathrm{R}_d \vdots \mathrm{R}_i] \tag{5.27}$$

where R_d and R_i are the sub-matrices containing the coefficients of the dependent ($\overline{\varepsilon}_{c1}$) and independent set of generalized coordinates respectively (i.e. $\overline{\varepsilon}_{n1}, \overline{\varepsilon}_{c2}$ and $\overline{\varepsilon}_{n2}$). Accordingly, the transformation matrix is thus given by

$$T_r = \begin{bmatrix} -R_d^{-1} R_i \\ I \end{bmatrix} \tag{5.28}$$

From equations (5.23) and (5.26) it is seen that $R_c^s T_r = 0$. Therefore, equations (5.22) and (5.23) can be combined to take the form

$$M_G \ddot{\overline{q}}_i + C_G \dot{\overline{q}}_i + K_G \overline{q}_i = F_s \tag{5.29}$$

where $$M_G = T_r^T \mu\, T_r;\; K_G = T_r^T \chi\, T_r;\; C_G = T_r^T \varsigma\, T_r;\; F_s = T_r^T F_T \tag{5.30}$$

Thus, equation (5.30) defines the modal matrices in terms of the independent variables $\overline{q}_i$ and equation (5.29) is subsequently solved. In addition, for the case of a limp panel over a common interface, only one constraint equation is defined by equation (5.16).

5.4 – Numerical Results

The simple one-dimensional example was considered here in order to illustrate the application of the CMS approach in structural-acoustic interaction problems. A comparison between the CMS approach and the one-dimensional analytical wave approach described in section 5.2 is made, in order to assess the performance of the method for sound transmission problems. In addition, the CMS model is later compared to the Modal model, which uses modes with uncoupled boundary conditions.

The configuration of the system used is shown in Figure 5.1. Three different models were used in order to illustrate the method. In the first two models, a comparison between the CMS and an analytical model is made in order to validate the CMS approach and formulation for force excitation. Subsequently, the modal method is compared to the CMS method in a third model which incorporates velocity excitation, as has previously been considered in the thesis.

5.4.1 Model 1 – The acoustic components are equal in length

For the first one (Model 1), the lengths of the rectangular acoustic volumes were both equal to 10 m (L_{x1} =L_{x2} =10 m). The volumes of both components were equal to 40 m^3. The thickness and cross sectional dimensions of the partition connecting both volumes were 0.01m and 2m x 2m respectively. A constant loss factor damping equal to $\eta = 0.01$ was used for both the normal and constraint modes. For the one-dimensional wave approach, a complex wavenumber k was selected for the propagating plane waves [48]. The loss factor used for the wave model was also $\eta = 0.01$.

For the *source* subsystem (component), 18 *free-fixed* normal modes and 1 constraint mode have been used. For the *receiving* subsystem, 17 *fixed-fixed* and 1 constraint mode have been considered. The first 11 uncoupled and coupled natural frequencies for Model 1 are shown in Table 5.1. The set of component modes is illustrated in Figure 5.2. No velocity is involved in the bulk compression mode n=0. There are other possible combinations of component modes, such as the free-interface normal modes plus attachment modes [69]. However, no other combination fulfil all criteria of mode selection, such as linear independence, low computational expense, accuracy, simplicity, etc., but for the one that employs constraint modes and fixed-interface normal modes [68].

The calculations were performed using only one-dimensional wave propagation. At high frequencies tangential modes cut-on, but these have been ignored for the purposes of comparison with the one-dimensional wave approach. The effect of oblique modes is discussed in Chapter 6 where a complete 3D implementation is described.

A frequency cut-off criterion was used to select the number of modes in each component. All normal axial modes, which are plane in the cross-section and have natural frequencies less than or equal to 300 Hz, were included. The overall system equation of motion, given in equation (5.29), is solved at each frequency.

Figures 5.3 and 5.4 show the frequency response of each subsystem in terms of the spatial-averaged mean square sound pressure level for a *limp* partition with nominal mass densities of $\rho h = 8.1$ kg/m^2 and $\rho h = 78.5$ kg/m^2 respectively. For both cases, the sound pressure levels were similar in behaviour. The CMS and one-dimensional wave model were nearly identical over most of frequency range. The CMS model comprised normal free-fixed velocity modes, which were excited by a plane force source located at the rear of the source component. In addition, the peaks in the frequency response corresponded to the resonance frequencies of the combined system, as expected.

In *the receiving* component, there are also insignificant differences between the CMS and the one-dimensional wave model. Both the CMS and wave models exhibited some peaks in the receiving volume at similar frequencies. These frequencies are related to the modes of the fixed-fixed receiving component. However, alternate peaks, which correspond to the resonance frequencies of the coupled system, can also be seen in the response of the receiver volume in these cases.

Figure 5.3-a shows that at very low frequencies (below 20 Hz), a difference of less than 2 dB can be seen at the resonance peaks. It is related to different sensitivities of the damping models used in both approaches at low frequencies.

Figures 5.5 and 5.6 show the mean square sound pressure and particle velocity distribution along the length of the source and receiving volumes at 80 Hz and 10 Hz respectively. The results for pressure distribution are shown in Figures 5.5a and 5.6a. It can be seen that there is a pressure discontinuity at the interface between the components for both approaches. The particle velocity results shown in Figures 5.5b and 5.6b (in dB) were normalized with respect to a volume velocity $Q_0 = 3\text{x}10^{-5}$ m^3/s divided by the partition area S = 2m x 2m. The calculated fluid particle velocity is non-zero and

continuous at the interface. For instance, this is not the case for the modal model where the particle velocity is zero at the interface. For the receiving room the differences shown in Figure 5.5-a and 5.5-b are due to differences in the damping models at that particular frequency. Moreover, in Figure 5.5-a the differences close to the source (x<-9) are due to the open end at x = -10. This implies that the dynamic component of pressure tends to zero at this open boundary. For the results in Figure 5.6 the difference between the CMS and the exact one-dimensional formulation is negligible and not discernible.

Figure 5.7 shows the comparison of the Noise Reduction NR [82] predicted in narrow bands. The NR was calculated using

$$\mathrm{NR} = 10\log_{10}\left(\frac{\left\langle \overline{p}_s^2 \right\rangle}{\left\langle \overline{p}_r^2 \right\rangle}\right) \text{in dB} \tag{5.32}$$

where $\left\langle \overline{p}_s^2 \right\rangle$ and $\left\langle \overline{p}_r^2 \right\rangle$ are the space-averaged mean square sound pressure in the source and receiving volumes respectively. Figure 5.7a is for the partition with mass per unit area ρh=8.1 kg/m^2 and Figure 5.7b is for a heavier partition with ρh= 78.5 kg/m^2. The narrow band results were obtained by subtracting the energy level in narrow bands for the source volume from the energy level in the same bands for the receiving volume. For instance, in Figure 5.4, the CMS and one-dimensional wave approach at about 18 Hz have a smaller peak in the receiving component but a trough in the source component. Therefore, the subsequent NR also exhibits a dip in these cases, which coincides. The NR values for the CMS and the 1-D wave approach were almost identical over the whole frequency range. In general, the trend in the NR results was similar for both models. The length in the receiving volume primarily governs the values of the resonance frequencies, and the absorption influences the variation of the maxima in the response respectively.

Figure 5.8 shows that the one-third octave bands NR values obtained via the CMS and wave models. The one third octave band results for NR were obtained by subtracting the total energy level in a specific band for the source component from the total energy level in the same band for the receiving component. The total energy in a one third octave band was obtained by the summation of the energies in each narrow band. Figure 5.8 shows the NR results for $\rho h = 8.1 kg/m^2$ and $\rho h = 78.5 kg/m^2$. It is seen that the models

produced very similar results. The differences between the two approaches were insignificant over most of the frequency range considered.

In summary, the excitation for the CMS and the wave models was formulated in terms of a unit imposed force on the source component boundary. A force excitation source puts energy primarily into modes which have large in-phase velocities at the surface of excitation. The CMS and one-dimensional wave approach predictions for the narrow and one-third octave frequency bands considered have had very good agreement.

5.4.2 Model 2 – Dissimilar acoustic components (unequal lengths)

For the second model (Model 2), two dissimilar length components were used. The lengths of the source and receiving volumes were equal to 12m and 7m respectively. (L_{x1} = 12m and L_{x2} = 7m). The source and receiving component volumes were 72m^3 and 42m^3 respectively. The thickness and dimensions of the partition connecting both volumes were 0.01m and 2m x 2m respectively. Likewise as considered in the previous model, a constant loss factor of $\eta = 0.01$ was used for both *components* of model 2.

For the *source* subsystem (component), 21 *free-fixed* normal modes and 1 constraint mode were used. For the *receiving* subsystem, 12 *fixed-fixed* and 1 constraint mode were considered. The first 9 uncoupled and coupled natural frequencies for Model 2 are shown in Table 5.2. Figures 5.9 and 5.10 present the frequency response of each subsystem in terms of spatial-averaged mean square sound pressure levels for ρh = 8.1 kg/m^2 and ρh = 78.5 kg/m^2 respectively. The CMS and one-dimensional wave model were similar and almost identical for most of the frequency range with more modes existing than for model 1.

Figures 5.11 and 5.12 show the mean square sound pressure and particle velocity distribution along the length of both source and receiving volumes at 80 Hz and 10 Hz respectively. The discontinuity of pressure at the interface between components is also evident. The particle velocity results in Figure 5.12b were normalized with respect to a volume velocity $Q_0 = 3\text{x}10^{-5}$ m^3/s divided by the panel area S. As in the results presented previously, for the CMS and wave techniques the fluid particle velocity is non-zero and continuous at the interface.

Figure 5.13 shows the NR results in narrow bands. The NR values for the CMS and the 1-D wave approach presented negligible differences over all of the frequency range. In general, the trend in the NR results was similar for both models 1 and 2.

Figure 5.14 shows the NR values in one-third octave bands. It is also seen that the differences between the CMS and the 1-D wave approach are not distinguishable for either partition densities used in the simulations.

Comparing these results with those of the previous section it appears that the fact of considering a smaller receiving component for Model 2, and subsequently a component with a lower number of modes compared to the source, has a significant effect on the calculation of the NR when velocity continuity (at the component interface) is imposed. Consequently, the NR values obtained for model 2 (Figure 5.14) via either the CMS or the one-dimensional wave model were lower and different than those obtained for model 1 over most of the frequency bands.

5.4.3 Model 3 – Baseline model used for comparison with the Modal model

The excitation for the modal model presented in chapter 2 is based on a constant volume velocity source, whereas the one for the CMS and the one-dimensional wave approach presented previously for Model 1 and 2 were described in terms of an imposed force on the moving boundary. The physical implications of this difference are explained as follows. Force excitation puts energy primarily into modes having large in-phase velocities at the plane of excitation. On the other hand, velocity sources excite modes having large pressures at the surface (i.e. the rigid-walled modes – if they are damped). Thus, the results obtained via the approaches are substantially different due to the dissimilar input powers to the models, the effect of which does not divide out when the results are considered in one-third octave bands [87].

In order to compare the CMS, one-dimensional and modal models, similar input powers were considered here. The type of excitation used in the CMS and one-dimensional wave approaches was modified to velocity source excitation. For the one-dimensional model, equation (5.3) was substituted by

$$\frac{A_s e^{jkL_{x1}} - B_s e^{-jkL_{x1}}}{\rho_o c_o} = v_o \text{ at } x = -L_{x1} \text{ for the velocity acting on the source volume} \quad (5.33)$$

where v_o is the imposed velocity.

For the CMS model, F_1 defined in equation (5.19) was substituted by F_1^S which is given by the relationship

$$F_1^S = j\omega\rho_o\dot{\varepsilon}_o S_1 \int \Psi_1 \, \delta(x - x_0)dx = j\omega\rho_o\dot{\varepsilon}_o S_1 \Psi_1(x_0) \tag{5.34}$$

where $x_o = -L_{x1}$, $\dot{\varepsilon}_o$ is the imposed normal surface velocity and S_1 is the cross-section area of component 1.

Equation (5.34) was derived by using the momentum equation [18] which establishes the relationship between acoustic pressure and particle fluid velocity. Alternatively, as the source component is subjected to an external imposed velocity, the corresponding generalized velocity could be directly determined by using the Virtual Work Principle [13], which is based on virtual displacements or virtual change of the system configuration. As a result of using either approach, one has the right-hand side of equation (5.29) expressed in terms of both generalized velocity and the acoustic pressure mode shape of the source room evaluated at the excitation point ($x = x_o$) instead of the generalized force and particle velocity mode shape (equation (5.19)).

For the third model (Model 3), two dissimilar length components were used. The lengths of the source and receiving volumes were equal to 5m and 3m respectively. (L_{x1} = 5m and L_{x2} = 3m). The source and receiving component volumes were 20m^3 and 12m^3 respectively. The thickness and dimensions of the partition connecting both volumes were 0.01m and 2m x 2m respectively. A constant loss factor $\eta = 0.01$ was used for both components.

For the *source* subsystem (component), 8 *fixed-fixed* normal modes and 1 constraint mode were used. This is different than previously used to accommodate the velocity excitation. For the *receiving* subsystem, 5 *fixed-fixed* and 1 constraint mode were considered instead (see Figure 5.15). Within the frequency range considered (0-300 Hz) a total of 9 and 5 resonance frequencies were considered for the source and receiving component respectively (see Table 5.3).

Figures 5.16 and 5.17 present the frequency response of each subsystem in terms of spatial-averaged mean square sound pressure levels for ρh = 8.1 kg/m^2 in narrow and one third octave bands respectively. Figures 5.16a and 5.16b show that the CMS and one-dimensional wave model were similar almost identical at frequencies greater than 20 Hz. On the other hand, the modal model presented significant differences. Figure 5.16a

shows that these differences are mainly associated with a shift in the resonance peaks. In Figure 5.16b it is also seen that at higher frequencies there is a difference of about 2 dB between the CMS and the modal model. Figure 5.17a and 5.17b shows that the differences (up to about 35 dB) between the Modal and the CMS model occur mainly in the one third band with centre frequency at 20 Hz.

At frequencies below 10 Hz, the modal and the one-dimensional wave models show a fairly good agreement. However, it is seen that there are significant differences between the CMS and the one-dimensional wave model. It can be explained by the fact that the CMS model does not incorporate in the present formulation the bulk mode of the sound pressure field. According to the CMS method implemented, a set of fixed-interface normal and constraint modes is selected for each component in terms of velocity modeshapes. Thus, the bulk pressure mode, which is also known as the equilibrium mode (zero particle velocity and constant pressure), cannot be represented herein using this type of formulation. Below 10 Hz the coupled system has no dynamic mode and can be considered as a quasi-static problem.

Figures 5.18 and 5.19 show the frequency response of each subsystem in terms of spatial-averaged mean square sound pressure levels for $\rho h = 78.5$ kg/m^2 in narrow and one third octave band respectively. Comparing these results with those for the lightweight partition, a better agreement is observed between the CMS and modal model, especially at low frequencies. This shows that the numerical modal model better represents the coupled system for the heavy partition, as expected.

Figures 5.20 and 5.21 show the mean square sound pressure and particle velocity distribution along the length of both source and receiving components at 50 Hz and 100 Hz respectively. The discontinuity of pressure at the interface between components is also evident. The particle velocity results in Figures 5.20b and 5.21b were normalized with respect to a source volume velocity $Q_0 = 3\text{x}10^{-5}$ m^3/s divided by the panel area S. As in the results presented previously, for the CMS and wave techniques the fluid particle velocity is non-zero and continuous at the interface.

In terms of pressure distribution Figures 5.20a shows that the CMS and one dimensional wave models present significant discrepancies in the source *component* (as x tends to $-L_{x1}$) at 50 Hz. Nevertheless, those differences are insignificant at 100 Hz, as there is less influence of the bulk pressure mode which is taken into account in the modal and

wave models. In the receiving component the pressure distribution for the CMS and one-dimensional wave model are very similar whereas the modal model presents some differences. Figures 5.20b and 5.21b show that at $x=-L_{x1}$ the particle velocity is zero for the CMS and modal model. For the one-dimensional wave model, the particle velocity at $x=-L_{x1}$ is imposed according to equation (5.33).

Figure 5.22 shows the NR results in narrow bands. The NR values for the CMS and the 1-D wave approach produced small differences over most of the frequency range. The NR values for the CMS model were slightly different from those for the 1-D wave model at frequencies less than 40 Hz. It can be seen that the modal model results present significant differences at low frequencies Nevertheless, the trend in the NR results generally was similar for all models.

Figure 5.23 shows the NR values for $\rho h = 8.1 kg/m^2$ and $\rho h = 78.5 kg/m^2$. The results are presented in one-third octave bands. The CMS and wave model values are very similar. Nevertheless, at low frequencies they are slightly greater than the values obtained using the Modal model. It is shown that at higher frequencies, a difference of less than 2 dB is observed between the CMS and the modal approach. At frequencies below 40 Hz, there is a difference of up to about 10dB. On the other hand, for the heavier partition this difference is only about 5dB. It shows the degree of sensitivity of the results when considering the frequency response with light partitions at very low frequencies.

Alternatively, a CMS model considering free-fixed normal modes for the source component (as used in models 1 and 2) has been formulated in order to be compared to Model 3, which is based on velocity excitation. The material and geometrical properties were the same as those of Model 3. However, in order to reconcile this alternative CMS model and the Modal model, the results were divided by the input impedance which was calculated by finding the particle velocity at the drive point (see Figure 5.24). Figure 5.25 shows a comparison between the CMS model 3 and this alternative model which considers force excitation. The results are nearly identical over most of the frequency range. At very low frequencies, a difference of less than 2 dB occurs between both models.

5.5 – Conclusions

The purpose of this chapter was to develop an original one-dimensional acoustic CMS model to analyse and calculate sound transmission through a *limp mass* panel between connected acoustic volumes. It is seen that the results for the CMS and one-dimensional wave approaches have shown excellent agreement with the force excitation formulation considered for Models 1 and 2.

The traditional modal method provided reasonable results for the higher mass density partitions, and in particular at higher frequencies. For instance, the modal analysis for Model 3, which comprises two dissimilar components, has shown good agreement with the CMS model at higher frequencies. In addition, at frequencies below 50 Hz, the modal model showed better agreement with the CMS model when considering the heavier partition. Basically, this behaviour indicates the importance of considering the kinematic effect of the partition on sound transmission when more complex systems are to be analysed, and the benefit of the CMS approach.

It is clear that particle velocity modes have been used and that no velocity is involved in the bulk compression mode, which is purely a static stiffness mode. Therefore, the CMS models used in this chapter do not include the bulk mode n=0 as strictly it should if it were possible to analyse the system in terms of displacement modes. The effect of the 0 Hz mode on the results was only significant at very low frequencies. This is confirmed by the fact the CMS model underestimated the spatially averaged mean square sound pressures as frequency tended to zero. Overall, the bulk mode is considerably important when small components or very low frequency ranges are considered in models driven by a volume velocity excitation. Thus, this is the case only for model 3 where the volume velocity is used.

The extension of the CMS approach to three-dimensional problems in acoustics will be discussed in the next chapter and evaluated for transmission between two acoustic spaces separated by a flexible partition, the latter also possessing modal behaviour.

In particular, the partition may or may not cover all of the common wall and it is not required that the components have identical cross-sections (as needed for the one-dimensional case) or that only axial acoustic modes perpendicular to the partition exist in the volumes. Equations (5.7)-(5.30) can therefore be generalised, the main differences being described in Chapter 6.

Tables

CMS model		One-dimensional model	
F_{N1}-F_{N2} (Hz)	F_C (Hz)	F_N (Hz)	F_C (Hz)
11.8 – 8.5	3.7	8.6	3.7
27.1 – 25.5	11.1	25.4	11.1
43.5 – 42.5	18.9	42.5	18.9
60.2 – 59.5	26.9	59.5	27.1
77.1 – 76.5	35.2	76.5	35.2
93.9 – 93.5	43.5	93.3	43.6
110.9 – 110.6	51.8	110.5	51.7
127.8 – 127.6	60.2	127.5	60.2
144.8 – 144.7	68.6	144.5	68.6
161.7 – 161.7	77.1	161.5	77.1
178.7 – 170.0	85.5	170.1	85.5

Table 5.1: The first 11 uncoupled (F_N) and coupled natural frequencies (F_C) for Model 1, which is a system comprising two identical volumes separated by a limp panel, obtained via the CMS and the one-dimensional wave models. The superficial mass density of the limp partition was $\rho h = 8.1 \text{kg/m}^2$. For the CMS model two different types of normal modes, i.e. free-fixed and fixed-fixed modes, plus constraint modes were used for the source and receiving volumes respectively.

CMS model		One-dimensional model	
F_{N1}-F_{N2} (Hz)	F_C (Hz)	F_{N1}-F_{N2} (Hz)	F_C (Hz)
10.13 – 12.1	4.1	7.1 – 12.3	4.5
22.8 – 36.4	10.5	21.3 – 36.4	10.7
36.4 – 60.7	21.9	35.4 – 60.7	21.8
50.3 – 85.0	26.8	49.6 – 85.0	26.6
64.3 – 109.4	36.4	63.8 – 109.3	36.3
78.4 – 133.7	49.1	77.9 – 133.6	48.7
92.5 – 158.1	50.9	92.1 – 157.9	50.8
106.6 – 182.6	64.3	106.3 – 182.1	64.6
120.7 – 207.2	73.6	120.4 – 206.4	73.5

Table 5.2: The first 9 uncoupled (F_N) and coupled natural frequencies (F_C) for Model 2, which is a system comprising two identical volumes separated by a limp panel, obtained via the CMS and the one-dimensional wave models. The superficial mass density of the limp partition was $\rho h = 8.1 \text{kg/m}^2$. For the CMS model two different types of normal modes, i.e. free-fixed and fixed-fixed modes, plus constraint modes were used for the source and receiving volumes respectively.

Modal Model		CMS model		One-dimensional model	
F_{N1}-F_{N2} (Hz)	F_C (Hz)	F_{N1}-F_{N2} (Hz)	F_C (Hz)	F_{N1}-F_{N2} (Hz)	F_C (Hz)
0 – 0	18.0	8.4 – 28.3	12.8	8.2 – 28.3	12.5
34.0 – 56.7	36.6	36.4 – 85.1	36.2	36.3 – 85.1	36.1
68.0 – 113.3	59.0	69.3 – 142.1	58.9	69.0 – 142.1	58.6
102.0 – 170.0	69.6	102.9 – 199.7	69.5	102.5 – 199.7	69.4
136.0 – 226.7	102.8	136.6 – 258.9	102.8	136.6 – 258.9	102.6
170.0 – 283.3	114.7	170.5 – -----	114.7	170.4 – -----	114.7
204.0 – -----	136.7	204.4 – -----	136.7	204.3 – -----	136.7
238.0 – -----	170.0	238.4 – -----	170.0	238.4 – -----	170.1
272.0 – -----	171.4	272.3 – -----	171.4	272.3 – -----	171.3

Table 5.3: The uncoupled (F_N) and coupled natural frequencies (F_C) for Model 3, which is a system comprising two dissimilar volumes separated by a limp panel, obtained via the Modal, CMS and one-dimensional wave models. The superficial mass density of the limp partition was $\rho h = 8.1 \text{kg/m}^2$. For the CMS model similar types of normal modes (fixed-fixed) plus a constraint mode were used for the source and receiving volumes.

Figures

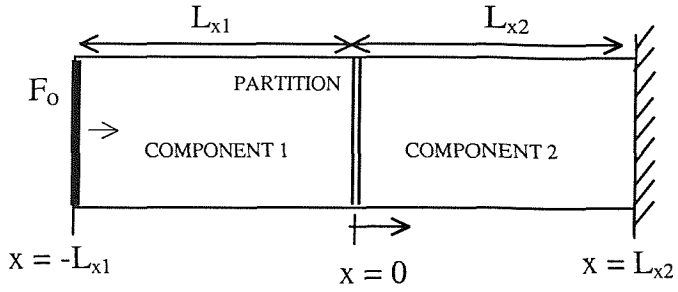

Figure 5.1: A piston driven acoustic tube divided into two components 1 and 2. Velocity continuity and force equilibrium conditions are imposed on the limp partition at the interface $x = 0$; F_o is the force excitation.

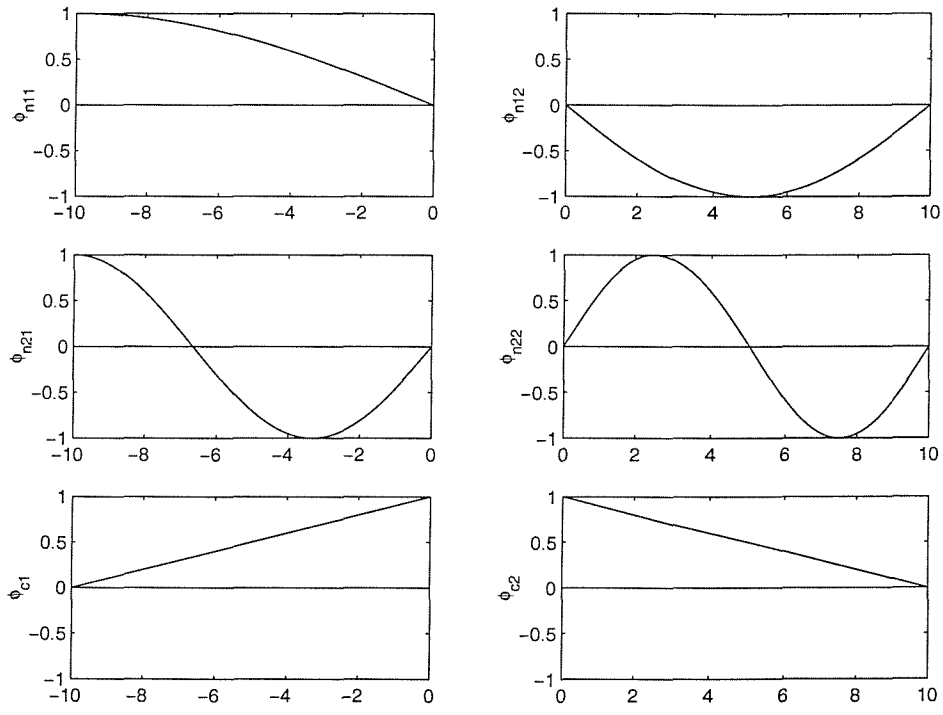

Figure 5.2: Set of component acoustic particle velocity modes used in Models 1 and 2 for the source (i) and receiver (ii) respectively. For instance, ϕ_{11} and ϕ_{21} represents the first two component free-fixed interface normal modes and ϕ_{c1} is the interface constraint mode for the source room. ϕ_{12} and ϕ_{22} are the first two component fixed-fixed modes and ϕ_{c2} is the interface mode for the receiving room.

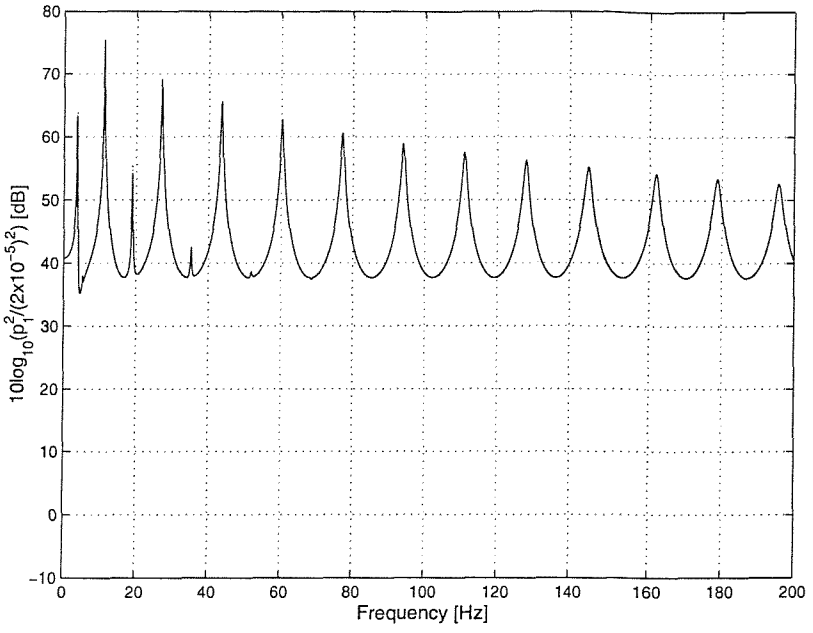

a)

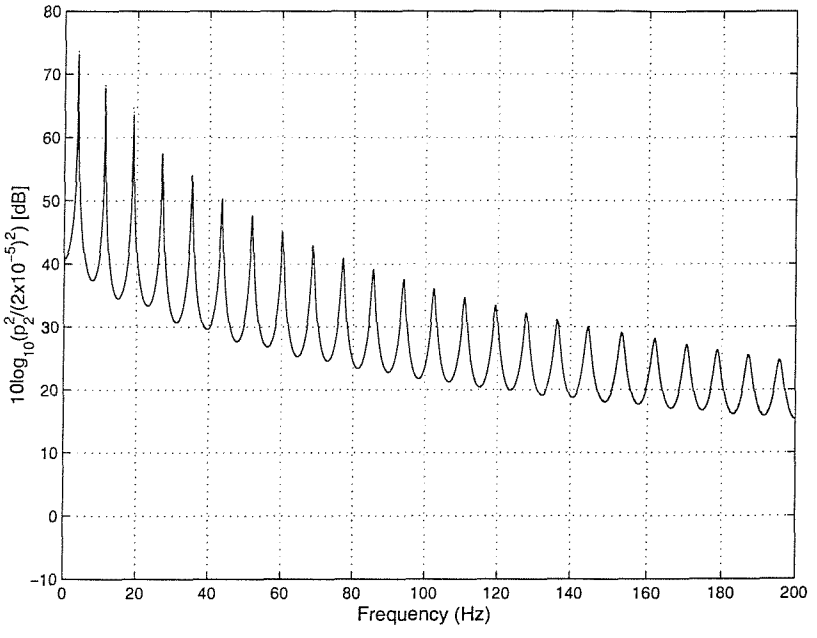

b)

Figure 5.3. Spatially averaged mean square sound pressure for the source (a) and receiving (b) volumes (in dB re $2x10^{-5}$ Pa) for Model 1. Lightweight partition (ρh=8.1 kg/m^2) ___ One-dimensional wave approach, ...CMS model.

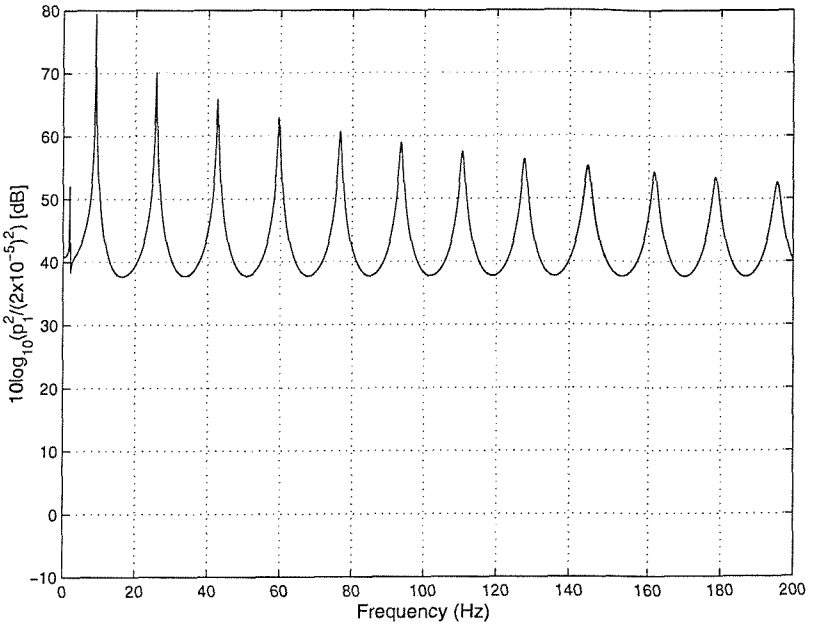

a)

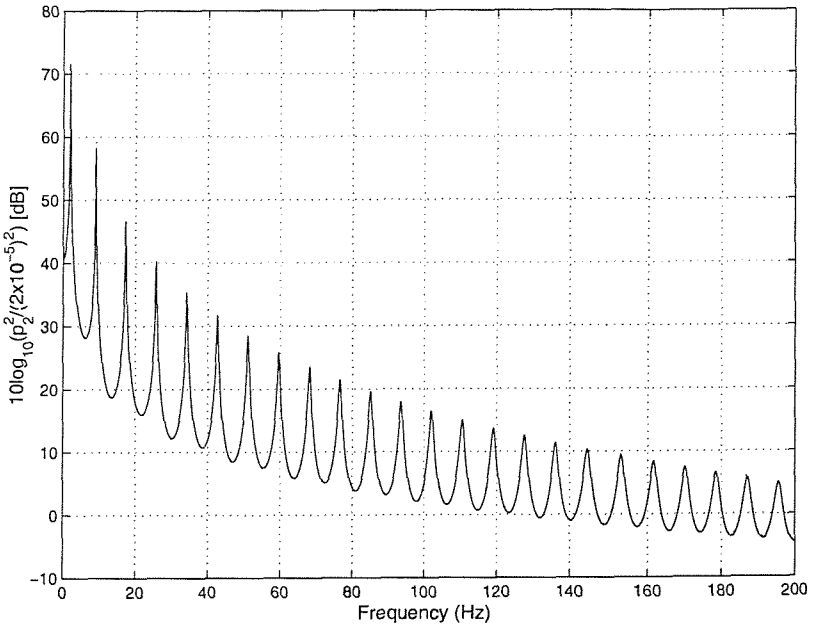

b)

Figure 5.4: Spatial-averaged mean square sound pressure for source (a) and receiving (b) volumes (in dB re $2x10^{-5}$ Pa) – Model 1. Heavy partition (ρh=78.5 kg/m^2) ___ One-dimensional wave approach, ...CMS model.

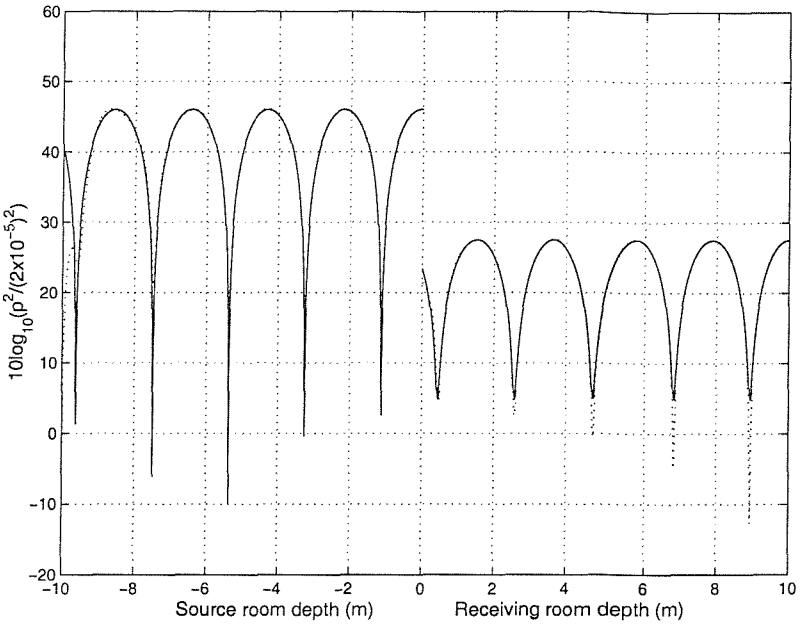

a)

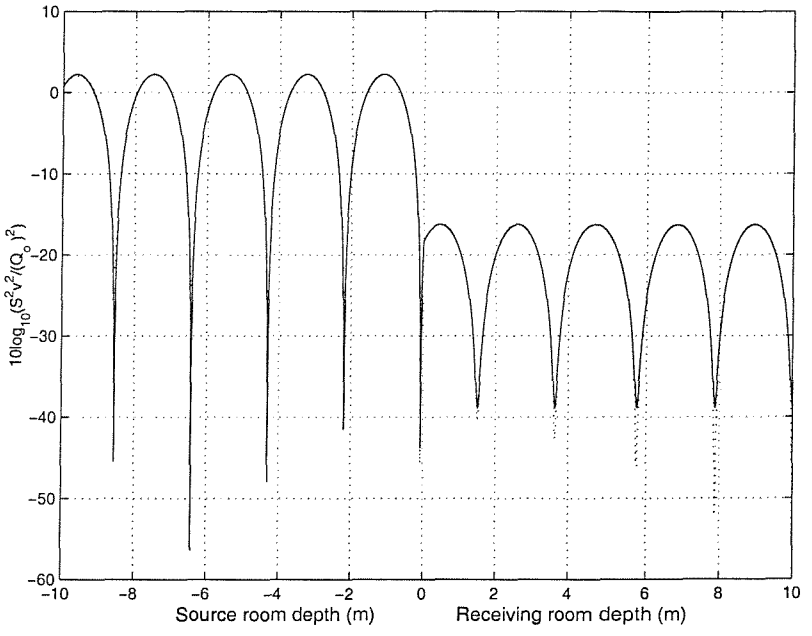

b)

Figure 5.5: The Spatial variation of mean square sound pressure (in dB re $2x10^{-5}$ Pa) (upper figure (a)) and particle velocity (normalized to Q_o/S where Q_o is the volume velocity which is equal to $3x10^{-5}$ m^3/s and S is the panel area as shown in the lower figure (b)) at 80 Hz (ρh=8.1 kg/m^2) – Model 1. ____ One-dimensional wave approach, ... CMS model.

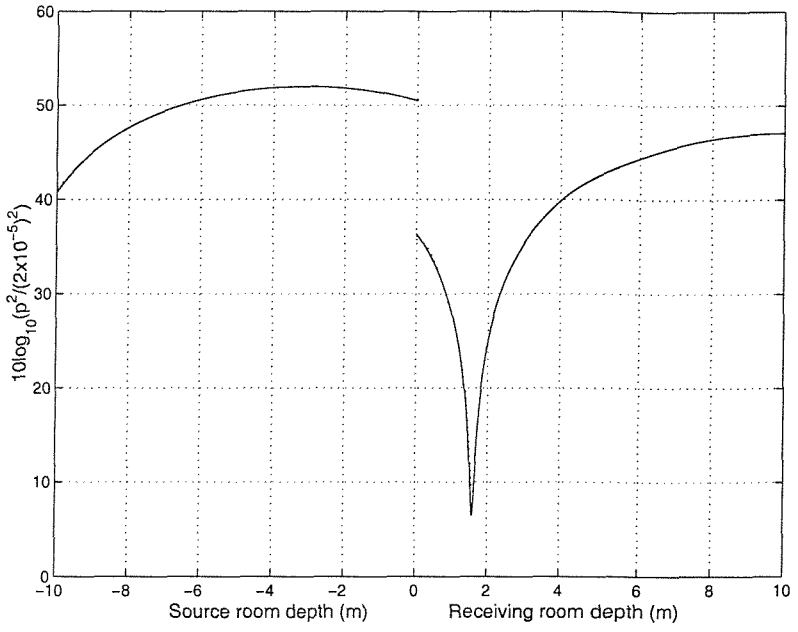

a)

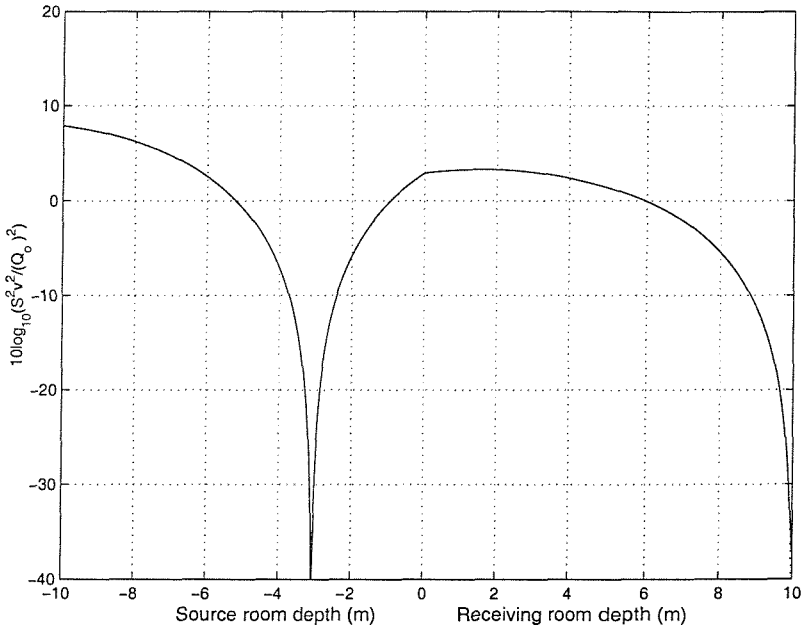

b)

Figure 5.6: The Spatial variation of mean square sound pressure (in dB re $2x10^{-5}$ Pa) (upper figure (a)) and particle velocity (normalized to Q_o/S where Q_o is the volume velocity which is equal to $3x10^{-5}$ m^3/s and S is the panel area as shown in the lower figure (b)) at 10 Hz (ρh=8.1 kg/m^2) for Model 1. ____ One-dimensional wave approach, ... CMS model.

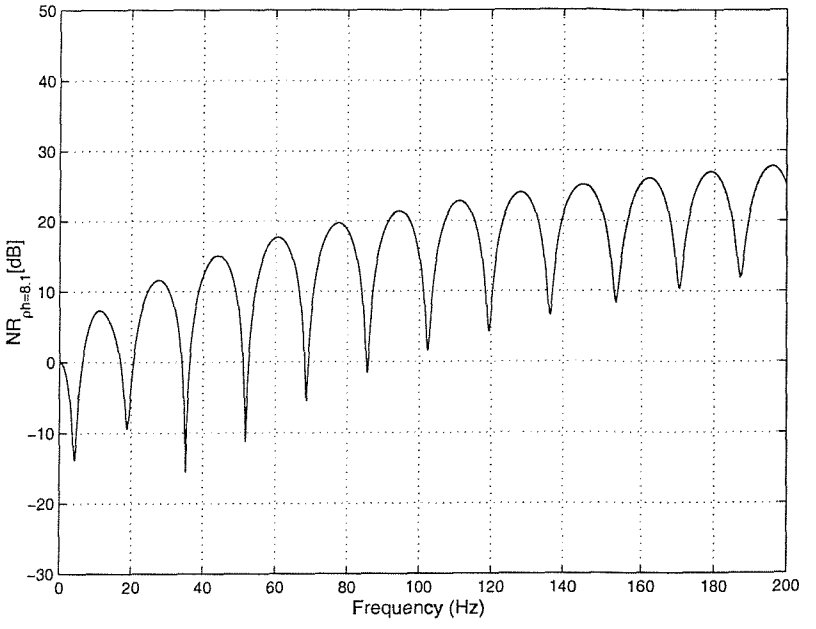

a)

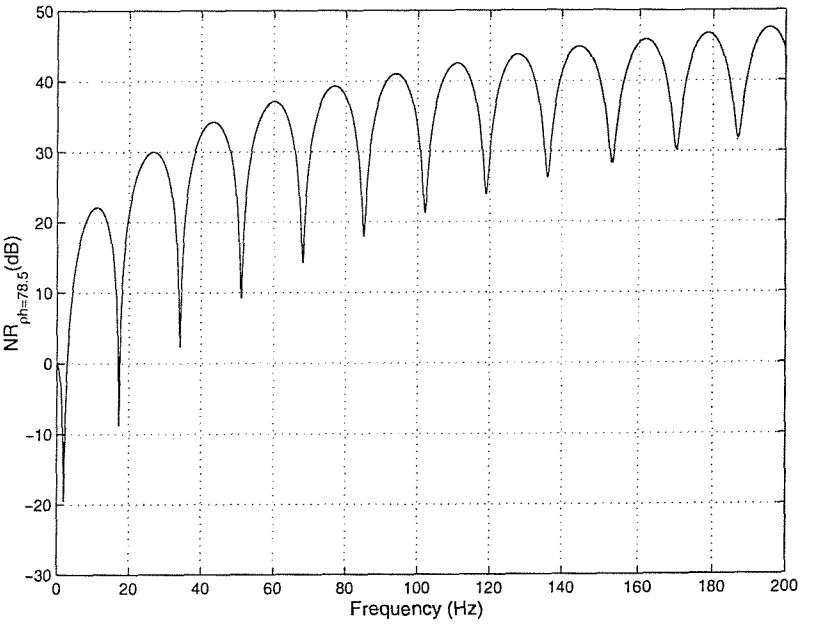

b)

Figure 5.7. Comparison of the Noise Reduction results, see equation (5.31), for two different panel mass densities (narrow bandwidth frequency) for Model 1. (a) ρh= 8.1 kg/m^2 , (b) ρh= 78.5 kg/m^2; ___One-dimensional wave approach, ...CMS model.

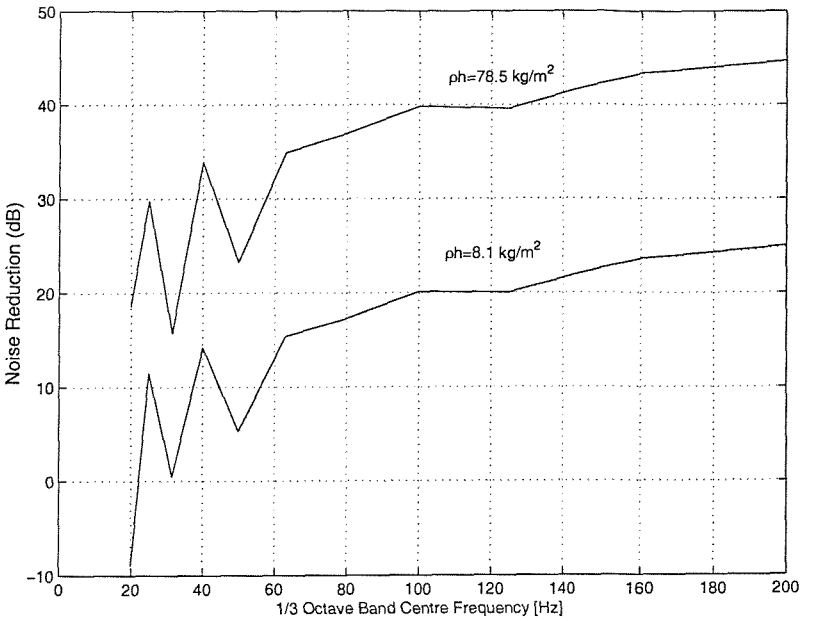

Figure 5.8. Comparison of the Noise Reduction (see equation (5.31)) for two different panel mass densities (1/3 octave bands) for Model 1. ___One-dimensional wave approach, ...CMS model.

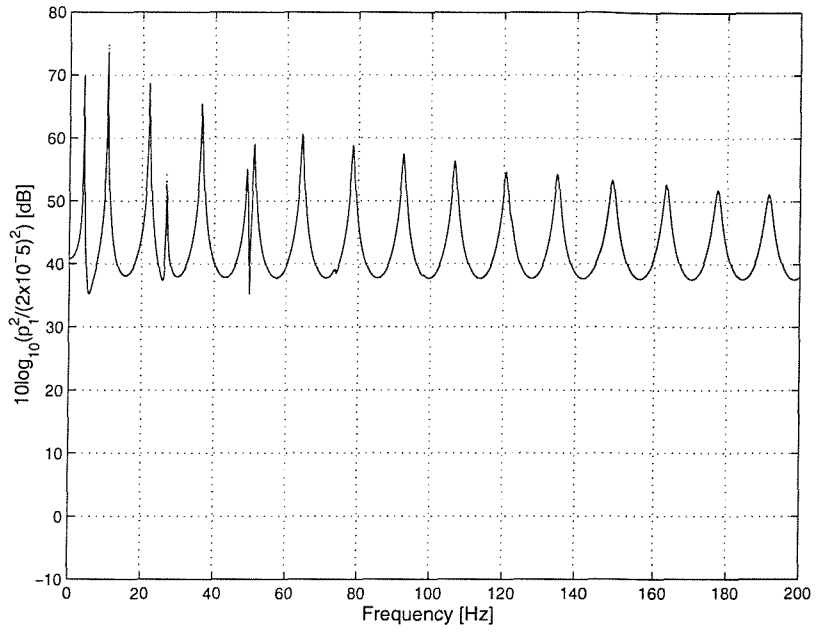

a)

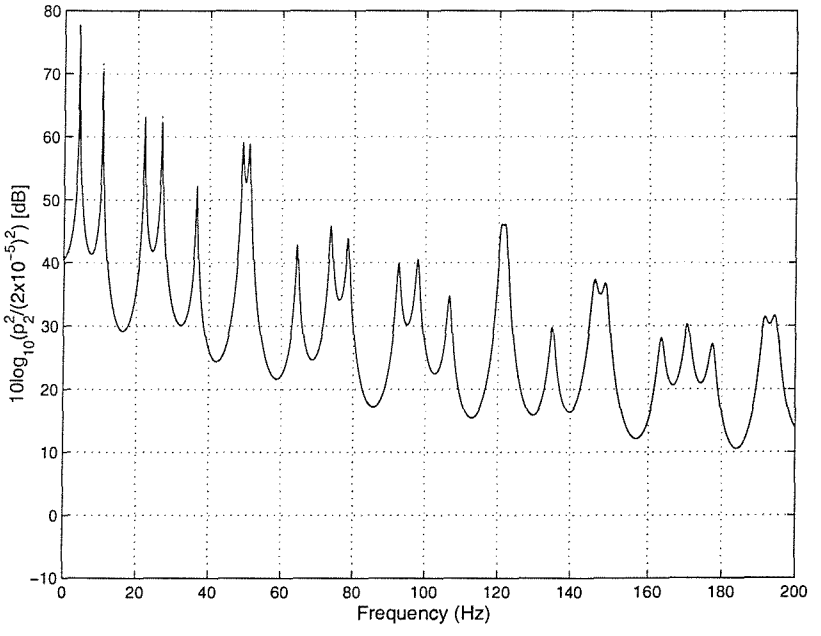

b)

Figure 5.9. Spatially averaged mean square sound pressure for the source (a) and receiving (b) volumes (in dB re $2x10^{-5}$ Pa) for Model 2. Lightweight partition (ρh=8.1 kg/m^2) ___ One-dimensional wave approach, ...CMS model.

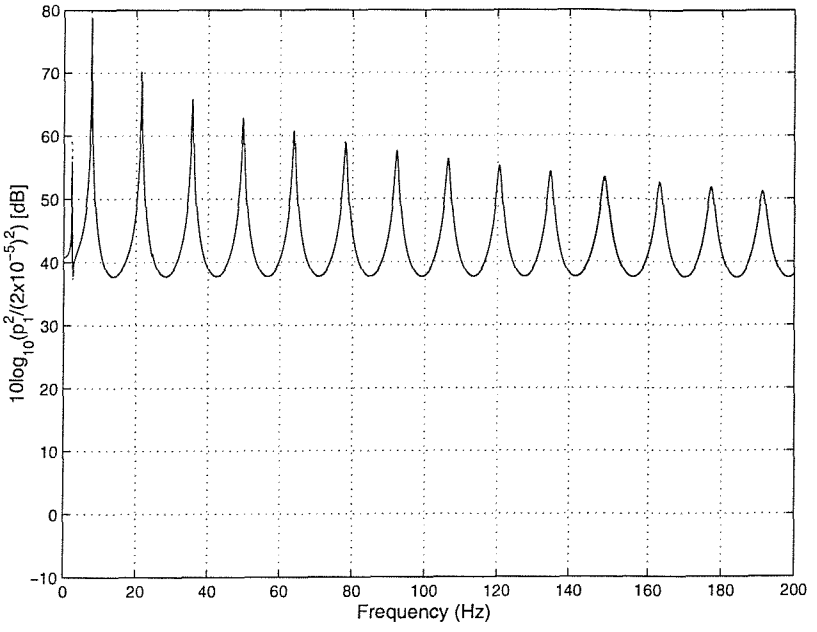

a)

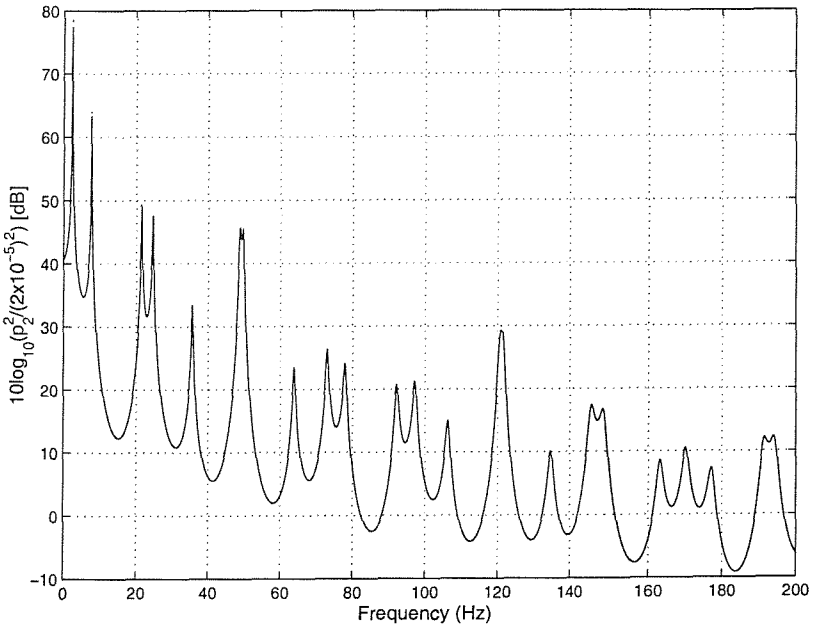

b)

Figure 5.10: Spatial-averaged mean square sound pressure for source (a) and receiving (b) volumes (in dB re $2x10^{-5}$ Pa) for Model 2. Heavy partition (ρh=78.5 kg/m^2) —— One-dimensional wave approach, ...CMS model.

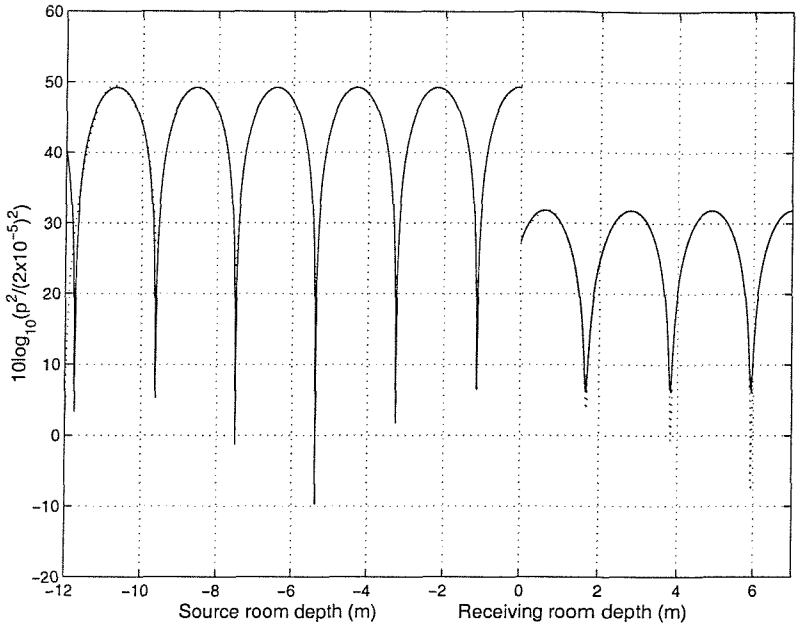

a)

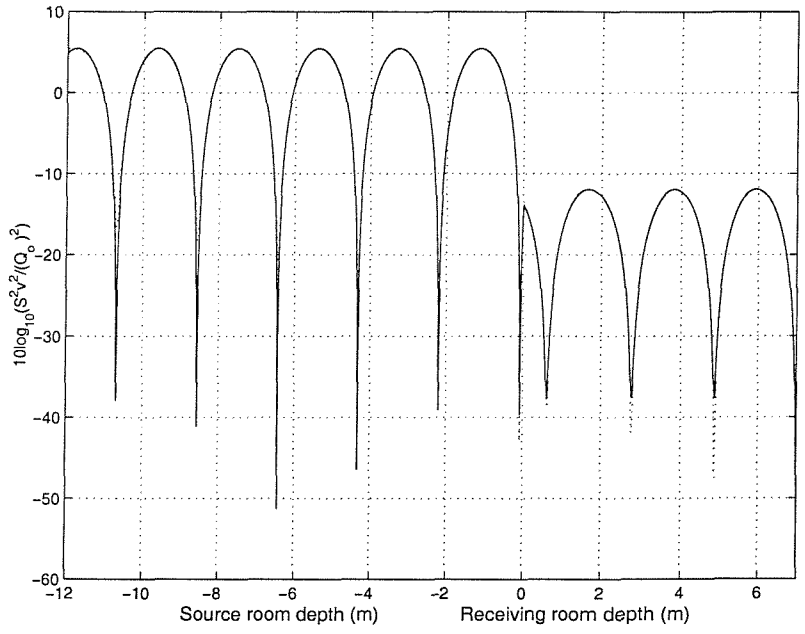

b)

Figure 5.11: The Spatial variation of mean square sound pressure (in dB re $2x10^{-5}$ Pa) (upper figure (a)) and particle velocity (normalized to Q_o/S where Q_o is the volume velocity which is equal to $3x10^{-5}$ m^3/s and S is the panel area as shown in the lower figure (b)) at 80 Hz (ρh=8.1 kg/m^2) for Model 2. ____ One-dimensional wave approach, ... CMS model.

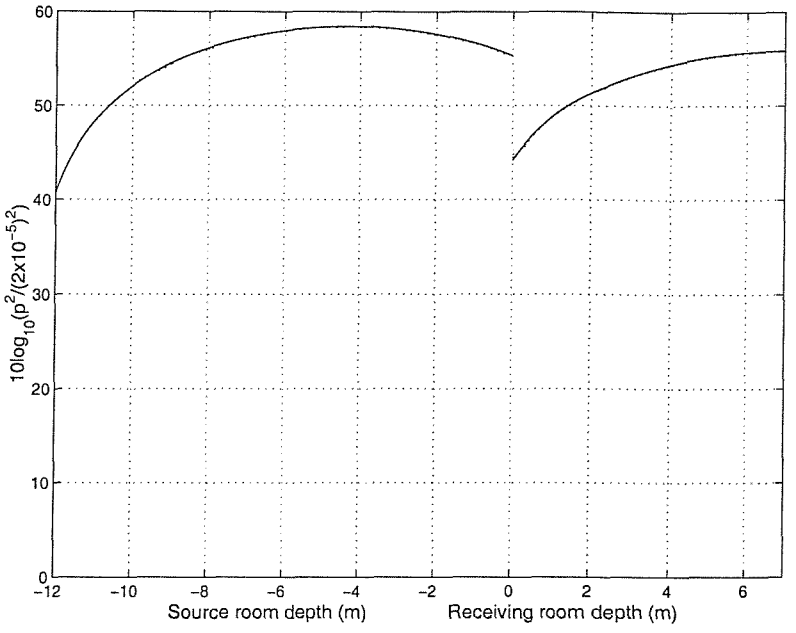

a)

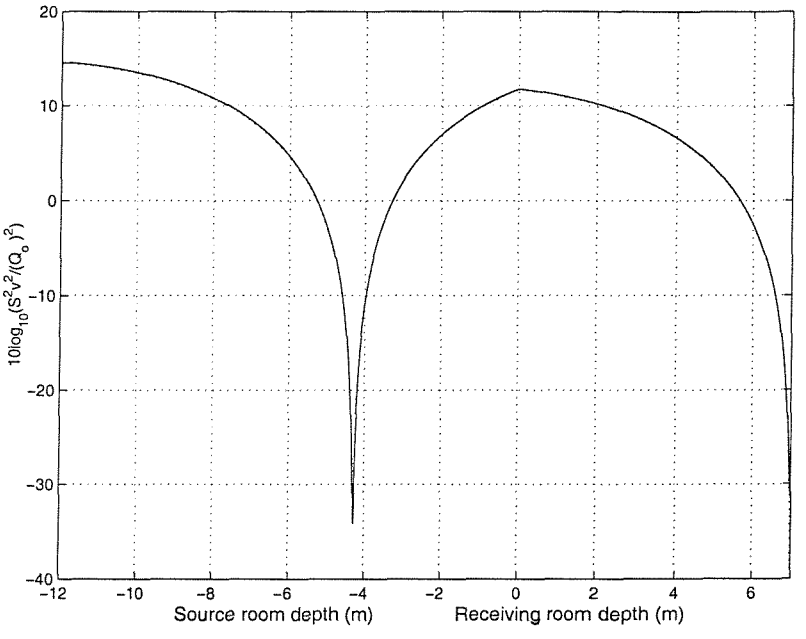

b)

Figure 5.12: The Spatial variation of mean square sound pressure (in dB re $2x10^{-5}$ Pa) (upper figure (a)) and particle velocity (normalized to Q_o/S where Q_o is the volume velocity which is equal to $3x10^{-5}$ m^3/s and S is the panel area as shown in the lower figure (b)) at 10 Hz (ρh=8.1 kg/m^2) for Model 2. ____ One-dimensional wave approach, ... CMS model.

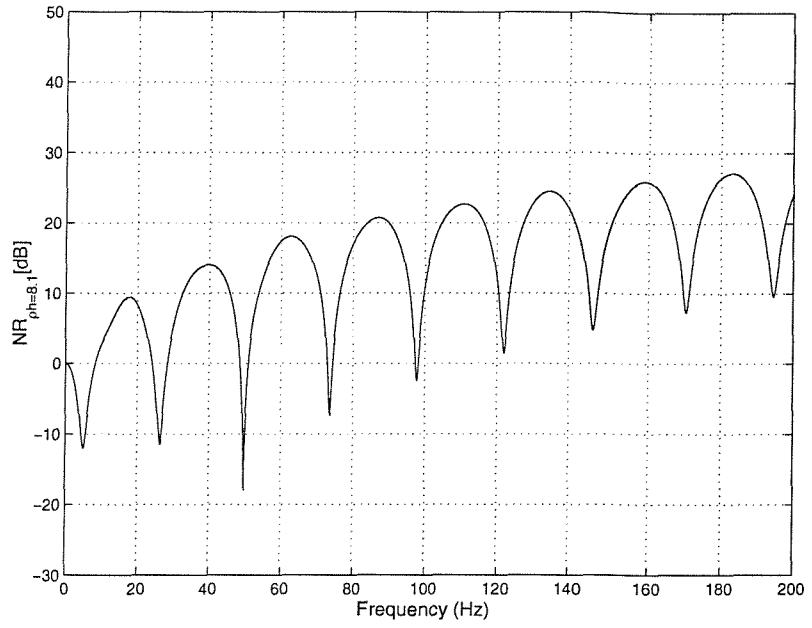

a)

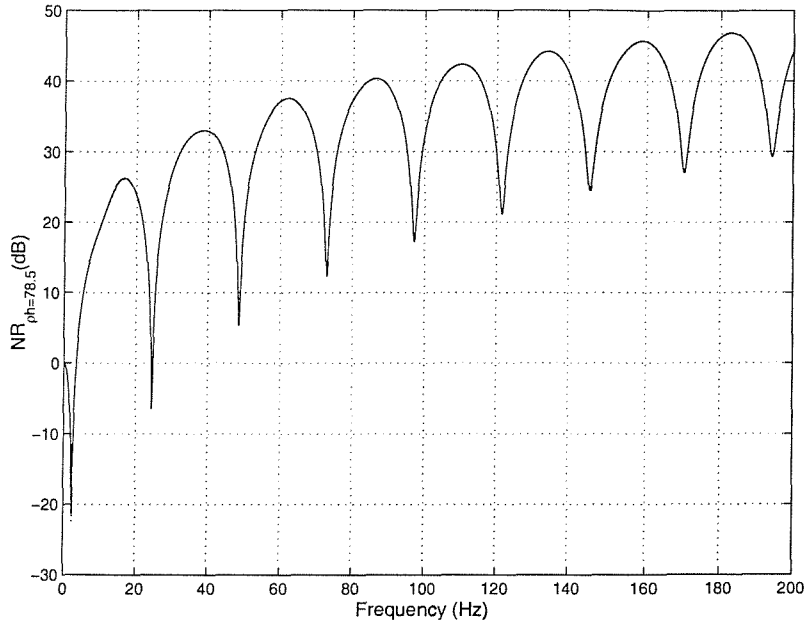

b)

Figure 5.13: Comparison of the Noise Reduction results, see equation (5.31), for two different panel mass densities (narrow bandwidth frequency) – Model 2. (a) ρh= 8.1 kg/m^2 , (b) ρh= 78.5 kg/m^2; ___One-dimensional wave approach, ...CMS model.

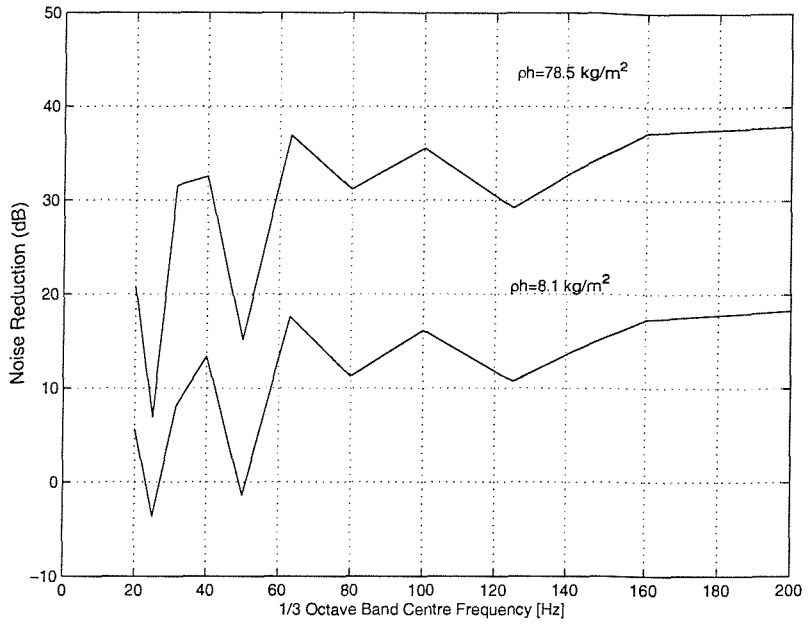

Figure 5.14: Comparison of the Noise Reduction for two different panel mass densities (in 1/3 octave bands) – Model 2. ___One-dimensional wave approach, ...CMS model.

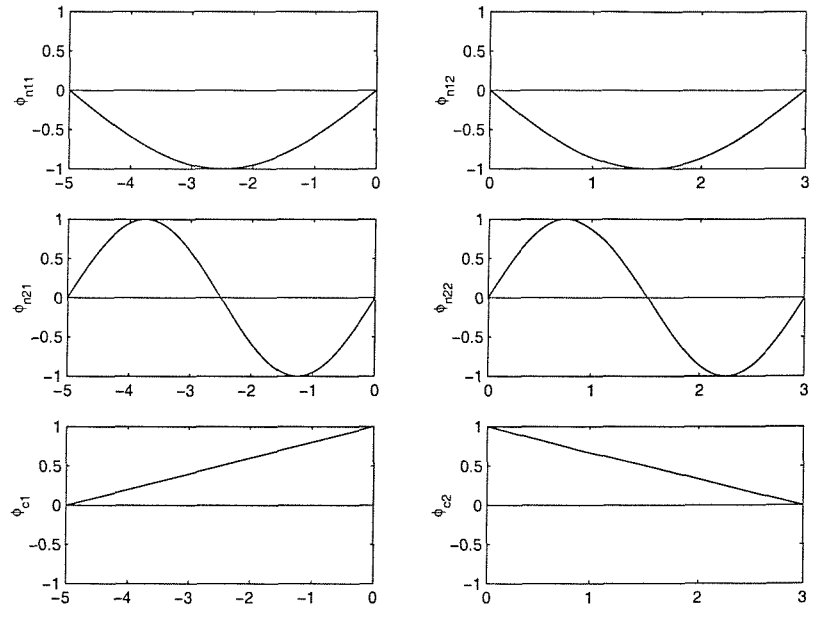

i) ii)

Figure 5.15: Set of component acoustic particle velocity modes used in Model 3 for the source (i) and receiver (ii) respectively. For instance, ϕ_{11} and ϕ_{21} represents the first two component fixed-fixed interface normal modes and ϕ_{c1} is the interface constraint mode for the source room. ϕ_{12} and ϕ_{22} are the first two component fixed-fixed modes and ϕ_{c2} is the interface mode for the receiving room.

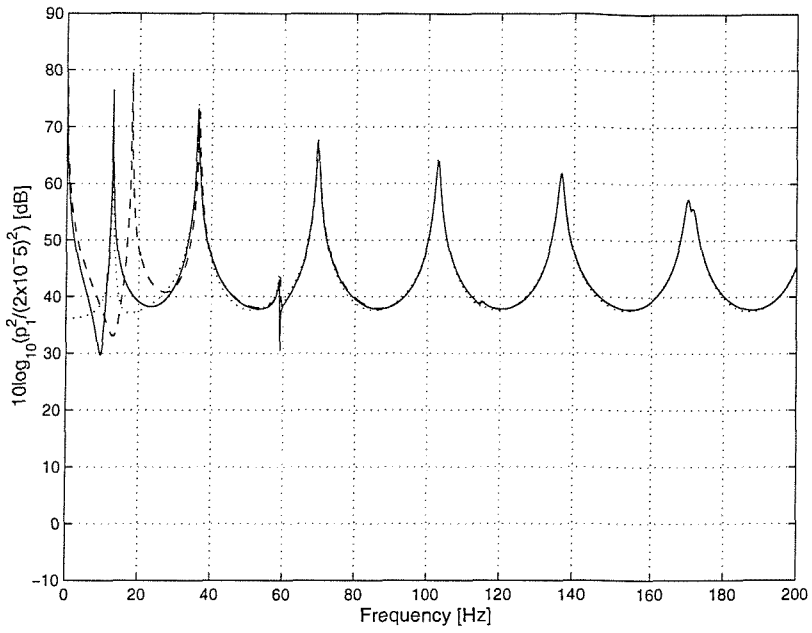

a)

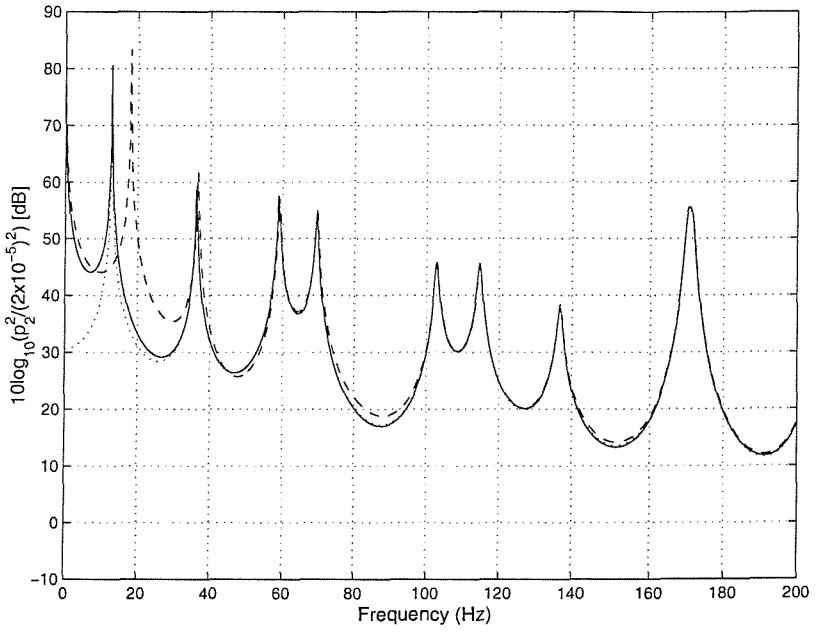

b)

Figure 5.16. Spatially averaged mean square sound pressure for the source (a) and receiving (b) volumes (in dB re $2x10^{-5}$ Pa) for Model 3. Lightweight partition (ρh=8.1 kg/m^2) ___ One-dimensional wave approach, ...CMS model and ----- Modal model.

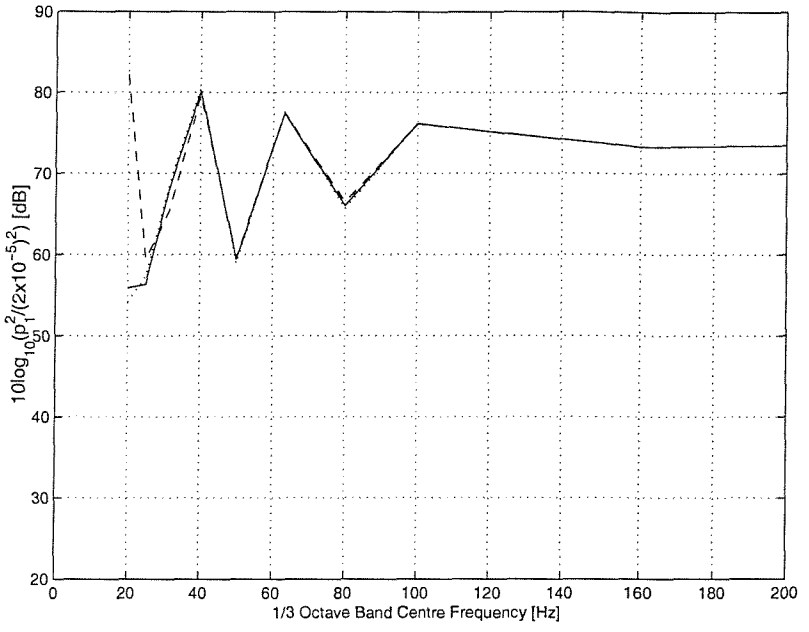

a)

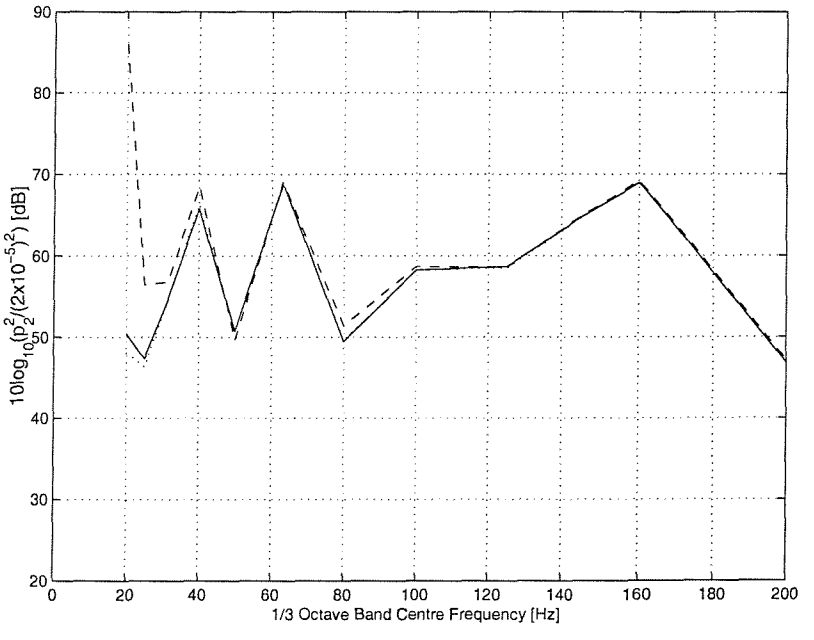

b)

Figure 5.17. Spatially averaged mean square sound pressure for the source (a) and receiving (b) volumes (in dB re $2x10^{-5}$ Pa) for Model 3 (one-third octaves). Lightweight partition (ρh=8.1 kg/m^2) ___ One-dimensional wave approach, ...CMS model and ----- Modal model.

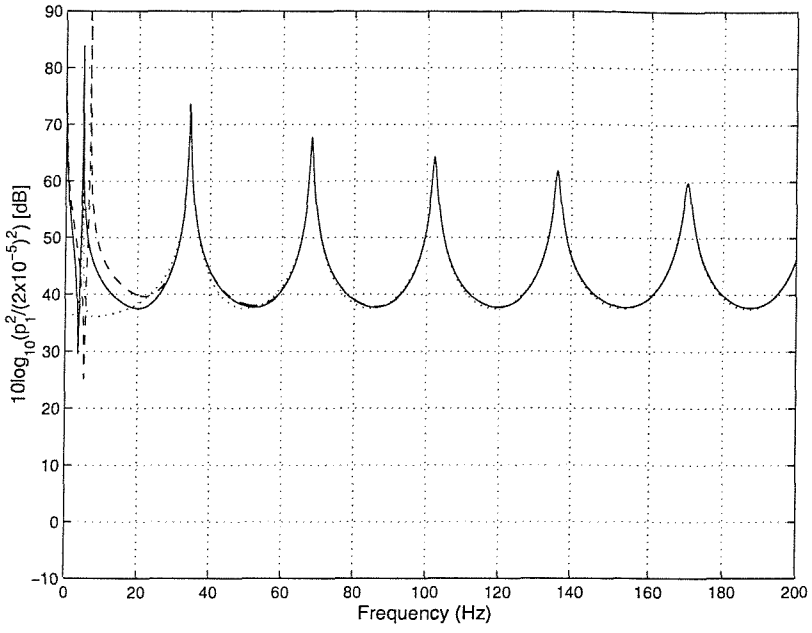

a)

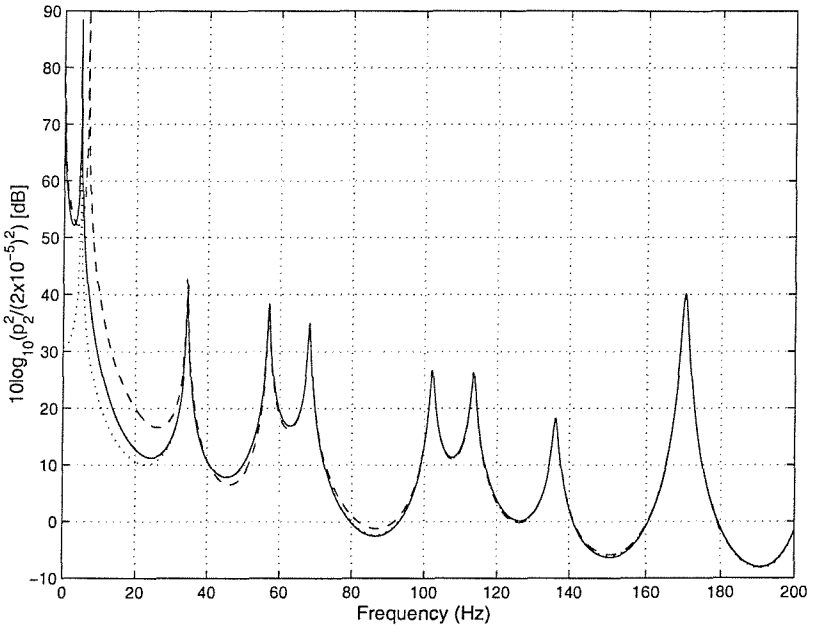

b)

Figure 5.18: Spatial-averaged mean square sound pressure for source (a) and receiving (b) volumes (in dB re $2x10^{-5}$ Pa) for Model 3. Heavy partition (ρh=78.5 kg/m^2) —— One-dimensional wave approach, ...CMS model and ----- Modal model.

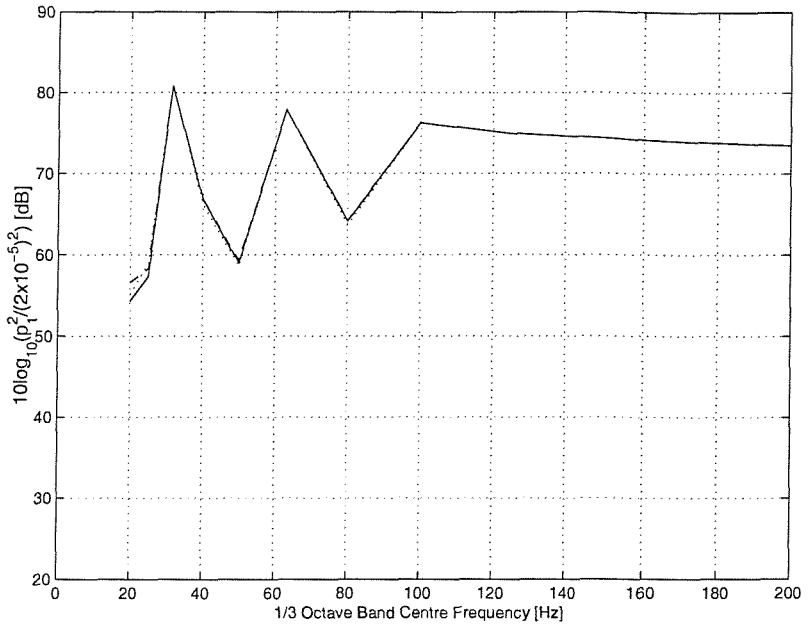

a)

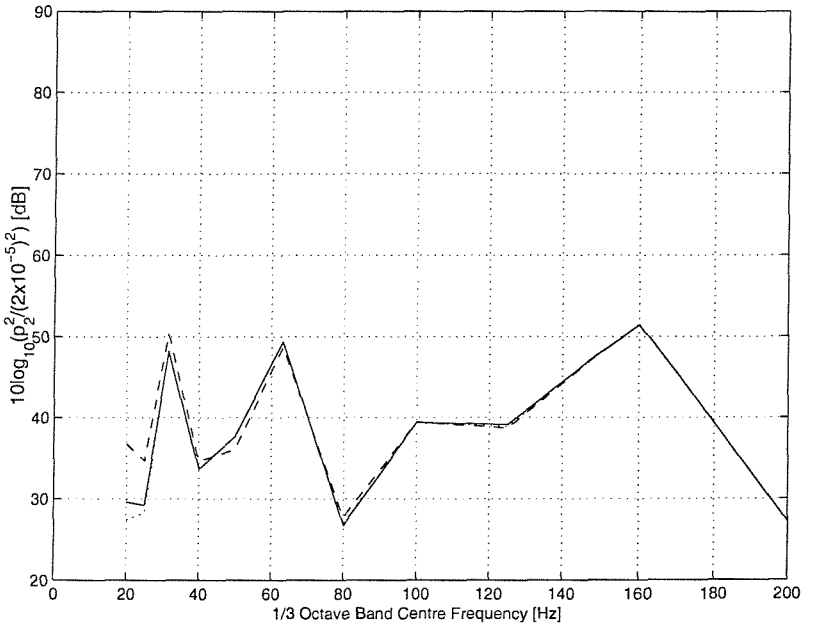

b)

Figure 5.19: Spatial-averaged mean square sound pressure for source (a) and receiving (b) volumes (in dB re $2x10^{-5}$ Pa) for Model 3 (one-third octaves). Heavy partition (ρh=78.5 kg/m^2) ___ One-dimensional wave approach, ...CMS model and ----- Modal model.

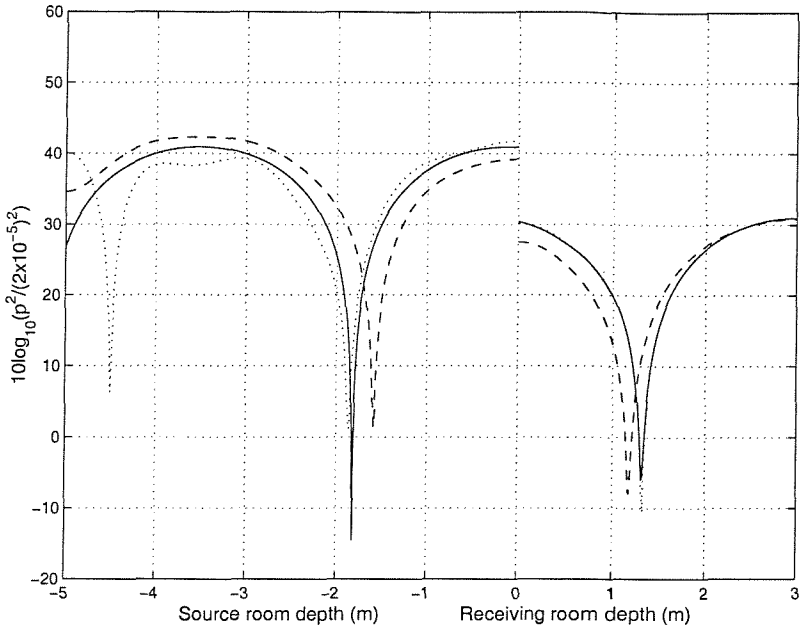

a)

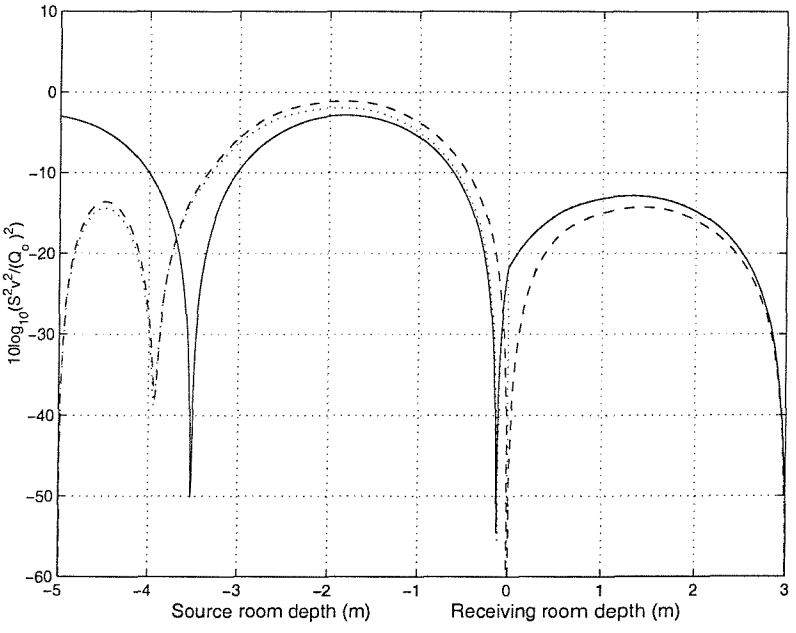

b)

Figure 5.20: The Spatial variation of mean square sound pressure (in dB re $2\text{x}10^{-5}$ Pa) (upper figure (a)) and particle velocity (normalized to Q_o/S where Q_o is the volume velocity which is equal to $3\text{x}10^{-5}$ m^3/s and S is the panel area as shown in the lower figure (b)) at 50 Hz (ρh=8.1 kg/m^2) for Model 3. ____ One-dimensional wave approach, ... CMS model and ---- Modal model.

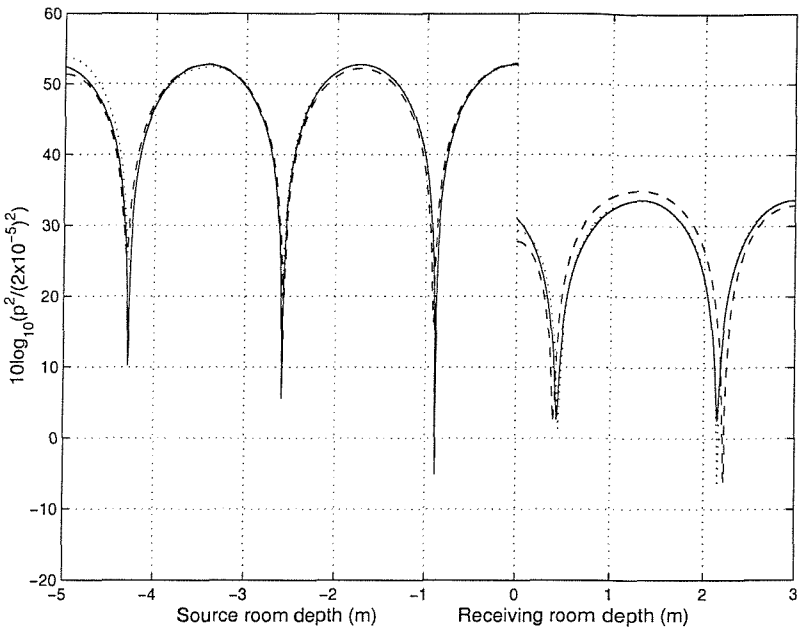

a)

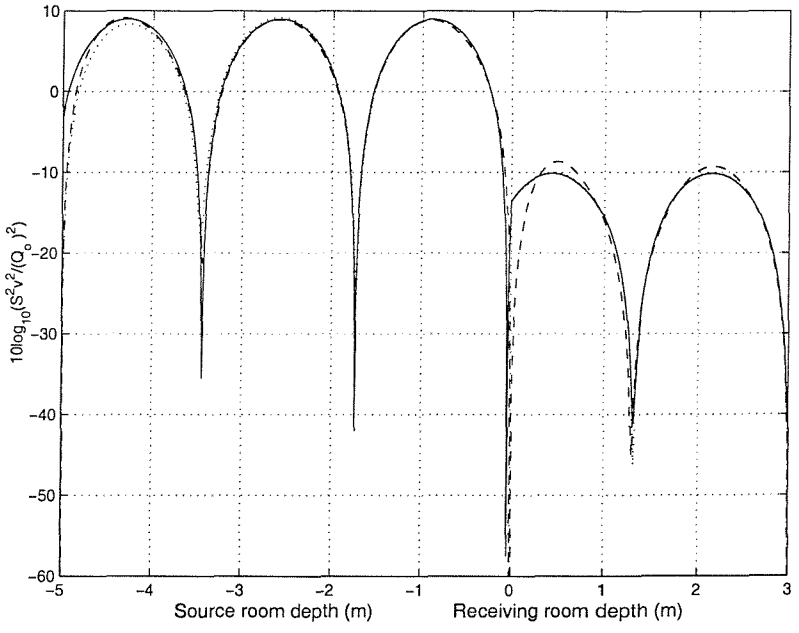

b)

Figure 5.21: The Spatial variation of mean square sound pressure (in dB re $2x10^{-5}$ Pa) (upper figure (a)) and particle velocity (normalized to Q_o/S where Q_o is the volume velocity which is equal to $3x10^{-5}$ m^3/s and S is the panel area as shown in the lower figure (b)) at 100 Hz (ρh=8.1 kg/m^2) for Model 3. ____ One-dimensional wave approach, ... CMS model and ----- Modal model.

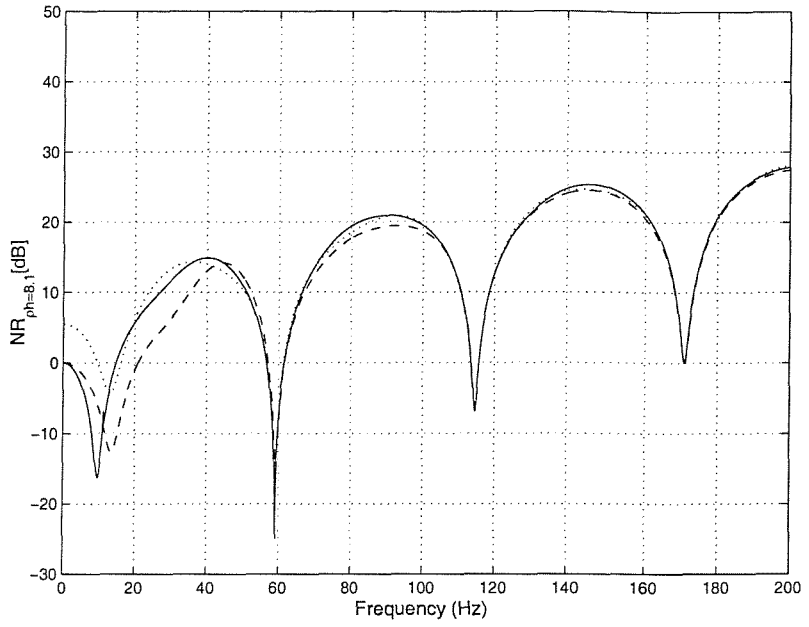

a)

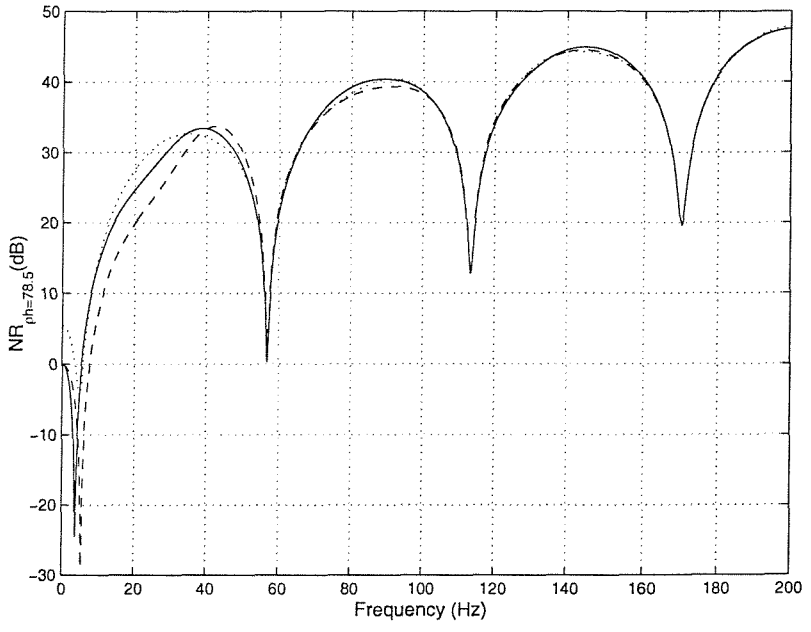

b)

Figure 5.22: Comparison of the Noise Reduction results, see equation (5.31), for two different panel mass densities (narrow bandwidth frequency) – Model 3. (a) ρh= 8.1 kg/m^2 , (b) ρh= 78.5 kg/m^2; ___One-dimensional wave approach, ... CMS model, and ---- Modal model.

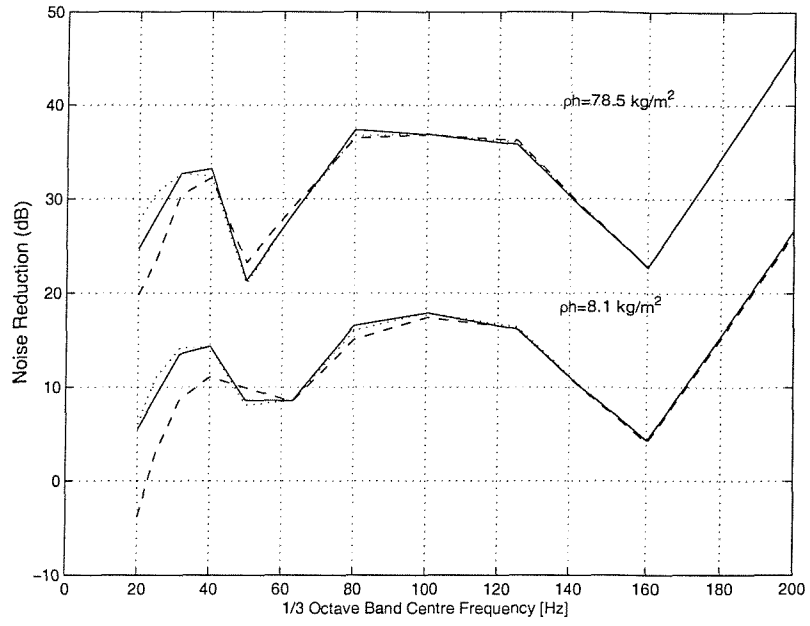

Figure 5.23: Comparison of the Noise Reduction for two different panel mass densities (1/3 octave bands) – Model 3. ___One-dimensional wave approach, ...CMS model, and ---- Modal model

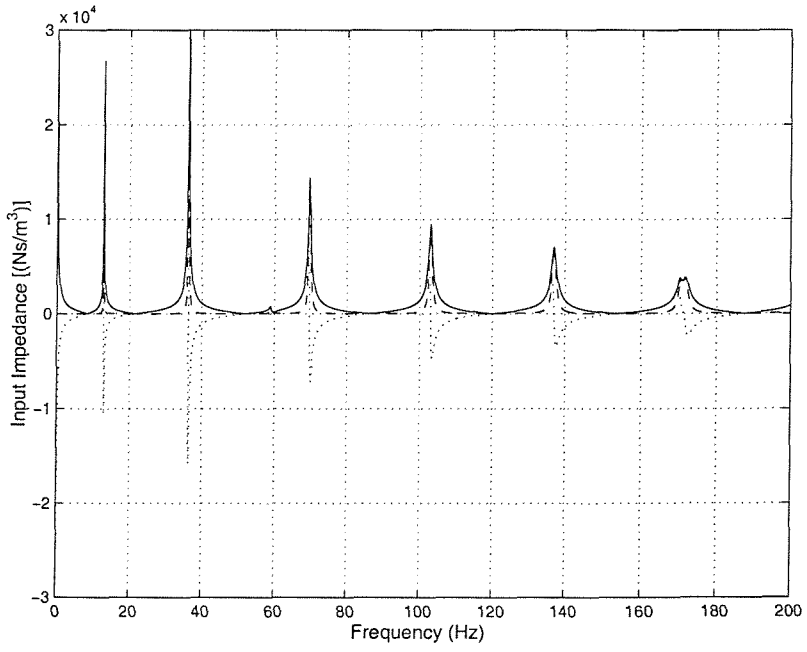

Figure 5.24: Input specific acoustic impedance for a CMS model considering force excitation and free-fixed normal modes for the source component (as used in models 1 and 2). The material properties and dimensions for this system are identical to those used in model 3. ___ magnitude, ----- real part; ..... imaginary part

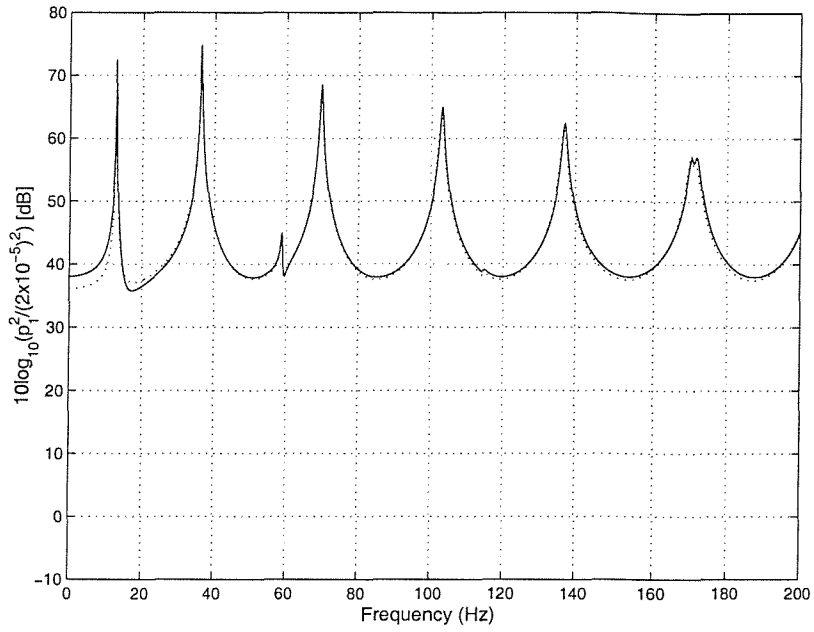

a)

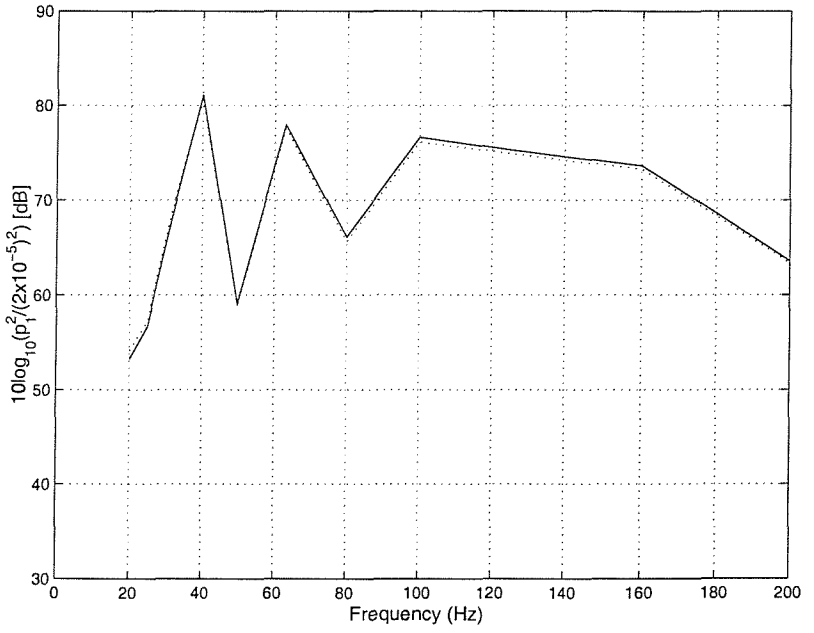

b)

Figure 5.25: Comparison of spatial-averaged mean square sound pressure for the source component (in dB re $2x10^{-5}$ Pa) between the CMS model 3 and an alternative CMS model which considers free-fixed normal modes (force excitation). a) narrow bands; b) one-third octave bands. (ρh=8.1 kg/m^2)___ CMS model using free-fixed velocity modes (force excitation), ...CMS model 3

Chapter 6

THE DEVELOPMENT OF A CMS MODEL FOR THREE DIMENSIONAL FLUID-STRUCTURE INTERACTION

6.1 – Introduction

The description, development and application of the CMS method for the one-dimensional fluid-structure interaction problem was presented in chapter 5, which can be used with some reservation on simple practical cases in engineering. On the other hand, most of the problems of sound transmission in buildings demand a three-dimensional model for better representation of the sound field distribution in acoustic spaces. In addition, the application of the 'limp' mass description is not entirely appropriate in frequency bands higher than the one which includes the fundamental resonance frequency of the partition.

The main aim of this chapter is to extend analytically the CMS model to the three-dimensional case (3D CMS model). This will be shown for simple room geometries, but in principle the same procedure can be developed when the component modes are obtained from numerical techniques, such as FE, and then applied in the described CMS methodology. The modal behaviour of rooms and partition is implemented in two steps. The first extension here is based on the one-dimensional model where the transverse acoustic modes of the rooms are incorporated into the formulation. The second extension, which is more general, considers not only the transverse acoustic modes of the rooms but also the structural modes of the partition.

The results obtained via the Modal Model predictions are then compared to the 3D CMS model. The 3D CMS model is tested and examined for the case of two coupled rooms connected by a lightweight partition. As described before, the difference between the results obtained via the experimental tests and the modal model for a lightweight partition was found to be due not only to experimental errors and limitations in the measurements, but also to the lack of kinematic continuity in the vicinity of the interface between the rooms.

In summary, the three-dimensional modal response in coupled rooms can then be analysed by application of the CMS approach. The main contents of this chapter are presented as follows.

Firstly, in section 6.2, a more general approach for the problem is presented. A CMS model is developed in terms of its acoustic components, which are separated by an elastic partition over the whole of the common wall interface. The constraint equations enforce kinematic compatibility and geometrical details. The partition is considered in terms of a series of independent modal components. The normal modes of a simply supported partition are considered here. Consequently, the constraint modes are defined in terms of geometrical coupling coefficients. Instead of using a transformation matrix technique, as described in chapter 5, the matrix description and implementation of the model are based here on the use of a Lagrange Multiplier technique [72]. This allows a more general geometry and interface to be defined.

Secondly, the numerical results of the three dimensional CMS model are presented in section 6.3 for the elastic partition case. They are compared to those obtained via the modal model and experimental tests. The discussion of the results, including the effect of the choice of modes and convergence, is also presented in section 6.3.

Finally, the summary of the main findings and conclusions are presented in section 6.4.

6.2 – The CMS Method for the 3D case – Matrix Formulation and Implementation of the Model

In this general approach, the CMS is applied to the three-dimensional case of two rooms separated by a common elastic partition. The constraint and fixed-interface normal modes for the acoustic components are used herein. In addition, the elastic partition is considered as a structural component, which is represented by its flexural normal modes. As for the one dimensional case, the implementation of the CMS method for the 3D case is also based on the selection of the sets of modes, definition of the constraint equations and system synthesis.

6.2.1 – The definition of sets of component modes

Two rigid-walled rooms with a common elastic partition at the interface were considered here as three distinct CMS components. The first one consists of the fluid volume, being

defined for $x = -L_{x1}$ to $x = 0$, $y = 0$ to $y = L_{y1}$ and $z = 0$ to $z = L_{z1}$. The second component is the receiving room, which is defined by a fluid volume varying from $x = 0$ to $x = L_{x2}$, $y = 0$ to $y = L_{y2}$ and $z = 0$ to $z = L_{z2}$. The third CMS component is a partition p defined by its flexural structural modes.

A constant volume velocity source, which undergoes harmonic oscillation, is placed in one corner of the room. It is assumed that the fluid velocity function $\dot{\varepsilon}(x,y,z,t)$ can be written in terms of generalized velocity potential $\dot{\Phi}$ (scalar quantity) by the modal transformation [74]

$$\dot{\varepsilon} = \left(\Psi_x \vec{i} + \Psi_y \vec{j} + \Psi_z \vec{k}\right)\dot{\Phi} \tag{6.1}$$

where Ψ_x, Ψ_y and Ψ_z are matrices which consist of pre-selected orthogonal normal modes plus constraint modes representing the fluid velocity distribution in the x, y and z directions respectively.

The modal matrices for the source component are given by

$$\Psi_{x1} = \left[\Psi_{n_1} \quad \Psi_{c_{x1}}\right] \tag{6.2}$$

$$\Psi_{y1} = \left[\Psi_{l_1} \quad \Psi_{c_{y1}}\right] \tag{6.3}$$

$$\Psi_{z1} = \left[\Psi_{q_1} \quad \Psi_{c_{z1}}\right] \tag{6.4}$$

where the subscript c_{x1} represents the constraint mode number; c_{y1} and c_{z1} are the modal numbers for the set of modes $\Psi_{c_{y1}}$ and $\Psi_{c_{z1}}$ respectively. The subscripts n, l, and q denote the normal mode number of a particular mode in the x, y and z directions respectively. The matrix Ψ_{x1} consists of a set of fixed-fixed interface normal modes (Ψ_{n_1}) plus a set of fixed-free constraint modes ($\Psi_{c_{x1}}$) in the x direction. The matrix Ψ_{y1} is comprised of a set of fixed-fixed interface normal modes (Ψ_{l_1}) plus another set of fixed-fixed modes ($\Psi_{c_{y1}}$) in the y direction, which is due to the contribution of the constraint modes $\Psi_{c_{x1}}$ to the fluid particle velocity in the y direction. Likewise, matrix Ψ_{z1} consists of a set of fixed-fixed interface normal modes (Ψ_{q_1}) plus the set of modes $\Psi_{c_{z1}}$, which is due to the contribution of the constraint modes $\Psi_{c_{x1}}$ to the fluid particle

velocity in the z direction. Although the set of constraint modes $\Psi_{c_{x1}}$ contributes to the fluid particle velocity distribution in both y and z directions, there is no need to have any other set of constraint modes. This is justified by the fact that the interface between components is only in the constant plane x = 0. The selected orthogonal normal and constraint modes were defined as shape functions satisfying the geometric boundary conditions for each acoustic component.

By application of the well-known relationship between velocity potential and particle velocity [5], the normal modes Ψ_{n_1} (in the x direction) and their contributions to the fluid particle velocity in the y and z directions (Ψ_{l_1} and Ψ_{q_1}) can be expressed by

$$\Psi_{n_1}(x,y,z,t) = -k_{n_1}\sin(k_{n_1}x)\cos(k_{l_1}y)\cos(k_{q_1}z) \quad \text{for } -L_{x_1} \le x \le 0 \tag{6.5}$$

$$\Psi_{l_1}(x,y,z,t) = -k_{l_1}\cos(k_{n_1}x)\sin(k_{l_1}y)\cos(k_{q_1}z) \text{ for } 0 \le y \le L_{y_1} \tag{6.6}$$

$$\Psi_{q_1}(x,y,z,t) = -k_{q_1}\cos(k_{n_1}x)\cos(k_{l_1}y)\sin(k_{q_1}z) \quad \text{for } 0 \le z \le L_{z_1} \tag{6.7}$$

where k_{n_1}, k_{l_1} and k_{q_1} are equal to $n_1\pi\, x/(L_{x1})$, $l_1\pi\, y/L_{y1}$ and $q_1\pi\, z/L_{z1}$ respectively.

An additional set of constraint modes Ψ_c, which satisfies zero velocity on x = -L_{x1} and unit velocity on x = 0 over the partition area is used for the source room. The elastic partition can either cover the whole of the common boundary (x = 0) or only part of the common interface. For the source room component, the constraint modes $\Psi_{c_{x1}}$ (in the x direction) and their contributions to the fluid particle velocity in the y and z directions ($\Psi_{c_{y1}}$ and $\Psi_{c_{z1}}$) are then given by

$$\Psi_{c_{x1}}(x,y,z,t) = \left(1+\frac{x}{L_{x1}}\right)\cos(k_{c_{y1}}y)\cos(k_{c_{z1}}z) \tag{6.8}$$

$$\Psi_{c_{y1}}(x,y,z,t) = -\left(1+\frac{x}{L_{x1}}\right)k_{c_{y1}}\sin(k_{c_{y1}}y)\cos(k_{c_{z1}}z) \tag{6.9}$$

$$\Psi_{c_{z1}}(x,y,z,t) = -\left(1+\frac{x}{L_{x1}}\right)k_{c_{z1}}\cos(k_{c_{y1}}y)\sin(k_{c_{z1}}z) \tag{6.10}$$

where $k_{c_{y1}}$ and $k_{c_{z1}}$ are equal to $c_{y1}\pi / L_{y1}$ and $c_{z1}\pi / L_{z1}$ respectively. Equations (6.8)-(6.10) apply over the area of the partition, even if it might only cover a partial area of the whole interface (common wall).

According to equation (6.8), it is observed that the number of constraint modes $\Psi_{c_{x1}}$ is directly related to the number of different modal orders c_{y1} and/or c_{z1}. In addition, a linear function was chosen to represent the particle velocity distribution in the x direction, as higher order functions did not provide better convergence.

As the particle velocity of a fluid is defined by the first order derivative of its velocity potential a sine function appears in equations (6.9) and (6.10), which represent the *constraint* modes velocity contributions in the y and z directions respectively.

Additionally, it is assumed that the set of normal structural modes ϕ_p results from the free flexural vibration of a simply supported rectangular thin plate (see Equations (C.2) and (C.12)). The derivation of the dynamic properties and the equation of motion for the structural component can be found in Appendix C. No constraint modes are necessary for the structural component.

The modal matrices for the receiving component can be expressed as

$$\Psi_{x2} = \left[\Psi_{n_2} \quad \Psi_{c_{x2}}\right] \tag{6.11}$$

$$\Psi_{y2} = \left[\Psi_{l_2} \quad \Psi_{c_{y2}}\right] \tag{6.12}$$

$$\Psi_{z2} = \left[\Psi_{q_2} \quad \Psi_{c_{z2}}\right] \tag{6.13}$$

The matrix Ψ_{x2} comprises of a set of fixed-fixed interface normal modes (Ψ_{n_2}) plus a set of free-fixed constraint modes ($\Psi_{c_{x2}}$) in the x direction. The matrix Ψ_{y2} is composed of a set of fixed-fixed interface normal modes (Ψ_{l_2}) plus another set of fixed-fixed modes ($\Psi_{c_{y2}}$) in the y direction, which is due to the contribution of the constraint modes $\Psi_{c_{x2}}$ to the fluid particle velocity in the y direction. In the same way, matrix Ψ_{z2} comprises a set of fixed-fixed interface normal modes (Ψ_{q_2}) plus a set of modes $\Psi_{c_{z2}}$, which is due to the contribution of the constraint modes $\Psi_{c_{x2}}$ to the fluid particle

velocity distribution in the z direction. As for the source room, the set of free-fixed constraint modes $\Psi_{c_{x2}}$ is sufficient for the formulation of the problem.

Additionally, the (x,y,z) particle velocity Cartesian components for the receiving room are given respectively by

$$\Psi_{n_2}(x,y,z,t) = -k_{n_2}\sin(k_{n_2}x)\cos(k_{l_2}y)\cos(k_{q_2}z) \text{ for } 0 \le x \le L_{x_2} \tag{6.14}$$

$$\Psi_{l_2}(x,y,z,t) = -k_{l_2}\cos(k_{n_2}x)\sin(k_{l_2}y)\cos(k_{q_2}z) \text{ for } 0 \le y \le L_{y_2} \tag{6.15}$$

$$\Psi_{q_2}(x,y,z,t) = -k_{q_2}\cos(k_{n_2}x)\cos(k_{l_2}y)\sin(k_{q_2}z) \text{ for } 0 \le z \le L_{z_2} \tag{6.16}$$

where k_{n_2}, k_{l_2} and k_{q_2} are equal to $n_2\pi\, x/L_{x2}$, $l_2\pi\, y/L_{y2}$ and $q_2\pi\, z/L_{z2}$ respectively.

The constraint modes c_2 in the x, y, and z directions have velocity components then given by

$$\Psi_{c_{x2}}(x,y,z,t) = \left(1-\frac{x}{L_{x2}}\right)\cos(k_{c_{y2}}y)\cos(k_{c_{z2}}z) \tag{6.17}$$

$$\Psi_{c_{y2}}(x,y,z,t) = -\left(1-\frac{x}{L_{x2}}\right)k_{c_{y2}}\sin(k_{c_{y2}}y)\cos(k_{c_{z2}}z) \tag{6.18}$$

$$\Psi_{c_{z2}}(x,y,z,t) = -\left(1-\frac{x}{L_{x2}}\right)k_{c_{z2}}\cos(k_{c_{y2}}y)\sin(k_{c_{z2}}z) \tag{6.19}$$

where $k_{c_{y2}}$ and $k_{c_{z2}}$ are equal to $c_{y2}\pi\, y/L_{y2}$ and $c_{z2}\pi\, z/L_{z2}$ respectively.

6.2.2 – Constraint Equations

Although the fluid particle velocity is considered in all directions (see equation (6.1)), for calculating the dynamic response of the acoustic components 1 and 2 the compatibility equations describing velocity continuity were only formulated in terms for the x direction normal to the partition or interface. In other words, although the fluid velocity function is equal to $\dot{\varepsilon} = (\dot{\varepsilon}_x, \dot{\varepsilon}_y, \dot{\varepsilon}_z)$, one only needs $\dot{\varepsilon}_x$ for the formulation of the constraint equations at the interface. When the structural partition is considered as an extra modal system, the compatibility equations are given by

$$C_1 = \int_S \left(\left(\frac{\partial \varepsilon_{x,1}}{\partial t} \right)\Big|_{x=0} - \left(\frac{\partial w}{\partial t} \right)\Big|_{x=0} \right)^2 dS = \int_S \left(\left(\dot{\varepsilon}_{x,1} \right)_{x=0} - \left(\dot{w} \right)_{x=0} \right)^2 dS = 0 \tag{6.20}$$

$$C_2 = \int_S \left(\left(\frac{\partial \varepsilon_{x,2}}{\partial t} \right)\Big|_{x=0} - \left(\frac{\partial w}{\partial t} \right)\Big|_{x=0} \right)^2 dS = \int_S \left(\left(\dot{\varepsilon}_{x,2} \right)_{x=0} - \left(\dot{w} \right)_{x=0} \right)^2 dS = 0 \tag{6.21}$$

where $\varepsilon_{x,1}$ and $\varepsilon_{x,2}$ are the fluid particle displacement in the x direction for components 1 and 2 respectively, w is the normal displacement of the partition (in the x direction) due to its flexural elastic deformation (see Appendix C) and S is the surface area of the partition. These equations relate to the velocity continuity between the source room and partition and receiving room and partition respectively. Thus, they are used to determine a reduced set of generalized coordinates equal to the difference between the number of component coordinates and the number of constraint equations.

As mentioned previously equations (6.8) to (6.10) can also be used for a partition covering only part of the boundary. In this situation the integrals in the constraint equations are evaluated only on the partition area.

It is implicit in equations (6.20) and (6.21) that the same reference coordinate is used for all components. Using the Least Squares Method to minimize the functions C_1 and C_2, and considering equation (6.1), the following matrix form can be obtained as

$$\frac{\partial C_1}{\partial \dot{\varepsilon}_{x,1}} = \frac{\partial C_1}{\partial \dot{w}_p} = \frac{\partial C_2}{\partial \dot{\varepsilon}_{x,2}} = \frac{\partial C_2}{\partial \dot{w}_p} = 0 \tag{6.22}$$

$$\text{or } R_c \overline{G} = 0$$

$$\text{where } \overline{G} = \left[\dot{\Phi}_{n1} \quad \dot{\Phi}_{c1} \vdots \quad \dot{w}_p \quad \vdots \dot{\Phi}_{n2} \quad \dot{\Phi}_{c2} \right]^T \text{ and } R_c = \left[R_1 \vdots R_p \vdots R_2 \right] \tag{6.23}$$

$$\text{and} \quad R_1 = \begin{bmatrix} 0 & R_{11} \\ 0 & R_{1p}^T \\ 0 & 0 \\ 0 & 0 \end{bmatrix}; \; R_p = \begin{bmatrix} -R_{1p} \\ -R_{pp} \\ -R_{pp} \\ -R_{2p} \end{bmatrix}; \; R_2 = \begin{bmatrix} 0 & 0 \\ 0 & 0 \\ 0 & R_{2p}^T \\ 0 & R_{22} \end{bmatrix} \tag{6.24}$$

The column vector $\overline{G}$ and the matrix R_c contain the system generalized coordinates and the geometrical coupling coefficients respectively.

The sub-matrices R_{11}, R_{1p}, R_{pp}, R_{2p} and R_{22} defining the geometrical coupling are given by

$$R_{11} = \int_S \left(\Psi_{c_{x1}}\right)^T \left(\Psi_{c_{x1}}\right) dS \tag{6.25}$$

$$R_{1p} = \int_S \left(\Psi_{c_{x1}}\right)^T \phi_p dS \tag{6.26}$$

$$R_{pp} = \int_S \phi_p^T \phi_p \, dS \tag{6.27}$$

$$R_{2p} = \int_S \left(\Psi_{c_{x2}}\right)^T \phi_p dS \tag{6.28}$$

$$R_{22} = \int_S \left(\Psi_{c_{x2}}\right)^T \left(\Psi_{c_{x2}}\right) dS \tag{6.29}$$

where the structural modal matrix ϕ_p is defined in equation (C.12) and the acoustic modal matrices Ψ_{x1} and Ψ_{x2} are defined in equations (6.2) and (6.11) respectively. S is the surface area of the structural partition.

No terms exist in coupling between the normal modes of the room (Ψ_{n_1} or Ψ_{n_2}) and the partition modes (ϕ_p), as the former have zero velocity at the interface ($x = 0$). The matrix R_{pp} is also a diagonal matrix due to orthogonality for the structural modes.

6.2.3 – Derivation of the General Dynamic Properties of the CMS acoustic components

In this sub-section the dynamic properties of an acoustic component driven by a volume velocity source are derived using the direct application of Lagrange's equations [69]. Therefore, the use of scalar quantities, which are the potential and kinetic energies, is necessary to employ these equations. The kinetic energy T_A for an acoustic volume V_1 can be expressed as [74]

$$T_A = \frac{1}{2} \rho_o \int_{V_1} \left((\dot{\varepsilon})^*\right)^T (\dot{\varepsilon}) \, dV \tag{6.30}$$

Substituting equation (6.1) into equation (6.30), the expression for the total kinetic energy using all of the modes employed in the formulation then becomes

$$T_A = \frac{1}{2}(\dot{\overline{\Phi}}^T)^* \rho_o \left\{ \int_{V_1} \left((\Psi_x)^T \Psi_x\right) dV_1 + \int_{V_1} \left((\Psi_y)^T \Psi_y\right) dV_1 + \int_{V_1} \left((\Psi_z)^T \Psi_z\right) dV \right\} (\dot{\overline{\Phi}}) \tag{6.31}$$

The potential energy of a fluid inside a volume V_1 is defined in terms of a velocity potential function $\dot{\Phi}$ as [74]

$$V_A = \frac{1}{2} \int_{V_1} \left(\kappa \rho_o^2 \frac{\partial (\dot{\Phi}^T)^*}{\partial t} \frac{\partial \dot{\Phi}}{\partial t} \right) dV_1 \tag{6.32}$$

where $\kappa = \dfrac{1}{\rho_o c_o^2}$ is the compressibility of the fluid (6.33)

Using the relationship between sound pressure and velocity potential [74], the potential energy can then be expressed in terms of pressure as

$$V_A = \frac{1}{2} \int_{V_1} \left(\kappa \left(p^*\right)^T p \right) dV_1 \tag{6.34}$$

By assuming that the acoustic disturbances in each component are sufficiently small, a linear relationship between pressure and the rate of change of the displacement of the fluid $\varepsilon(x, y, z, t)$ can be written as [74]

$$p = \frac{1}{\kappa} div(\varepsilon) \tag{6.35}$$

and

$$div(\varepsilon) = \left(\frac{\partial \Psi_x}{\partial x} + \frac{\partial \Psi_y}{\partial y} + \frac{\partial \Psi_z}{\partial z} \right) \overline{\Phi} \tag{6.36}$$

where κ is defined in equation (6.33) and $\overline{\Phi}$ is the displacement potential of the fluid.

Therefore, substituting equation (6.35) and (6.36) into equation (6.34), the expression for potential energy becomes

$$V_A = \frac{1}{2\kappa} (\overline{\Phi}^T)^* \left\{ \int_{V_1} \left(\frac{\partial (\Psi_x)^T}{\partial x} \frac{\partial \Psi_x}{\partial x} \right) dV_1 + \int_{V_1} \left(\frac{\partial (\Psi_y)^T}{\partial y} \frac{\partial \Psi_y}{\partial y} \right) dV_1 + \int_{V_1} \left(\frac{\partial (\Psi_z)^T}{\partial z} \frac{\partial \Psi_z}{\partial z} \right) dV_1 \right\} (\overline{\Phi}) \tag{6.37}$$

For non-conservative systems, a dissipation function [75, 76] must be included. For an acoustic component, it can be expressed as

$$D=\frac{1}{2}(\dot{\overline{\Phi}}^T)^*\rho_o\left\{\int_{V_1}\left((\Psi_x)^T 2\omega_N\zeta_N\Psi_x\right)dV_1+\int_{V_1}\left((\Psi_y)^T 2\omega_N\zeta_N\Psi_y\right)dV_1+\right.$$

$$\left.\int_{V_1}\left((\Psi_z)^T 2\omega_N\zeta_N\Psi_z\right)dV_1\right\}\dot{\overline{\Phi}} \tag{6.38}$$

where ζ_N is the modal damping ratio matrix for the components and ω_N is the modal matrix of natural frequencies. The damping matrix can then be derived from the above expression. It is seen that linear viscous damping was adopted for the purpose of simplification. This is a reasonable choice for highly reverberant acoustic spaces [5].

The system equations of motion can be obtained for a damped system by using Lagrange's equation of motion [69] as follows

$$\frac{\partial}{\partial t}\left(\frac{\partial L}{\partial \dot{q}_i}\right)-\frac{\partial L}{\partial q_i}+\frac{\partial D}{\partial \dot{q}_i}=Q_i \qquad i = 1, 2, \ldots n \tag{6.39}$$

where L is Lagrangian for the system of coupled components described below, D is the damping dissipation function and q_i are the elements of the generalized coordinate $\overline{\Phi}$. In addition, it is assumed that the modes are real. Q_i is the time-dependent generalized volume velocity source strength in the case of a source within an acoustic volume or generalized force for a general system. The Lagrangian is defined by [72]

$$L=T_A-V_A+\lambda^T R_c\overline{G} \tag{6.40}$$

where λ is a Lagrange multiplier vector which enforces interface compatibility.

For instance, the dynamic properties of a separate acoustic component 1 may be determined via Lagrange's equations (6.39), which lead to the following equation of motion

$$M_1^{3D}\ddot{\overline{\Phi}}_1+C_1^{3D}\dot{\overline{\Phi}}_1+K_1^{3D}\overline{\Phi}_1-(R_1)^T\lambda_1=Q_1^{3D} \tag{6.41}$$

where $M_1^{3D}=\rho_o\left\{\int_{V_1}\left((\Psi_{x1})^T\Psi_{x1}\right)dV_1+\int_{V_1}\left((\Psi_{y1})^T\Psi_{y1}\right)dV_1+\int_{V_1}\left((\Psi_{z1})^T\Psi_{z1}\right)dV_1\right\}$ (6.42)

$$K_1^{3D}=\rho_o c_o^2\int_{V_1}\left(\frac{\partial(\Psi_{x1})^T}{\partial x}\frac{\partial\Psi_{x1}}{\partial x}\right)dV_1+\int_{V_1}\left(\frac{\partial(\Psi_{y1})^T}{\partial y}\frac{\partial\Psi_{y1}}{\partial y}\right)dV_1+\int_{V_1}\left(\frac{\partial(\Psi_{z1})^T}{\partial z}\frac{\partial\Psi_{z1}}{\partial z}\right)dV_1 \tag{6.43}$$

$$C_1^{3D} = 2\omega_N \rho \left\{ \int_{V_1} \left((\Psi_{x1})^T \zeta_N \Psi_{x1} \right) dV_1 + \int_{V_1} \left((\Psi_{y1})^T \zeta_N \Psi_{y1} \right) dV_1 + \int_{V_1} \left((\Psi_{z1})^T \zeta_N \Psi_{z1} \right) dV_1 \right\} \tag{6.44}$$

$$Q_1^{3D} = j\omega \rho_o Q_o \int \Psi_{x1} \delta_o (x - x_o, y - y_o, z - z_o) dx \tag{6.45}$$

where $\delta_o(x-x_o, y-y_o, z-z_o)$ is the three-dimensional Dirac delta function representing a point volume velocity source at (x_o, y_o, z_o), and M_1^{3D}, K_1^{3D}, and C_1^{3D} are scalar quantities representing the modal mass, stiffness and damping matrices for the fluid volume respectively. Q_1^{3D} is the column matrix of generalized volume velocity source strength where the individual terms relate to the excitation of individual model components. R_1 is the matrix defined in equation (6.23). λ_1 is a column vector with a number of rows equal to the total number of constraint modes in component 1 plus the total number of constraint modes in component 2.

As a consequence of classifying the modes into two categories, namely constraint modes and normal modes, the mass, stiffness and damping matrices are partitioned into sub-matrices as follows

$$M_1^{3D} = \begin{bmatrix} m_{NN} & m_{NC} \\ m_{NC}^T & m_{CC} \end{bmatrix}; \; K_1^{3D} = \begin{bmatrix} k_{NN} & k_{NC} \\ k_{NC}^T & k_{CC} \end{bmatrix}; \; C_1^{3D} = \begin{bmatrix} c_{NN} & c_{NC} \\ c_{NC}^T & c_{CC} \end{bmatrix}; \tag{6.46}$$

The sub-matrix m_{NN}, k_{NN} and c_{NN} are diagonal matrices. This is true due to the orthogonality property of the natural component modes. The order of these matrices depends upon the number of modes chosen for the analysis. On the other hand, the sub-matrices m_{CC}, k_{CC} and c_{CC} are square matrices associated with the constraint modes; their orders are equal to the number of constraints. Finally, the rectangular matrices m_{NC}, k_{NC} and c_{NC} are associated with the coupling between the normal and constraint modes, as these are not generally orthogonal and cross-terms exist in the potential and kinetic energy expressions as well as in the dissipation function.

6.2.4 –System Synthesis

The equations of motion for the source room (acoustic component 1), the structural partition (component p) and the receiving room (acoustic component 2) are expressed in terms of their generalized coordinates $\overline{\Phi}$ as

$$M_1^{3D}\ddot{\overline{\Phi}}_1 + C_1^{3D}\dot{\overline{\Phi}}_1 + K_1^{3D}\overline{\Phi}_1 - R_1^T\lambda_1 = Q_1^{3D} \tag{6.47}$$

$$M_p\ddot{w}_p + C_p\dot{w}_p + K_p w_p - R_p^T\lambda_p = 0 \tag{6.48}$$

$$M_2^{3D}\ddot{\overline{\Phi}}_2 + C_2^{3D}\dot{\overline{\Phi}}_2 + K_2^{3D}\overline{\Phi}_2 - R_2^T\lambda_2 = 0 \tag{6.49}$$

where λ_1, λ_p and λ_2 are column vectors of Lagrange multipliers for components 1, p and 2 respectively. The set of equations presented above as well as the dynamic properties of the acoustic components M^{3D}, C^{3D}, and K^{3D} and the generalized volume velocity source strength Q^{3D} can all be derived as shown in subsection 6.2.3 using Lagrange's equations of motion. The dynamic properties of the structural component (M_p, C_p and K_p) are derived in detail in Appendix C.

The coupled set of equations for the entire system is then given by

$$\mu\ddot{\overline{G}} + \varsigma\dot{\overline{G}} + \chi\overline{G} - \lambda R_c = Q_s \tag{6.50}$$

and

$$R_c\overline{G} = 0 \tag{6.51}$$

where

$$\lambda = \begin{Bmatrix}\lambda_1\\ \lambda_p\\ \lambda_2\end{Bmatrix};\ \mu = \begin{bmatrix}M_1^{3D} & 0 & 0\\ 0 & M_p & 0\\ 0 & 0 & M_2^{3D}\end{bmatrix};\ \varsigma = \begin{bmatrix}C_1^{3D} & 0 & 0\\ 0 & C_p & 0\\ 0 & 0 & C_2^{3D}\end{bmatrix};\ \chi = \begin{bmatrix}K_1^{3D} & 0 & 0\\ 0 & K_p & 0\\ 0 & 0 & K_2^{3D}\end{bmatrix};$$

and $Q_s = \begin{bmatrix}Q_1^{3D} & 0 & 0\end{bmatrix}^T$. The matrices μ, ς and χ are the modal mass, damping and stiffness matrices respectively. Q_s is the column vector containing the generalized 'forces' exerted on the components. It can also be shown that the coordinates $\overline{G}$ are not linearly independent in the set of equations (6.50), due to the constraint equations (6.51).

The matrix of generalized coordinates $\overline{G}$ cannot easily be rearranged and partitioned into dependent and linearly independent coordinates as in the one-dimensional case. Therefore, the transformation technique, which was described previously, has not been adopted here. Alternatively, equations (6.50) and (6.51) may be written in the partitioned form [73]

$$\begin{bmatrix}\left(\chi - \omega^2\mu + j\omega\varsigma\right) & -R_c\\ R_c^T & 0\end{bmatrix}\begin{Bmatrix}\overline{G}\\ \lambda\end{Bmatrix} = \begin{Bmatrix}Q_s\\ 0\end{Bmatrix} \tag{6.52}$$

The use of the Lagrange's Multiplier technique for the present situation, whilst more tedious than the transformation matrix technique used in the previous chapter, permits the incorporation of the constraint equations in a systematic manner. Equation (6.52) can be solved numerically by the application of a pseudo-inversion technique using Singular Value Decomposition (SVD) [77].

6.3 – Numerical Results

In this section the results of some numerical simulations are presented in order to illustrate the use of the CMS method in 3D fluid-structure interaction problems. All results are presented for the three dimensional problem, which also includes the modal contribution of the partition.

The spatial results are presented in terms of normalized mean square pressure and particle velocity distribution at 55 Hz, 120 Hz and 190 Hz over certain positions (planes) that have been specified *a priori*. These particular frequencies, which do not necessarily coincide with the fundamental room modes, were arbitrarily chosen below and above the lowest natural frequency of the receiving room, above which tangential and oblique acoustic modes are generated in the receiving room.

Subsequently, a comparison between the CMS and the Modal model described in chapter 2 is made in terms of spatially averaged mean square sound pressure variation and Noise Reduction (NR).

6.3.1 – A three dimensional CMS model considering an elastic partition (over the whole common wall)

A flexible partition with dimensions and density equal to 2m x 2m and 806 kg/m^3 respectively was considered over the whole common interface. The thickness, Young's modulus and Poisson's ratio for the partition were 0.01m, 2.12x10^{-9} N/m^2, and 0.24 respectively. Its fundamental natural frequency is 3.8 Hz. The source and receiving room dimensions were as before equal to 5m x 2m x 2m and 3m x 2m x 2m respectively. A constant volume velocity source was placed at one corner of the source room (-5,0,0).

As mentioned above, the following results are presented in terms of the mean square pressure and particle velocity distribution at 55 Hz, 120 Hz and 190 Hz. The mean square values are normalized to their maximum value in the plane. The normal particle

velocity values presented in this section were considered in the x direction normal to the partition. The mean square pressure and particle velocity distributions were symmetric with respect to the principal axes of both rooms.

Figure 6.1 shows the distribution of the normalized mean square sound pressure over the horizontal plane x-z (at the room mid-plane y = 1 m) at 55 Hz. The x and z direction correspond to the rooms' depth and width respectively. Figures 6.1 (a) and (b) show the variation of mean square pressure using a three dimensional surface plot mesh and contour levels respectively. It is seen that the pressure variation over the horizontal plane x-z of the source and receiving rooms is symmetric, in particular it is plane across the width of the receiving room (see Figure 6.1 (b)). This can be explained by the fact that the first tangential mode in the receiving room occurs at about 59 Hz. There is also pressure discontinuity at $x = 0$.

Figures 6.2 (a) and (b) show the normalized mean square particle velocity distribution in the x direction with respect to the horizontal mid-plane y = 1 m at a frequency equal to 55 Hz. At the partition location the particle velocity is close to zero.

Figure 6.3 shows the distribution of the normalized mean square sound pressure over the plane x-z (at the room mid-plane y = 1 m) at 120 Hz. The x and z direction correspond to the rooms depth and width respectively. It is seen that the pressure variation over the horizontal x-z plane of the receiving room is symmetric across the width of the room but not plane as tangential modes are excited at this frequency. Figures 6.4 (a) and (b) show the normalized mean square particle velocity distribution in the x direction with respect to the horizontal mid-plane y = 1 m at 120 Hz. It is seen that plane waves are not generated as in the case shown in Figure 6.2. By comparing Figures 6.3 and 6.4 with those of the modal model (Figures 2.19 and 2.20), it is seen that the CMS solution shows a different spatial distribution of sound pressure and particle velocity, especially in the receiving room. At this frequency, the modal model is close to a resonance and the CMS model is at an anti-resonance.

At particular frequencies, it is usually difficult to make a comparison between the two models in terms of mean-square pressure and/or particle velocity spatial distributions. It may be explained by the fact that for the modal model the acoustic pressure is assumed to be the sum of the pressure distributions in the acoustic modes of a rectangular rigid-walled room. On the other hand, for the CMS model 'additional' modes (constraint

modes) are also included in the summation and the responses at particular frequencies are not necessarily very similar.

Figures 6.5 and 6.6 show the normalized mean square pressure distribution with respect to the vertical plane *x-z* along the centre line length of the room (y = 1 m) at 140 Hz and at 190 Hz respectively. The pressure at the end wall x = -5m, where the source was located, assumed a maximum value. It can be seen that good agreement was found between the modal and CMS model for the mean square pressure distributions at both frequencies. Similarly there is good agreement for the mean square particle velocity distribution (not shown). The results are close to particular modes of both rooms. For instance the natural frequency at 190.1 Hz corresponds to the modes (5,0,1) and (3,0,1) for the source and receiving rooms respectively. Nevertheless, in terms of mean square pressure distribution the results obtained via the Modal and CMS models present some differences for the receiving room. Figure 6.8 later shows the effect of these differences in the absolute pressure levels at about 190 Hz.

In Figure 6.7 a comparison is made between the one dimensional CMS model, which considers a limp partition and was presented previously in Chapter 5, and the actual three-dimensional CMS model in terms of average mean square sound pressure. Figures 6.7a and 6.7b show the results for the source and receiving room respectively. It is seen that the resonance peaks for the CMS-1D model tend to match those for the CMS-3D model as frequency increases. According to the Figure, the first resonance peak for the 1D case is lower than the one for the 3D case, which considers an 'elastic' partition. This is due to the effect of the partition elastic properties, which is considered in the 3D CMS model. Some agreement can be seen near the 1D modes as expected.

Figures 6.8 (a) and (b) show a comparison between the CMS and the Modal model in terms of mean square sound pressure for both source and receiving rooms respectively. The results are shown in narrow frequency bands. A total of 90 modes (77 normal modes and 13 constraint modes) were used for the source room. For the receiving room, 59 modes (46 normal modes and 13 constraint modes) were considered.

The effect of the 0 Hz mode in the Modal model has been checked by eliminating it from the calculations (not shown). As a result, the variation of sound pressure in the source and receiving rooms tended to zero at frequencies below their first 'elastic' modes, i.e. at 34 Hz and 56.7 Hz. Peaks at 34 Hz and 68 Hz can be seen in both the source and receiving rooms. However, there are some 'extra' peaks in the receiving room which

correspond to the coupled modes of the system. For example, the peak at about 19 Hz corresponds to the coupled mode 19.3 Hz shown in Table 6.2.

Both models present slight differences in terms of their coupled resonance frequencies in the frequency range considered although generally the agreement is very good in the source room above 50 Hz and reasonably good in the receiver room. The first ten natural frequencies for the coupled system consisting of the rooms and partition are listed in Tables 6.1 and 6.2. These correspond to the eigenvalues of the unforced system (equation (6.52) with no volume velocity source), which are obtained using an eigenvalue solver. Due to the square cross-section of the rooms there are repeated modes apparent in the tables due to this symmetry. The peaks shown in the room responses, Figure 6.8 for example, can be identified in the natural frequencies calculated, some of which are given in the tables. For instance, it is seen that the first peak for the CMS predictions shown in Figure 6.8a is at about 8 Hz and is seen in the modes listed in Table 6.2

Figure 6.9 shows a comparison between the models in terms of variation of spatial-average mean square sound pressure with frequency in 1/3 octave bands. Figure 6.9(a) presents the results for the source room. It is seen that a difference of less than 2 dB occurs between the models for frequencies above 100 Hz. Below 100 Hz there are differences of up to 10 dB. On the other hand, Figure 6.9(b) shows differences of up to 20 dB for frequencies below 100 Hz. This might be explained by the fact that few acoustic 'room' modes are excited at frequencies below 100 Hz in the receiving room. However, it is seen that a difference of less than 5 dB occurs in the 1/3 octave bands with centre frequencies greater than 100 Hz.

In general the differences became less important at higher frequencies, where the acoustic field became more diffuse and the system boundary conditions did not have as much effect on the mean square sound pressure averaged over the acoustic volume.

Figures 6.10a and 6.10b show the Noise Reduction values in narrow and 1/3 octave bands respectively. The variation of the NR between the CMS and Modal models in 1/3 octave bands tends to be less than about 6 dB at centre frequencies greater than 100 Hz. In this frequency range the results show low convergence. On the other hand, there is a fair agreement between the CMS model and Leppington's approach as frequency increases.

Figures 6.11a and 6.11b show a comparison of the spatially averaged mean square normal velocity of a lightweight partition calculated using the CMS and the Modal models. A difference of about 20 dB between the models occurs at very low frequencies. Nevertheless, a difference of less than 2 dB is found at frequencies greater than 100 Hz.

Figures 6.12a and 6.12b present a comparison between the CMS and Modal model in terms of the variation of the mean square sound pressure for the source and receiving rooms respectively. The results shown are shown in narrow band and for a heavyweight partition. It is seen that a reasonable agreement is found between both models over most of the frequency range and it is better than that for the lighter partition shown in Figure 6.8. The first ten natural frequencies for the rooms, partition and the coupled system are listed in Tables 6.3 and 6.4. It is seen that there are some degenerate modes due to the symmetry of the rooms.

Figure 6.12a shows a slight difference between the models at approximately 12 Hz. Figure 6.12b shows that there are peaks at 85 Hz and 120 Hz in the modal model but not in the CMS model. This might be explained by the fact that the CMS did not incorporate 'rigid-body' modes in the formulation. Therefore, as the compatibility equations were only formulated in terms in the x direction normal to the partition, there was no net volume associated with the particle velocity modes $(0, l_2, q_2)$ in the receiving room. Likewise, the one-dimension CMS model implemented in Chapter 5 did not incorporate the zero velocity bulk mode in its formulation.

In Figures 6.13a and 6.13b the corresponding one third octave bands results are shown. Figure 6.13a shows at frequencies greater than 100 Hz a difference of less than 1 dB is found between both models for the source room. At frequencies below 100 Hz they show some differences of up to approximately 6 dB. On the other hand, Figure 6.13b shows differences of up to 15 dB in one third octave bands with centre frequencies below 160 Hz for the receiver room. Figure 6.12 shows that there are peaks at 85 Hz and 120 Hz in the modal model but not in the CMS and that these would contribute significantly to the third octave band level differences. Above 160 Hz the fairly good narrow band agreement produces third octave band differences of less than 2 dB.

Figures 6.14a and 6.14b show the NR values for the heavier partition in narrow and one third octave bands respectively. It is shown that significant differences between the models occur at low frequencies. As the frequency increases, a fairly good agreement is obtained between the models. Moreover, the CMS result shows fairly good agreement

with those obtained via Leppington's approach and with the field incidence Mass Law. For the model considered the incidence Mass Law appears to still be underestimating the NR at the higher frequencies being considered here.

Figures 6.15a and 6.15b show the results comparing the partition vibration according to the CMS and the Modal model for a heavyweight partition. It is seen that at higher frequencies the results tend to a better agreement as expected. Differences of less than 3 dB occur at frequencies greater than 100 Hz.

6.3.2 –Comparison between the results obtained experimentally and via the numerical models.

In this subsection some results are presented for comparison between the predictions (i.e. those obtained via the Modal and CMS models) and the measured values obtained via experimental tests described in Chapter 3. In order to compare the results obtained in Chapter 3 (i.e. using the Modal model and measured values) with those obtained via the CMS-3D model, the same geometrical and material properties for the partition and rooms were adopted herein. In addition, the same volume velocity, which was measured from the loudspeaker for using in the Modal model calculations (see Figure 3.15), was also considered in the CMS model.

Figures 6.16a and 6.16b show a comparison between measured and predicted sound pressure levels in 1/3 octave bands for the source and receiving rooms respectively. The results obtained via the Modal model and experimental tests were reproduced here from Figures 3.45 and 3.46. They show that significant differences occur between the CMS and Modal models at very low frequencies. On the other hand, it is seen that a difference of less than 6 dB occurs between the CMS and the Modal model at frequencies greater than 100 Hz. Overall, a poorer agreement is found between the measured and predicted results for the receiving rooms at high frequencies. As mentioned in Chapter 3, the main reason for this discrepancy was due to the poor signal-to-noise ratio of the measurements made in the receiving room.

Figure 6.17 shows that as frequency increases, both theoretical models tend to diverge from the measured Noise Reduction values. As explained previously, this is possibly due to the poor signal to noise ratio measured values. The noise floor for the measurements in the receiver room was not substantially lower than the measured sound pressure level. Despite significant differences occuring between the CMS and the Modal model at very low frequencies, these differences tend to be less than 3 dB at higher frequencies.

Figure 6.18 presents a comparison between the experimental test, the CMS and Modal models in terms of the partition normal velocity. It is seen that as frequency increases the results seem to converge as expected. The measured damping was used in the calculations. It is seen that at higher frequencies both the CMS and Modal models show good agreement.

6.4 – Conclusions

The CMS approach for the one-dimensional problem has been extended in this chapter to the more general three-dimensional case. The application described the coupling of two, in general, dissimilar rectangular volumes separated by an elastic partition which might form only partial coverage of a common interface with all of the rest being rigid. In principle, apart from the choice of the component and constraint modes, which for irregular volumes may require numerical (e.g. FE) calculations, the approach is very general and could be implemented within existing commercial software.

For the present examples considered it has been possible to use existing analytical expressions for the modes under certain assumptions, e.g. simply-supported edges for the partition, and then rapid numerical calculations for the coupled systems have been possible. As previously seen in the one-dimensional case, there is a significant change in the detailed pressure and velocity spatial variations when correct velocity continuity is included but which is not so important if the spatially averaged quantities or higher frequencies are considered. The most important findings from the simulations performed are as follows, where comparison is made between the CMS and the original Modal Model approach.

It was seen that the spatial distribution of sound pressure and particle velocity in the rooms are very complex. It usually depends on several factors such as source position, room and partition dimensions, frequency, etc. For the cases presented herein the response in the receiving volume was directly related to the degree of coupling between the structural and the transverse acoustic modes.

Firstly, an elastic partition was incorporated and considered as another modal component. The results have shown a fairly good agreement between the CMS and the Modal model in terms of spatially averaged mean square pressure. Similarly reasonably good agreement between the models was obtained at higher frequencies. One possible

explanation is that the modal model, which considers rigid-walled modes, is more representative at higher frequencies where the system boundary conditions are much less important. Nevertheless, it still cannot replicate exactly the partition velocity compared to the CMS method.

Secondly, some experimental results obtained in Chapter 3 are compared to the numerical models. It is seen that in contrast to the sound pressure in the receiving room, a better agreement between the measured and predicted results, which were obtained using the CMS and Modal models, was obtained for the source room. This is particularly evident from inspection of the frequency response of the sound pressure in both rooms. In Chapter 3, it was seen that the sound pressure measurements in the receiving room were significantly affected by external factors such as poor signal to noise ratio.

In summary, the number of modes, and hence the order of the equations, increases significantly and for practical computational and numerical reasons the CMS approach is primarily useful for low frequency predictions. This comment is also applicable to the existing modal methods and is a consequence of the high modal density with increasing frequency for acoustic volumes and is a reason why statistical approaches (e.g. SEA) have been developed.

In principle, the constraint equations could also be used for the application of further conditions based on the impedance of the walls, for example, if one requires the distribution of absorbing material characterized as locally reacting and quantified by a normal impedance.

For irregular volumes then more general approximate methods, such as the numerical FE/BEM and the Trefftz techniques [71], might be more appropriate unless the normal modes are found numerically in advance of applying the CMS method.

The incorporation of the approach into existing software packages for acoustics would be worth investigation in future studies.

Tables

f_1(Hz)	f_2(Hz)	f_p(Hz)	F_c(Hz)
0.0	0.0	3.8	0.00
34.0	56.7	9.5	9.02
68.0	85.0	9.5	9.02
85.0	85.0	15.2	10.98
85.0	102.2	18.9	14.72
91.5	102.2	18.9	18.57
91.5	113.3	24.6	19.04
102.0	120.2	24.6	19.04
108.9	132.9	32.2	24.26
108.9	141.7	32.2	24.26

Table 6.1: The first ten undamped natural frequencies of rooms and partition for the Modal Model considering a flexible partition with dimensions 2m x 2m. Mass per unit area and Young's Modulus are ρh = 8.06 kg/m^2 and E = 2.12x10^9 N/m^2 respectively. 'f_1' and 'f_2' are the 'eigenvalues' corresponding to the fixed-fixed normal modes for the source and receiving rooms respectively. 'F' is the coupled frequency with subscripts 1, 2, 'p' and 'c' representing the source room, receiving room, partition and the coupled system respectively. N.B. Note degenerate modes for the coupled models because of symmetry in the square cross-section of the panel and volumes.

f_1(Hz)	f_2(Hz)	f_p(Hz)	$F_{c,3D}$(Hz)	$F_{c,1D}$(Hz)
34.0	56.7	3.8	8.1	12.8
68.0	85.0	9.5	11.2	36.2
85.0	85.0	9.5	11.2	58.9
85.0	102.2	15.2	15.8	69.5
91.5	102.2	18.9	19.3	102.8
91.5	113.3	18.9	19.3	114.7
102.0	120.2	24.6	24.5	136.7
108.9	132.9	24.6	24.5	170.0
108.9	141.7	32.2	34.6	171.4
			34.6	
			37.8	

Table 6.2: The first nine undamped 'eigenvalues' of rooms and partition for the CMS Model considering a flexible partition with dimensions 2m x 2m. Mass per unit area and Young's Modulus are ρh = 8.06 kg/m^2 and E = 2.12x10^9 N/m^2 respectively. 'f_1' and 'f_2' are the 'eigenvalues' corresponding to the fixed-fixed normal modes for the source and receiving rooms. 'F' is the coupled frequency with subscripts 1, 2 and 'p' representing the source room, receiving room and partition respectively. The subscripts c,3D and c,1D represent the 3D and 1D CMS models respectively.
N.B. Note degenerate modes for the coupled models because of symmetry in the square cross-section of the panel and volumes.

f_1(Hz)	f_2(Hz)	f_p(Hz)	F_c(Hz)
0.0	0.0	12.1	0.00
34.0	56.7	30.2	12.53
68.0	85.0	30.2	30.01
85.0	85.0	48.3	30.01
85.0	102.2	60.4	34.17
91.5	102.2	60.4	34.17
91.5	113.3	78.5	48.12
102.0	120.2	78.5	56.56
108.9	132.9	102.7	60.22
108.9	141.7	102.7	60.49

Table 6.3: The first ten natural frequencies of rooms and partition for the Modal Model considering a flexible partition with dimensions 2m x 2m. The mass per unit area and Young's Modulus are ρh = 78.5 kg/m^2 and E = 210x10^9 N/m^2 respectively. 'f_1' and 'f_2' are the 'eigenvalues' corresponding to the fixed-fixed normal modes for the source and receiving rooms respectively. 'F' is the coupled frequency of the undamped system. The subscripts 1, 2, 'p' and 'c' represent the source room, receiving room, partition and the coupled system respectively.

f_1(Hz)	f_2(Hz)	f_p(Hz)	F_c(Hz)
34.0	56.7	12.1	12.2
68.0	85.0	30.2	19.6
85.0	85.0	30.2	31.2
85.0	102.2	48.3	31.2
91.5	102.2	60.4	34.0
91.5	113.3	60.4	48.1
102.0	120.2	78.5	56.7
108.9	132.9	78.5	56.7
108.9	141.7	102.7	60.2
120.2	141.7	102.7	68.3

Table 6.4: The first ten 'eigenvalues' of rooms and partition for the CMS Model considering a flexible partition with dimensions 2m x 2m. The mass per unit area and Young's Modulus are ρh = 78.5 kg/m^2 and E = 210x10^9 N/m^2 respectively. 'f_1' and 'f_2' are the 'eigenvalues' corresponding to the fixed-fixed normal modes for the source and receiving rooms. 'F_c' is the coupled frequency of the undamped system. The subscripts 1, 2 and 'p' represent the source room, receiving room and partition respectively.

Figures

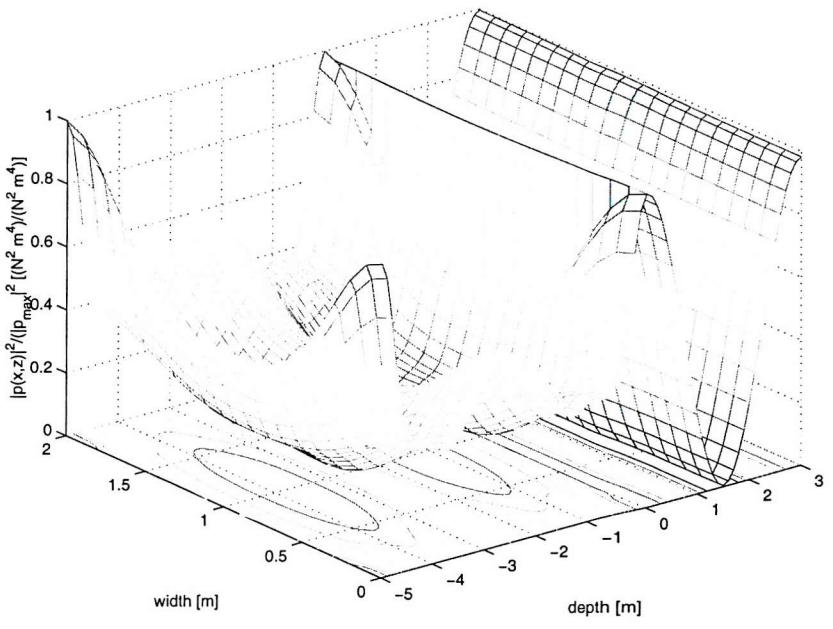

a)

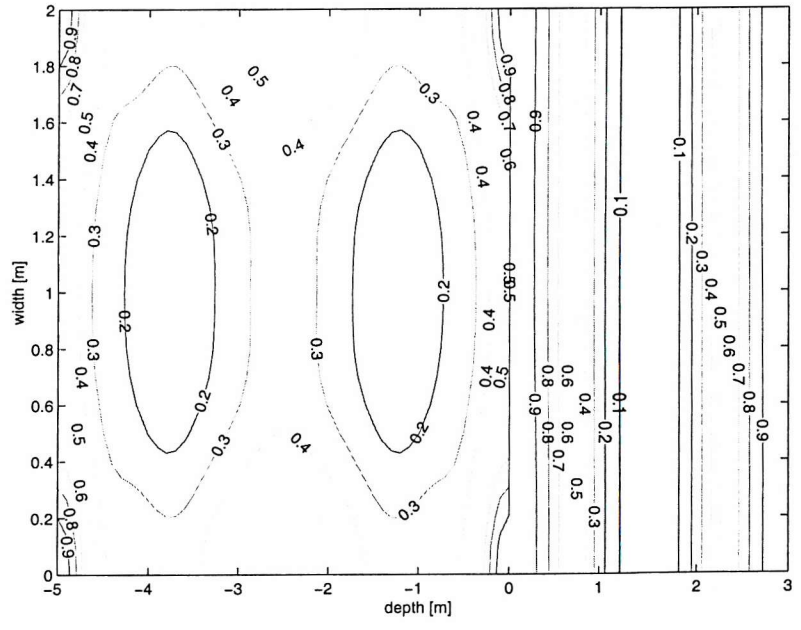

b)

Figure 6.1: Normalized mean square pressure distribution with respect to the horizontal plane y = 1m at 55 Hz. The square elastic partition has dimensions, mass per unit area and Young's Modulus equal to 2m x 2m, ρh = 8.06 kg/m^2 and E = 2.12x10^9 N/m^2 respectively. (a) Surface plot and (b) Contour levels in relative pressure to the maximum in the plane.

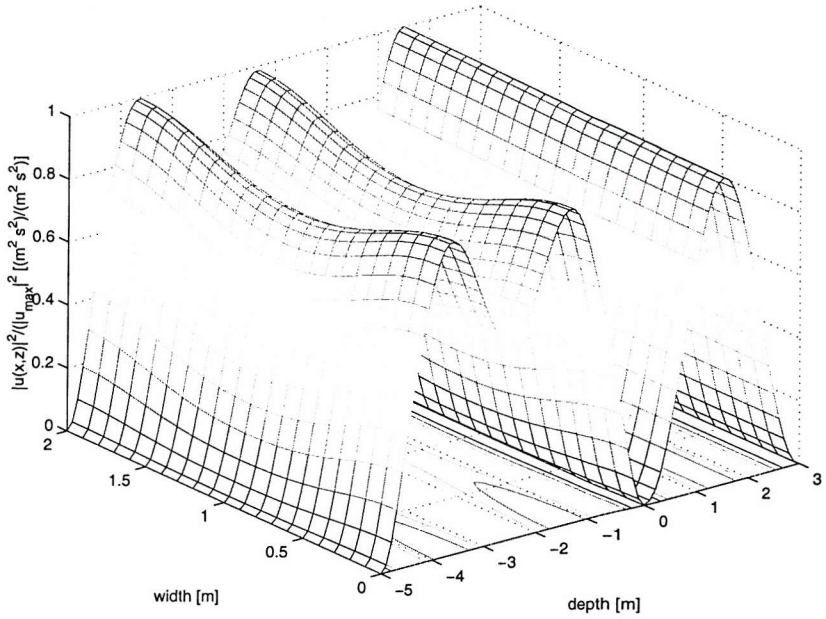

a)

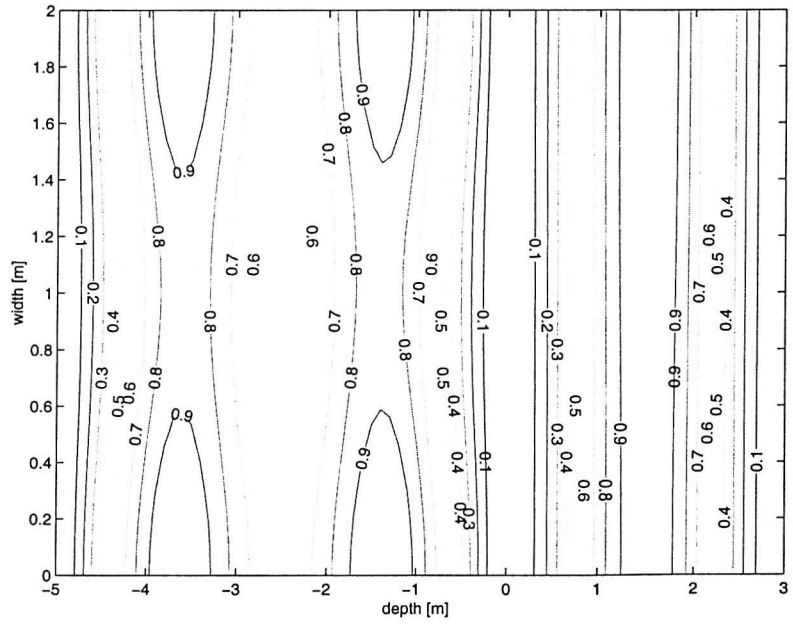

b)

Figure 6.2: Normalized mean square particle velocity distribution in the x-direction with respect to the horizontal plane y = 1m at 55 Hz. The square elastic partition has dimensions, mass per unit area and Young's Modulus equal to 2m x 2m, $\rho h = 8.06$ kg/m^2 and E = 2.12x10^9 N/m^2 respectively. (a) Surface plot and (b) Contour levels in relative pressure to the maximum in the plane.

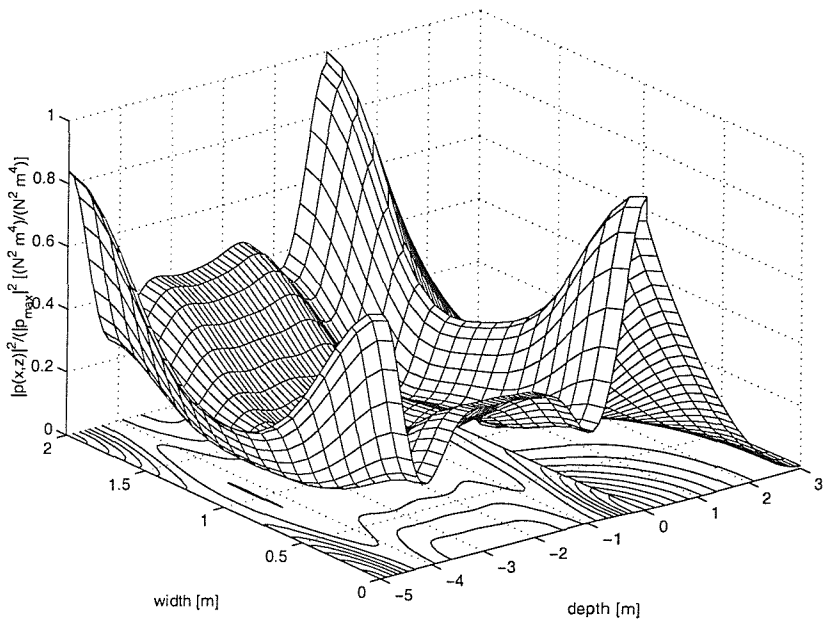

a)

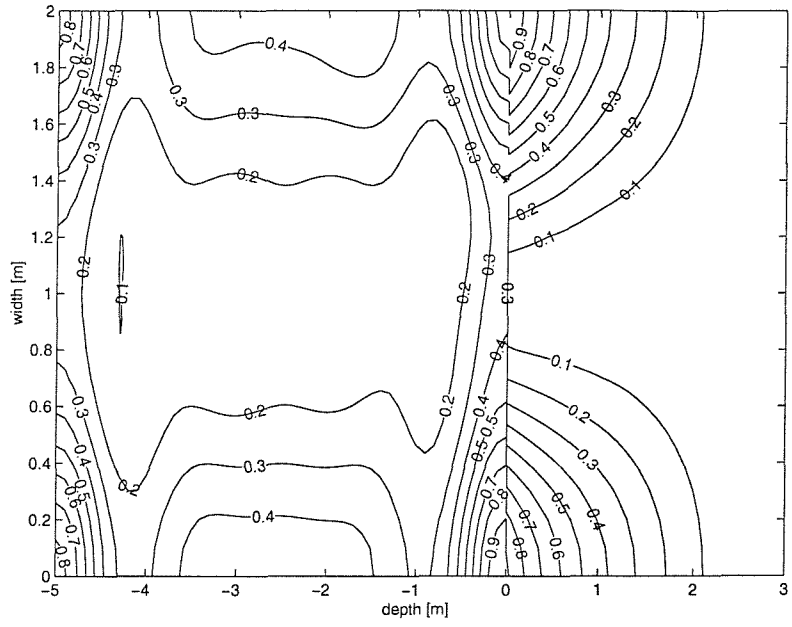

b)

Figure 6.3: Normalized mean square pressure distribution with respect to the horizontal plane y = 1m at 120 Hz. The square elastic partition has dimensions, mass per unit area and Young's Modulus equal to 2m x 2m, ρh = 8.06 kg/m^2 and E = 2.12x10^9 N/m^2 respectively. (a) Surface plot and (b) Contour levels in relative pressure to the maximum in the plane.

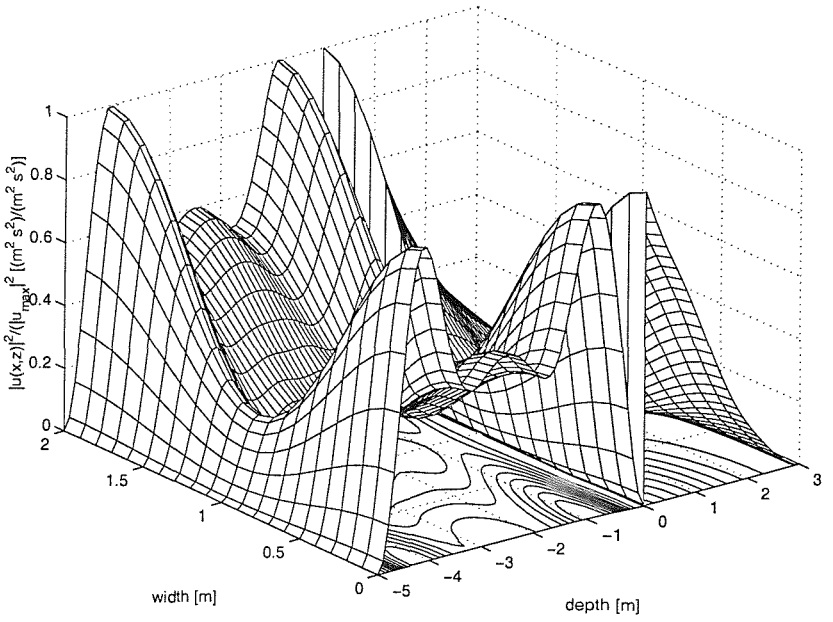

a)

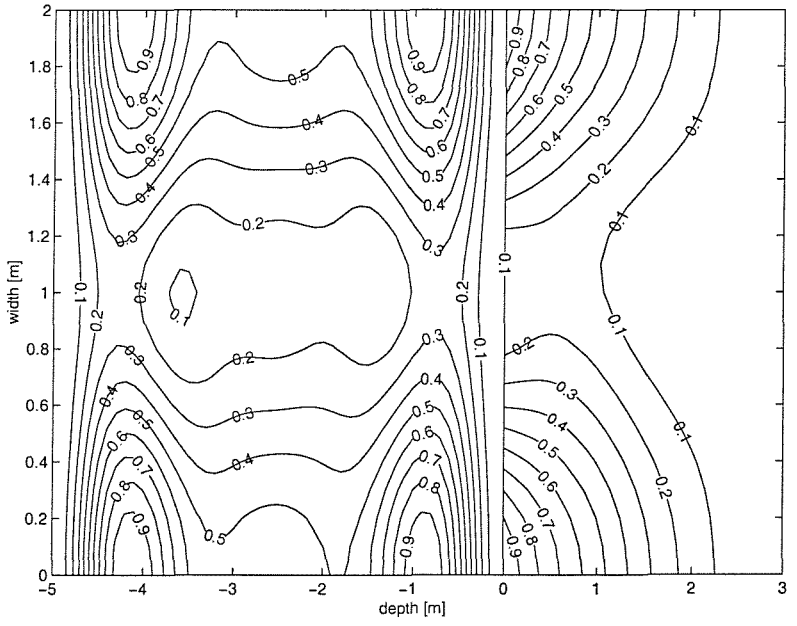

b)

Figure 6.4: Normalized mean square particle velocity distribution in the x-direction with respect to the horizontal plane y = 1m at 120 Hz. The square elastic partition has dimensions, mass per unit area and Young's Modulus equal to 2m x 2m, ρh = 8.06 kg/m^2 and E = 2.12x10^9 N/m^2 respectively. (a) Surface plot and (b) Contour levels in relative pressure to the maximum in the plane.

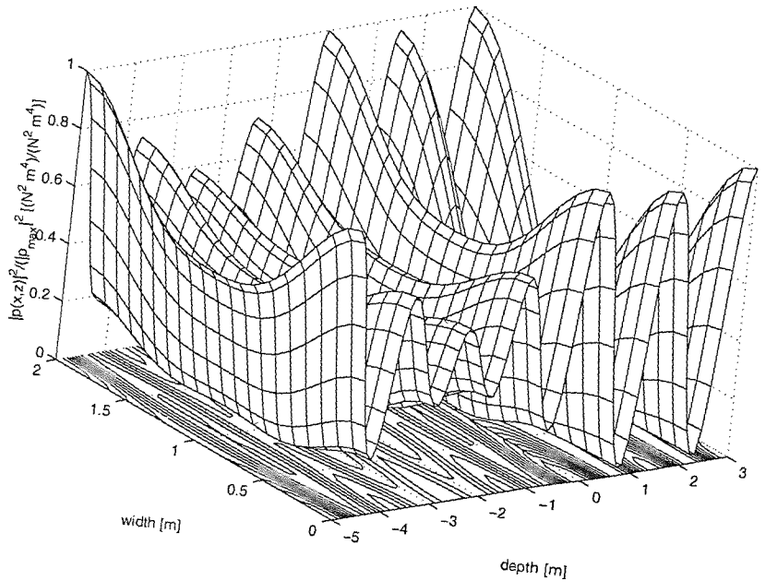

a)

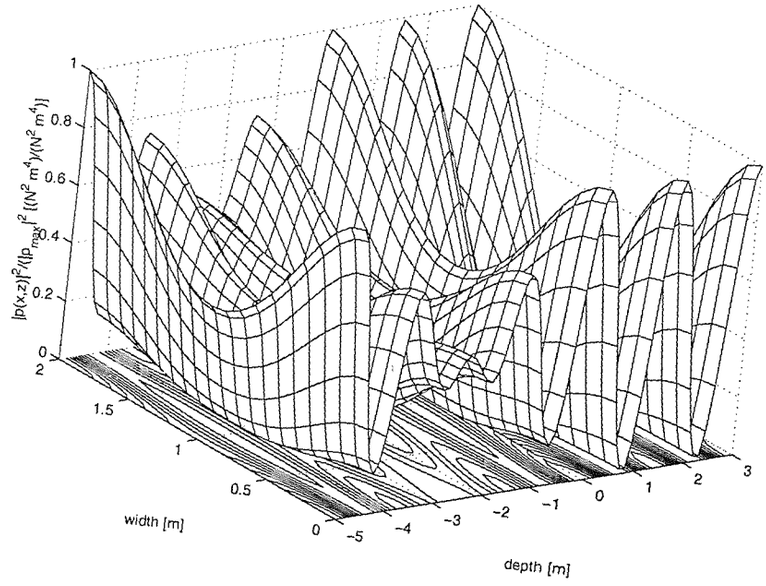

b)

Figure 6.5: Normalized mean square pressure distribution with respect to the horizontal plane y = 1m at 140 Hz. The square elastic partition has dimensions, mass per unit area and Young's Modulus equal to 2m x 2m, $\rho h = 8.06$ kg/m^2 and $E = 2.12 \times 10^9$ N/m^2 respectively. (a) CMS model and (b) Modal model in relative pressure levels to the maximum in the plane.

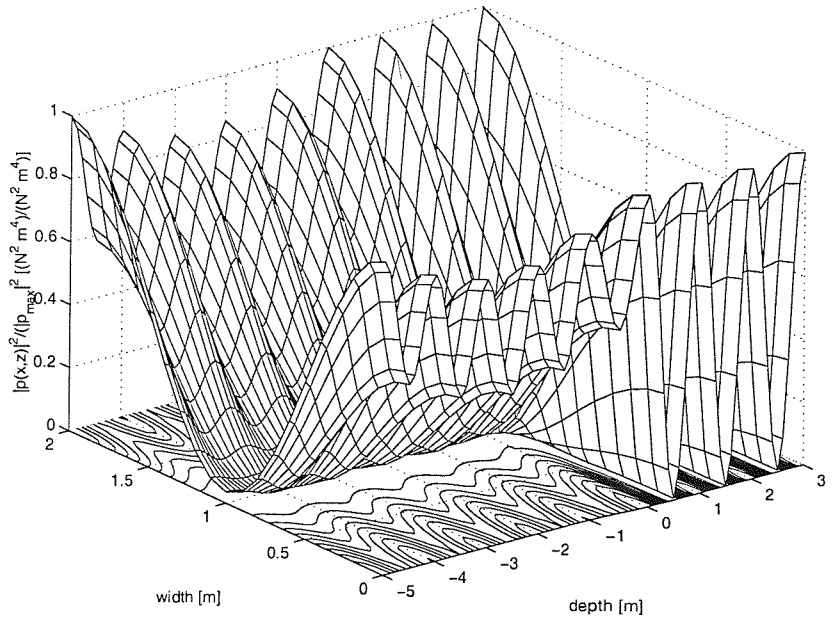

a)

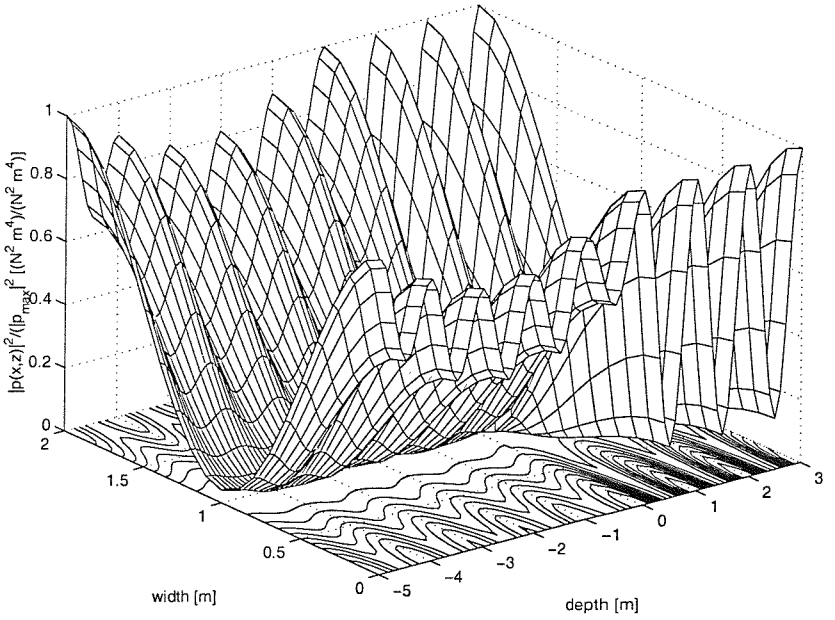

b)

Figure 6.6: Normalized mean square pressure distribution with respect to the horizontal plane y = 1m at 190 Hz. The square elastic partition has dimensions, mass per unit area and Young's Modulus equal to 2m x 2m, ρh = 8.06 kg/m^2 and E = 2.12x10^9 N/m^2 respectively. (a) CMS model and (b) Modal model in relative pressure levels to the maximum in the plane.

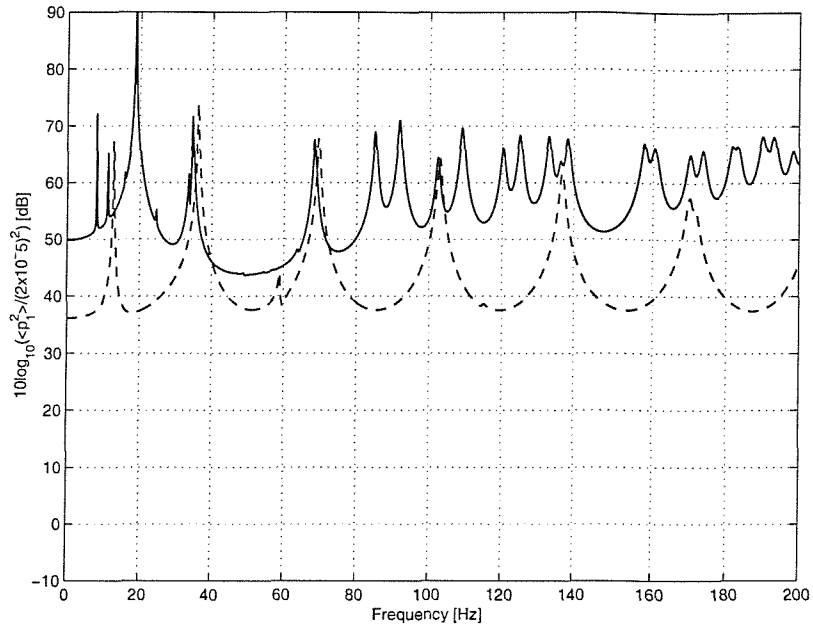

a)

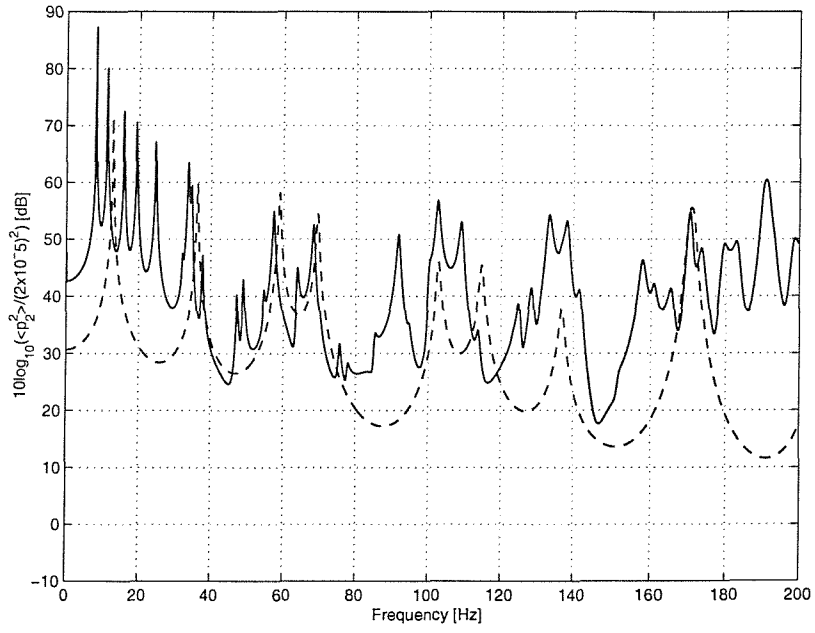

b)

Figure 6.7: Comparison between the CMS-1D and the CMS-3D models in terms of the variation of spatial-average mean square sound pressure with frequency (0.1 Hz resolution). The square elastic partition has dimensions, mass per unit area and Young's Modulus equal to 2m x 2m, ρh = 8.06 kg/m^2 and E = 2.12x10^9 N/m^2 respectively. (a): $10\log_0\left(\left\langle \bar{p}_1^2 \right\rangle / p_o^2\right)$ [dB re 2x10^{-5} Pa] ;(b): $10\log_0\left(\left\langle \bar{p}_2^2 \right\rangle / p_o^2\right)$ [dB re 2x10^{-5} Pa]. The subscript 1 and 2 indicates source and receiving rooms respectively; — CMS-3D model; ------ CMS-1D model.

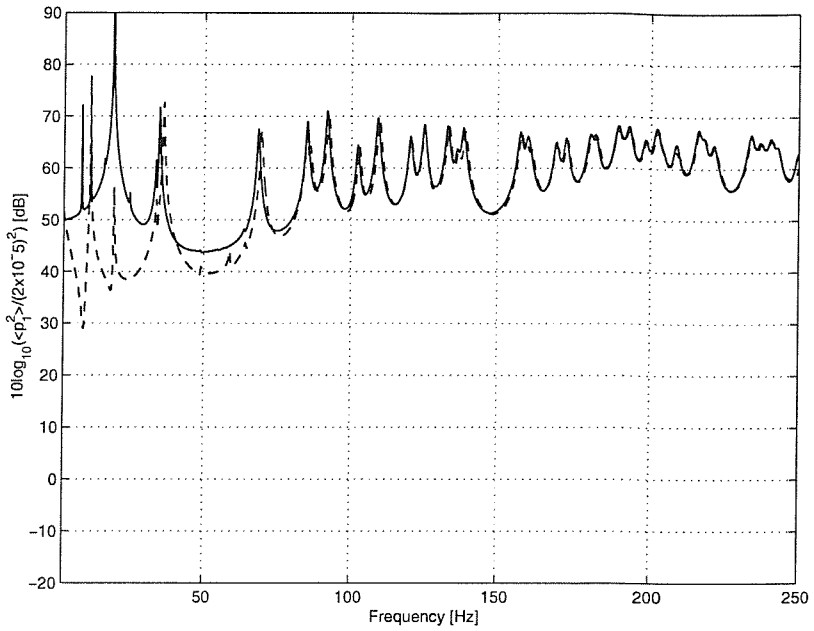

a)

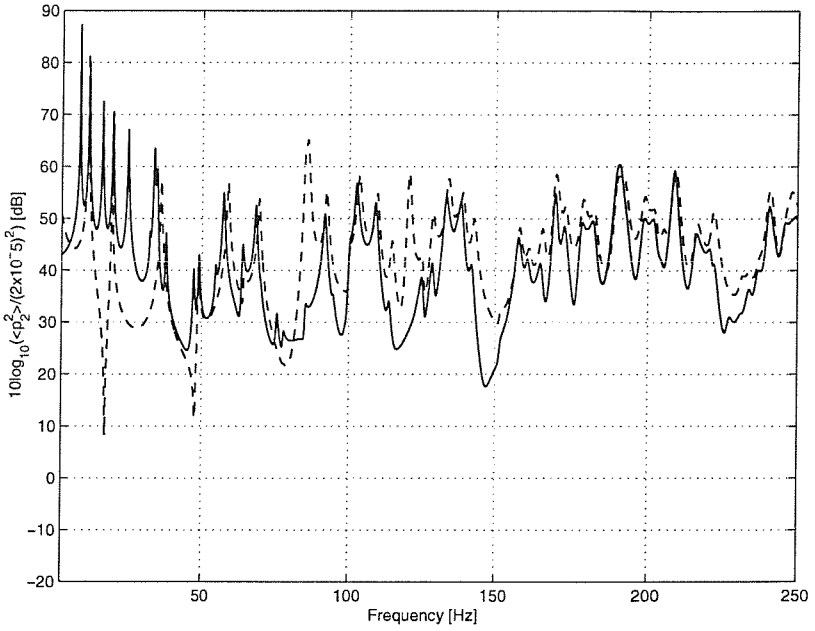

b)

Figure 6.8: Comparison between the CMS and the Modal model in terms of the variation of spatial-average mean square sound pressure with frequency (0.1 Hz resolution). The square elastic partition has dimensions, mass per unit area and Young's Modulus equal to 2m x 2m, ρh = 8.06 kg/m^2 and E = 2.12x10^9 N/m^2 respectively. (a): $10\log_0\left(\langle \bar{p}_1^2 \rangle / p_o^2\right)$ [dB re 2x10^{-5} Pa] ;(b): $10\log_0\left(\langle \bar{p}_2^2 \rangle / p_o^2\right)$ [dB re 2x10^{-5} Pa]. The subscript 1 and 2 indicates source and receiving rooms respectively; — CMS model; ---- Modal model.

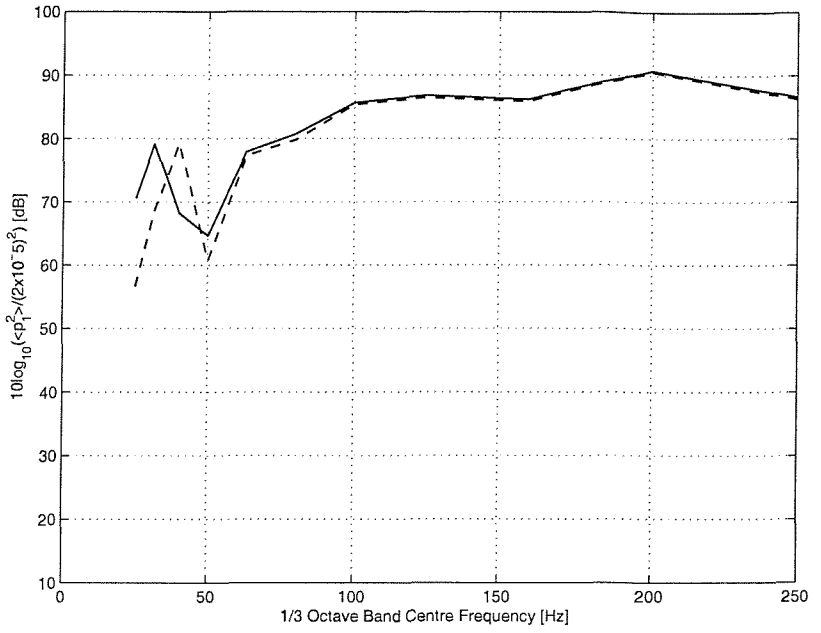

a)

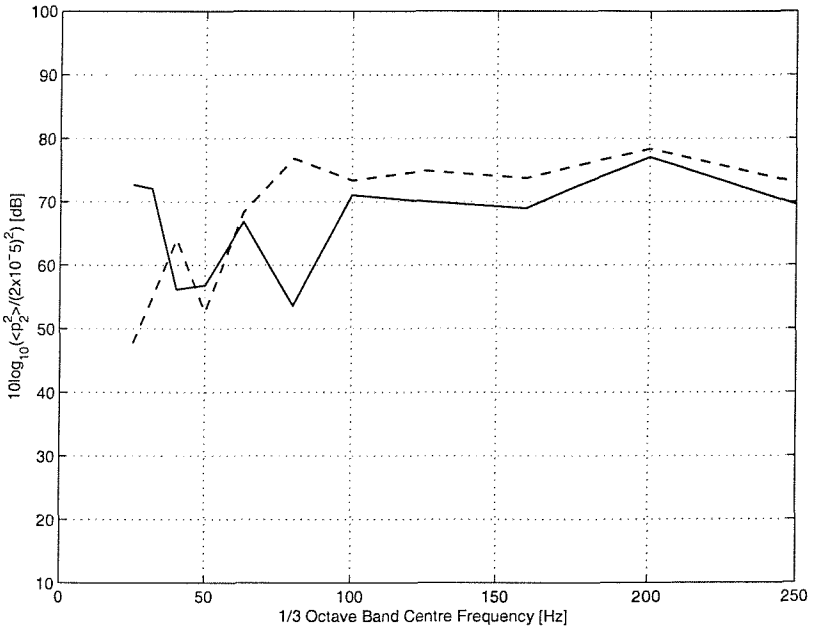

b)

Figure 6.9 Comparison between the CMS and the Modal model in terms of the variation of spatial-average mean square sound pressure with 1/3 octave bands. The square elastic partition has dimensions, mass per unit area and Young's Modulus equal to 2m x 2m, ρh = 8.06 kg/m^2 and E = 2.12x10^9 N/m^2 respectively. (a): $10\log_{10}\left(\langle \bar{p}_1^2 \rangle / p_o^2\right)$ [dB re 2x10^{-5} Pa] ;(b): $10\log_{10}\left(\langle \bar{p}_2^2 \rangle / p_o^2\right)$ [dB re 2x10^{-5} Pa]. The subscript 1 and 2 indicates source and receiving rooms respectively; — CMS model; ---- Modal model.

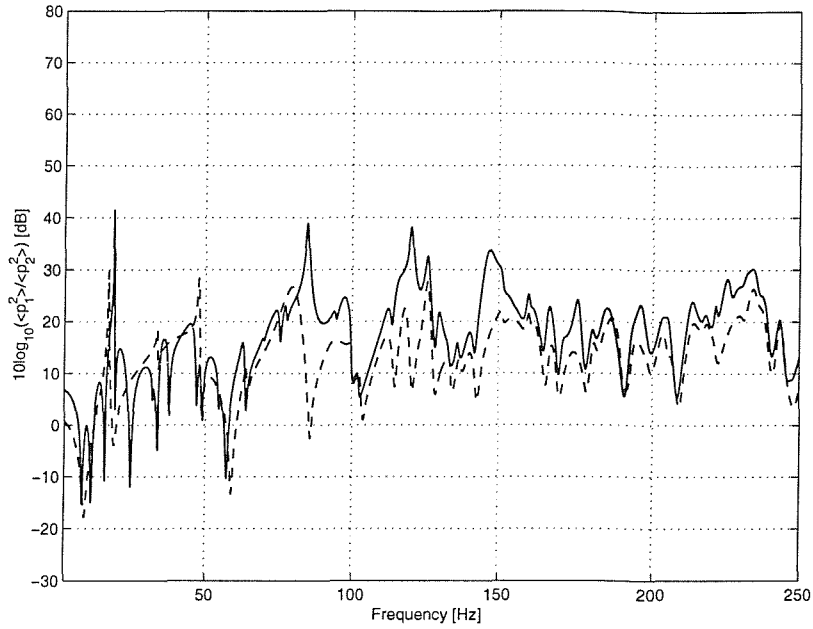

a)

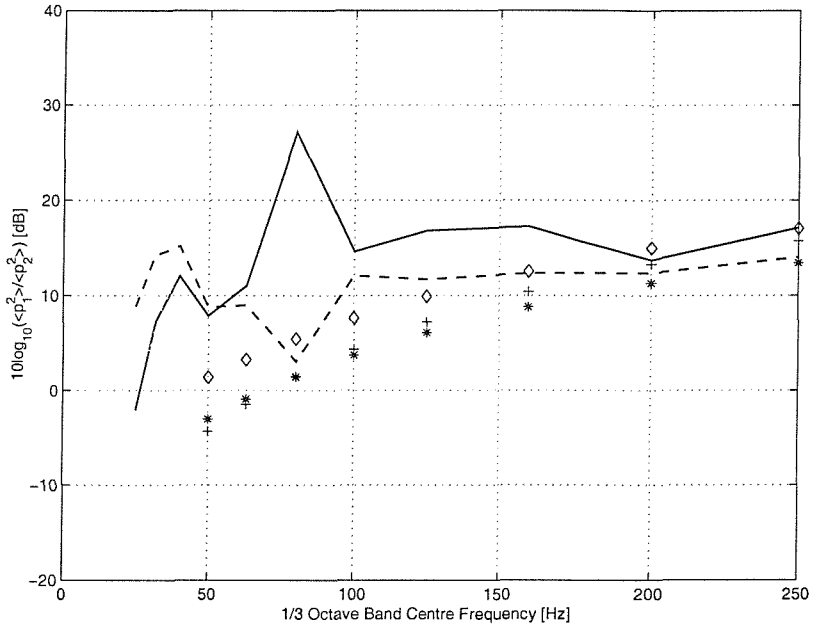

b)

Figure 6.10: Comparison between the CMS and the Modal model in terms of the variation of Noise Reduction (NR). The square elastic partition has dimensions, mass per unit area and Young's Modulus equal to 2m x 2m, ρh = 8.06 kg/m^2 and E = 2.12x10^9 N/m^2 respectively. (a): $10\log_0\left(\left\langle \bar{p}_1^2 \right\rangle / \left\langle \bar{p}_2^2 \right\rangle\right)$ [dB re 1] versus frequency ;(b): $10\log_0\left(\left\langle \bar{p}_1^2 \right\rangle / \left\langle \bar{p}_2^2 \right\rangle\right)$ [dB re 1] in 1/3 octave bands. The subscript 1 and 2 indicates source and receiving rooms respectively; — CMS model; --- Modal model; *** Diffuse incidence Mass Law; +++ Field incidence Mass Law; ◊◊◊ Leppington's prediction.

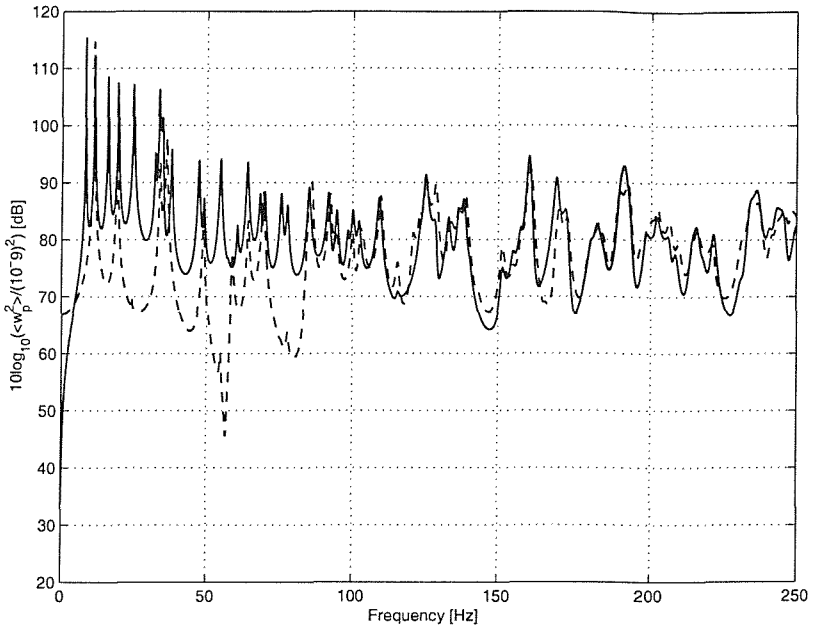

a)

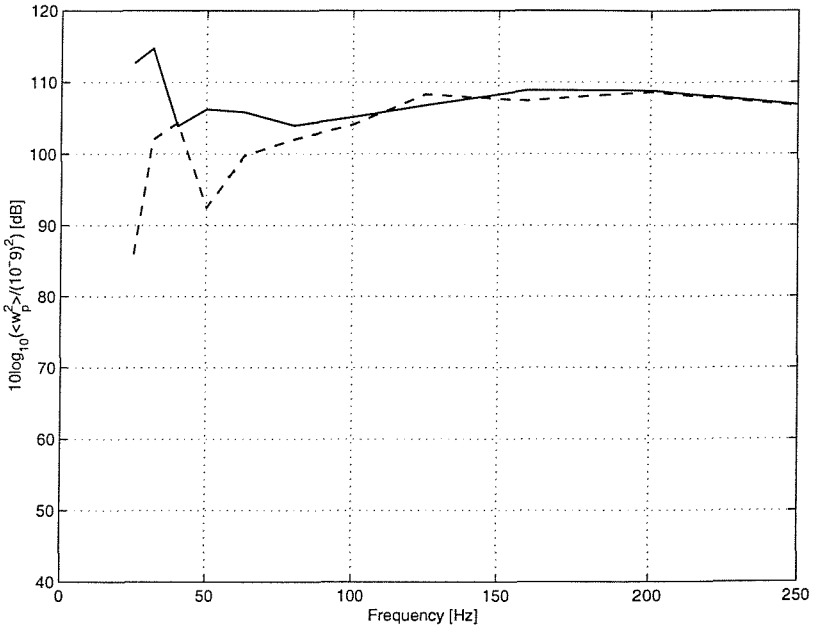

b)

Figure 6.11: Comparison between the CMS and the Modal model in terms of the variation of the spatially averaged mean square normal velocity of the partition (dB re 10^{-9} m/s). The square elastic partition has dimensions, mass per unit area and Young's Modulus equal to 2m x 2m, ρh = 8.06 kg/m^2 and E = 2.12x10^9 N/m^2 respectively. (a) in narrow bands; (b) in 1/3 octave bands. — CMS model; --- Modal model.

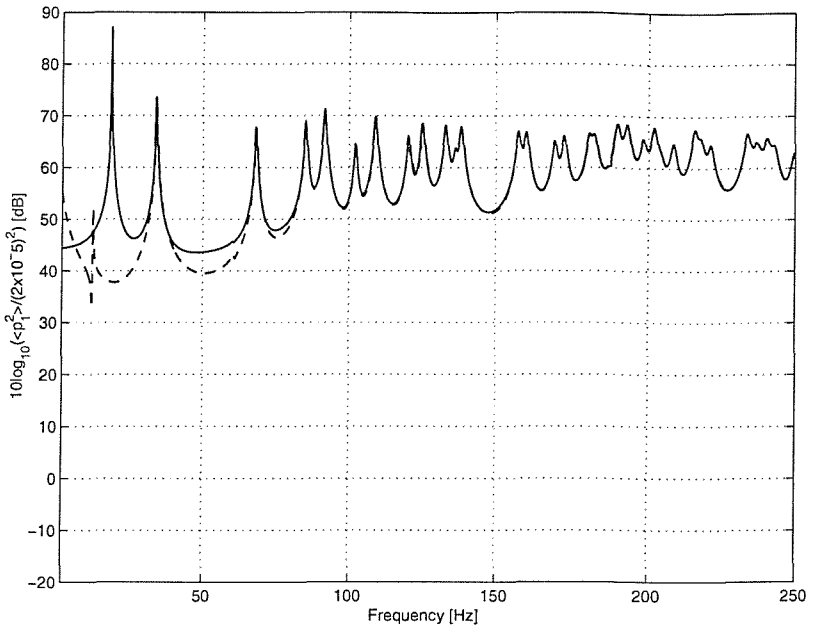

a)

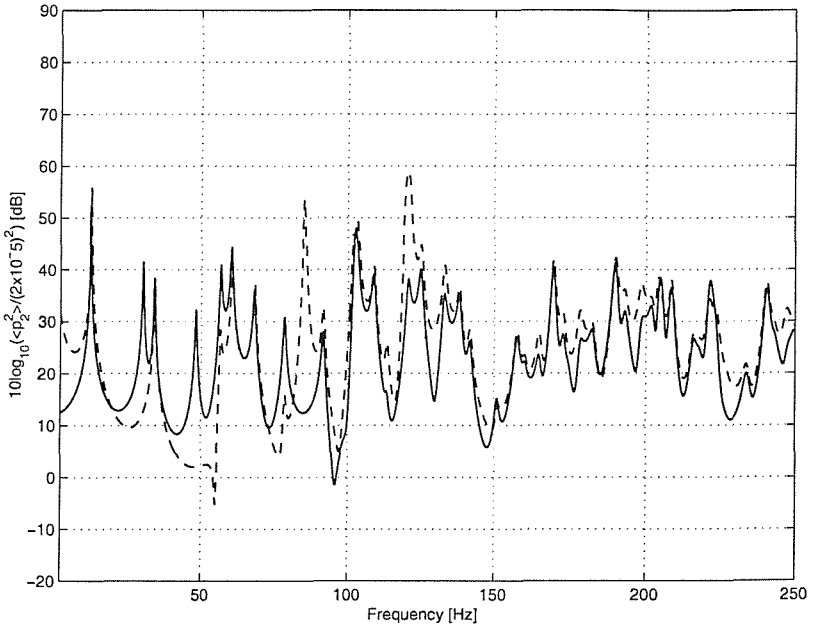

b)

Figure 6.12: Comparison between the CMS and the Modal model in terms of the variation of spatial-average mean square sound pressure with frequency (0.1 Hz resolution). The square elastic partition has dimensions, mass per unit area and Young's Modulus equal to 2m x 2m, ρh = 78.5 kg/m^2 and E = 210x10^9 N/m^2 respectively. (a): $10\log_{10}\left(\langle \bar{p}_1^2 \rangle / p_o^2\right)$ [dB re 2x10^{-5} Pa] ;(b): $10\log_{10}\left(\langle \bar{p}_2^2 \rangle / p_o^2\right)$ [dB re 2x10^{-5} Pa]. The subscript 1 and 2 indicates source and receiving rooms respectively; — CMS model; ---- Modal model.

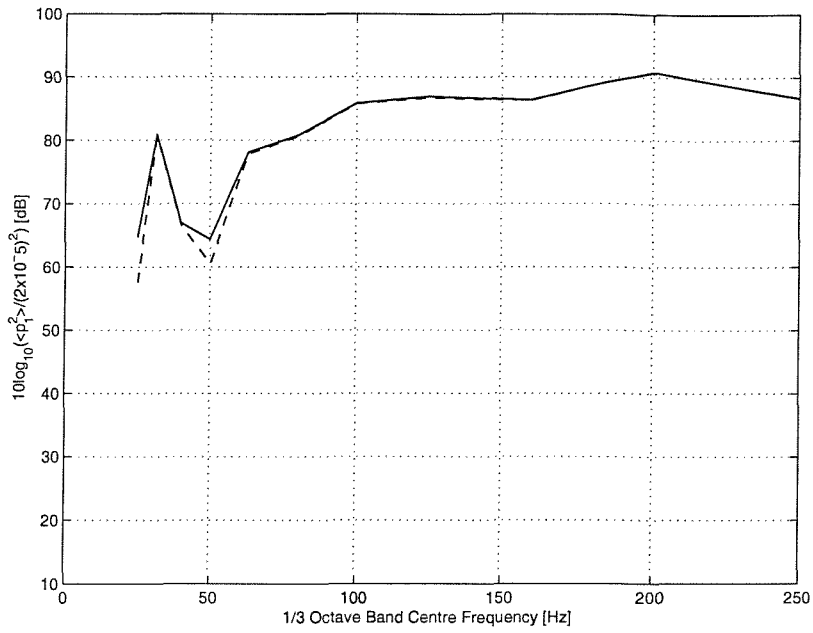

a)

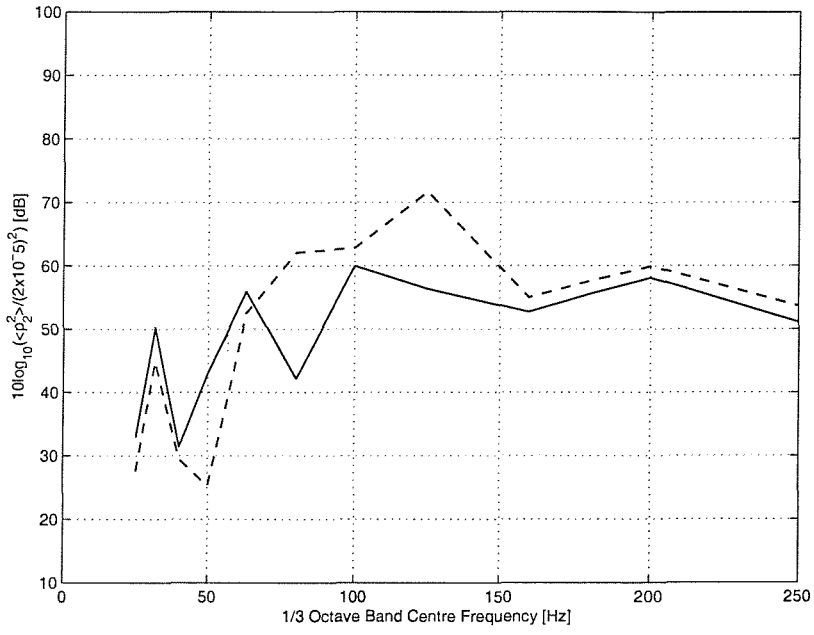

b)

Figure 6.13 Comparison between the CMS and the Modal model in terms of the variation of spatial-average mean square sound pressure with 1/3 octave bands. The square elastic partition has dimensions, mass per unit area and Young's Modulus equal to 2m x 2m, ρh = 78.5 kg/m^2 and E = 210x10^9 N/m^2 respectively. (a): $10\log_0\left(\left\langle \bar{p}_1^2 \right\rangle / p_o^2\right)$ [dB re 2x10^{-5}Pa] ;(b): $10\log_0\left(\left\langle \bar{p}_2^2 \right\rangle / p_o^2\right)$ [dB re 2x10^{-5} Pa]. The subscript 1 and 2 indicates source and receiving rooms respectively; — CMS model; ---- Modal model.

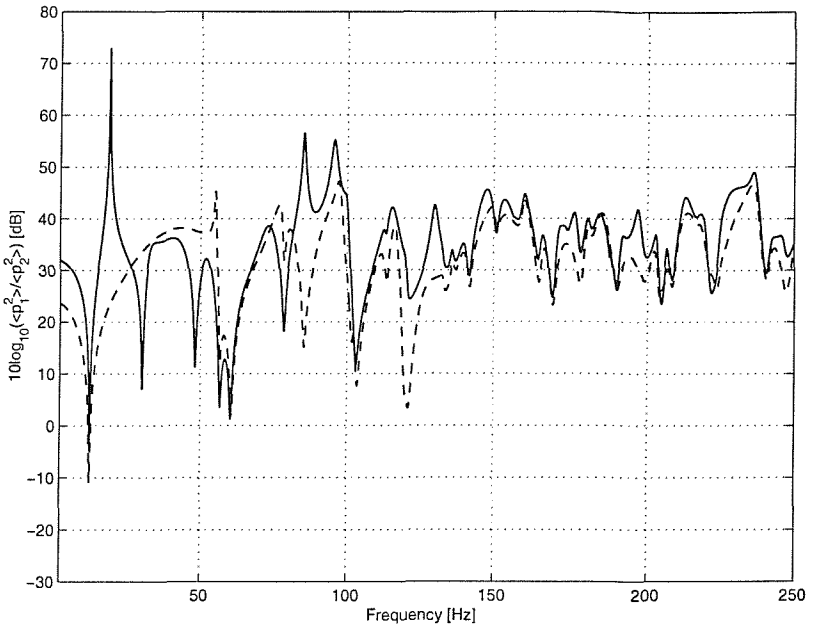

a)

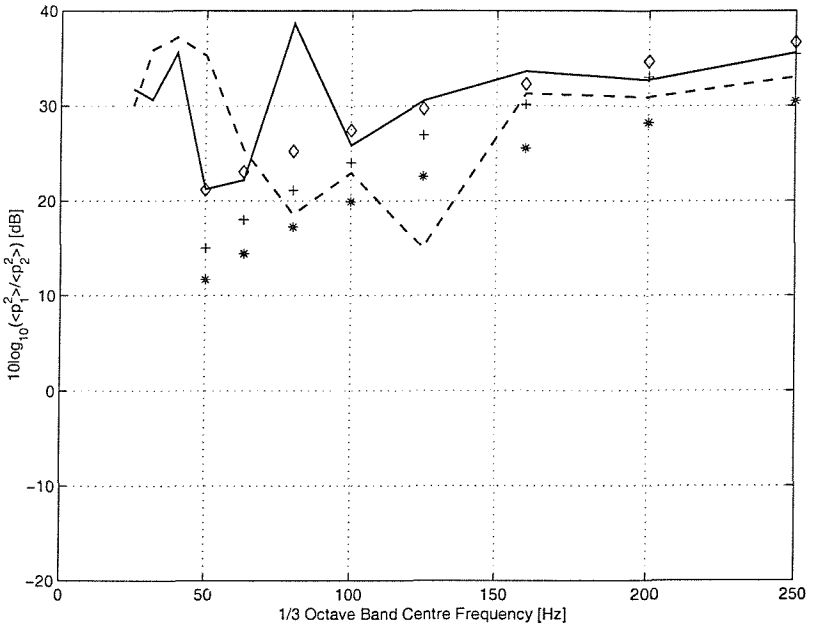

b)

Figure 6.14: Comparison between the CMS and the Modal model in terms of the variation of Noise Reduction (NR). The square elastic partition has dimensions, mass per unit area and Young's Modulus equal to 2m x 2m, ρh = 78.5 kg/m^2 and E = 210x10^9 N/m^2 respectively. (a): $10\log_{10}\left(\langle \bar{p}_1^2 \rangle / \langle \bar{p}_2^2 \rangle\right)$ [dB re 1] versus frequency ;(b): $10\log_{10}\left(\langle \bar{p}_1^2 \rangle / \langle \bar{p}_2^2 \rangle\right)$ [dB re 1] in 1/3 octave bands. The subscript 1 and 2 indicates source and receiving rooms respectively; — CMS model; --- Modal model; *** Diffuse incidence Mass Law; +++ Field incidence Mass Law; ◊◊◊ Leppington's prediction.

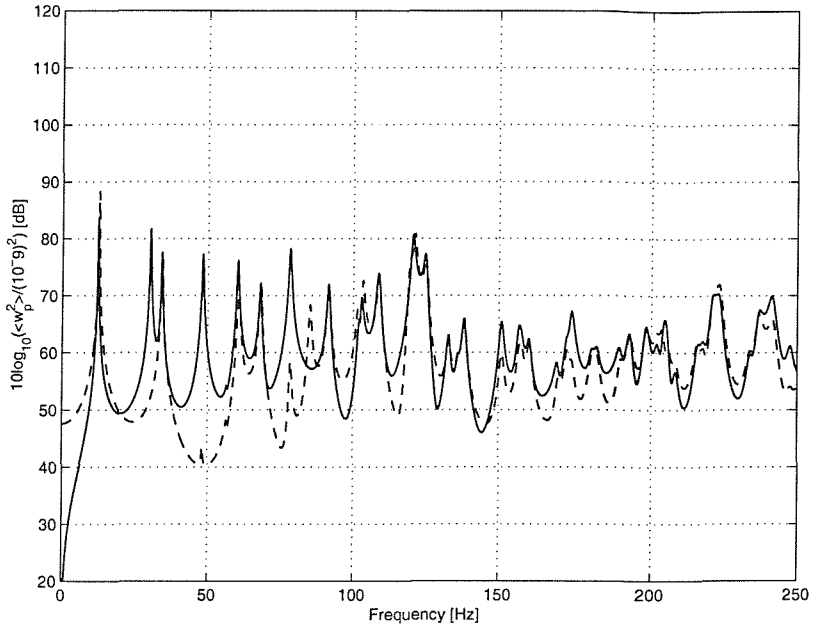

a)

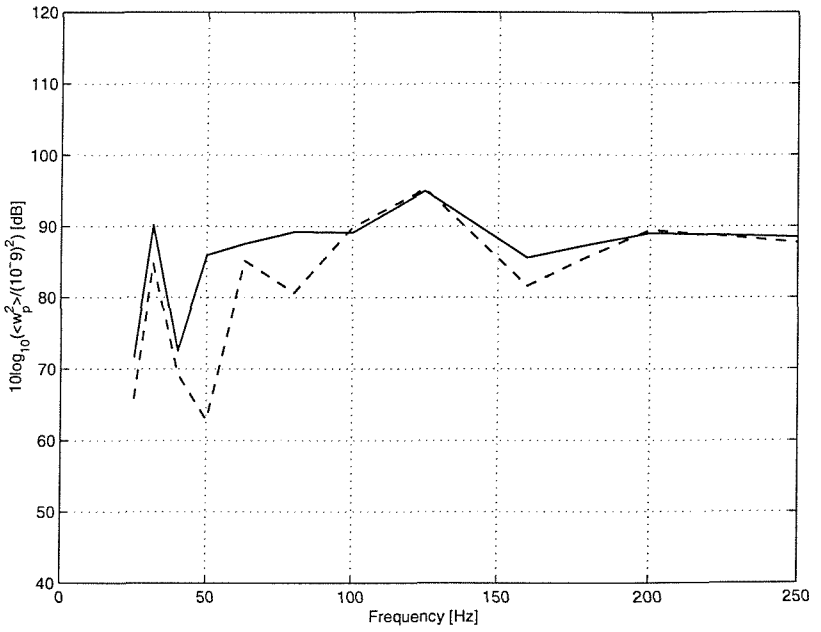

b)

Figure 6.15: Comparison between the CMS and the Modal model in terms of the variation of the spatially averaged mean square normal velocity of the partition. The square elastic partition has dimensions, mass per unit area and Young's Modulus equal to 2m x 2m, ρh = 78.5 kg/m^2 and E = 210x10^9 N/m^2 respectively. (a) in narrow bands; (b) in 1/3 octave bands. — CMS model; --- Modal model.

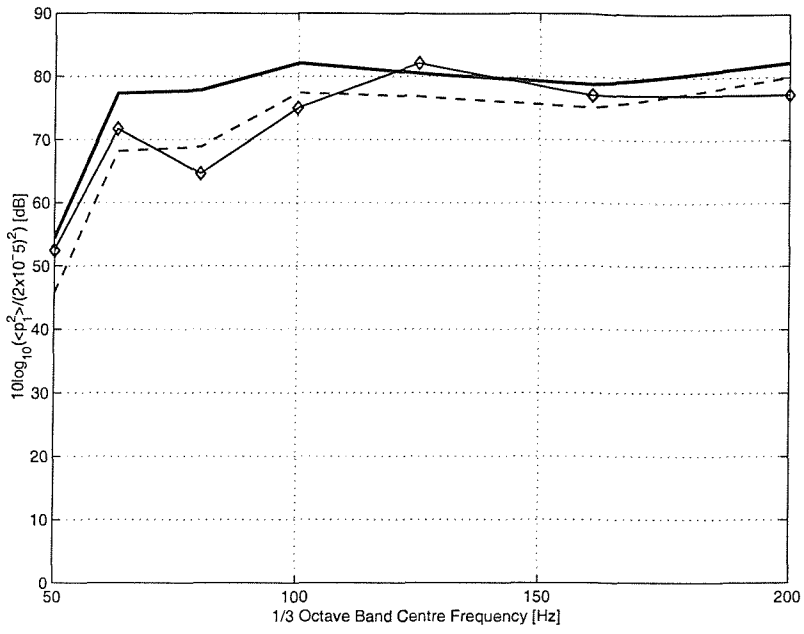

a)

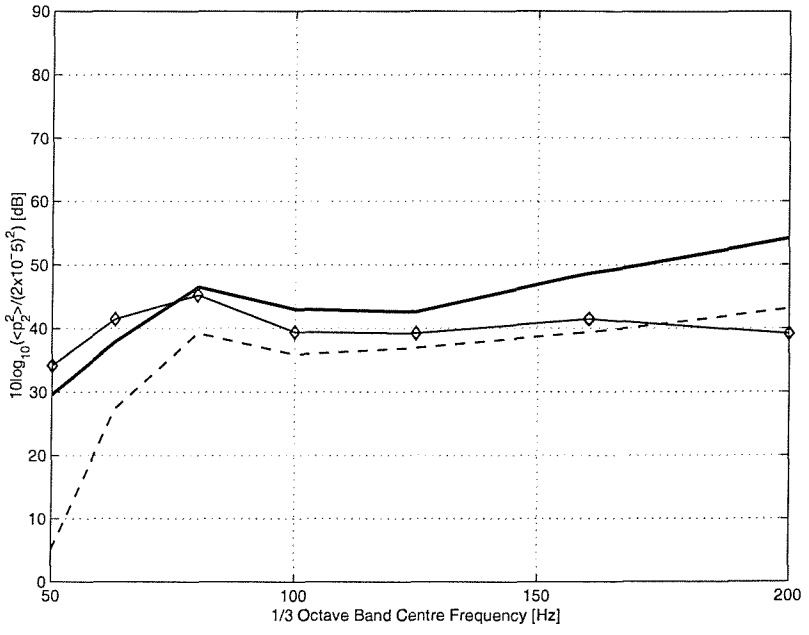

b)

Figure 6.16: Comparison between the measured and predicted (using the CMS and Modal models) spatial-average mean square sound pressure in 1/3 octave bands. The square elastic partition has dimensions, mass per unit area and Young's Modulus equal to 0.7m x 0.7m, ρh = 6.83 kg/m^2 and E = 2.53x10^9 N/m^2 respectively. (a): $10\log_0\left(\left\langle \overline{p}_1^2 \right\rangle / p_o^2\right)$ [dB re 2x10^{-5} Pa] ;(b): $10\log_0\left(\left\langle \overline{p}_2^2 \right\rangle / p_o^2\right)$ [dB re 2x10^{-5} Pa]. The subscript 1 and 2 indicates source and receiving rooms respectively; —— Measured; -◊- CMS model; ---- Modal model.

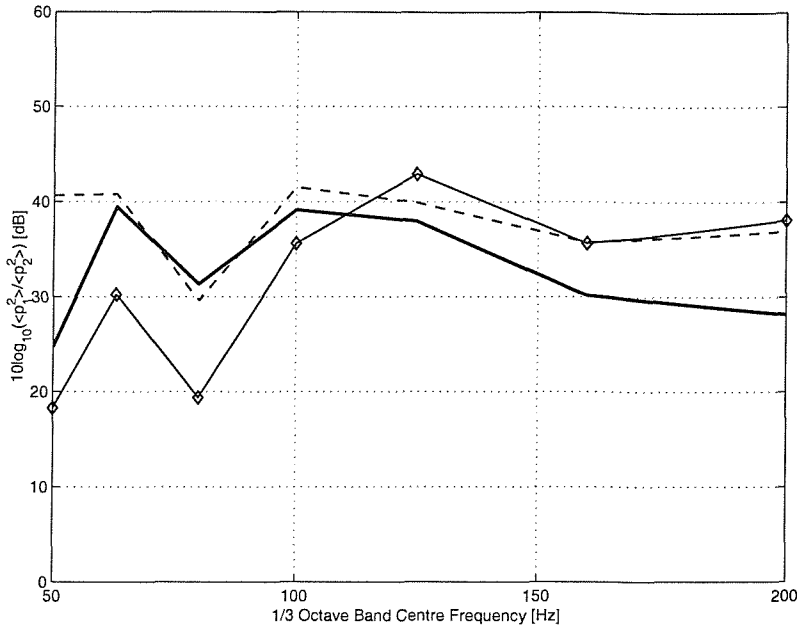

Figure 6.17: Comparison between the predicted and measured Noise Reduction (NR) values in 1/3 octave bands. The square elastic partition has dimensions, mass per unit area and Young's Modulus equal to 0.7m x 0.7m, ρh = 6.83 kg/m^2 and E = 2.53x10^9 N/m^2 respectively. —— Measured; -◊-.CMS model; ---- Modal model.

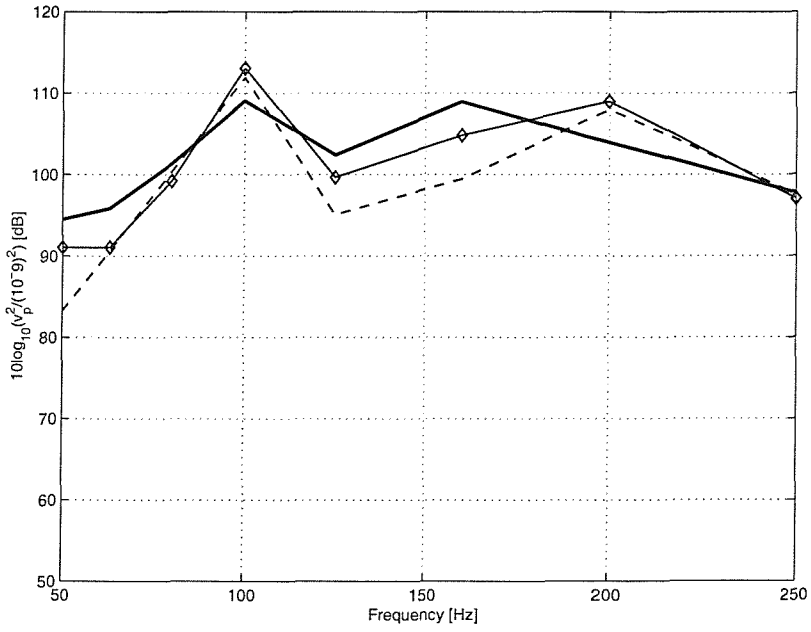

Figure 6.18: Comparison between the predicted and measured spatially averaged mean square normal velocity of the partition in 1/3 octave bands. The square elastic partition has dimensions, mass per unit area and Young's Modulus equal to 0.7m x 0.7m, ρh = 6.83 kg/m^2 and E = 2.53x10^9 N/m^2 respectively. —— Measured; -◊-.CMS model; ---- Modal model.

Chapter 7

CONCLUSIONS AND RECOMMENDATIONS FOR FUTURE WORK

7.1 – Introduction

This research was undertaken as a result of the need to improve the available analytical tools, such as Modal Analysis and classical methods, for prediction of sound transmission through partitions at low frequencies. For instance, nowadays there is a trend to design lighter structural elements and smaller rooms in order not only to optimize the use of space but also to generate higher profits. In addition, the simplification of assuming 'rigid-walled' modes in the calculations may not be reliable under certain conditions e.g. when the knowledge of the spatial distribution of the sound field is of primary importance. Furthermore there is little published work that considers noise transmission and structural acoustic coupling at low frequencies. These problems include the effect of the room geometry and absorption, the partition properties, geometry and its location and the effect of non-reverberant acoustic volumes. Therefore, this work was mainly motivated by these reasons and aimed at developing approaches and tools which could address some of the important issues.

The development and validation of mathematical models, using Modal Analysis and the Component Mode Synthesis (CMS) Method, were the main goals of this research. The implementation of a general modal model, which allows for a detailed parametric study, involved the task of expanding the set of equations presented in ref. [5] to a system comprising two-coupled rooms. To the author's knowledge, the development of the CMS model described and the application of a 'sub-structuring' technique, which was mainly developed for solving complex structural dynamics problems, for fluid-structure interaction problems was novel as regards its application to sound transmission in buildings.

7.2 – Summary of results and conclusions of each individual chapter

In this section, a review of the most important findings is presented.

In chapter 2, the results using an existing modal model formulation have shown the importance of the several phenomena that are directly related to the sound insulation provided by building partitions. Firstly, the geometrical coupling coefficients had a direct significant influence on the sound transmission between two coupled rooms. They indicate the degree of spatial matching between structural and acoustic modes. Therefore, the coupling terms were related to the size of the partition, its location and transverse dimensions of the rooms.

Although the best fluid-structure matching condition cannot occur at frequencies below the critical frequency of the panel, it has been shown that for a simply-supported elastic partition over the whole common interface, the symmetric rigid-walled acoustic modes (even modes) were better coupled to the symmetric (even) modes of the panel than to the antisymmetric (odd) structural modes, which led to substantial deterioration in the sound insulation. Secondly, the room volumes (considering similar or dissimilar rooms), were also important for predicting the sound insulation. A large variation in the Noise Reduction (NR) was observed and is mainly due to the low modal density in the rooms considered.

Furthermore, it was seen that similar rooms had a pronounced effect on reducing the NR due to the occurrence of similar modes in both source and receiving rooms, which have identical natural frequencies [78].

By assuming light and evenly distributed damping in the rectangular cross-section rooms, real and orthogonal cosinusoidal modes were selected for the calculations. In other words, the modal model considered the damping effect in the rooms basically in terms of each individual modal damping in the subsequent formulation and equations of motion.

With regard to the Mass Law and Leppington's approaches, it has been found that these underestimated the NR values in the very low frequency range, as the diffuse field condition is assumed in their formulation. However, the predicted NR levels obtained via the Modal model converged to those calculated using the Mass Law and Leppington's formulations at high frequencies. Overall, the modal model was capable of reproducing reasonably well some of the results presented in the published literature.

The main aim for Chapter 3 was to validate experimentally the Modal Model presented in the previous chapter. Firstly, the measurement of the frequency response for the sound pressure inside a single room and the quantification of the source volume velocity of a conical loudspeaker provided a critical insight into the assessment of the measurement accuracy. Secondly, the comparison and correlation of experiment and prediction was made for a system comprising two rooms coupled by a single-leaf partition. Thirdly, the analysis of the frequency response for the partition was made, by investigating which peaks corresponded to either structural or acoustic modes.

The experimental results and predictions have shown a reasonably good agreement for the single-room experimental test, within a tolerance of +/- 3dB (in one-third octaves). Although the experimental and predicted results for the two coupled rooms models presented significant discrepancies for the sound pressure in the receiving room, a reasonable agreement was obtained for the source room measurements.

One of the main difficulties was to assess the acoustic model damping at low frequencies and light absorption using a reverberation time technique, which is ideally suited for measurements in a diffuse and reverberant field. In addition, the low signal-to-noise ratio in the receiving room also affected the quality of the results measured. Moreover, considering the determination of the partition normal velocity the influence of noise in the SLDV measurements might have been significant. For instance, the problems associated with the signal-to-noise ratio mainly depend on the target (a surface which is capable of reflecting the laser beam adequately), type of scan and measurement frequency range [49].

Overall, the main goal of the chapter has been achieved and the modal model was therefore reasonably well validated for the purposes of further sensitivity and variability investigations.

The sensitivity and variability of the modal model in terms of geometric factors, panel position, room absorption and panel damping were reported in Chapter 4. Firstly, the results indicated a strong dependency of NR on room dimensions at low frequencies. This may be explained by the fact that the transmitted intensity through the partition depends on the degree of spatial matching between the partition structural modes and the acoustic modes of the receiving room.

Nevertheless, above a certain frequency, the differences between configurations were substantially reduced. Therefore, the room dimensions became large compared to the

acoustic wavelength and also there were many modes in the rooms and the acoustic field became more diffuse. Thus, the rooms became alike in terms of possessing high numbers of modes and the NR was no longer greatly affected by variation in either room's dimensions. Furthermore, it is seen that the difference between the diffuse incidence Noise Reduction NR_{ML} and the 'actual' Noise Reduction NR^{ij}_{modal} tended to zero, as expected.

As mentioned previously in Chapter 1, at high frequencies the results tend to be more dependent solely on the partition transmission properties and the absorption of the receiving room (see also equations (1.1) and (2.49)). It is well known that at high frequencies the NR values are mainly influenced by the variation in the receiving room absorption, area and transmission efficiency of the partition rather than the source room properties. On the other hand, at low frequencies there are few modes and the interpretation of the results is considerably more difficult. Furthermore, the results obtained have not considered any flanking transmission contribution although in practice this also may occur.

The reverberation time T_{60} had a significant effect on the NR differences in the frequency range where there were no modes. It might be explained by the fact that in this region only the Mass Law results varied with T_{60}.

The influence of panel position on sound transmission was not significant in the frequency range where there were no acoustic modes. However, there were significant variations in certain frequency bands where the panel dimensions and wavelengths were of similar orders of magnitude.

For the frequency range considered, the 'empirical model' for the variability of CLF developed in ref. [58] was reasonably applicable for enveloping most of the numerical results presented in Chapter 4.

Chapter 5 emphasized the significance of considering velocity continuity effects on the prediction of sound transmission via the implementation of a one-dimensional CMS model. An excellent agreement between the CMS and the one-dimensional analytical model was achieved. In comparison with the CMS model, the Modal Model produced slightly lower spatially averaged sound pressure levels at the very low frequencies.

An exception occurred at the system resonance frequencies, which corresponded to the coupled natural frequencies of the rooms where similar values were found for both

approaches. For the heavier partition, better agreement between the Modal and the CMS model has been obtained. Therefore, for the results in one-third octave bands small differences between the models were observed and noted.

Finally, the purpose of Chapter 6 was to extend the CMS model from the 1D-case to the three-dimensional case (3D-case), where the application of the method becomes more representative of real problems. Thus, additional particular features were necessary in the extension. For instance, the normal and constraint modes were for the whole volume, where the latter were of the form $(1+x/L_{x1})\cos(c_{y1}\pi\, y/L_{y1})\cos(c_{z1}\pi\, z/L_{z1})$ in the rectangular source volume $V_1(L_{x1}\,x\,L_{y1}\,x\,L_{z1})$ for example. In addition, the constraint equations were generalized and a summation over all axial, tangential and oblique modes taken into account.

The simulations were performed in order to compare the results obtained via the CMS and the Modal model. In general, significant differences (up to about 10 dB) between the models were mainly observed at very low frequencies (e.g. in the one-third octave band with centre frequency of 40 Hz). This is due to the effect of having only one or two modes in a particular frequency band, so that for models having different natural frequencies the results present some differences in the corresponding band. Most results have shown that these differences tended to be less pronounced at higher frequencies where the boundary conditions, e.g. at the interface between rooms, appear to have less significant effect on the spatially averaged results.

7.3 – Main outcomes for the project

The development and implementation of refined and improved mathematical models have been presented. These were based on the modal expansion method and CMS for the prediction of sound transmission through partitions at low frequencies and are important contributions to the field. For example, the models can also be developed or extended by other researchers for their own academic purposes. Likewise, it will be feasible to use the CMS approach with a numerical technique, e.g. FEM, the latter being used to obtain the individual component modes required to input into the CMS approach for a coupled system.

In addition, the simulation of real problems can still be made with these models. Although the applicability of the presented improved models, e.g. in building acoustics, is greatly

restricted to certain conditions, such as low frequencies, small and regular components, light damping, etc., the models may still be used in practice. For instance, the results may be useful for predicting the Coupling Loss Factor (CLF) which is an important parameter in SEA analysis. The procedure developed will allow such a parameter to be based on more realistic features of the physical model.

The main conclusion of the CMS work is that at least for the 1D-case, the predictions have shown that the CMS method can better represent the fluid particle velocity continuity at the flexible interface between the components than the modal model. Nevertheless, the CMS model cannot predict the spatially averaged mean square sound pressure and fluid particle velocity correctly to zero Hz. This might be explained by the fact that the CMS did not incorporate the bulk mode in the present formulation.

In addition, using the CMS method, which is basically a substructure technique for dynamic analysis, large fluid-structure interaction problems can be handled in a more efficient way. Although the CMS model presented in this thesis is more complex and certainly no smaller numerically than the modal model, it might be more accurate and could be generalized.

7.4 – Discussion and recommendation for future work

Further research is needed in order to extend the applicability of the CMS model to more general sound transmission problems in buildings, such as rooms with irregular shapes and heavy damping, clamped partitions, etc. Thus, an alternative parametric study can be made in terms of the variability and sensitivity of the transmission efficiency. This might be very extensive because of the wide range and number of parameters. In principle, it would be possible to vary, say, the room natural frequencies and predict the variations in the coupled system response using the CMS formulation and provide relationships between the statistical variations of the inputs and outputs in various forms. In this way, as required for SEA, ensemble averaged results could be obtained.

In addition, when one uses the CMS and have the fixed-fixed modes in the receiver room, be it one or three dimensional, it would be useful to include the bulk mode in the formulation. This could be done by considering the rigid-body mode, which is a special case of the constraint modes (e.g. using velocity potential mode shapes). In the rigid-body mode the frequency is zero and the fluid is deformed statically and elastically but there are

no inertial terms, i.e. like a spring. It can be defined to any set of boundary coordinates that is just sufficient to restrain the rigid-body motion of the component [13, 68].

The transmission models can provide an enhancement for incorporation within SEA modelling, which is an accepted tool for practical building acoustics and design but has usual assumptions of reverberant acoustic spaces and a high enough modal overlap. The acoustic predictions from the models presented do not require either of these conditions to be fulfilled. Similarly the effect of partition location can be incorporated.

Alternatively, the use of the CMS model in fluid-structure interaction problems other than sound transmission in buildings is also another interesting application of the method. For example, the prediction of sound transmission between two enclosures containing fluids of different characteristic impedances for underwater applications could be considered as well as the application of constraint techniques also allowing for more complex geometric coupling to be undertaken, if necessary.

The problem of low frequency noise reduction still remains an issue, which this project has not been able to resolve, because basically the laws of physics for existing configurations do not provide any possibility for further significant reduction. Alternatives that could be considered, and for which the CMS approach might be a useful tool, are the possibility of inhomogeneous panels, panels with mass distribution, attached tuned neutralizers or absorbers, etc., and these could be readily simulated within the CMS models as only the partition model formulation would require modification. Once potential contenders for design have been identified, a complementary detailed numerical calculation (e.g. a coupled FEM-BEM model) might be appropriate for the next stage and the work of the CMS model might then have reached a good conclusion in assisting the design process.

In summary, as can be seen above, there are significant opportunities for further development and implementation of the models derived in this study and the author will attempt to continue in the field and publish on it.

REFERENCES

[1] W. KROPP, A. PIETRZYK AND T. KIHLMAN 1994 *Acta Acustica* **2,** 379-392. On the meaning of the sound reduction index at low frequencies.

[2] A. D. PIERCE 1981 *Acoustics: An Introduction to its Physical Principles and Applications,* New York: McGraw-Hill.

[3] F. J. FAHY 1995 *Sound Intensity*, Second Edition, E & FN SPON, U.K.

[4] L. E. KINSLER et al 1982 *Fundamentals of Acoustics;* John Wiley & Sons, Inc., New York.

[5] F. J. FAHY 1985 *Sound and Structural Vibration*, Academic Press, U.K.

[6] S. MALUSKI AND B. GIBBS 2000 *Proc. I. O A.* **22 (2).** Sound Insulation between dwellings at low frequencies using a Finite Element Method.

[7] A. HEPBERGER, H. H. PRIEBSCH, W. DESMET, B. VAN HAL, B. PLUYMERS AND P. SAS 2002 *ISMA-International Conference on Noise and Vibration Engineering, KUL, Belgium.* Application of the Wave Based Method for the Stead-State Acoustic Response Prediction of a Car Cavity in the Mid-Frequency Range.

[8] R. J. M. CRAIK 1996 *Sound Transmission through Buildings using Statistical Energy Analysis*, Gower Publishing Limited, U.K.

[9] E. H. DOWELL, G. F. GORMAN AND D. A. SMITH 1977 *Journal of Sound and Vibration* **52(4),** 519-542. Acoustoelasticity: General Theory, Acoustic Natural Modes and Forced response to sinusoidal excitation, including comparisons with experiment.

[10] D. TAKAHASHI 1995 *The Journal of the Acoustical Society of America* **98(5)**, 2598-2606. Effects of panel boundedness on sound transmission problems.

[11] S. MALUSKI AND B. M. GIBBS 1998 *Euro noise 98*, 681-685. The influence of partition boundary conditions on sound level difference between rooms at low frequencies.

[12] A. OSIPOV, P. MESS AND G. VERMEIR 1997 *Applied Acoustics* **52 (3-4)**, 273-288. Low-Frequency Airborne Sound Transmission Through Single Partitions in Buildings.

[13] R. R. CRAIG JR. 1981 *Structural Dynamics – An Introduction to Computer Methods;* Inc. New York, N. Y: John Wiley &Sons.

[14] L. GAGLIARDINI AND J. ROLAND 1991 *Journal of Sound Vibration* **145(3)**, 457-478. The Use of a Functional Basis to Calculate Acoustic Transmission Between Rooms.

[15] F. G. LEPPINGTON, F. R. S. BROADBENT AND K. H. HERON 1982 *Proceedings of the Royal Society of London*, **A 382,** 245-271. The acoustic radiation efficiency of rectangular panels.

[16] F. G. LEPPINGTON, K. H. HERON, F. R. S. BROADBENT AND S. M. MEAD 1987 *Proceedings of the Royal Society of London*, **A 412,** 309-337. Resonant and Non-Resonant Acoustic Properties of elastic Panels. II. The transmission Problem

[17] F. G. LEPPINGTON 1989 *Proceedings of the Royal Society of London*, **A 426,** 153-165. The Transmission of Randomly Incident Sound Through an Elastic Panel.

[18] F. J. FAHY 2000 *Foundations of Engineering Acoustics,* Academic Press, U.K.

[19] H. NELISSE, O. BESLIN AND J. NICOLAS 1998 *Journal of Sound Vibration* **211(2)**, 207-225. A Generalized Approach for the Acoustic Radiation from a Baffled or Unbaffled Plate with Arbitrary Boundary Conditions, Immersed in a Light or Heavy Fluid.

[20] P. SANTOS AND A. TADEU 2002 *Journal of Sound and Vibration* **257(5),** 945-965. Acoustic Insulation Provided by a Single Wall Separating Two Contiguous Tunnels Via BEM.

[21] R. J. M. CRAIK AND R. S. SMITH 2000 *Applied Acoustics* **61**, 223-245. Sound Transmission Through Double Leaf Lightweight Partitions part I: Airborne Sound.

[22] P. SANTOS AND A. TADEU 2003 *Journal of Sound and Vibration* **261,** 185-191. A Note on the Acoustic Insulation Between Two-Dimensional Acoustic Spaces at Low Frequencies.

[23] J. MATHYS 1993 *Applied Acoustics* **40(3),** 185-200. Low Frequency Noise and Acoustical Standards.

[24] J. LANG 1997 *Applied Acoustics* **52,** 225-238. A Round Robin Sound Insulation in Buildings.

[25] M. VILLOT, J. ROLAND AND G. CHAVERIAT 1992 *Journal of the Acoustical Society of America* **91(1),** 187-195. Phonoscopy – an Acoustical-Holography Technique for Plane Structures Radiating in Enclosed Spaces.

[26] M. PETYT, G. H. KOOPMAN, AND R. J. PINNINGTON 1977 *Journal of Sound and Vibration* **53(1),** 71-82. The Acoustic Modes of a Rectangular Cavity Containing a Rigid, Incomplete Partition.

[27] M. C. BHATTACHARYA. AND R. W. GUY. 1972 Acustica **26,** 344-348. The influence of the measuring facility on the measured sound insulating property of a panel.

[28] L. C. FOTHERGILL 1980 *Applied Acoustics* **13,** 171-187. Recommendations for the measurement of sound insulation between dwellings.

[29] J. LANG 1972 *Applied Acoustics* **5,** 21-37. Differences between acoustical insulation properties measured in the Laboratory and results of measurements in situ.

[30] R. W. GUY, A. DE MEY, and P. SAUER 1985 *Applied Acoustics* **18,** 81-98. The effect of some physical parameters upon the laboratory of sound transmission loss.

[31] R. J. M. CRAIK 1992 *Applied Acoustics* **35,** 25-46. The influence of the Laboratory measurements of walls performance.

[32] J. ROLAND 1995 *Proceedings of Inter-noise* 95, 1113-1115. Adaptation of existing test facilities to low frequencies measurements.

[33] H. GOYDKE 1998 *Proceedings of Inter-Noise 98,* 480. Investigations on the precision of laboratory measurements of sound insulation of building elements according to the revised Standard ISO 140.

[34] INTERNATIONAL STANDARD ISO 140-2; *Acoustics- Measurement of sound insulation in buildings and of building elements – part 2: Statement of precision requirements*, First Edition 1978.

[35] H. V. FUCHS, X. ZHA, M. SPAH AND M. POMMERER 1998 *Proceedings of Euro-Noise 98* **2**, 657-662. Qualifications of small free-field and reverberation rooms for low frequencies.

[36] D. C. PEDERSEN 1997 *DAGA 97, Kiel*, 105-106. Laboratory measurement of the low frequency sound insulation.

[37] S. MALUSKI, B. M. GIBBS AND H. BOUGDAH 1997 *Journal Building Acoustics* **4(2)**, 73-86. Predicted and measured low frequency response of small rooms.

[38] S. MALUSKI 1999 *PhD thesis; Sheffield Hallam University.* Low frequencies sound insulation in Dwellings.

[39] J. C. LAI AND S. BURGESS 1991 *Applied Acoustics* **34,** 77-87. Application of the sound intensity technique to measurement of field sound transmission loss.

[40] R. E. HALLIWELL AND C. C. WARNOCK 1985 *The Journal of the Acoustical Society of America* **77 (6)**, 2094-2103. Sound transmission loss: Comparison of conventional techniques with sound intensity techniques.

[41] INTERNATIONAL STANDARD BS EN ISO 140-3 1995 *Acoustics- Measurement of sound insulation in buildings and of building elements – part 3: Laboratory measurements of airborne sound insulation of building elements.*

[42] M. D. C. MAGALHAES AND N. S. FERGUSON 2001 *Proceedings of Inter Noise – The Hague* 4pp. Low frequency airborne sound transmission.

[43] INTERNATIONAL STANDARD ISO 354 1985 *Acoustics – Measurement of sound absorption in a reverberation room;* First Edition

[44] M. R. SCHROEDER 1965 *The Journal of the Acoustical Society of America* **37,** 409-412. New method of measuring reverberation time.

[45] E. H. DOWELL 1978 *The Journal of the Acoustical Society of America* **64(1),** 181-191. Reverberation Time, Absorption, and Impedance.

[46] J. DEVORE AND N. FARNUM 1999 *Applied Statistics for Engineers and Scientists;* Duxbury Press – ITP.

[47] M. TOHYAMA, H. SUZUKI AND Y. ANDO 1995 *The nature and technology of acoustic space;* Academic Press.

[48] L. CREMER, M. HECKL AND E. E. UNGAR 1988 *Structure-borne Sound*; Berlin: Springer-verlag.

[49] POLYTEC SOFTWARE MANUAL – Polytec Scanning Vibrometer software 7.1.

[50] F. JACOBSEN AND H. DING 1982 *Journal of Sound and Vibration* **81(3),** 405-412. Decay rate and wall absorption at low frequencies.

[51] J. S. BENDAT AND A. G. PIERSOL 2000 *Random Data: Analysis and Measurement Procedures*; John Wiley &Sons, Inc.

[52] K. A. MULHOLLAND AND R. H. LYON 1973 *Journal of the Acoustical Society of America* **54(4),** 867-873. Sound Insulation at Low Frequencies.

[53] A. C. C. WARNOCK 1982 *Proceedings of Internoise 82, San Francisco, USA,* 833-836. Sound Insulation at Low Frequencies.

[54] T. KIHLMAN AND A. C. NILSSON 1972 *Journal of Sound and Vibration* **24(3),** 349-364. The Effects of Some Laboratory Designs and Mounting Conditions on Reduction Index Measurements.

[55] S. D. CONTE AND C. DE BOOR 1980 *Elementary Numerical Analysis – An Algorithmic Approach.* Third Edition – Mc Graw- Hill Book Company.

[56] T. KIHLMAN, A. PIETRZYK AND W. KROPP 1997 *Optimisation of Sound Insulation at Low frequencies.* Report F 97-04, Department of Applied Acoustics, Chalmers University of Technology, Gothenburg.

[57] W. KROPP AND A. PIETRZYK 1999 *Statistic Analysis of the Influence of the Room Dimensions on the Sound Insulation at Low Frequencies.* Report F 99-03, Department of Applied Acoustics, Chalmers University of Technology, Gothenburg.

[58] W. S. PARK, D. J. THOMPSON AND N. S. FERGUSON 2001 *Institute of Sound and Vibration Research – ISVR. Technical Memorandum* **874.** An Empirical Model for the Variability of the Coupling Loss Factor.

[59] H. KUTTRUFF 2000 *Room Acoustics* (4th edition). E &F N Spon, London.

[60] M. J. CROCKER AND A. J. PRICE 1969 *Journal of Sound and Vibration* **9,** 469-486. Sound Transmission Using Statistical Energy Analysis of Vibrating Systems.

[61] R. J. M. CRAIK, J. A. STEEL AND D. I. EVANS 1991 *Journal of Sound and Vibration* **144(1),** 95-107. Statistical Energy Analysis of Structure-Borne Sound Transmission at Low Frequencies.

[62] F. X. MAGRANS 1992 *Journal of Sound and Vibration* **165(2),** 277-283. Definition and Calculation of Transmission Paths Within An S.E.A. Framework.

[63] R. J. M. CRAIK 1981 *Journal of Sound and Vibration* **82(4),** 505-516. The Prediction of Sound Transmission Through Buildings Using Statistical Energy Analysis.

[64] R. H. LYON AND R. G. DEJONG 1995 *Theory and Application of Statistical Energy Analysis.* Boston: Butterworth-Heinemann – Second Edition.

[65] D. A. BIES AND S. HAMID 1980 *Journal of Sound and Vibration* **70(2),** 187-204. *In Situ* Determination of Loss and Coupling Loss Factors by the Power Injection Method.

[66] S. N. HOU 1969 *The Shock and Vibration Bulletin, Bulletin* **40(4)** *Naval Research Lab.*, 25-39. Review of Modal Synthesis Techniques and a New Approach.

[67] W. A. BENFIELD AND R. F. HRUDA 1971 *AIAA journal* **9(7),** 1255-1261. Vibration Analysis of Structures by Component Mode Substitution.

[68] R. R. CRAIG JR 2000 *Proceedings of the 18th IMAC Conference on Computational Challenges in Structural Dynamics 2000* **1** and **2,** 899-908. A Brief Tutorial On Substructure Analysis And Testing.

[69] R. R. CRAIG JR 1981 *Structural Dynamics - An Introduction to Computer Methods.* New York: John Wiley & Sons Inc.

[70] W. C. HURTY 1965 *AIAA Journal* **3(4),** 678-685. Dynamic Analysis of Structural System Using Component Modes.

[71] B. PLUYMERS, W. DESMET, D. VANDEPITTE AND P. SAS 2002 *ISMA-International Conference on Noise and Vibration Engineering, KUL, Belgium.* Application of the wave based prediction technique for the analysis of the coupled vibro-acoustic behaviour of a 3D cavity.

[72] N. S. FERGUSON 2000 *Structural Dynamics – Recent Advances - Proceedings of the 7th International Conference* **1,** 309-319. The Lagrange Multiplier Method Revisited for Free and Forced Vibration of a Constraint Structure.

[73] L. MEIROVITCH 1967 *Analytical Methods in Vibrations,* Macmillan, New York.

[74] P. M. MORSE AND K. U. INGARD 1986 *Theoretical Acoustics*; Princeton, New Jersey: Mc Graw-Hill Inc.

[75] K. H. GHLAIM AND K. F. MARTIN *Proc. Int. Conf. On Modal Analysis; Schenectady, N. Y. Union College,* 683-689. Reduced Component Modes in a Damped System.

[76] L. R. KLEIN AND E. H. DOWELL 1974 *Journal of Applied Mechanics,* 527-528. Analysis of Modal Damping by Component Modes Method Using Lagrange Multipliers.

[77] T. P. GIALAMAS, D. T. TSAHALIS, D. OTTE, H. VAN DER AUWARAER AND D. A. MANOLAS 2001 *Journal of Applied Mechanics* **62**, 1211-1219. Substructuring Technique: Improvement by Means of Singular Value Decomposition (SVD).

[78] C. L. MORFEY 2000 *Dictionary of Acoustics.* Academic Press, London, UK.

[79] E. KREYSZIG 1999 *Advanced Engineering Mathematics.* Eighth Edition, John Wiley & Sons, Inc.

[80] S. M. KIM AND M. J. BRENNAN 1999 *Journal of Sound and Vibration* **223(1),** 97-113. A Compact Matrix Formulation Using the Impedance and Mobility Approach for the Analysis of Structural-Acoustic Systems

[81] A. PIETRZYK 1997 *Sound Insulation at Low Frequencies.* Report F 97-01, Department of Applied Acoustics, Chalmers University of Technology, Gothenburg.

[82] L. L. BERANEK and I. L. VER 1992 *Noise and Vibration Control Engineering,* John Wiley & Sons, Inc. USA

[83] F. M. WHITE 1999 *Fluid Mechanics,* McGraw-Hill International Editions, Fourth Edition, Singapore.

[84] L. L. BERANEK and I. L. VER 1971 *Noise and Vibration Control,* Mc Graw-Hill Book Company.

[85] R. W. GUY AND M. C. BHATTACHARYA 1973 *Journal of Sound and Vibration* **27(2),** 207-223. The Transmission of Sound Through a Cavity-Backed Finite Plate.

[86] D.A. BIES AND C. H. HANSEN 1996 *Engineering Noise Control – Theory and practice.* E &FN SPON – Second Edition.

[87] M. D. C. MAGALHAES AND N. S. FERGUSON 2003 *Applied Acoustics* **64,** 1049-1067. Acoustic-Structural Interaction Analysis Using the Component Mode Synthesis Method.

[88] R. D. B. BLEVINS 1995 *Formulas for Natural Frequency and Mode Shape.* Krieger Publishing Company

Appendix A.

The Eigenvalue Problem – Matrix Formulation

This appendix describes the implementation of the Modal model using a matrix formulation. Firstly, the eigenvalue problem, which was implemented in MATLAB, is presented. Secondly, the matrix implementation for the calculation of the system frequency response is shown.

Basically, a eigenvalue problem is described in its standard form as

$$[A-\lambda I][y]=0 \tag{A.1}$$

where A is the dynamic matrix, I is the identity matrix and y is the response function.

The solution of the eigenvalue problem, for the fluid-structure interaction case described in chapter 2, led to a system of a standard second order differential equations in the form

$$[M][\ddot{y}]+[C][\dot{y}]+[K][y]=0 \tag{A.2}$$

where $[M]$, $[C]$ and $[K]$ are the mass, damping and stiffness matrices respectively and $[y]$ is the column vector representing the generalized coordinates of the system.

Using a MATLAB code for the conversion of a second order differential equation to a system of two first-order differential equations, the first-order system for equation (A.2) can then immediately be obtained by [79]

$$\frac{\partial y_{n-1}}{\partial t} = y'_{n-1} = y_n \tag{A.3}$$

Therefore, setting $y^T = [y_1 \quad y_2]$ and using equations (A.2) and (A.3), one can obtain the following relationship

$$y' = \begin{bmatrix} 0 & I \\ -M^{-1}K & -M^{-1}C \end{bmatrix} y = A\,y \tag{A.4}$$

Thus, the characteristic equation for the eigenvalue problem defined by equation (A.1) is

$$\det(A-\lambda I)=\begin{vmatrix}\begin{bmatrix}\lambda_1 & 0 & 0\\ 0 & \ddots & \vdots\\ 0 & \cdots & \lambda_n\end{bmatrix} & [I_n]\\ [-M^{-1}K] & -[M^{-1}C]-\begin{bmatrix}\lambda_1 & 0 & 0\\ 0 & \ddots & \vdots\\ 0 & \cdots & \lambda_n\end{bmatrix}\end{vmatrix}=[0]_n^T \tag{A.5}$$

The dynamic matrix for the modal model described in Chapter 2 was

$$A=\begin{bmatrix}0 & I\\ \omega_{n1,p,n2} & Z_{n1,p,n2}\end{bmatrix} \tag{A.6}$$

and

$$\omega_{n1,p,n2}=\begin{bmatrix}-\omega_{n1}^2 & 0 & 0\\ 0 & -\omega_p^2 & 0\\ 0 & 0 & -\omega_{n2}^2\end{bmatrix} \tag{A.7}$$

$$Z_{n1,p,n2}=\begin{bmatrix}-\beta_{n1} & G_1 & 0\\ -T_1 & -\beta_p & T_2\\ 0 & -G_2 & -\beta_{n2}\end{bmatrix} \tag{A.8}$$

where ω_{n1}, ω_{n2} and ω_p are the natural frequencies (in radians) for the source room, receiving room and partition respectively. β_{n1}, β_{n2} and β_p are the modal damping matrices for the source room, receiving room and partition. These variables are all defined in the context of Chapter 2. Accordingly, the matrices G_1, G_2, T_1 and T_2 were given by

$$G_1=\frac{c_o^2 S\, C_{n_1 p}}{\Lambda_{n_1}};\ G_2=\frac{c_o^2 S\, C_{n_2 p}}{\Lambda_{n_2}} \tag{A.9}$$

$$T_1=\frac{\rho_o S\, C_{n_1 p}}{\Lambda_p};\ T_2=\frac{\rho_o S\, C_{n_2 p}}{\Lambda_p} \tag{A.10}$$

where c_o and ρ_o are the sound speed and density of air respectively, S is the partition surface area, $C_{n_1 p}$ and $C_{n_2 p}$ are the spatial coupling coefficients, Λ_{n_1} and Λ_{n_2} are the modal volume of the source and receiving room, and finally Λ_p is the partition modal surface area. These variables are also defined in the context of Chapter 2.

Appendix B.

The accuracy of the measurements – Statistical Parameters

The most frequently used statistical parameter, which is simply the arithmetic average of n values, is often considered by comparing measured and predicted sample mean values. The sample mean $\bar{x}$ is defined as [46]

$$\bar{x} = \frac{\sum_{i=1}^{n} x_i}{n} \tag{B.1}$$

The probability distribution of data obtained from noise and vibration measurements within a subsystem may often be assumed to be normal [64]. Thus, the statistical calculations done in this work assume that the acquired data are normally distributed. Hence, the measure of accuracy used in this work is the 95% confidence interval. It is defined as the range of values for which the true mean value μ is expected to lie 95% of the time when the tests are repeated. Thus, the confidence interval for μ with a confidence level of approximately 95% is given by

$$\frac{\bar{x} - t_{0.975,n-1}\, s}{\sqrt{n}} < \mu < \frac{\bar{x} + t_{0.975,n-1}\, s}{\sqrt{n}} \tag{B.2}$$

$$s = \sqrt{\frac{\sum (x_i - \bar{x})^2}{n-1}} \tag{B.3}$$

where $t_{0.975,n-1}$ is the value of the *Student t* distribution function and s is the sample standard deviation [64]. The parameter $t_{0.975,n-1}$ tends to 1.96 as $n \to \infty$. Thus, equation B.2 may be written

$$\frac{\bar{x} - s\,1.96}{\sqrt{n}} < \mu < \frac{\bar{x} + s\,1.96}{\sqrt{n}} \tag{B.4}$$

Appendix C.

Derivation of the Dynamic Properties of a Elastic Panel

The kinetic energy T_S for a plate in flexure is defined as [69]

$$T_S = \frac{1}{2}\int_S \frac{\partial w^*}{\partial t}\,\rho_s h\,\frac{\partial w}{\partial t}\,dS \tag{C.1}$$

Using the modal expansion, an approximated expression for the plate normal velocity $\dot{w}(t)$ is given by

$$\dot{w}\,(t) = \sum_{p=1}^{P} \dot{w}_p\,(t)\;\phi_p(y,z) \tag{C.2}$$

where $\phi_p(y,z)$ and P represent a mode shape p and the total number of assumed-modes for the structural partition respectively;

Substituting equation (C.2) into equation (C.1), yields

$$T_S = \frac{1}{2}\sum_{p=1}^{P}\sum_{q=1}^{P}\left(\dot{w}_p \dot{w}_p^*\right)\int_S m\;\phi_p^T\,\phi_q\,dS \tag{C.3}$$

where m = mass per unit area of the plate. By using the orthogonality condition [69], the cross terms are then eliminated from the calculations. Equation (C.3) may then be evaluated as

$$T_S = \frac{1}{2}\sum_{p=1}^{P}\left|\dot{w}_p\right|^2\int_S m\;\phi_p^T\,\phi_p\,dS \tag{C.4}$$

Likewise, the potential strain energy V_S is defined as [69]

$$V_S = \frac{1}{2}\sum_{p=1}^{P}\left(\left|w_p\right|^2\right)\int_S D\left[\left(\frac{\partial^2\phi_p}{\partial z^2}\right)^2 + 2\upsilon\left(\frac{\partial^2\phi_p}{\partial z^2}\right)\left(\frac{\partial^2\phi_p}{\partial y^2}\right) + \left(\frac{\partial^2\phi_p}{\partial y^2}\right)^2\right]dS \tag{C.5}$$

where D is the plate flexural rigidity.

For non-conservative systems, a dissipation function D [75, 76] may be included. For a flexible structural plate with viscous damping, it can be expressed as

$$\mathrm{D} = \frac{1}{2}\sum_{p=1}^{P}\sum_{q=1}^{Q}\omega_p\left(\dot{w}_p\dot{w}_p^*\right)\int_S m\,\phi_p^T\eta_p\,\phi_q\,dS \tag{C.6}$$

where η_p is the modal loss factor for the plate and ω_p is the natural frequency which corresponds to the mode number p. The damping matrix can then be derived from the above expression. It is seen that linear viscous damping was adopted for the purpose of simplification.

The dynamic properties of the plate can be obtained by substituting the kinetic and potential energy and the dissipation function expressions into Lagrange's equation given in ref. [69]. Thus, the damped system of equations of motion for a mode p of a uniform plate can then be written as

$$M_p\ddot{w}_p + C_p\dot{w}_p + K_p w_p = F_p \tag{C.7}$$

where

$$M_p = m\int_S \phi_p^T\,\phi_p\,dS \tag{C.8}$$

$$C_p = \omega_p m\int_S \phi_p^T\eta_p\,\phi_q\,dS \tag{C.9}$$

and

$$K_p = D\int_S\left(\frac{\partial^2\phi_p}{\partial z^2}\right)^2 + 2\upsilon\left(\frac{\partial^2\phi_p}{\partial z^2}\right)\left(\frac{\partial^2\phi_p}{\partial y^2}\right) + \left(\frac{\partial^2\phi_p}{\partial y^2}\right)^2 dS \tag{C.10}$$

$$F_p = \int_S p(y,z,t)\,\phi_p\,dS \tag{C.11}$$

where the parameters M_p, K_p, C_p and F_p represent the modal mass, modal stiffness, modal damping and generalized force on the plate respectively.

The analytical mode shape ϕ_p for a simply-supported rectangular plate *in vacuo* is exactly described by

$$\phi_p(r,s) = \sin(k_{r_Y})\sin(k_{s_Z}) \tag{C.12}$$

where $k_{r_Y} = \frac{r\pi}{L_{y_p}}$ and $k_{s_Z} = \frac{s\pi}{L_{z_p}}$ are plate wavenumbers in the y and z directions respectively.

Substituting equation (C.12) into equations (C.8), (C.9) and (C.10) then leads to the following results

$$M_p = \frac{mS}{4} \tag{C.13}$$

$$C_p = \frac{\omega_p \eta_p mS}{4} \tag{C.14}$$

and $$K_p = M_p \omega_p^2 \tag{C.15}$$

where $$\omega_p = \left(\frac{D}{m}\right)^{\frac{1}{2}} \left(k_{r_Y}^2 + k_{s_Z}^2\right) \tag{C.16}$$

where ω_p represents the angular natural frequency of mode $p(r, s)$.